Aston University

Some pages of this thesis may have been removed for copyright restrictions.

If you have discovered material in AURA which is unlawful e.g. breaches copyright, (either yours or that of a third party) or any other law, including but not limited to those relating to patent, trademark, confidentiality, data protection, obscenity, defamation, libel, then please read our Takedown Policy and contact the service immediately

MULTI - FUNCTION CONTROLLERS

FOR A HYDRAULIC PUMP

by

PETER TOVEY B Sc, M Sc.

A thesis submitted in fulfilment of the requirements for the degree of Doctor of Philosophy.

THE UNIVERSITY OF ASTON IN BIRMINGHAM

SEPTEMBER 1980

MULTI-FUNCTION CONTROLLERS FOR A HYDRAULIC PUMP

PETER TOVEY

DOCTOR OF PHILOSOPHY

1980

SUMMARY

This project has been undertaken for Hamworthy Hydraulics Limited. Its objective was to design and develop a controller package for a variable displacement, hydraulic pump for use mainly on mobile earth moving machinery. A survey was undertaken of control options used in practice and from this a design specification was formulated, the successful implementation of which would give Hamworthy an advantage over its competitors.

Two different modes for the controller were envisaged. One consisted of using conventional hydro-mechanics and the other was based upon a micro-processor.

To meet short term customer prototype requirements the first section of work was the realisation of the hydro-mechanical system. Mathematical models were made to evaluate controller stability and hence aid their design. The final package met the requirements of the specification and a single version could operate all sizes of variable displacement pumps in the Hamworthy range. The choice of controller options and combinations totalled twenty-four.

The hydro-mechanical controller was complex and it was realised that a micro-processor system would allow all options to be implemented with just one design of hardware, thus greatly simplifying production. The final section of this project was to determine whether such a design was feasible. This entailed finding cheap, reliable transducers, using mathematical models to predict electro-hydraulic interface stability, testing such interfaces and finally incorporating a micro-processor in an interactive control loop.

The study revealed that such a system was technically possible but it would cost 60% more than its hydro-mechanical counterpart. It was therefore concluded that, in the short term, for the markets considered, the hydro-mechanical design was the better solution.

Regarding the micro-processor system the final conclusion was that, because the relative costs of the two systems are decreasing, the electro-hydraulic controller will gradually become more attractive and therefore Hamworthy should continue with its development.

CONTROLLERS : CONTROL : PUMPS : SERVO-MECHANISMS

ACKNOWLEDGEMENTS

I should like to express my gratitude to everyone concerned with the project, especially my supervisors Prof K Foster, Mr B M Bell, Mr B Wynn, Mr D C Hickson and Mr F G Willets, for their continual support and guidance.

I should like to thank also my colleagues at Hamworthy, particularly Mr G Hale, Mr C Holloway and Mr R Wilmot for their enthusiasm and co-operation.

My especial thanks must go to Mrs E Baines for her perseverance in typing this thesis.

Finally, I should like to thank my wife for her inspiration and understanding throughout the project.

CONTENTS

APPENDIX

Page Number

APPENDIX

APPENDIX

APPENDIX

LIST OF FIGURES

NOMENCLATURE

SYMBOL	DEFINITION	UNITS
A	Limit cycling amplitude of pressure compensating spool	m
A'	Limit cycling amplitude of main spool in CCS control	m
a	Pressure compensating valve damping orifice area	m^2
a(in)	Flow area into a valve	m^2
a(out)	Flow area out of a valve	m^2
a_c	Area of pressure compensating spool	m^2
a_p	Flow area of a port	m^2
a_v	Flow area of the loading valve	m^2
a_1	Power piston area	m^2
a_2	Follow-up piston area	m^2
a_3	Pressure compensating piston area	m^2
a_4	Flow area out of the pressure compensating valve	m^2
a_5	Larger area of stepped pressure compensating spool	m^2
a_6	Smaller area of stepped pressure compensating spool	m^2
a_7	CCS sensing orifice area	m^2
a_8	CCS piston area	m^2
a_9	CCS damping orifice area	m^2
a_{10}	Flow area of CCS directional control valve	m^2
a_{11}	Flow area of flats on CCS piston	m^2
a_{12}, a_{13}	Pressure dividing orifice areas in pressure compensated CCS circuit	m^2
a_{14}	Stroking piston area in solenoid design	m^2
a_{15}	Spool area in solenoid design	m^2

SYMBOL	DEFINITION	UNITS
a_{16}	Stroking piston areas in flapper/nozzle design	m^2
B_1)	Magnitudes of terms in the CCS flow	
)		m^2
B_2)	equations	
C_d	Coefficient of discharge for orifices and valves	-
C_p	Meter-in pressure flow gain of follow-up servo	$(m^3/s)/Pa$
C'_p	Meter-out pressure flow gain of follow-up servo	$(m^3/s)/Pa$
C_x	Meter-in position flow gain of follow-up servo	$(m^3/s)/m$
C'_x	Meter-out position flow gain of follow-up servo	$(m^3/s)/m$
C_z	Meter-in position flow gain of pressure compensating valve	$(m^3/s)/m$
C'_z	Meter-out position flow gain of pressure compensation valve	$(m^3/s)/m$
C_1	Reaction area of pump in the plane of the controller	m^2
C_2	Meter-in flow force pressure gain of solenoid controller	N/Pa
C_3	Meter-in flow force position gain of solenoid controller	N/m
C_4	Meter-out flow force pressure gain of solenoid controller	N/Pa
C_5	Meter-out flow force position gain of solenoid controller	N/m
C_6	Meter-in position flow gain of solenoid controller	$(m^3/s)/m$
C_7	Meter-in pressure flow gain of solenoid controller	$(m^3/s)/Pa$
C_8	Meter-out position flow gain of solenoid controller	$(m^3/s)/m$
C_9	Meter-out pressure flow gain of solenoid controller	$(m^3/s)/Pa$

SYMBOL	DEFINITION	UNITS
F	CCS spring pre-load	N
F(in)	Meter-in flow force - solenoid controller	N
f(in)	Small changes of F(in)	N
F(out)	Meter-out flow force - solenoid controller	N
f(out)	Small changes of F(out)	N
f(W)	CCS directional control valve opening ($=a_{10}$)	m^2
f(X)	CCS piston variable orifice ($=a_{11}$)	m^2
F_s	Solenoid force	N
f_s	Small changes in F_s	N
[G]	Forward loop transfer function (FLTF)	$(m^3/s)/Pa$
$[G_1]$	Transfer function for the main spool	m/Pa
$[G_2]$	Transfer function for the follow-up servo	-
$[G_3]$	Transfer function for the pump	$(m^3/s)/m$
$[G_4]$	Transfer function for the valve, pump and load (A8)	Pa/N
$[G_5]$	Transfer function for the pressure transducer and amplifier (A9)	V/Pa
$[G_6]$	Transfer function for electrical compensation (A9)	-
$[G_7]$	A transfer function for the servo-valve	$(m^3/s)/A$
$[G_8]$	Transfer function for electrical compensation (A9)	-
$[G_9]$	Transfer function for the current amplifier	A/V
$[G_{10}]$	A transfer function for the pump (A9)	$m/(m^3/s)$
H	Depth of the CCS notch in the directional control valve	m
H_Z	Distance between metering holes in the pressure compensating valve	m
H_1	Co-ordinate for the CCS notch circle centre	m
H_2	Pressure flow gain for the servo-valve	$(m^3/s)/Pa$

SYMBOL	DEFINITION	UNITS
$[H]$	Transfer function for the hydraulic load	$Pa/(m^3/s)$
$[H_1]$	Transfer function for the pressure transducer, electrical control circuit and solenoid	N/Pa
$[H_2]$	A transfer function for the pump	$(m^3/s)/Pa$
$[H_3]$	A transfer function for the servo-valve	$(m^3/s)/Pa$
$[H_4]$	Transfer function for the position transducer	V/m
$[H_5]$	A transfer function for the pump	Pa/m
i	Small changes in current	A
j	The imaginary number $\sqrt{-1}$	
K	Pump return spring	N/m
K_1	Pump displacement control valve spring	N/m
K_2	Pre-load spring for power controller	N/m
K_3	Pressure compensation main spool return spring	N/m
K_4	Pressure compensating valve spring	N/m
K_5	Main spool return spring used in initial design	N/m
K_6	Main spool return spring used in revised design	N/m
K_7	CCS main spool return spring	N/m
K_8	Pump stroking spring (A8)	N/m
K_9	Pump return spring (A8)	N/m
K_{10}	Feed-back spring (A8)	N/m
K_{11}	Internal solenoid spring (A8)	N/m
ΣK	Summated spring rate of the power controller springs	N/m
L_N	Length of CCS metering notch	m
L_V	Spool metering land length (A8)	m
L_Z	Underlap of the pressure compensating valve	m
L_1	Main spool damping coefficient	N/(m/s)
L_2	Underlap of the follow-up servo	m

SYMBOL	DEFINITION	UNITS
L_3	Spool damping coefficient (A8)	N/(m/s)
$\dot{m}$	Mass flow rate	Kg/s
M_Z	Mass of pressure compensating spool	Kg
M_1	Mass of main spool	Kg
M_2	Mass of moving parts in the pump	Kg
M_3	Mass of spool (A8)	Kg
N	Rotational speed of the pump	rpm
N_1)	General speeds in the description of a constant speed controller	rpm
N_2)		rpm
N_3)		rpm
$\hat{P}$	Maximum pressure	Pa
P_c	Pressure compensating crack pressure	Pa
$\hat{P}_L$	Maximum load pressure	Pa
P_{L_1}	Electronic CCS pressure signal for pump 1	V
P_{L_2}	Electronic CCS pressure signal for pump 2	V
P_{L_3}	Electronic CCS pressure signal for pump 3	V
P_m	Metered pressure	Pa
p_m	Small changes in P_m	
P_r	Pressure ripple in pressure compensation	Pa
P'_r	Pressure ripple in CCS control	Pa
P_1	Pressure of pump 1	Pa
P'_1	Pressure compensating CCS pressure	Pa
p_1	Small changes in P_1	
P_2 (	Follow-up piston pressure	Pa
(	Pressure of pump 2 (ch's 2 & 4)	
(		Pa
p_2	Small changes in P_2	
P_3	Pressure of pump 3	Pa

SYMBOL	DEFINITION	UNITS
p_3	Small changes in P_3	Pa
P_4	Stroking piston pressure (A8)	Pa
p_4	Small changes in P_4	Pa
ΔP	Differential servo-valve pressure	Pa
Δp	Small changes in ΔP	Pa
ΔP_1	Change in pressure of pump 1	Pa
Q	General flow term	m^3/s
q	Small changes in servo valve flow	m^3/s
Q(in)	Flow into a valve	m^3/s
$\hat{Q}$(in)	Maximum flow into a valve	m^3/s
q(in)	Changes in Q(in)	m^3/s
Q(out)	Flow out of a valve	m^3/s
q(out)	Changes in Q(out)	m^3/s
Q_c	Compressibility flow	m^3/s
q_c	Small changes in Q_c	m^3/s
Q_{ccs}	Pump flow demanded by CCS controller subroutine	m^3/s
q_{fb}	Flow feed-back	m^3/s
Q_i	General flow term. i = 1 to 3 for pumps 1 to 3	m^3/s
Q_p	Pump flow	m^3/s
q_p	Small changes in Q_p	m^3/s
Q_{pc}	Pump flow demanded by pressure compensating controller subroutine	m^3/s
Q_s	Service flow	m^3/s
Q_v	Flow through the loading valve	m^3/s
q_v	Small changes in Q_v	m^3/s
$Q_{1\ to\ 3}$	General flow terms	m^3/s
R	Radius of CCS notch	m
r	Radius of follow-up servo metering holes	m

SYMBOL	DEFINITION	UNITS
r_z	Radius of the metering holes of the pressure compensating valve	m
R_1	Radius of CCS piston	m
r_2	Radius of metering hole (A8)	m
s	The Laplace operator	-
S_z	Spool length in the pressure compensating valve	m
T	Servo-valve time constant	s
t	Time	s
T_1 to s	Electrical compensating time constants	s
u	Position of metering area on CCS piston	m
v	Volume of oil constituting the least stable load	m^3
V_p	Volumetric displacement of the pump	m^3/rev
V_1	Volume of oil between the servo-valve and pump	m^3
Δv	Change in volume v	m^3
W	Travel of CCS directional control valve	m
X	Spool travel	m
x	Small changes in X	m
$\dot{X}$	Spool velocity	
$\dot{x}$	Small changes in $\dot{X}$	m/s
$\ddot{X}$	Spool acceleration	m/s^2
$\hat{X}$	Maximum spool travel	m
Y	Pump travel	m
y	Small changes in Y	m
$\dot{Y}$	Pump velocity	m/s
$\hat{Y}$	Maximum pump travel	m
y_d	Demanded pump position	m
y_{fb}	Pump position feedback	m

SYMBOL	DEFINITION	UNITS
Z	Pressure compensating valve spool travel	m
z	Small changes in Z	m
$\dot{Z}$	Pressure compensating valve spool velocity	m/s
$\dot{z}$	Small changes in $\dot{Z}$	m/s
$\ddot{Z}$	Pressure compensating valve spool acceleration	m/s^2
$\ddot{z}$	Small changes in $\ddot{Z}$	m/s^2
$\hat{\dot{Z}}$	Maximum pressure compensating valve spool velocity	m/s
α	Meter-in pressure flow gain of pressure compensating valve	$(m^3/s)/Pa$
α'	Meter-out pressure flow gain of pressure compensating valve	$(m^3/s)/Pa$
β	Bulk modulus of hydraulic oil	Pa
γ, γ_1 to $_4$	Dummy variables	
δ_1 to $_3$	Dummy variables	
θ	Angle of tapered flats on CCS piston	degrees
λ, λ_1 to $_7$	Dummy variables	
ϕ_1 to $_7$	Dummy variables	
μ, μ'	Dummy variables	
ρ	Density of hydraulic oil	Kg/m^3
ω	Angular speed	rad/s

CHAPTER 1

INTRODUCTION

This thesis describes the synthesis, simulation, design and development of controllers for a range of variable displacement hydraulic pumps. The work undertaken was for a particular firm and formed a fundamental part of its research and development effort. Consequently the Company expected results in normal industrial time scales.

The project has been made possible by the close co-operation between the University of Aston in Birmingham and Hamworthy Hydraulics Limited of Poole, through the Inter-Disciplinary Higher Degree (IHD) scheme.

The IHD scheme enables students to undertake industrial problems and use the resources of the University to help solve them. As a further back up for technology students, the scheme incorporates a series of lectures on such subjects as management, accountancy and innovation of technology, which provide a useful insight into industry and enables students to communicate more effectively with different people within their organisations.

Hamworthy approached Aston University in 1977 to discuss the possibility of recruiting a student to undertake one of two possible projects. These were a computer aided design program for control valves or the design of a series of pump controllers.

To explain how the choice of project was made it is necessary to give a brief history of Hamworthy Hydraulics Limited. The company originally bought the designs of hydraulic gear pumps and control valves from Hydreco, its sister company in the United States of America, just after the Second World War. Since then the market for these products has steadily expanded and Hamworthy has been contented to satisfy this demand. However, in the pump market, there is now a trend towards more complex equipment such as variable displacement piston pumps because of their higher efficiencies, longer working lives and potential energy saving modes of operation.

From this information, the relative importance of the two projects can be established. The computer aided design of control valves involved consolidating the experience within the company and presenting this information in a suite of programs. This would improve the company's competitiveness in the marketplace by reducing design costs and also by providing a more efficient design service. However the project on pump controllers involved working on the company's new product, a radial, variable displacement, piston pump. From the marketing information available this new pump would perhaps be the life blood of the company in the future and so the controller project was chosen, because of the pump's greater importance to the company's future profitability.

At the start of this project the radial pump was in its late stages of development and two control options had satisfactorily been designed and tested. However, a third variant proved to be unstable.

Looking at the project objectively it was clear that there were two questions to answer. Firstly, what control modes should be included and secondly, what form should the final "package" take? To determine an answer to the first of these questions a review of the control modes used in the mobile earth moving, crane, mining and marine markets was undertaken and the various options are described in Chapter 2. This chapter continues with a discussion on the requirements of the overall controller package, outlining how Hamworthy could establish its own "niche" in a very competitive market by offering a very wide selection of control options with its pump. Finally, these requirements are included in a design specification for the complete controller package.

Having decided upon the requirements of the controller package, two principle modes of solution were evident. The most obvious was to take the original controller design and expand it to meet the multi-function requirements of the specification. This had the advantage that a lot of experience in the

design and manufacture of hydro-mechanical equipment existed within Hamworthy and such a controller would easily fit into the organisation. Also, the end users of such equipment are familiar with this type of technology and hence there would be no market resistance.

However, the traditional hydro-mechanical solution would have several serious disadvantages due to the necessary complexity of such a package to meet the specification and these are:-

1. It would contain a large number of components requiring high capital investment in machine tools and a large amount of stock.
2. Assembly and test would be expensive.
3. A well organised team of specialists would be required to plan, organise and manage the production and assembly of the product.

An alternative design solution would be to use electro-hydraulics. A brief study into the different electronic approaches such as analogue, digital or hybrid, revealed that only the versatility of a micro-processor would satisfy all of the design requirements. The advantages of such a solution are:

1. The controller design would be very simple and thus require less capital investment.
2. The package would be extremely flexible and with sufficient programing back-up, could be made to operate in any reasonable control mode.
3. All controllers would be identical except for the program within the micro-processor. Thus the cost of the controllers would be low because mass production techniques could be used.
4. Due to the simpler design, the stock level would be low.
5. The assembly and test times would be relatively short and hence inexpensive.

The main disadvantage of this approach is the very high unit cost involved. It was estimated that the electro-hydraulic design would be some five times

more expensive than an equivalent hydro-mechanical solution. However, because of the advent of the micro-processor there could be a large demand for cheap electro-hydraulic servo-valves and transducers and that, if this was true, the price of an electro-hydraulic controller package could be much lower than anticipated.

At the outset of this project Hamworthy desperately required a controller package to meet its customer prototype requirements. It was therefore decided that the primary objective of this project was to design and develop a hydro-mechanical controller package and this work is described in Chapter 3. However, the advantages of the electro-hydraulic system were very attractive and it was decided to undertake a detailed feasibility study into the electro-hydraulic alternative which is given in Chapter 4.

The final chapter contains the conclusions for both types of controller and gives suggestions regarding the course of action Hamworthy should take in the near future.

CHAPTER 2

REVIEW OF CONTROL OPTIONS

2.1 INTRODUCTION

The information in this review has been obtained from several different sources. A great deal of it has come from conversations with people at Hamworthy and this has been supplemented by extracts from published papers, patent specifications and the advertising literature of other hydraulic pump manufacturers. This information has been collated and is presented under individual controller headings. In the final section the stratagem of the controller package is discussed and the types and combinations of controllers required are listed.

2.2 MANUAL

This is the simplest method of pump control and produces flow proportional to a demanded input. It can be achieved in many different ways. For example a purely mechanical design is given by STRICKLAND and is shown in Fig 2.1. This approach is perfectly adequate when the pump is accessible. However, in the majority of applications it is not and so remote forms have been developed.

The first of the "remote manual" controllers uses a hydraulic cylinder to alter the stroke of the pump. The pressure acting upon this actuator is controlled by a valve which is connected to the pump by hydraulic hoses. A schematic diagram of a typical system is given in Fig 2.2.

The second form of "remote manual" control utilises an electro-hydraulic servo valve as illustrated by CLARK and JOYAL. A schematic for such a controller is given in Fig 2.3. The main advantage of this form of remote control is that only electrical wires connect the potentiometer to the pump and so the two could be considerable distances apart. However, electro-hydraulic servo valves are very expensive and so the hydraulic remote manual controller is more commonly used in the mobile machinery, mining and marine markets.

2.3 CONSTANT POWER

This type of controller strives to ensure that the hydraulic pumps take the maximum amount of power from the prime mover. To understand the advantages of such a system compared with one using a gear pump, consider Fig 2.4. Here a variable displacement pump with a constant power controller and a gear pump are considered to be separately coupled to a prime mover and their respective pressure/flow characteristics plotted.

Before any conclusions can be drawn from Fig 2.4 the way in which the pump size was selected must be considered. To start with consider the gear pump. The maximum flow is proportional to the maximum speed of a particular service and the maximum pressure can be calculated by considering the peak forces associated with the system. Thus the power rating of the prime mover can be determined as the maximum product of pressure and flow (plus an allowance for efficiency). Coupling a variable displacement pump (maximum flow Q_2) with a constant power controller to the same engine enables the same maximum flow (Q_1) to be achieved at the same ultimate pressure P_1. It also allows the system to take a higher flow (Q_2) at lower pressures and hence effectively speed up the operation of the system by the extra flow ($Q_2 - Q_1$).

Another way of looking at the system when a pump is fitted with a constant power controller is to consider whether the maximum flow Q_1 is actually required at peak pressure P_1. If it is not and a lower flow of Q_3 is quite satisfactory (whilst Q_1 is still required at lower pressures) then it is possible to use a smaller prime mover, as indicated by the lower power curve on the diagram.

Thus the advantages are that, either the engine can be worked harder for a higher proportion of the system's working cycle and hence more useful work can be done, or a smaller motor (or diesel engine) can be fitted to save some capital expenditure. Whether any money will really be saved depends upon the required characteristic. This is due to the fact that the extra cost

of fitting a variable displacement pump, may exceed the savings associated with a smaller prime mover.

There are several different configurations for achieving this control mode. A very simple scheme is given by CLAAR, who approximates the constant power curve to a straight line for a single pump and by KNOELKER & MAZUR who demonstrates a more complex circuit to take into account two variable displacement piston pumps as well as an auxiliary gear pump.

However, both of the above systems are similar in operation to the design developed by Hamworthy prior to this study and so an account of how this operates will illustrate the general principle. A schematic of the Hamworthy power controller for a dual pump unit is shown in Fig 2.5. The basic operation of the controller is that as the pump pressures increase, the small pistons force the spools to move to the right, against their respective spring packs. As the spools move, the follow-up servos ensure that the stroking mechanisms of the pumps follow their movement and in this example, as the spools are moved to the right, the pumps are de-stroked. As the spools move further to the right, more springs in the packs are engaged and so their progress is increasingly hindered. A typical characteristic for such a controller is shown in Fig 2.6. It illustrates that the slope of the controller's characteristic increases as more springs are engaged. The controller developed by Hamworthy contains a total of five springs per pack, which guarantees that the error between the two curves is very small.

Another important feature of this design is that both controllers are identically set and so the flow from each pump is nominally the same. The reason for this feature is that often each pump supplies flow to one track of a hydrostatic drive. If the machine is to travel in a straight line, without too much operator correction , then naturally the flow from each pump must be very similar.

2.4 PRESSURE COMPENSATION

This controller, to a large extent, replaces the relief valve of a system. Such a controller destrokes the pump once a pre-set pump pressure has been exceeded, as shown in Fig 2.7(a). Hence, instead of destroying unwanted energy by operating a relief valve, the hydraulic pump simply refuses to take more power than the system services require. This point is illustrated by the pressure/power curve of Fig 2.7(b). The power used steadily rises as pressure rises (for constant flow) and rapidly decays once the cracking pressure of 145 bar has been exceeded. When the pressure is 175 bar, the pump is fully de-stroked and produces no flow.

Thus, such a controller directly contributes to saving energy and reducing running costs. Another less obvious advantage is that using such a system it may be possible to either use a smaller hydraulic oil cooler or eliminate the need for one altogether.

Another possible advantage of using a pressure compensating controller is that only a small relief valve is required to cater for transient pressure peaks. However, for safety reasons hydraulic circuits still tend to include a fully rated relief valve.

The design of pressure compensating controllers varies between manufacturers. However, they do tend to fall into two main categories, namely those which either incorporate a spool or a poppet valve as the active element in the circuit. For example, MEISEL and ERNST illustrate circuits with poppet valves, whereas BOULDEN, DREYMULLER, RUPPELT & SCHLINKE and CLICKMAN describe systems which use a spool valve.

The fundamental operation of all the above controllers however is very similar and as an example a schematic of the one given by MEISEL is shown in Fig 2.8. The relief valve is set to crack at the desired pump destroking pressure (P_c). Once this pressure is exceeded, flow passes through the relief valve to tank, via an orifice. This orifice creates a pressure (P_m) downstream

of the relief valve proportional to the square of the flow. This pressure (P_m) acts upon the actuator and destrokes the pump. The higher the pump pressure (P_1) is above the relief valve cracking pressure (P_c) then the more flow passes through the relief valve and orifice. The higher this flow, the greater the metered pressure (P_m) and hence the further the actuator destrokes the pump.

This concludes the description of the pressure compensating controller. However, it is often used in conjunction with other control modes and an example of this is illustrated in the next section.

2.5 CONSTANT POWER WITH PRESSURE COMPENSATION

These two controllers can be combined to give a characteristic shown in Fig 2.9. This controller behaves in an identical manner to the power controller described in Section 2.3 until the pressure (P_c) is attained. If the pressure rises above this value then a compensating network is activated which destrokes the pump. A detailed description of a typical system is given by CLAAR.

2.6 LOAD SENSING

The controllers described so far in this review have limited either the power or pressure of systems and so it is only natural that a controller capable of controlling the flow from the pump should be required. The advantage of fitting a load sensing controller to a pump is that only sufficient flow to satisfy the requirements of the load is produced. A very basic load sensing circuit is described by CLAAR. However, a more practical hydraulic circuit design is given in Fig 2.10 and is used by Hydreco. The system depends upon the directional control valve giving a signal to the pump demanding a particular flow. A detailed description of how the circuit in Fig 2.10 operates is given below.

1. When both directional control valves are initially closed pump pressure (P_1) rises. This pressure (P_1) acts upon the pump displacement controller and displaces it to the right. This increases the metered pressure (P_m) acting upon the pump stroke

actuator and destrokes the pump. Ideally this should represent no flow but the system must supply enough flow to raise a control pressure of up to 20 bar.

2. The fundamental operation of the circuit is to maintain the pressure drop across the directional control valve at a constant value, which is typically 15 bar. When a directional control valve is initially operated, there is no flow and hence no pressure drop across the spool. This upsets the hydro-static balance of the displacement control valve and the metered pressure (P_m) falls, thus increasing the flow from the pump. The flow continues to increase until the pressure drop across the spool is 15 bar and the controller then maintains this flow.

   If the opening of the directional control valve is now reduced, the pressure drop increases. This increases the metered pressure (P_m) and thus reduces the flow from the pump. This flow continues to fall until, again, the pressure drop equals 15 bar.

3. When a second directional control valve is opened some of the flow from the pump will be directed to this new load. The controller now operates by the principle of flow taking the path of least resistance. The lightest load attracts flow at the expense of the higher one. However, a series of check valves ensures that the service at the higher pressure is sensed by the displacement control valve. Thus the pump strives to fulfil the requirements of the greater load while the other service receives as much oil as it requires because it is the easier path. Thus the flow requirements of both services are fulfilled without any surplus being produced.

Another type of load sense controller is shown in Fig 2.11. This circuit was developed by Hydreco and is deemed Centre Core Sensing (CCS) as the

flow through the centre core of the valve casting is used to control the flow from the pump. The CCS circuit works as follows:-

1. If both directional control valves are unselected the flow passes through the sensing orifice. This orifice is fairly small and a large flow creates a high metered load sense pressure (P_m). Once this pressure (P_m) exceeds a nominal 20 bar the pump actuator is fully extended and the pump is in a minimum flow condition.

2. If one of the directional control valves is selected the flow is divided between the sense line and the service. As the sense line flow drops, the load sense pressure falls and the pump actuator retracts increasing the flow from the pump. Thus the flow demanded by the directional control valve is met.

3. When the second directional control valve is selected the flow through the sensing orifice falls and again the sensing pressure (P_m) is reduced. This is sensed by the actuator and the pump is increased to fulfil this higher demanded flow rate.

The two methods of achieving load sensing mentioned above describe the operation of most commercially available circuits. However, regardless of which method is adopted they both have the same energy saving potential. Consider an idealised flow/displacement characteristic for a directional control valve where flow is proportional to spool travel. If such a valve is connected to a constant displacement pump then the flow not taken by the service is dumped to tank. However, all the flow produced is at the pressure required to move the load and the power wasted is therefore the product of the dumped flow and the pump pressure. This power saving is shown in Fig 2.12 against travel of the directional control valve. However, in practice some flow is required to operate the load sense circuit and the power saved by replacing a gear pump with a variable displacement pump with a load sensing controller is slightly less

than at first imagined and this is also shown in Fig 2.12.

This saving shown in Fig 2.12 varies with the flow to the service. For instance, for high flows the saving is small, whereas at low load flows it is very significant. The total amount of energy saved therefore depends upon the working cycle of the service. If for example the working cycle is as described in Fig 2.13 then a load sensing system will save some 50% of the energy used by a conventional circuit. Alternatively if the working cycle is closer to that illustrated in Fig 2.14 then only 25% of the energy will be saved.

It is therefore difficult to determine the actual energy saved by an individual machine fitted with a load sensing system, but as indicated above, the potential is large. This saving can be still further increased by adding a pressure compensating controller to the pump. These two energy saving devices together ensure that all of the power taken by the hydraulics does useful work with the exception of the small amount of power used by the controllers. Such a system would therefore reduce running costs to an absolute minimum. Also the extra cost of installing a piston pump, rather than a gear pump, could probably be offset by not having to fit an oil cooler to the machine.

2.7 CONSTANT FLOW

This control option has already been described in the previous section on load sensing. The system shown in Fig 2.10 uses the same concept for controlling flow as does the constant flow controller described by RUPPELT & SCHLINKE and illustrated in Fig 2.15 except that the spool valve has been replaced by an orifice. The pump controller maintains a set pressure drop across this orifice thus ensuring that, for a particular orifice area, the flow remains constant.

2.8 CONSTANT ENGINE SPEED

This type of controller is primarily used on diesel engines and it operates by changing the stroke of the pump to keep the engine speed constant. In practice the speed of the engine may vary slightly but it can be maintained to

within 5% of the optimum speed setting for maximum power. The engine therefore produces virtually a constant power output for the majority of operating conditions. Typical diesel engine torque/speed and power/speed characteristics are shown in Fig 2.16. The speeds N_1 and N_2 represent the desired control band for the engine to maintain the power of the engine to within 5% of maximum. The area on the diagram to the right of speed N_3 represents the speed range controlled by the governor on the diesel engine. In order to eliminate any interaction between the two controllers and also to ensure that the governor is demanding full fuel to the engine, the pump controller speed band must not overlap this area. Hence N_1 is just less than N_3.

Speed sensing has many advantages over the previous type of "constant power controller", described in Section 2.3 namely:-

1. Sensing the speed of the engine will take into account any combinations of hydraulic pumps, whereas on a "power controller" all of the pumps should be variable capacity and the design described operates at its best when all pumps have the same volumetric displacement.
2. As the diesel engine wears it will tend to give less power. A speed sensing controller would automatically account for this, but the other type of "power controller" would still demand the power produced by a new unit. This could lead to the engine continually stalling.
3. The design of such a controller is much simpler than the "constant power" equivalent and hence cheaper to manufacture.
4. A speed sense controller is far quicker to set and therefore still less cost is involved in its production.

A schematic diagram of how Linde achieve this form of control is given by KNOELKER & MAZUR. For convenience a copy of this circuit is shown in Fig 2.17 and its operation is as follows.

The servo pump produces a flow proportional to speed. This flow passes through the sensing orifice and creates a pressure drop across it. The controller strives to maintain this pressure drop constant at 2 bar. If the load on the engine increases then the speed falls. This change in speed results in a drop in flow through the orifice and hence the pressure drop across it is also reduced. A very sensitive control valve senses this pressure change and directs flow to the controller which destrokes the pump. This change in stroke reduces the torque on the engine and hence the engine speed increases to maintain the status quo. Similarly if the engine load decreases then the engine speeds up but the controller counteracts this by increasing the pump stroke and hence increasing torque on the engine.

This system works when the throttle is set to demand maximum speed. If the engine is throttled back, then this is sensed as a very high load and the hydraulic pumps are destroked. This is not a satisfactory situation and it is overcome by a linkage connecting the throttle to the sensing orifice. If the engine is now throttled back the orifice area is reduced and thus a smaller flow can maintain the required differential pressure of 2 bar. The controller can then function normally about this lower speed setting.

2.9 THE STRATEGEM FOR THE HAMWORTHY CONTROLLER PACKAGE

Hamworthy is to sell this new pump in a well established market. Technically the pump has few advantages over the competition therefore, in order to attract new business, it must offer potential customers either a lower price or some other advantage.

Lower price is very difficult to achieve initially as Hamworthy will be producing far fewer pumps than its competitors and cannot therefore benefit from the lower unit costs associated with large quantity production.

However, from discussions with potential customers and such articles highlighting the cost of wasting power by YEAPLE, BOULDEN and YOUNG, it was evident that there was a definite market movement towards more

sophisticated pump control with energy saving as one of the prime motivators of this trend. It was realised that this was an area in which Hamworthy could offer a new advantage to their customers by producing a controller package which incorporated all of the most popular control options.

The disadvantage of this approach is that the cost of a simple controller is high compared with the competition. However, if the customer requires a complex combination of controllers, which only Hamworthy can supply, then the pump can command a prime price to cover the higher unit cost.

From the review of the controllers the following four options were regarded as the most favourable to form a basis for the package:manual, constant power (as described in Section 2.3), pressure compensation and CCS.

Load sensing was not adopted because of problems associated with cavitation when the system is used to control overhauling loads.

The "constant power" controller was included instead of speed sensing because of problems related to the life of the diesel engine. When pumps with such controllers were initially fitted, due to their exacting nature, the life of the diesel engines was dramatically reduced. In defence of their products the engine manufacturers started to quote two power levels for their engines. One for intermittent use and a lower one for constant power applications. With the constant "power controller" the hydraulic pumps can be set to the lower level (for constant power) and auxiliary services which are not continuously in use are permitted to raise the power taken from the engine to the higher, intermittent rating. However, when hydraulic pumps are fitted with speed sensing controllers they always take the maximum power available. The only way to achieve a reasonable engine life is to derate the governor. This ensures that the engine cannot produce more power than that quoted for constant power applications. Unfortunately this results in the loss of capability to use the intermittent rating for short periods. This is a considerable disadvantage as, for example, Perkins quote an intermittent level of 100.7 KW for their turbo

charged T6.354 engine and a constant power level of only 83.6 KW. Thus with a speed sensing controller the 17.1 KW difference cannot be used thus negating the advantage of using such a controller.

Returning to the discussion on control option selection, Hamworthy had received requests for combinations of manual, constant power and pressure compensation. It therefore seemed reasonable to include combinations of any three of these in the package. Similarly with CCS, constant power and pressure compensation, these form another very useful and versatile combination.

With respect to the manual and CCS control modes, the CCS controller supersedes the manual option and so it was decided that the combination of all four control modes was not required.

The final list of control variants and combinations is listed below and it was believed that this would form one of the most universal pump controllers on the market:-

1. Manual Control
2. Constant Power
3. Pressure Compensation
4. CCS
5. CCS + Pressure Compensation + Constant Power
6. CCS + Pressure Compensation + Manual Control
7. CCS + Pressure Compensation
8. Pressure Compensation + Constant Power + Manual Control
9. Pressure Compensation + Constant Power
10. Pressure Compensation + Manual Control
11. Constant Power + Manual Control

These control options have been included in a design specification for the controller which is given in Appendix A1. It includes the detailed requirements for each option and states the working limits and conditions for the package.

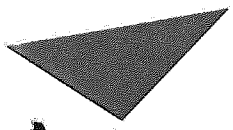

Aston University

Content has been removed for copyright reasons

Fig 2.1 MANUAL DISPLACEMENT CONTROL OF A RADIAL PISTON PUMP BY STRICKLAND

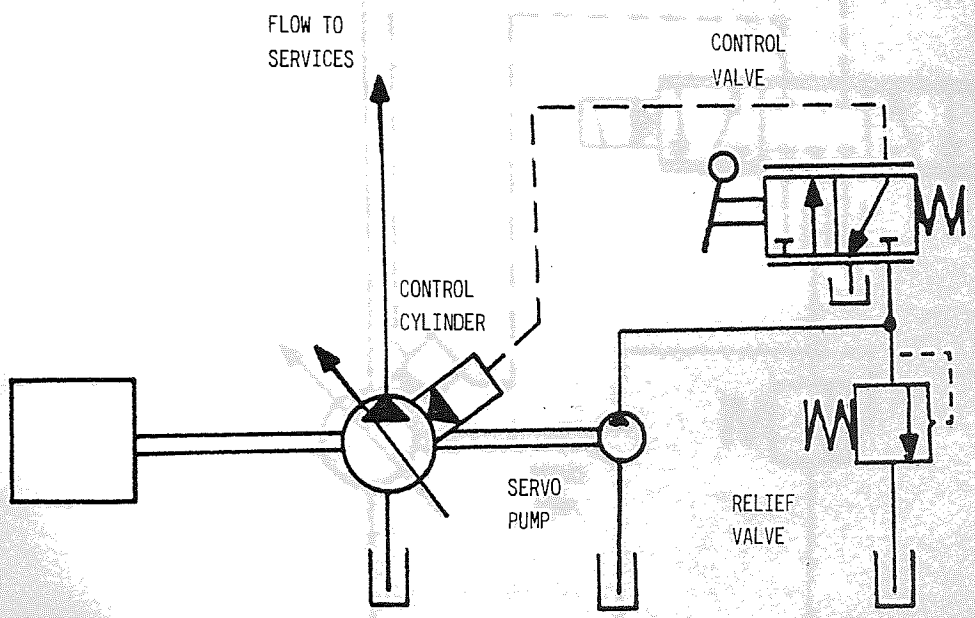

Fig 2.2 SCHEMATIC DIAGRAM OF A REMOTE HYDRAULIC MANUAL CONTROLLER

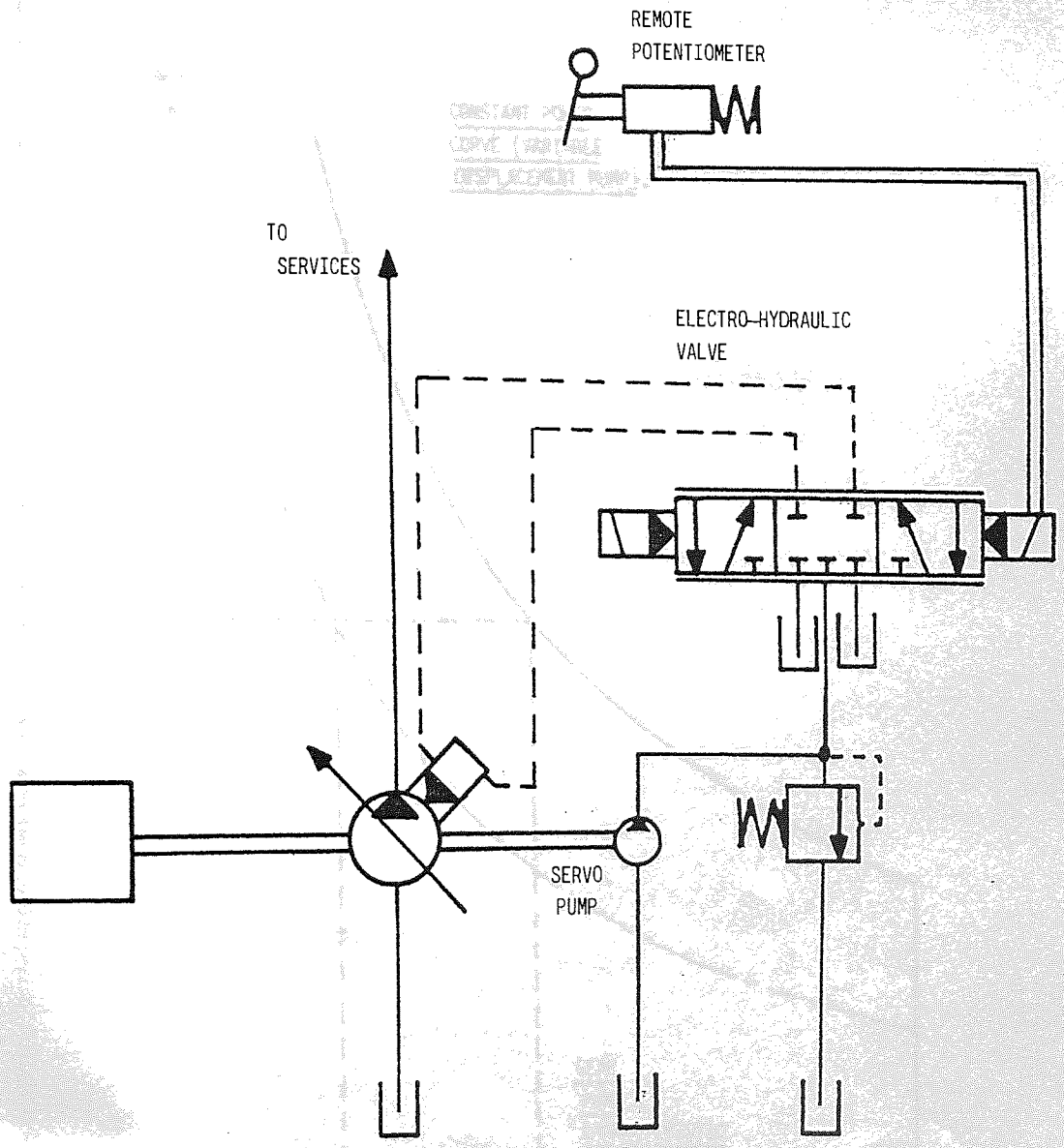

Fig 2.3 SCHEMATIC DIAGRAM OF A REMOTE ELECTRO-HYDRAULIC CONTROLLER

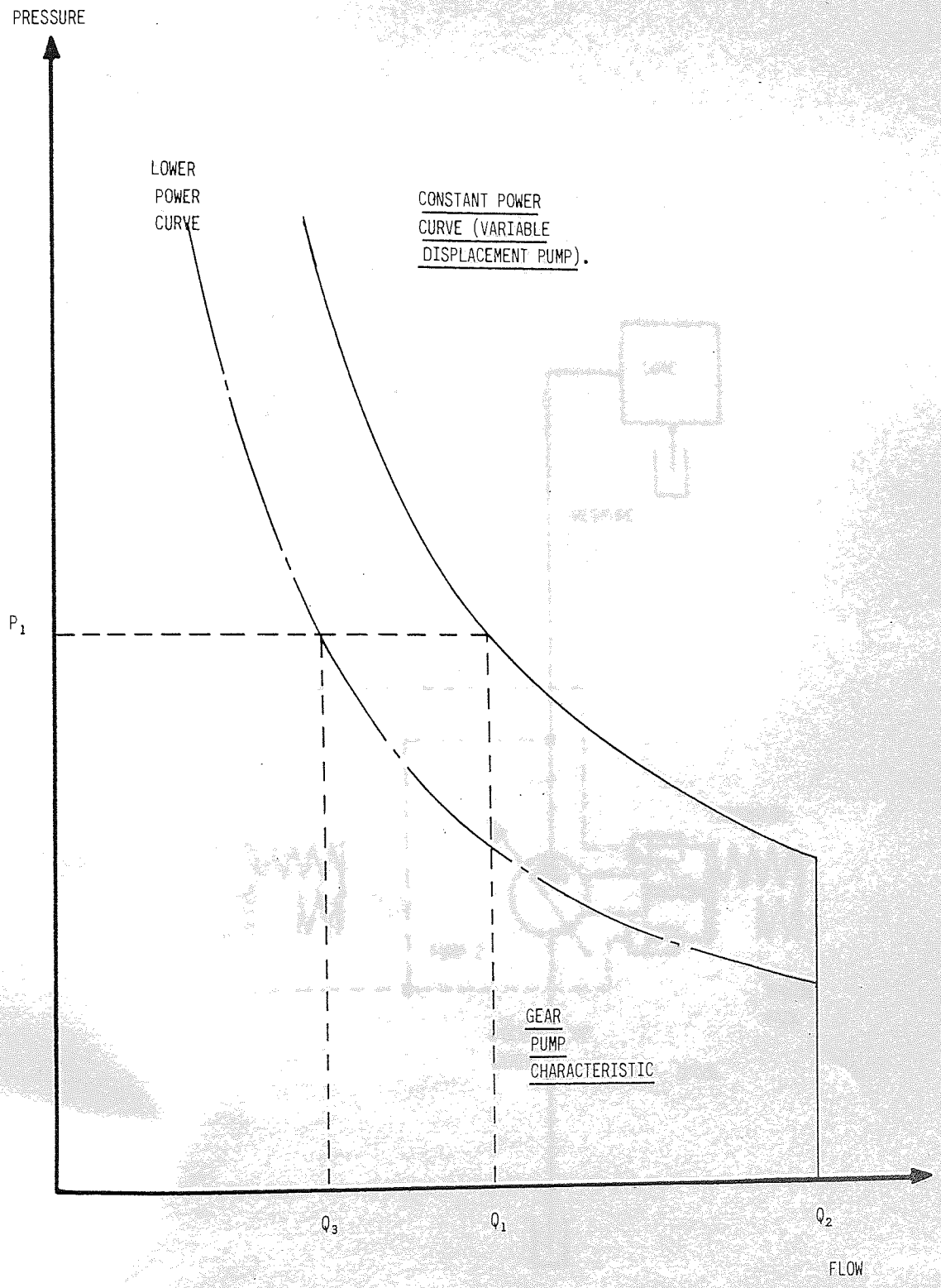

Fig 2.4 COMPARISON OF PRESSURE/FLOW CHARACTERISTICS FOR A VARIABLE DISPLACEMENT PUMP WITH A CONSTANT POWER CONTROLLER WITH A GEAR PUMP

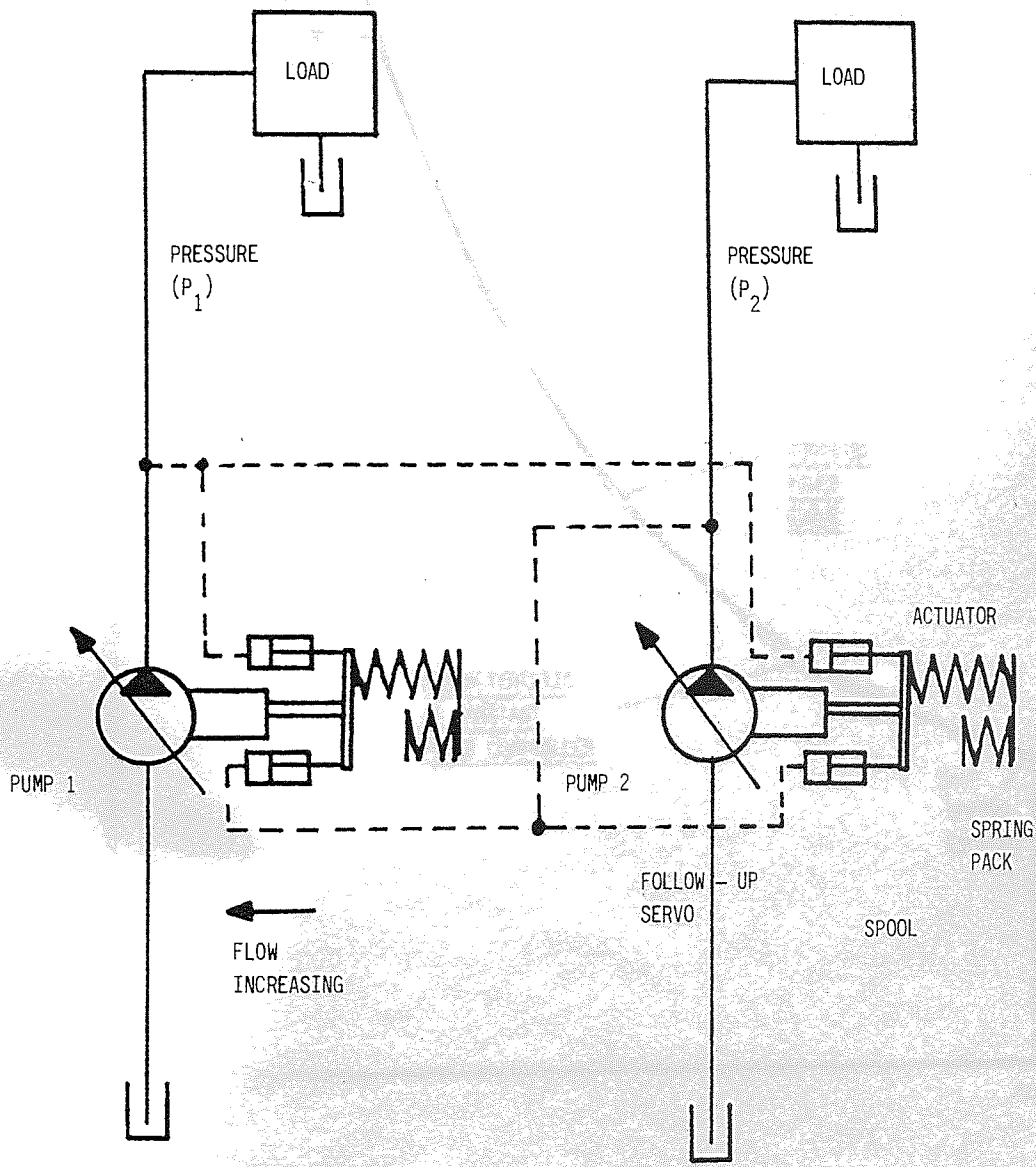

Fig 2.5 SCHEMATIC DIAGRAM OF THE HAMWORTHY POWER CONTROLLER FOR A DUAL PUMP

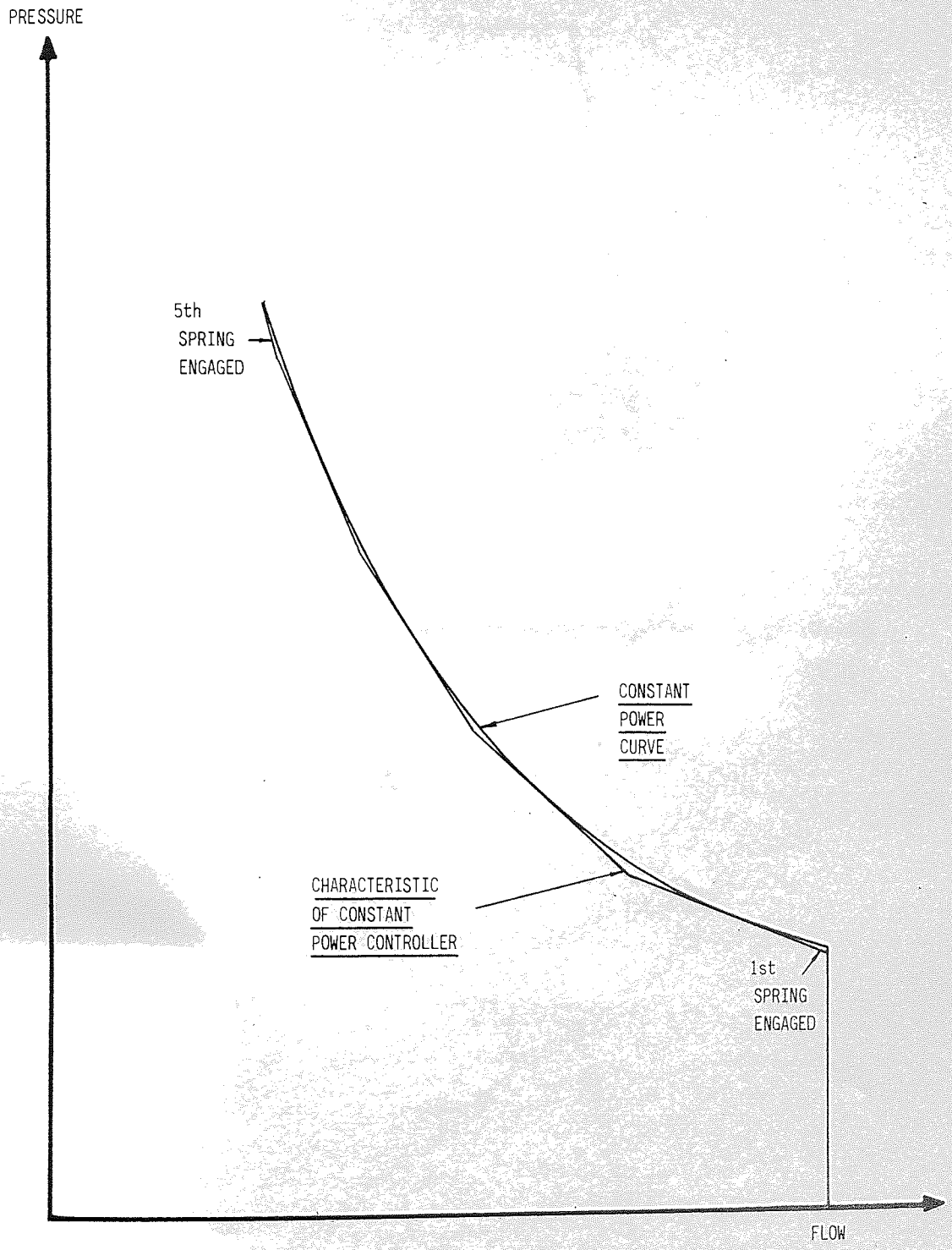

Fig 2.6 A CONSTANT POWER CURVE AND THE APPROXIMATION TO IT OF A CONSTANT POWER CONTROLLER

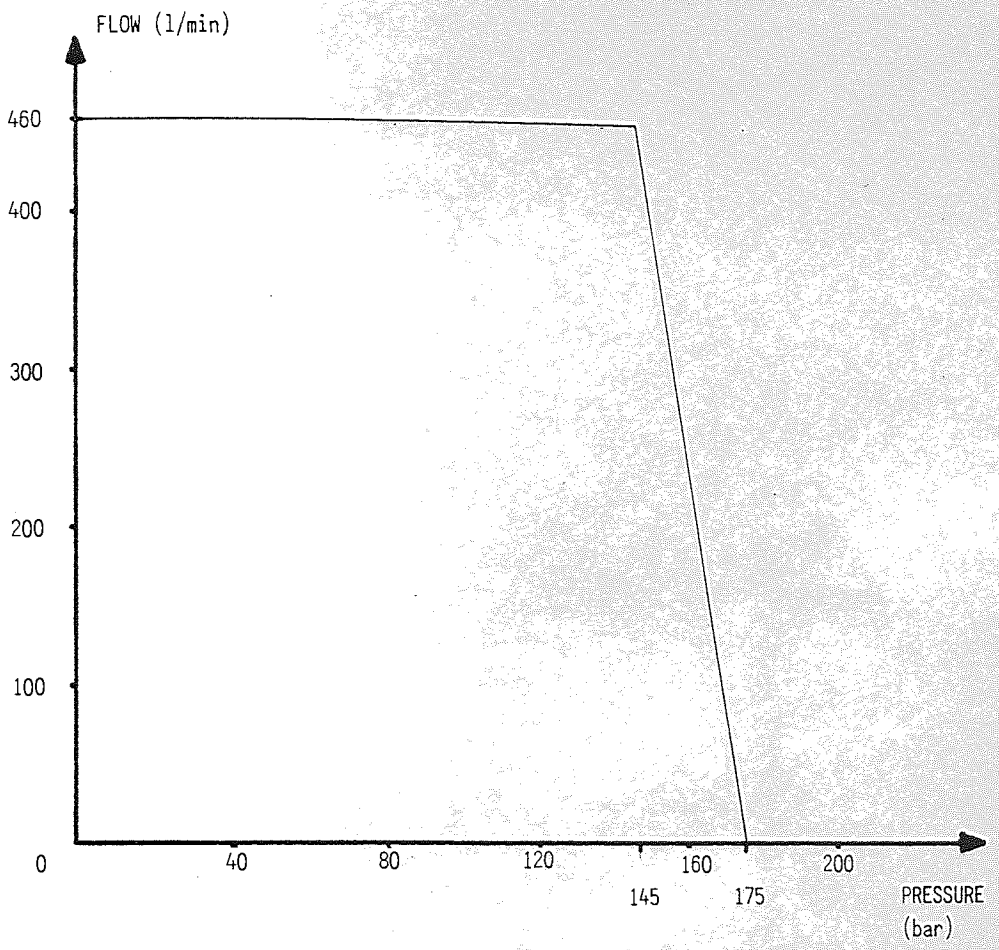

(a) PRESSURE/FLOW

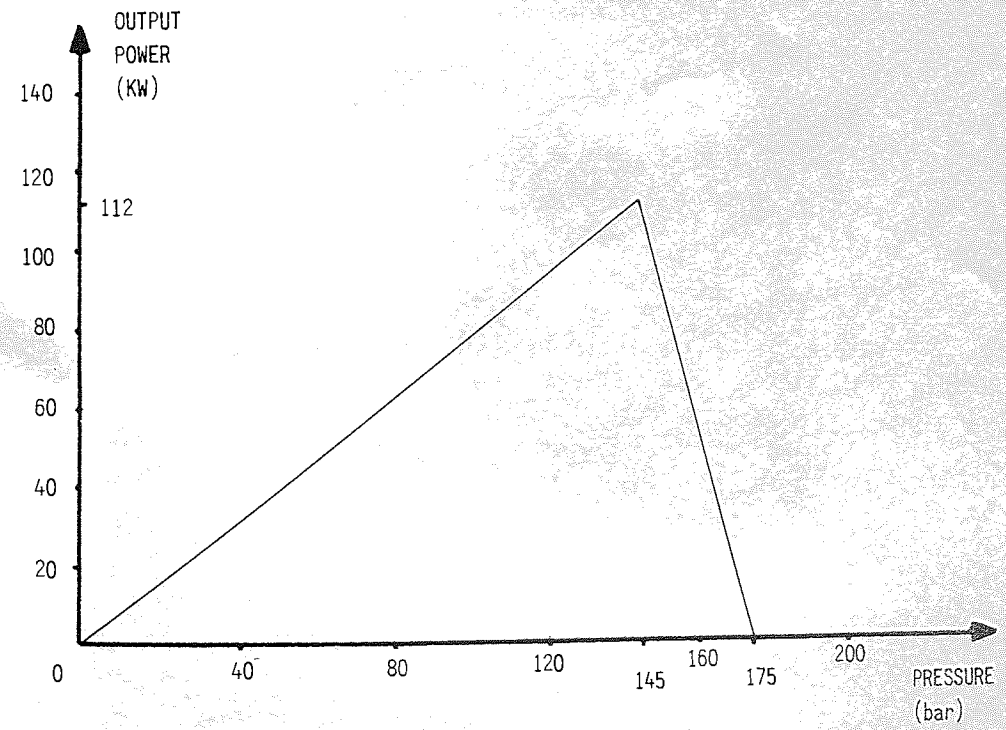

(b) PRESSURE/POWER

Fig 2.7 TYPICAL PRESSURE COMPENSATING CHARACTERISTICS FROM CATERPILLAR

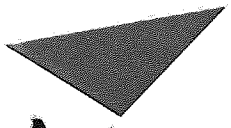

Aston University

Content has been removed for copyright reasons

Fig 2.8 PRESSURE COMPENSATING NETWORK PRESENTED BY MEISEL

Aston University

Content has been removed for copyright reasons

Fig 2.9 CONSTANT POWER CONTROL WITH PRESSURE COMPENSATION OVERRIDE - EXTRACT FROM CLAAR

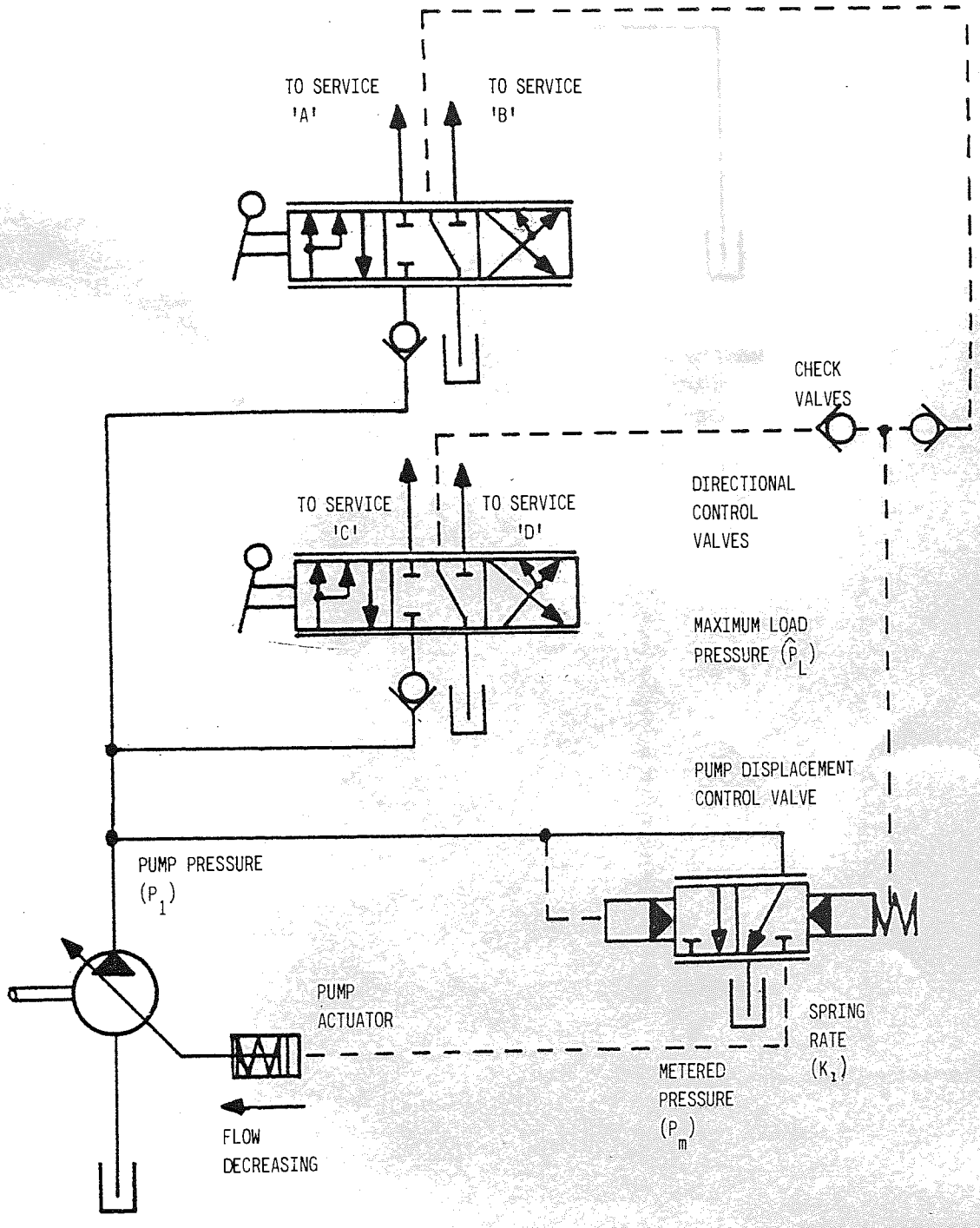

Fig 2.10 HYDRECO LOAD SENSING CIRCUIT

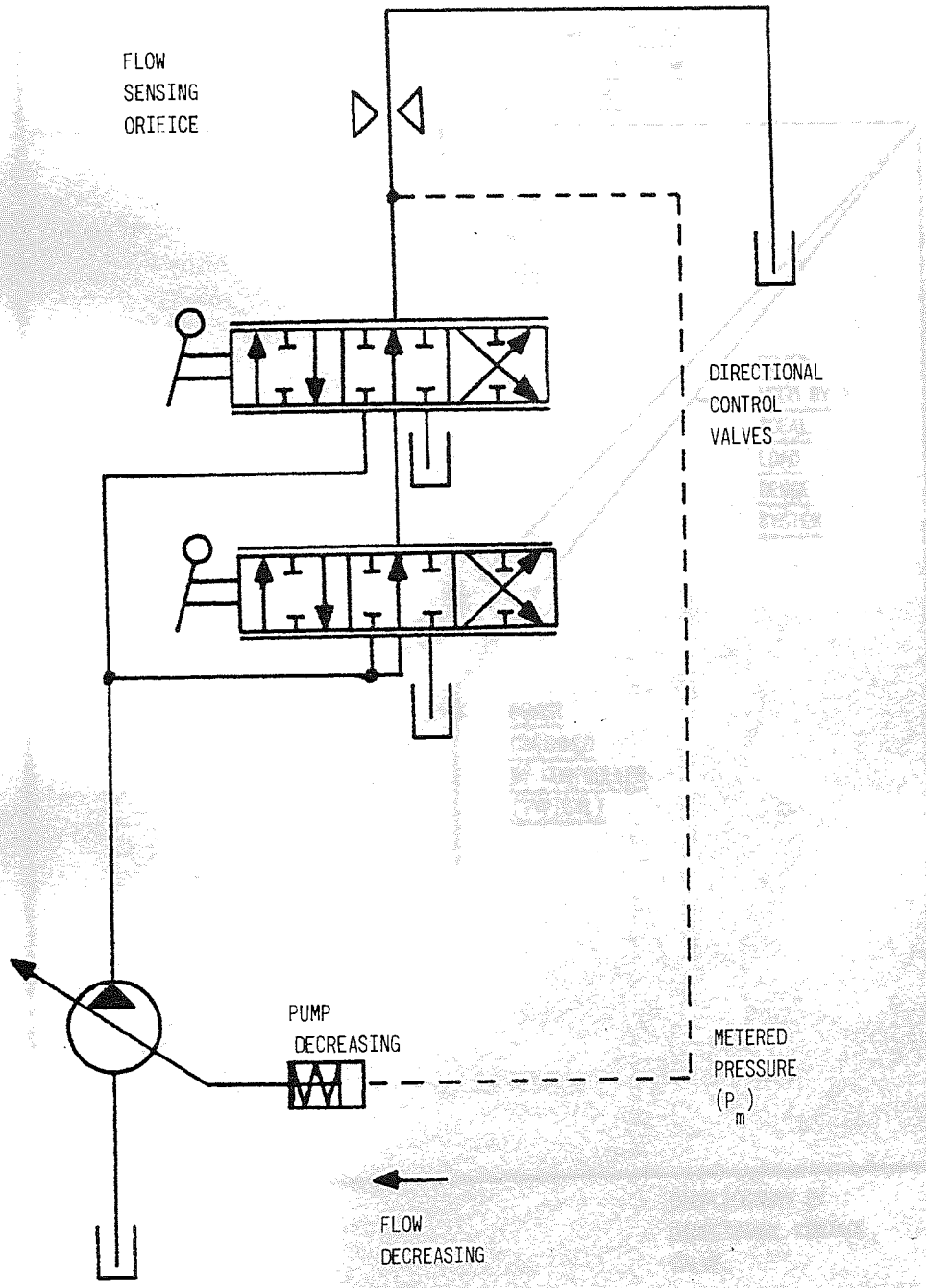

Fig 2.11 HYDRECO CENTRE CORE SENSING (CCS) CIRCUIT

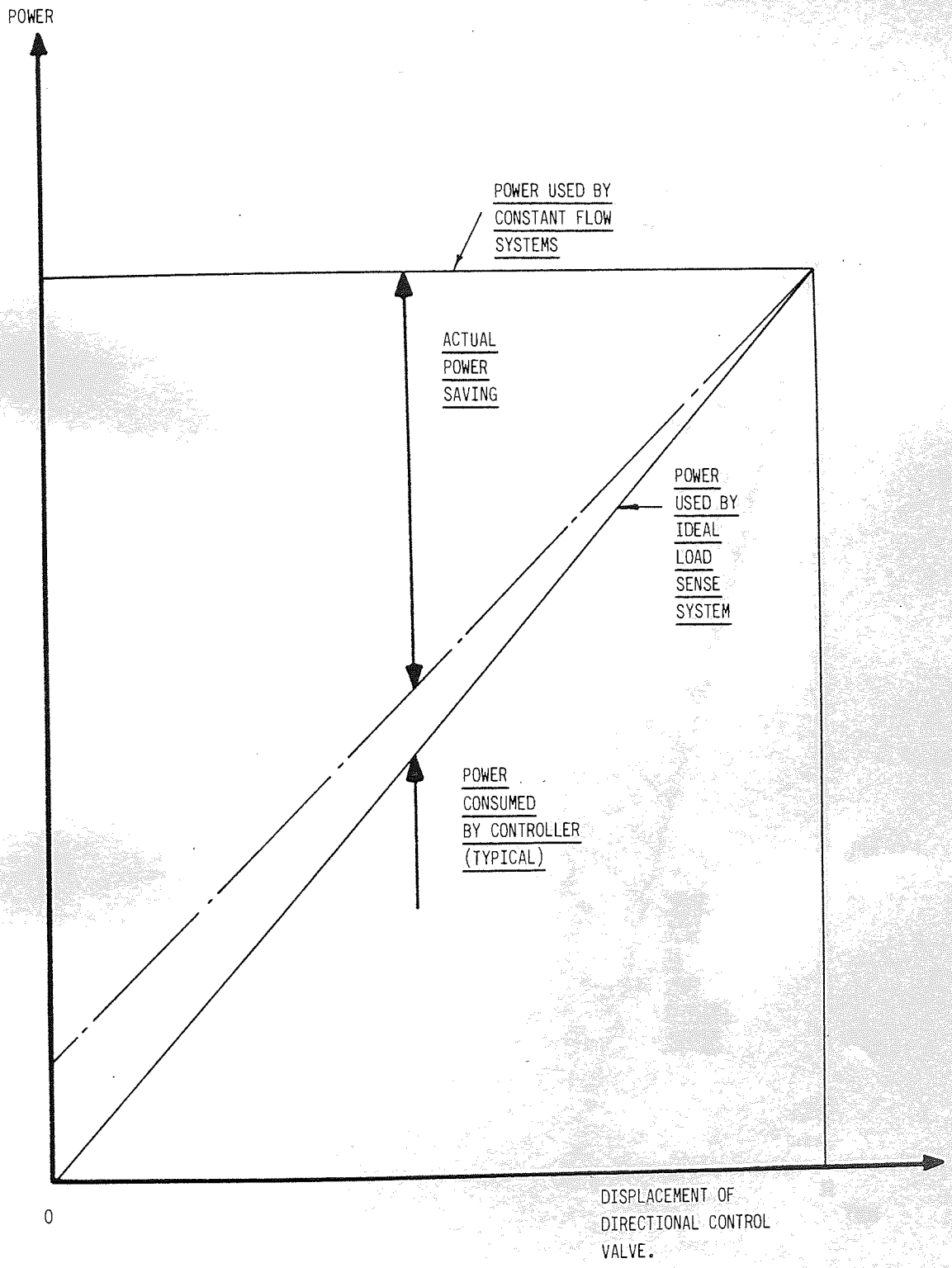

Fig 2.12 POWER SAVING POTENTIAL OF A LOAD SENSING CONTROL SYSTEM

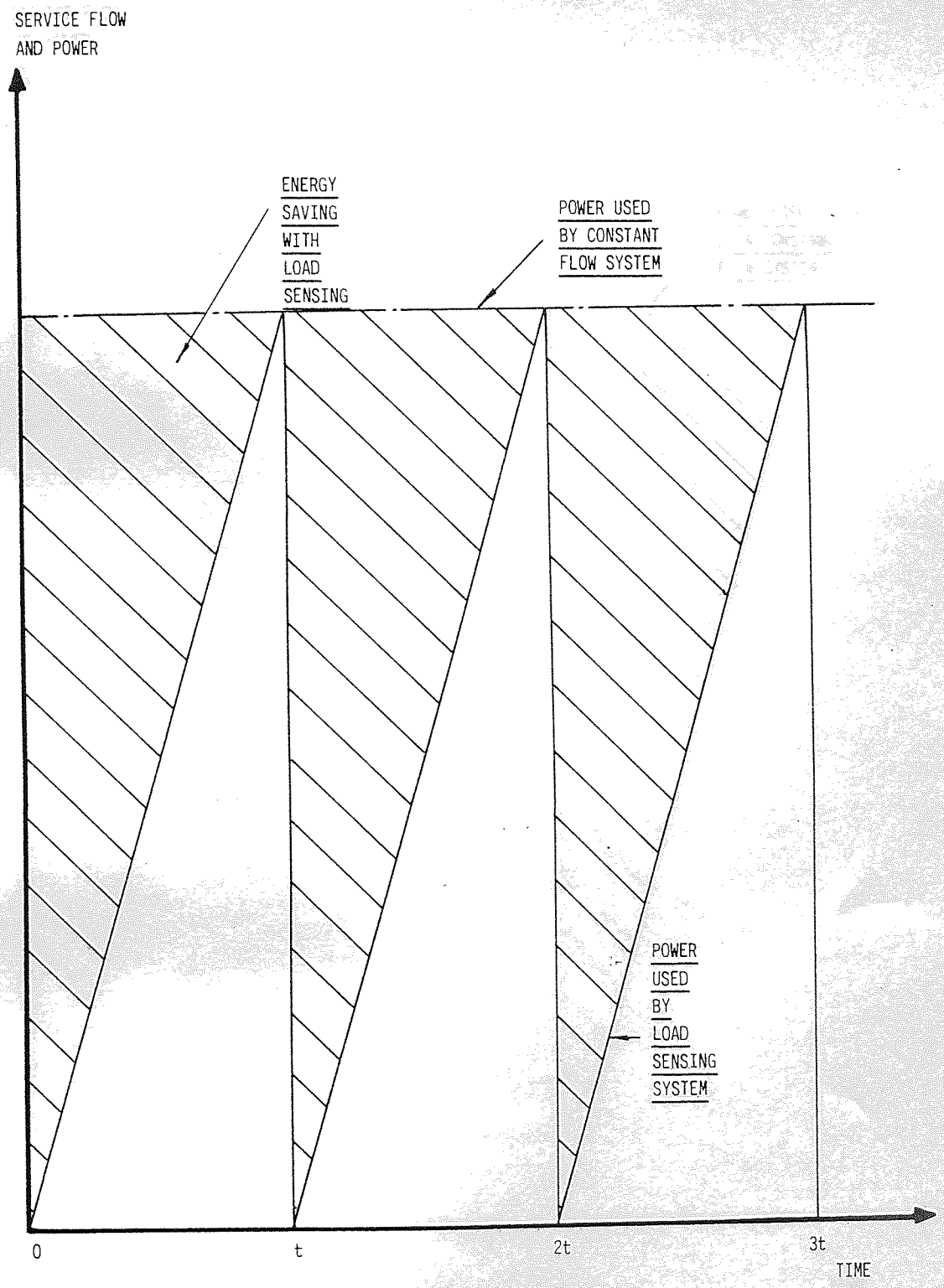

Fig 2.13 ENERGY SAVING POTENTIAL OF LOAD SENSING WITH LOADING CYCLE NUMBER 1 (CONSTANT PRESSURE AND SPEED)

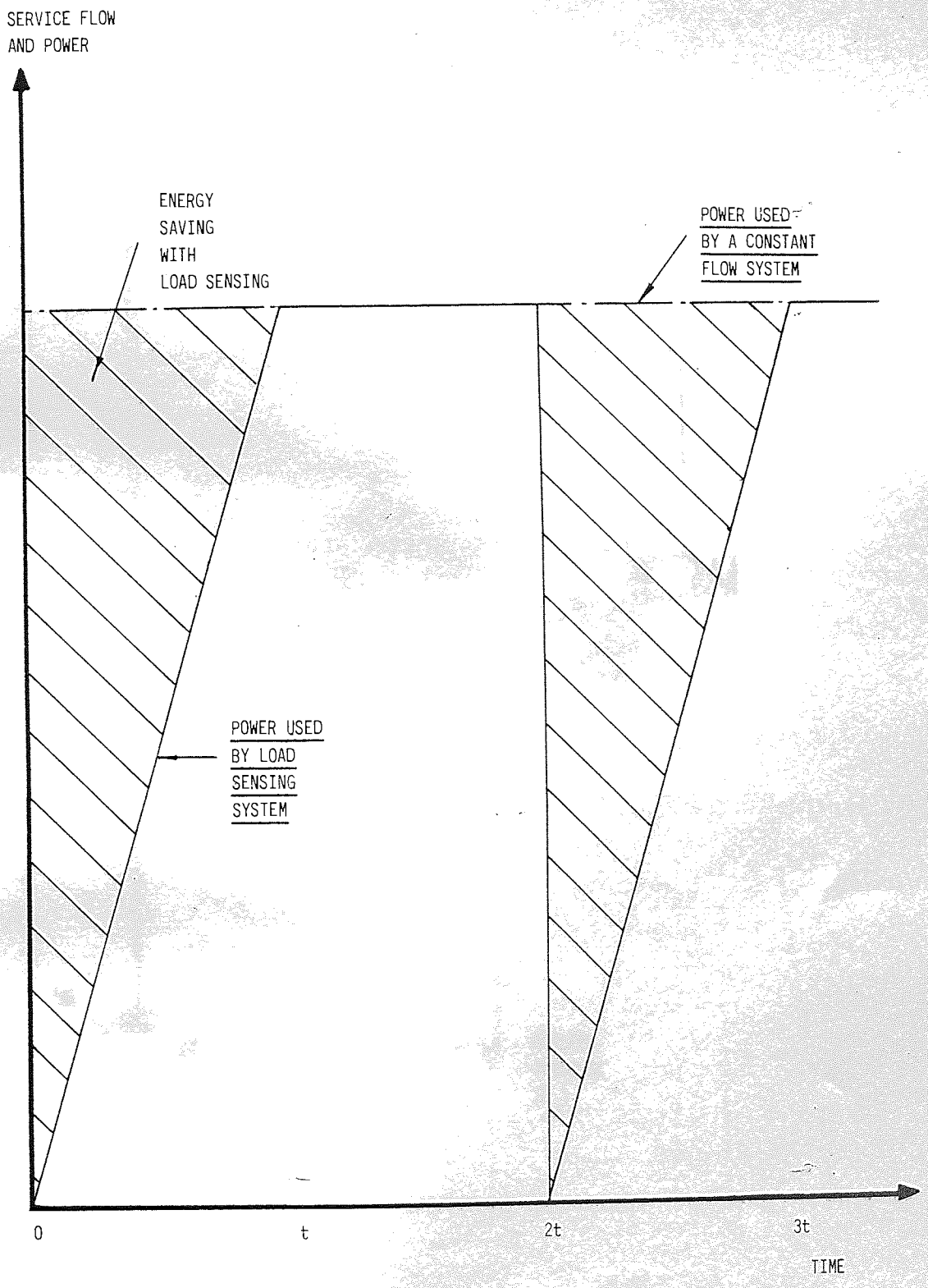

Fig 2.14 ENERGY SAVING POTENTIAL OF LOAD SENSING WITH LOADING CYCLE NUMBER 2 (CONSTANT PRESSURE AND SPEED)

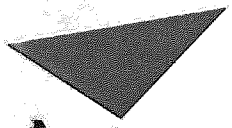

Aston University

Content has been removed for copyright reasons

Fig 2.15 FLOW CONTROL SYSTEM GIVEN BY RUPPELT AND SCHLINKE

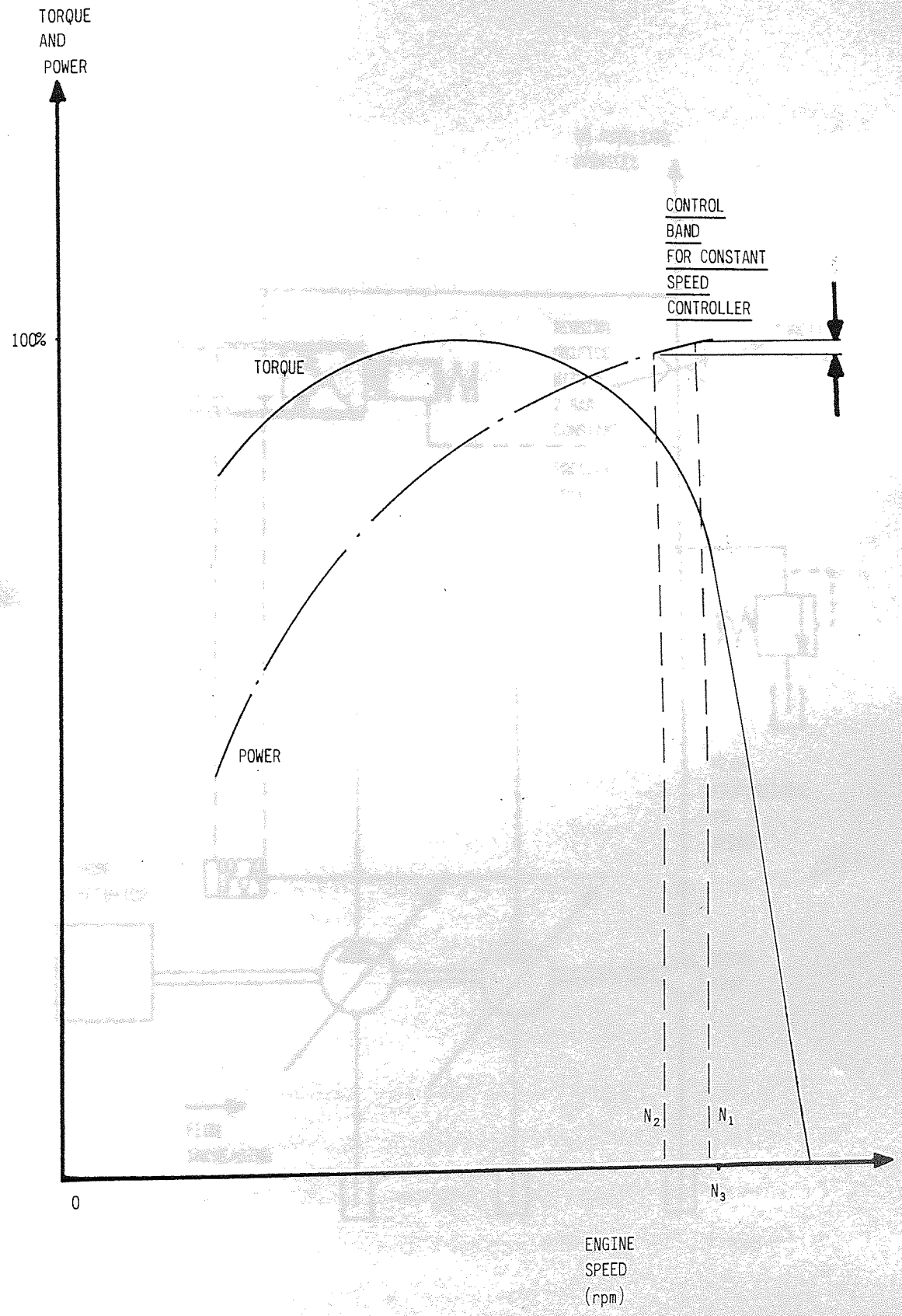

Fig 2.16 TYPICAL TORQUE/SPEED AND POWER/SPEED CHARACTERISTICS OF A DIESEL ENGINE

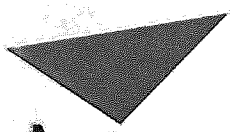

Aston University

Content has been removed for copyright reasons

Fig 2.17 SPEED SENSING POWER CONTROLLER AS PROPOSED BY KNOELKER AND MAZUR

CHAPTER 3

THE REALISATION OF THE HYDRO-MECHANICAL CONTROLLER PACKAGE

3.1 INTRODUCTION

Prior to this study Hamworthy had successfully designed and developed constant power and manual controllers but a design for a pressure compensating network proved to be extremely unstable.

From the results of this pressure compensating circuit it was clear that mathematical models of systems were going to be required to predict their stability. A study was made to find a suitable modelling method which resulted in the use of the small pertabation technique and frequency domain analysis. The accuracy of this method was proven by comparing results with known stable and unstable systems.

Once the accuracy of the modelling technique had been determined a design programme for the controller package was formulated. It was decided that the first priority was to use the mathematical modelling technique to produce a stable pressure compensating system. If necessary this could then be supplied to customers on a prototype basis in the short term, whilst a more comprehensive investigation could be made into the design of the overall package.

From the results of the model of the pressure compensating controller it was realised that such a network was difficult to stabilize. Eventually a design was found which was theoretically acceptable and so a prototype was manufactured and tested. After considerable development the network functioned correctly, but it had a poor response time and was expensive to produce. It could however fulfil the short term objectives of the project and so attention was then focused upon the CCS system and the overall package.

Before the package could be designed it was necessary to adapt the CCS controller to the Hamworthy pump. Although Hydreco had devised the idea, their prototypes suffered from hunting in the stand-by condition. A

mathematical model of the CCS controller coupled to the Hamworthy pump was made and confirmed that this design would also hunt. Using the model to theoretically test the effect of various damping orifices and piston areas, a suitable combination was determined which limited the magnitude of the oscillation to an acceptable level.

To bring all of the required control modes into one package proved to be quite a challenge. The design specification given in Appendix A1 required that it should be capable of controlling the pump in up to three different control modes simultaneously. In practice this meant that each of the control modes should be active but only the one demanding the lowest flow should actually control the stroke of the pump. After much thought two ways of achieving this were devised. Firstly each control mode could have a spool valve and the metered pressure of each valve would be inversely proportional to the demanded flow. A series of check valves could then be used to direct the highest pressure (lowest demanded flow) to a destroking piston acting upon the pump. This idea was very attractive because the package could comprise of modular units which could be stacked together as required. However, from the work on the pressure compensating networks it was realised that such spool valves introduce considerable phase lags which would probably lead to severe stability problems. The second idea for the package involved the control modes acting directly upon the pump stroking device and thus eliminating the need for the extra spool valves. This latter idea had been used for the original model of the CCS controller and it proved that this control mode was only just acceptable without an auxiliary spool valve. The introduction of such a valve to the CCS controller could make it virtually impossible to stabilize. This concept of direct acting controllers was therefore adopted for the constant power, manual and CCS controllers. However, the pressure compensating controller remained indirect.

A controller package was then manufactured and tested. With some

modifications the power and manual controllers worked well. The CCS controller was stable, but its metering characteristics were very poor. Basically the CCS controller was a direct adaptation of the Hydreco system and their claims for it had been accepted. However, when a Hydreco CCS system was tested at Hamworthy it also had poor metering characteristics and was affected by changes in load pressure. As it stood the CCS system was not particularly marketable. Hydreco suggested a modification to the CCS de-stroking piston which improved the system slightly but did not affect the sensitivity of the system to pressure. It was clear that some effort was required to improve the performance of the controller and so a mathematical model was made to predict its metering characteristics. To eliminate the pressure dependence of the system several networks were devised and tested using the model. One such network proved to be very effective and was subsequently tested on the controller. It behaved as predicted and virtually eliminated its pressure dependence. Once the system was independent of pressure, it was a relatively easy task to extend the metering range of the controller by various de-stroking piston designs.

At this stage the controller package had been fully developed and worked well. The only reservation about it was the cost and poor response of the pressure compensating network. Traditionally, pressure compensating networks are indirect because of the difficulty associated with designing a spring for a direct acting system. A breakthrough in this concept was to use a hydraulic pre-load. The design of the CCS controller leant itself to this concept and so a series of development tests were performed on direct acting pressure compensating networks. The result of this work was most rewarding. A new compensating system was devised which outperformed the previous design and was only one third of its cost.

After the work on the new pressure compensating network and CCS systems, the original controller required updating. These modifications were

then incorporated into a pre-production design.

3.2 THE DEVELOPMENT OF A SUITABLE MATHEMATICAL MODELLING TECHNIQUE

An investigation into which mathematical method to use revealed that there were two alternative approaches. Firstly a time domain technique from which the behaviour of the individual components of the system could be determined in response to different excitation signals and hence the stability of the system could be deduced. The alternative, described by BLACKBURN[1] et.al, was to use frequency domain analysis and to linearise the system equations. Of these the second method was favoured because the time involved in model building and computation was estimated to be only half of that associated with the time domain approach.

Having selected a mathematical technique it was necessary to prove its accuracy. It had been noticed that if the Hamworthy power controller was incorrectly set then under certain conditions it would be unstable. The exact conditions under which this occurred were noted and a model of the system was devised which is fully documented in Appendix A2. These operating conditions were then used in the model with the exception of the dynamic damping coefficient for the main spool running in the seal collar. By considering the viscous drag between these two components this was calculated to have a value of between 2 and 10 N/(m/s) and so a nominal, mid-way valve of 7 N/(m/s) was used in the model. The results from the model are shown on a Nyquist chart in Fig 3.1. The first curve is for when the controller was incorrectly set and the second locus represents the results from the model when it simulated the system with the correct controller setting. The Nyquist stability criterion states that if a curve passes to the right of the "-1" point then the system is stable. Applying this to the two curves resulted in the model correctly predicting the state of both systems.

The modelling technique was in error regarding the resonant frequency.

It predicted an oscillation at 44 Hz but in practice it was only about 6 Hz. FOSTER reported a similar experience when comparing the actual and predicted resonant frequencies for a relief valve. His explanation was that the valve was saturating and hence it lost its hydraulic stiffness. Thus the natural frequency of the spool was dependent solely upon a light spring. The same explanation is applicable to the follow-up servo of the controller. At resonance the relative displacement between the spool and piston will become large and the metering holes will be either fully open or closed. This will adversely effect the hydraulic stiffness of the follow-up servo and hence the natural frequency of the control ring. With no hydraulic stiffness and just the stroking spring, the natural frequency of the pump can be calculated to be 6.2 Hz. Thus the small pertabation technique accurately predicted the state of the system but it could not be expected to determine its resonant frequency. However, it was concluded that this would be adequate as a design tool as the resonant frequency was of no real interest whilst the system remained stable.

As a further test for the technique the model of the constant power controller was extended to include the unstable pressure compensating network. The details of this new model are given in Appendix A3. Inserting the unstable operating conditions into the model resulted in the Nyquist plot shown in Fig 3.2. This correctly shows that as pressure increases, the pump is destroked and the system becomes progressively more unstable.

These two test cases gave a reasonable amount of confidence in the accuracy of the modelling technique and so it was decided to use it at the design stage as a tool to investigate system stability. Its first application was in the search for a stable pressure compensating design, the details of which are included in the next section.

3.3 THE DESIGN AND DEVELOPMENT OF A STABLE PRESSURE COMPENSATING CIRCUIT

The mathematical model of the original Hamworthy power controller with a pressure compensating circuit was used to evaluate the effect of each parameter. By changing the metering of the valve and increasing the flow through it, a stable network was devised. Such a valve was made but in practice, the compensating controller proved to be unstable when pump flow was at 15% of maximum.

When evaluating the stability of the network it had been assumed that the least stable state was when the pump was stalled and there was no flow. As a result of the network's behaviour the model was used to predict theoretical stability margins for various pump strokes. The model proved that at 15% of full flow the system was indeed at its most unstable and that this was due to the phase lag of the complete system being slightly offset by a decrease in phase lag of the valve as it opened. The overall effect was that for this particular system, the phase lag for all frequencies, was largest when the flow was 15% of maximum. These results verified that the modelling technique was reasonably accurate. Also a valuable lesson had been learnt, namely, that the stability at all operating conditions should be evaluated before a system is tested.

From the work on this modified compensating system it was becoming clear that to design a stable circuit was going to be a difficult task. The problem of stability was made even more difficult by the requirement for the pressure/flow characteristic of the system to have a pressure rise of only 10% of cracking pressure from the crack point to the stalled condition. The previous design was required to operate only in conjunction with a constant power controller where a steeper characteristic (over a shorter flow range) was acceptable. The equivalent pressure rise of this system over the full flow range was 100% of the cracking pressure, which implied that a

satisfactory compensator would require a gain ten times that of the previous network and hence be ten times less stable.

The first step in finding a suitable design was to study the circuits given in the controller review of Section 2.4. The various circuits presented used either a poppet or a spool valve. The mathematical model of Appendix A3 was used to investigate the effect of replacing the spool type valve in the pressure compensating network by a poppet design. The results indicated that, for the same characteristic, the spool valve produced the more stable results.

The use of a spool valve was therefore continued and in an attempt to improve the stability of the system a damping orifice was included in the same position as used by DREYMULLER and shown in Fig 3.3. Details of the new model for this design are given in Appendix A4. The effect of the orifice was to dampen the compensator spool to the square of its velocity. This implied that there would only be a damping effect while the spool was in motion. The consequence of this was that the design would continually oscillate or limit cycle. Results from the model indicated that if this limit cycle was to be kept to a reasonable level of $\pm$ 0.5 bar, then the diameter of the damping orifice must be 0.086 mm. Clearly this was not a satisfactory solution because such a small hole would rapidly become blocked by the contaminant in the hydraulic oil.

RIGBY had the same problem and he overcame it by the incorporation of a "phase lead" piston. This is an additional piston which moves when the compensator operates thus forcing more oil through the damping orifice. Therefore the same damping effect can be achieved using a larger orifice. This was modified in the next compensator design. Instead of using a separate chamber, the spool diameter was increased which created the same effect.

A sketch of the resulting valve is shown in Fig 3.4. The spool is hollow and this passage is used to direct flow to both of its ends via small damping orifices. Due to the seal collar the areas at high pressure are different at each end of the spool $(a_5 > a_6)$ and this creates the hydrostatic force to

move the spool. As pump pressure increases this force increases until, at the compensator crack pressure, it overcomes the pre-load in the spring. As the spool moves flow passes through the metering holes and is dumped to tank via the vent orifice, thus creating a metered pressure (P_m). This is sensed by the cut-off piston in the controller which de-strokes the pump.

The model of this new valve was slightly different to the previous one and the necessary modifications are included in Appendix A4. The parameters of the system were altered in an attempt to maximise its stability and the resulting Nyquist plot, for the least stable operating conditions, is shown in Fig 3.5. The new stability criterion for this system, described in Appendix A4, states that where the curves intersect, at a common frequency, gives the frequency and amplitude of the resulting limit cycle. From Fig 3.5 these curves intersect at 20 Hz and, from equation A4.20, a 0.48 mm diameter damping orifice must be used to keep the pressure ripple to $\pm$ 0.5 bar.

This orifice diameter was still rather small and so attention was given to improving the performance of the follow-up servo. A model of its frequency response, described in Appendix A5, indicated that the design could be dramatically improved by changing the diameter of the piston (a_2) and by altering its metering. It was estimated that this new design would give 28.7° less phase lag at 10 Hz than the old design.

The model of the larger diameter compensating spool valve was altered to incorporate this new servo design. The results indicated that the pressure ripple could be kept below $\pm$ 0.5 bar with a 0.66 mm diameter damping orifice. Such an orifice, with suitable filtration, was considered to be satisfactory from a contamination viewpoint.

One potential problem of the design was that the damping orifice would adversely effect the response time of the system. A quick check was made on its theoretical response to a 25 bar step input above the cracking pressure. This indicated that the valve would fully respond within the 300 ms stipulated in

the design specification given in Appendix A1.

Such a valve was then manufactured and tested. The immediate results indicated that the steady state characteristics were quite acceptable but that the stability of the system was fairly complex. With a 0.66 mm diameter damping orifice the system was stable if the load was gradually changed. However, when subject to a step change in pressure the system went unstable. This was overcome by using a 0.40 mm diameter orifice. With respect to the predicted limit cycle, none was observed as it was impossible to distinguish from the general level of pressure ripple present.

The consequence of using a smaller damping orifice was that the system would have a slower response. Pressure was measured against time in response to a step input of 25 bar above the valves cracking pressure. The results indicated that the valve's response was 700 ms.

The conclusion from the performance of the valve was that it could be used to meet short term customer requirements, as its response could be improved if the volume of oil at high pressure, for a particular installation, was larger than that described as the "worst" load in Appendix A2.

Thus attention was turned towards the design of the CCS system and overall controller package, with a view to incorporating any ramifications of the package into the compensating valve and improving its performance at a later date.

3.4 THE DESIGN AND DEVELOPMENT OF THE CCS CONTROLLER AND THE COMPLETE CONTROLLER PACKAGE

A description of how the CCS controller works is given in Section 2.6 and a schematic for adapting the Hamworthy pump to accept it is shown in Fig 3.6. In this case the centre core pressure acts upon a piston/spring arrangement which pushes on the main spool in the controller. The higher the sensing pressure the further the spool is moved and the less flow the pump produces. As more flow is demanded by the selection of the control valve, the centre core pressure falls and hence the stroke of the pump increases.

In practice Hydreco had reported that the system was stable when flow was supplied to the services but that it did tend to limit cycle when in the stand-by condition. To aid the design of the Hamworthy system a mathematical model, using the same technique as used for the pressure compensating system, was devised and is described in Appendix A6. Results from this model confirmed that in the stand-by condition there was indeed a tendency to hunt but this could be greatly reduced by the inclusion of a damping orifice. The size of orifice required was dependent upon the area of the controller piston and the sensitivity of the orifice to contamination. To limit the overall size of the controller it was necessary to keep the diameter of the controller piston to a minimum. The final design incorporated a 13.0 mm diameter controller piston and a 0.40 mm diameter damping orifice. A Nyquist plot of this system is given in Fig 3.7 and this indicated that the stand-by pressure ripple would be $\pm$ 3 bar at a frequency of 14 Hz.

This ripple was considered to be acceptable because, unlike the pressure compensating network, the pump would not be supplying flow to a service whilst oscillating. The reason for this is that at stand-by, the phase lag from the follow-up servo is very large due to the low pressure. However, when a service is selected, pump pressure rises to meet this load and hence the phase lag of the follow-up servo diminishes and the CCS system becomes stable.

The inclusion of such a small orifice was of concern on two accounts. Firstly it would slow down the response of the controller and secondly, it would be sensitive to contamination.

A quick check on the theoretical response of the system indicated that it should meet the 300 ms target stipulated in the design specification given in Appendix A1.

Regarding the sensitivity to contamination it was argued that because the flow through the orifice was oscillatory it would have a self cleaning action. Therefore, so long as the oil entering this chamber was filtered by a 100 μm mesh and that the system was thoroughly cleaned before assembly, then this

should not create a problem.

At this stage all of the necessary control functions had been designed and it was possible to concentrate upon the controller package. The design specification stipulated that the package must have the facility to control a pump in up to three different options simultaneously. In practice this required the pump to be monitored by a combination of controllers and the one demanding the minimum flow should override all others.

The first scheme proposed to achieve this is shown in Fig 3.8. Each function controls the metered pressure of a spool valve. The higher the metered pressure then the less flow is demanded and so by a series of check valves the highest metered pressure is switched to control the stroke of the pump. Initially this appears to be quite an attractive solution. The design lends itself to modular construction with more valves being added to accommodate additional control options. In fact there is no theoretical limit to the number of modules which could be used. However, the main disadvantage of this design was that the control valves would reduce the stability of each function. For example CCS was only just acceptable when it acted directly upon the main spool. The inclusion of the extra valve would certainly lead to stability problems.

This idea was dropped in favour of a direct acting design which is sketched in Fig 3.9. The individual control functions are combined to form a compact package. In this design the stroke of the pump is controlled by the function which has moved furthest to the right. To illustrate how this operates a pump with CCS and pressure compensating control functions is shown in Figs 3.10. Initially, in Fig 3.10(a), the pressure is below the compensator cracking pressure and the pump is controlled by the CCS system. As the cracking pressure is exceeded, Fig 310(b), the pressure compensating piston is pressurised and it acts upon the spool. As the pump pressure is further increased, Fig 3.10(c), the compensator pressure increases further and the

compensator piston overrides the CCS piston and wins control of the pump. An additional feature of this system is that interaction between the two control functions is minimised by the property that as one function overrides another, the signal to the former is reduced. Thus, returning to Fig 3.10(c), as the compensator takes over from the CCS controller, the flow from the pump to the service is less than the CCS system requires (rather like an increase in flow to the service) and it compensates for this by trying to demand more flow. Thus, as it is overridden, the CCS piston moves to the left and away from the spool.

The design of the package is shown in Fig 3.11. It consists of a main spool with a 'key' piece locked on to it. This 'key' piece can be moved by either the CCS piston, the spring holder or the pressure compensating piston. Thus each controller is totally independent of the others and the one which moves furthest to the right takes control of the pump.

The physical size of the controller was kept to an absolute minimum in order to save material and to limit the installation envelope of the pump. However, it was designed to be fully interchangeable on all three sizes of piston pumps (which had strokes of 6.50, 7.50 and 8.70 mm) and so the size of the controllers for the smaller pumps was slightly larger than they need have been.

The design in Fig 3.11 incorporates equal area, opposing CCS pistons. Although this feature was not necessary for the proposed control options, the extra piston was included to increase the versatility of the package for future development work. For example they could be used by constant flow or speed controllers and, as will be seen later, they proved invaluable in the development of the new CCS and pressure compensation controllers.

Another feature of the CCS design was that the same hardware could be used by the remote manual control function alleviating the need for additional components to satisfy the requirements of this control mode.

The design of the power controller was basically the same as the original Hamworthy controller except that it was now larger. This implied that the offset loads were going to be higher and so a PTFE/lead bearing was incorporated between the controller body and spring housing shaft.

Such a controller was manufactured and tested. The power controller was the first function to be evaluated and the results indicated that the controller worked as well as the original with negligible hysteresis. The manual controller was then tested and a graph of flow against control pressure is shown in Fig 3.12. This result was not so satisfactory and some design modifications were made to reduce the amount of hysteresis.

It was believed that there were two main sources of hysteresis. Firstly if the opposing pistons were out of line then this would create a side load upon the pistons and hence increase the level of coulomb friction. The second area of hysteresis was due to the offset load created by the spool return spring and the CCS/manual control piston. These two problems were overcome by the design shown in Fig 3.13 where the spool return spring was moved to be in line with the CCS/manual piston and the opposing piston interface was changed to include a connecting bar. Subsequent tests revealed that using this design the hysteresis of the characteristic had been eliminated.

The manual controller was then replaced by the CCS circuit shown in Fig 3.14. The inclusion of the additional servo pump was to ensure that the load pressure could be maintained constant and that the characteristic of the relief valve at low flow would not interfere with the test. The resulting volume of oil at high pressure was estimated to be five times that of the 'worst load', described in Appendix A2, and consequently in the stalled state the CCS system was adequately stable without a damping orifice.

The results of the tests were disappointing. Hydreco had claimed that the metering band should be from 20% to 80% of the valve's travel regardless of pressure. The results obtained from the Hamworthy system demonstrated that the metering band was only 2% and that pressure affected the characteristic.

A subsequent investigation revealed that Hydreco had used a pump actuator piston with ground, tapered flats on it. These acted as variable orifices as the pump stroke altered and improved the performance of the controller. This idea was tried on the Hamworthy CCS system and two resulting characteristics are shown in Fig 3.15. These curves indicated that metering band had been improved but also that the system was still pressure dependent.

To aid the design of a pressure compensating network a mathematical model was made to predict the metering characteristic of the CCS controller and this is described in Appendix A7. The accuracy of the model was assessed by comparing predicted results with measured curves and such a comparison is shown in Fig 3.16. The correlation was certainly to within the accuracy of the data and so the model was used to predict the affect of various pressure compensating networks. The system which was successful is shown in Fig 3.17 and the theoretical metering characteristics for pressures of 35 and 350 bar are shown in Fig 3.18. A description of how this network operates is included in Appendix A7.

The CCS controller was then re-tested with this pressure compensating network. The results demonstrated that the system behaved as predicted and that the metering characteristics had been greatly improved.

Attention was then turned to the interaction effects of the controllers. The first two control modes to be used together were constant power and pressure compensation. The resulting characteristic was similar to Fig 2.9 and the system did not demonstrate any instability or distortion of the characteristics at the override point.

The pressure compensating controller was then replaced by a manual one. The initial tests indicated that there was a rounding effect of the characteristics as one controller overrode the other. This effect was reduced to an acceptable level by reducing the rate of the spool return spring

and compensating for this by increasing that of the manual and power controller springs. The resulting characteristic is shown in Fig 3.19.

The final test on the controller package was to determine the response time of the pump. The circuit used for this test is shown in Fig 3.20. For convenience a needle loading valve was used and pressure plotted against time. As flow was proportional to the square of the pressure full flow was attained when the pressure was at its maximum. Similarly when the pressure was zero this indicated that there was no flow. The response time for the pump to de-stroke was measured using both the new and old follow-up servo designs. The corresponding traces of pressure against time are shown in Fig 3.21 and from these it was determined that the response time of 0.3 seconds using the original follow-up servo was halved with the introduction of the new, smaller one. Thus not only did the new follow-up servo improve the stability of the controller but it also greatly improved the pumps response time.

The developed controller package was now significantly different from the original design. However, before the drawings were updated to the preproduction stage, it was decided to undertake a brief development exercise in an attempt to find an improved pressure compensating network.

3.5 THE DEVELOPMENT OF AN IMPROVED PRESSURE COMPENSATING NETWORK

From the results of the mathematical models of pressure compensating networks it was evident that the main problem in achieving stability was how to account for the phase lag introduced by the spool valve. If this valve could be eliminated then the stability of the network could be dramatically improved without affecting its steady state characteristic or dynamic response.

This valve was initially included because of the difficulty in designing a spring for a system which directly controls the position of the main spool in the controller package. To achieve this controller characteristic requires a high spring pre-load and a low rate. These two requirements can be met but the resulting spring is large (approximately 0.3 m long) as shown by ERNST

and is difficult to include in a neat controller design.

The breakthrough that enabled a direct acting system to be evaluated came with the concept of using a hydraulic pre-load. The two equal area opposing CCS pistons could be used in pressure compensation by maintaining a hydro-static force to oppose the de-stroking piston and using a light spring to control the shape of the characteristic.

The circuit tested was very similar to the ones shown by ERNST and DREYMULLER and a schematic of it is shown in Fig 3.22. Once pump pressure exceeds the cracking pressure of the relief valve, flow passes through the 1.78 mm diameter orifice and creates a pressure difference between the opposing pistons. This upsets the hydro-static balance of the two pistons and, as they moved to the right, they de-stroked the pump.

Initially no damping orifices were used and the system was unstable. However, when a 0.75 mm diameter damping orifice was put in the supply line to each piston, the system became adequately stable.

The characteristics obtained using the above pressure compensating network are shown in Fig 3.23. They are for a range of pressures from 150 to 300 bar and yet the same network was used for all of them. The only difference was the cracking pressure of the relief valve.

The characteristics show a tendency to cut-off the corner of the curve. This was caused by the relief valve opening below cracking pressure. The extra pre-load to increase the cracking pressure was supplied by the spring. Unfortunately the envelope for the spring was designed to give this pre-load and it could not easily be eliminated. It was decided that this could be taken into account when the controller package was re-designed and so no further work was done to improve the characteristic.

The next test on this new controller network was to measure its time response. The pump pressure was raised to 170 bar and the test rig relief valve set to 220 bar. The needle loading valve was then rapidly shut and the

resulting pressure against time trace is given in Fig 3.24. The trace shows that in response to the input, the pump pressure overshoots and after approximately 0.22 seconds it settles down to the stalled pressure of the pump. There were however some pressure oscillations which decayed after a further 0.05 seconds.

The final test on this network was to determine the maximum leakage flow. The system was set to a cracking pressure of 300 bar and the pressure raised to 310 bar which was sufficient to stall the pump. In this condition the leakage flow was 4.5 litres/min.

This latter compensating system fulfilled all of the design specification requirements and it even exceeded a few. For instance, it was adequately stable with operating slopes below 5% of cracking pressure which is better than the original requirement by a factor of two. Similarly the time response was 0.22 seconds which was a considerable improvement upon the 0.30 seconds specified.

However, the main advantage of this new design was its cost. It was estimated to be only one third of the cost of the other proposed design shown in Fig A4.4.

The new network was therefore combined with the other modifications to the design package and integrated to form the pre-production standard of the controller package which is discussed in the following section.

3.6 THE PRE-PRODUCTION DESIGN OF THE CONTROLLER PACKAGE

The results from the development of the original controller package indicated that the following design modifications were required.

1. Replace the pressure compensating valve and cut-off pin by the new compensating network.
2. Replace the original CCS controller by the load compensated version.
3. Adopt the opposing piston interface shown in Fig 3.13.

In addition to these changes it was also proposed to reduce the cost of the controller by making castings of as many components as possible.

The design changes to the original package were reasonably simple to achieve as space for the additional opposing pistons was already available. Indeed there was sufficient room for a third pair of opposing pistons should this ever be required. An isometric section of the new controller is shown in Fig 3.25. It shows the new controller package with power, load compensated CCS and pressure compensating control functions.

Fig 3.26 illustrates how the controller works. Initially, in Fig 3.26(a) the manual controller (biased to zero flow) is demanding minimum flow. The flow from the pump is increased, in Fig 3.26(b), by a reduction in the pressure acting upon the manual control piston.

Fig 3.26(c) illustrates how, as the load pressure of the pumps increases, the spring carrier moves upwards and destrokes the pump. The diagram shows the spring pack and how more springs are engaged as the pump is further destroked.

If the load pressure exceeds the pressure compensator setting, Fig 3.26(d), then the compensator piston pushes the "key" piece (and hence spool) off the constant power setting to a lower flow state.

To accommodate the new CCS and pressure compensating network a new block was fitted to the package as shown in Fig 3.27. It was decided to make it a separate unit, rather than integrating it into the complete package, in order to save cost when neither of these two control options were required. In such an instance the block is replaced by a blanking plate.

This concludes the description of the hydro-mechanical controller package. The next chapter deals with the feasibility study into the possibility of replacing the above controller by a competitively priced micro-processor based, electro-hydraulic system.

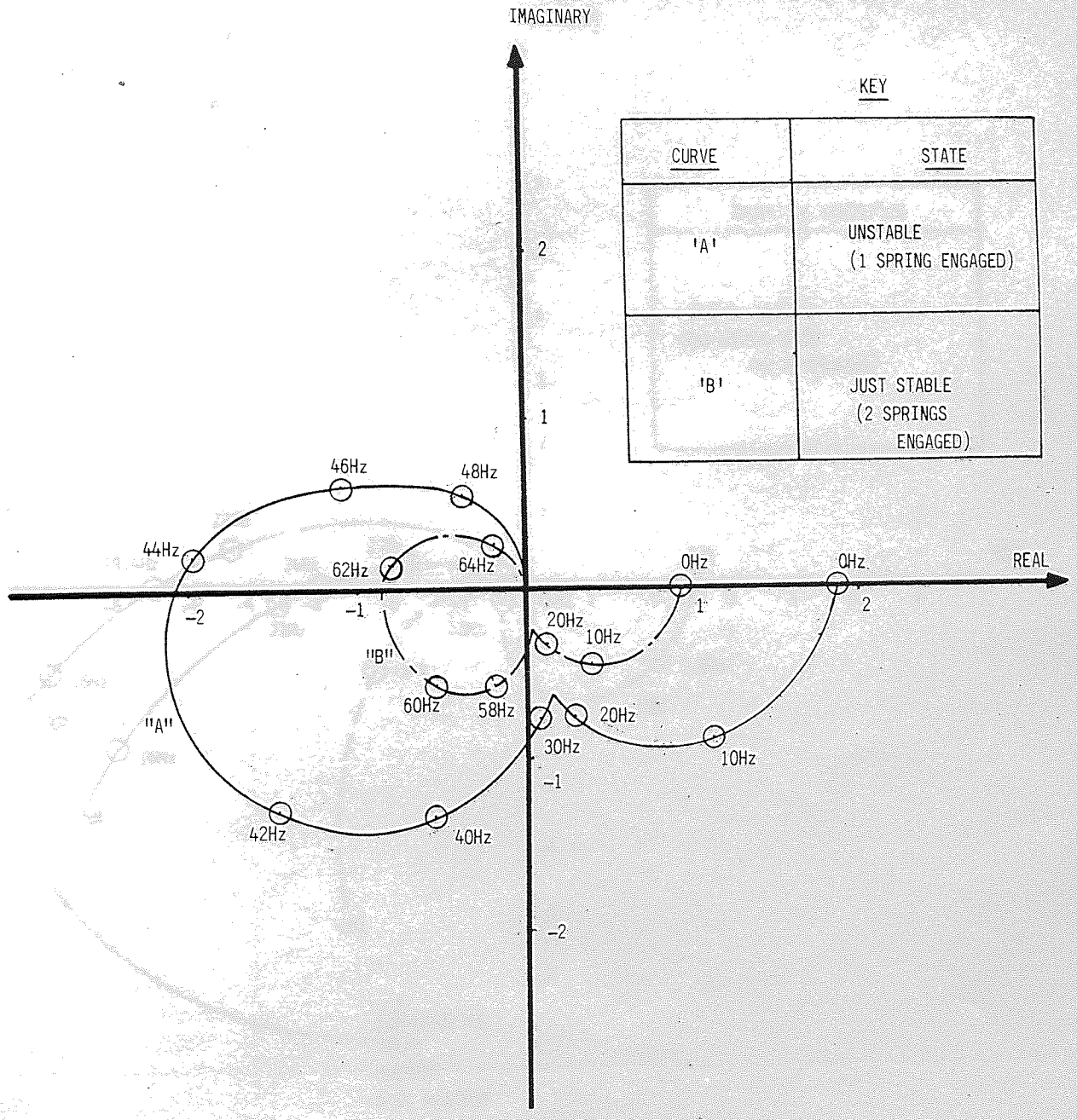

Fig 3.1 NYQUIST PLOT FOR THE ORIGINAL POWER CONTROLLER

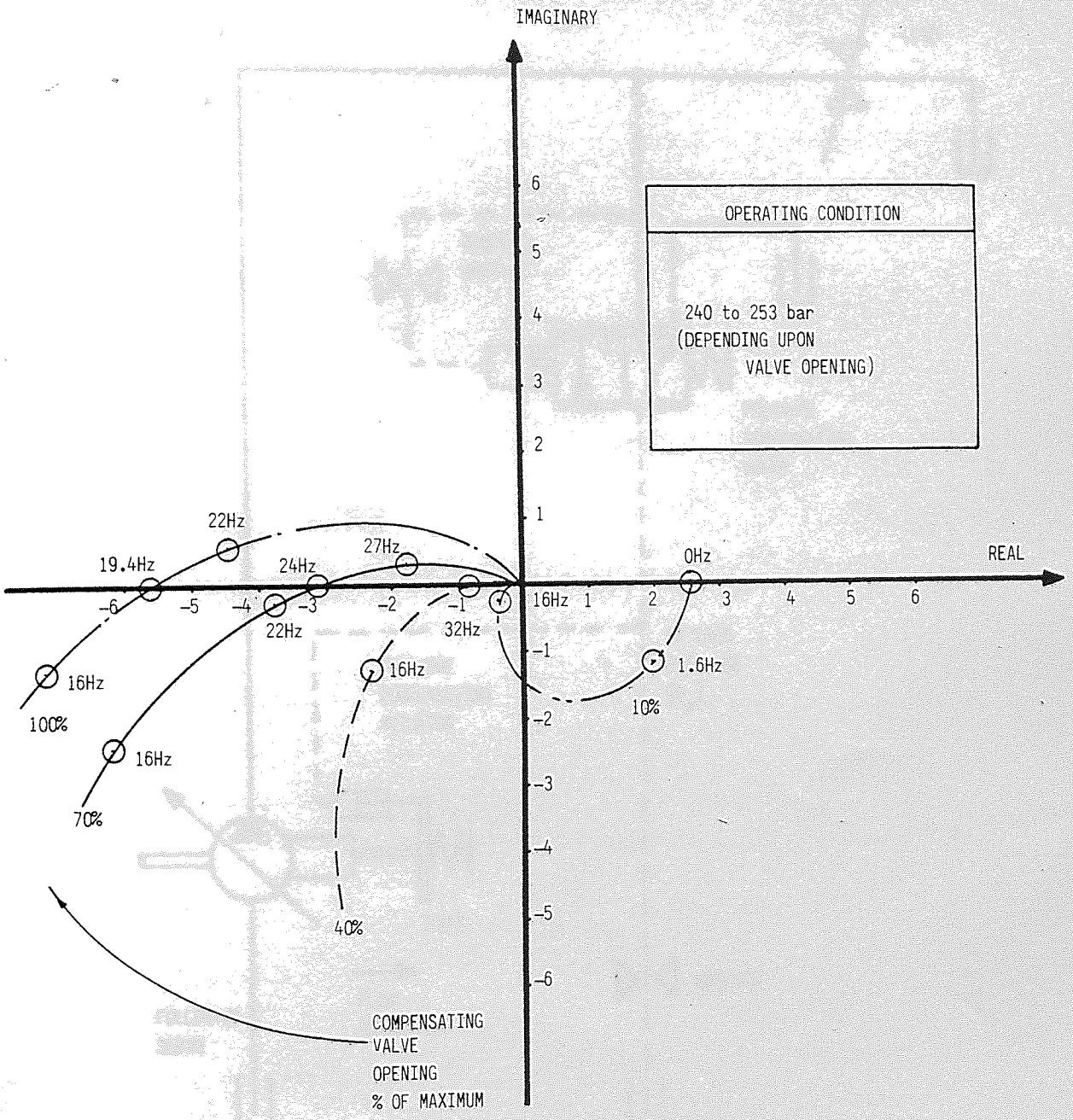

Fig 3.2 NYQUIST PLOT FOR THE ORIGINAL POWER CONTROLLER WITH PRESSURE COMPENSATION

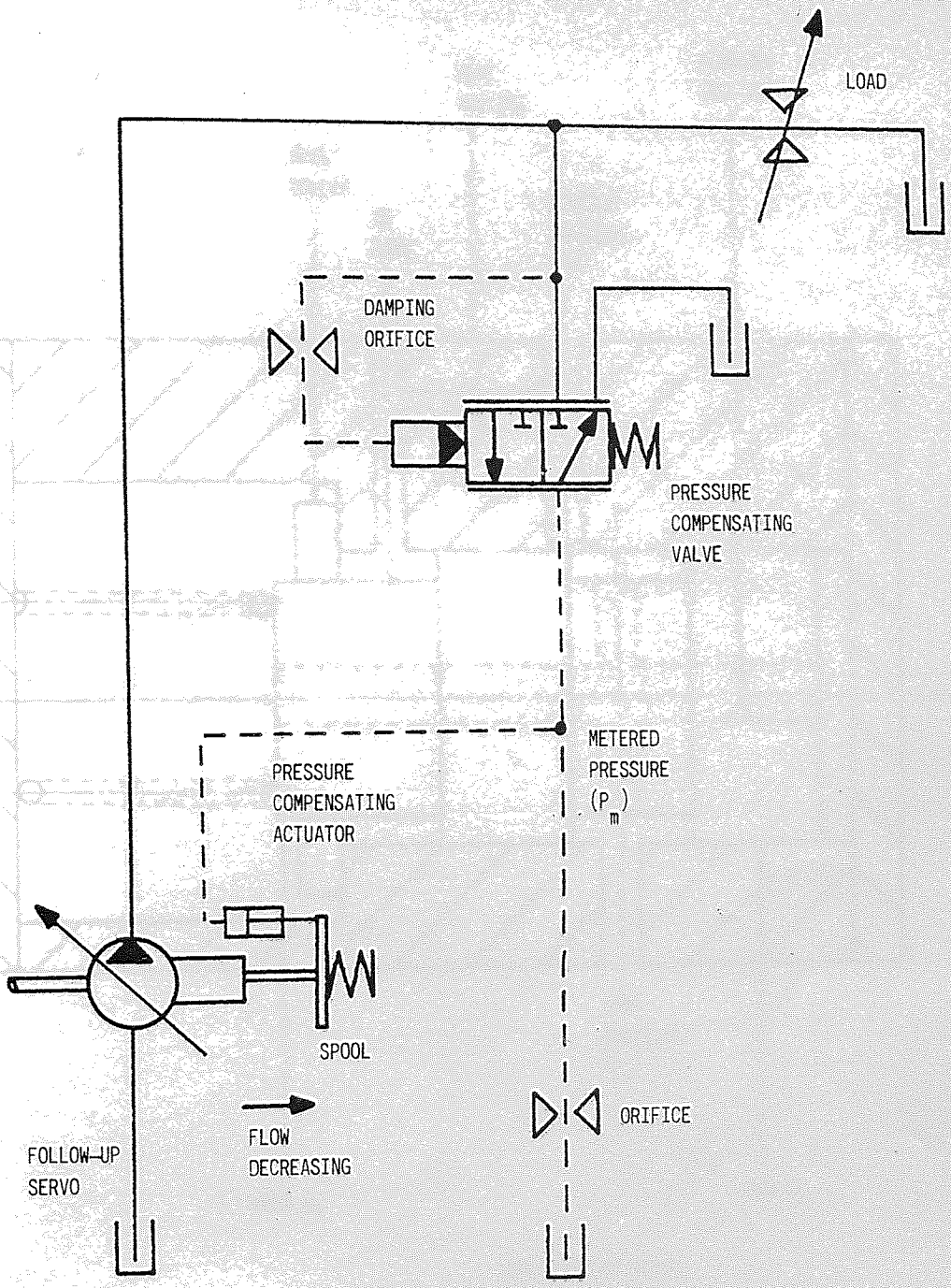

Fig 3.3 A DIAGRAM TO SHOW THE POSITION OF THE DAMPING ORIFICE FOR THE PRESSURE COMPENSATING VALVE

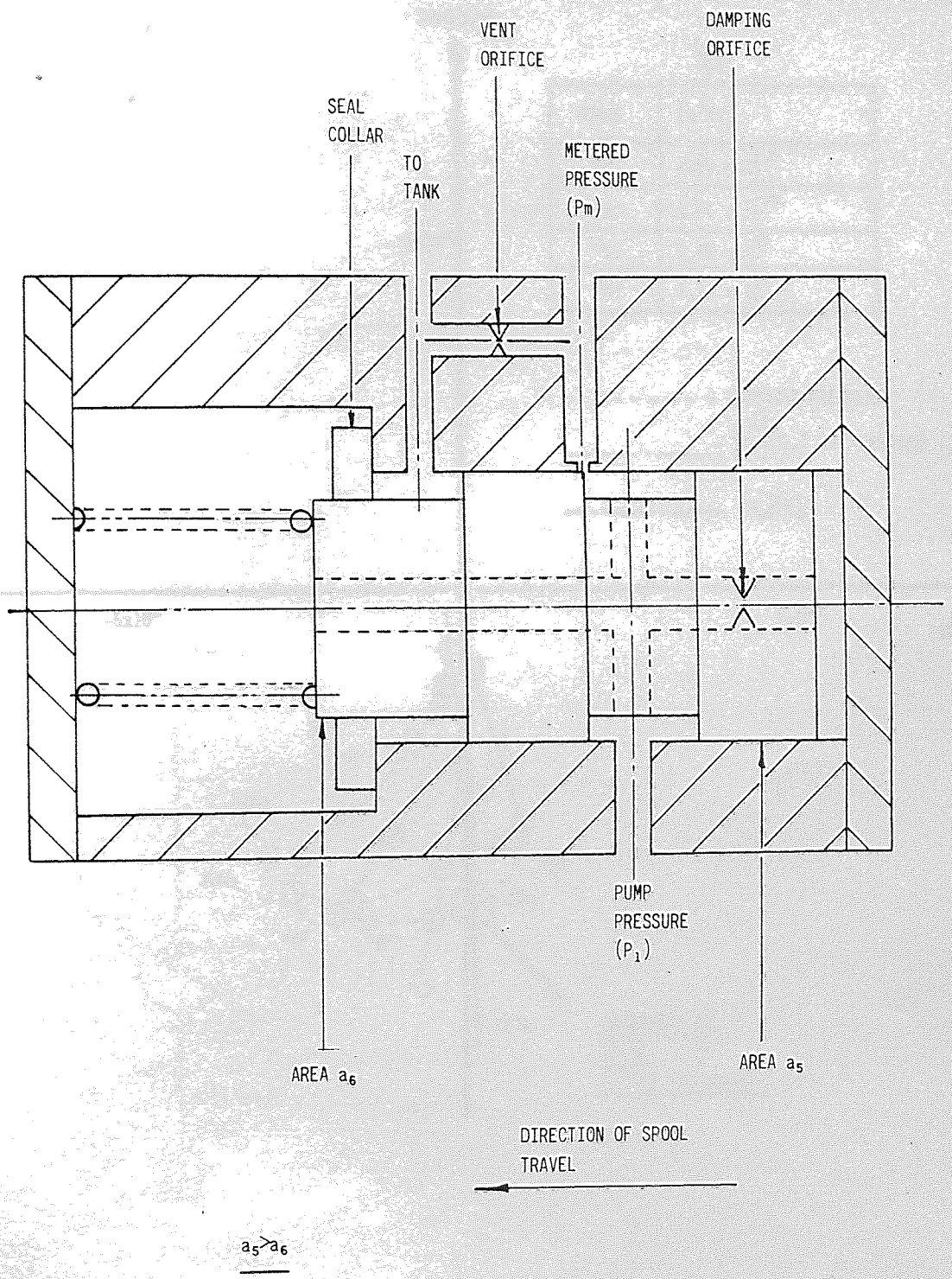

Fig 3.4 A SKETCH OF A PRESSURE COMPENSATING VALVE WITH A STEPPED PISTON AND A SEAL COLLAR

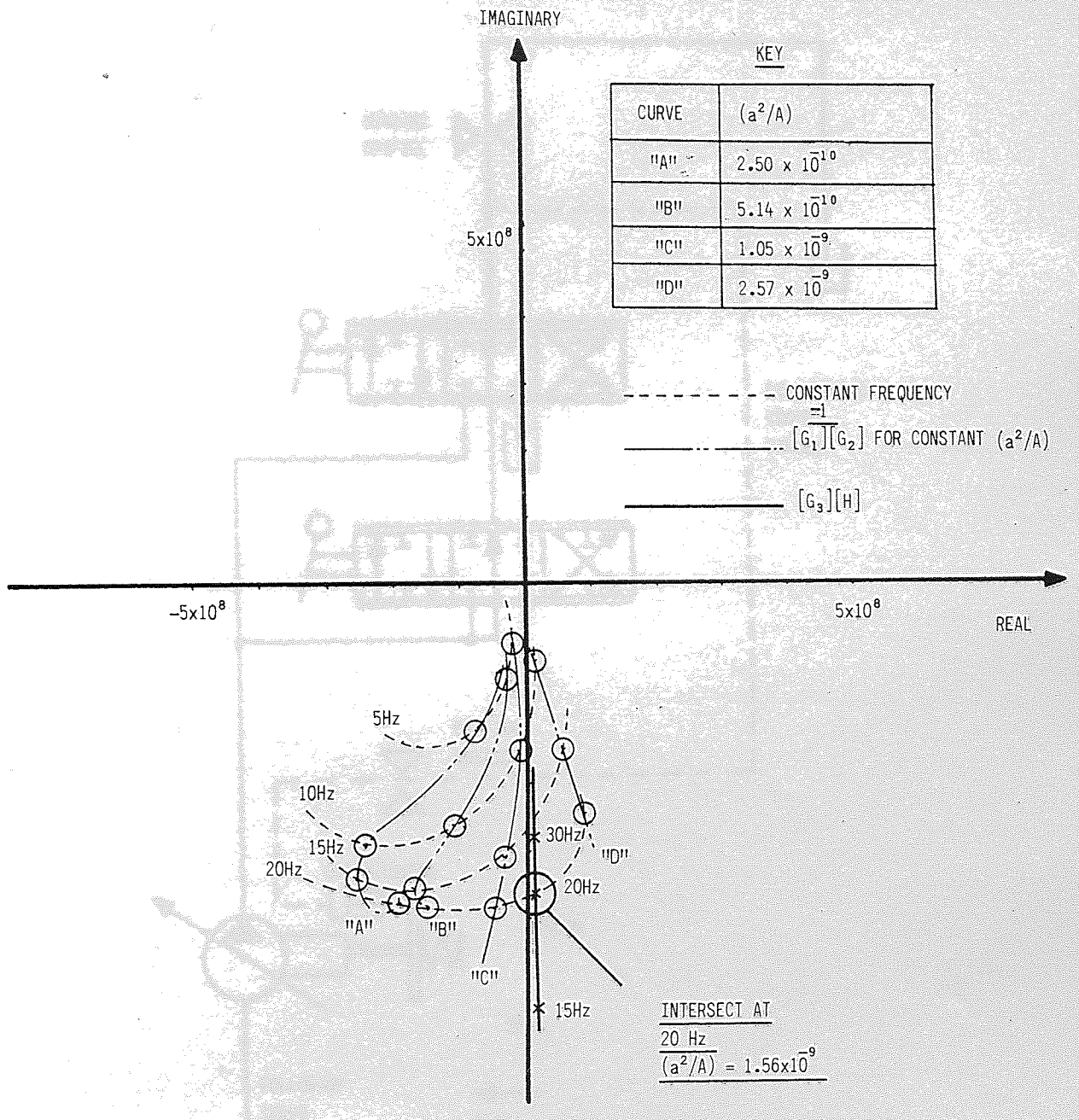

Fig 3.5 NYQUIST PLOT FOR THE NEW PRESSURE COMPENSATING SYSTEM INCORPORATING THE LARGE DIAMETER SPOOL VALVE

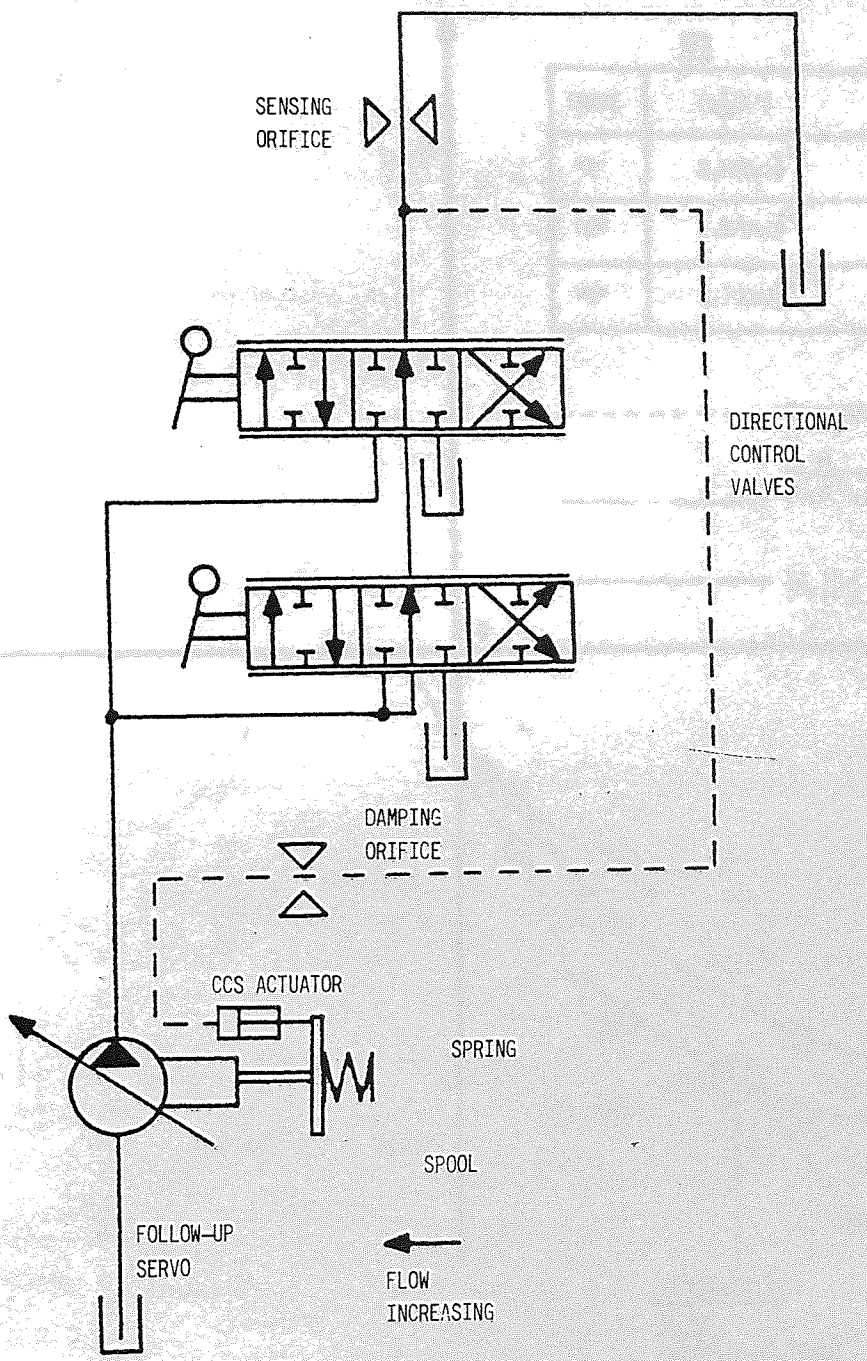

Fig 3.6 A SCHEMATIC DIAGRAM OF THE PROPOSED CCS SYSTEM FOR THE HAMWORTHY CONTROLLER PACKAGE

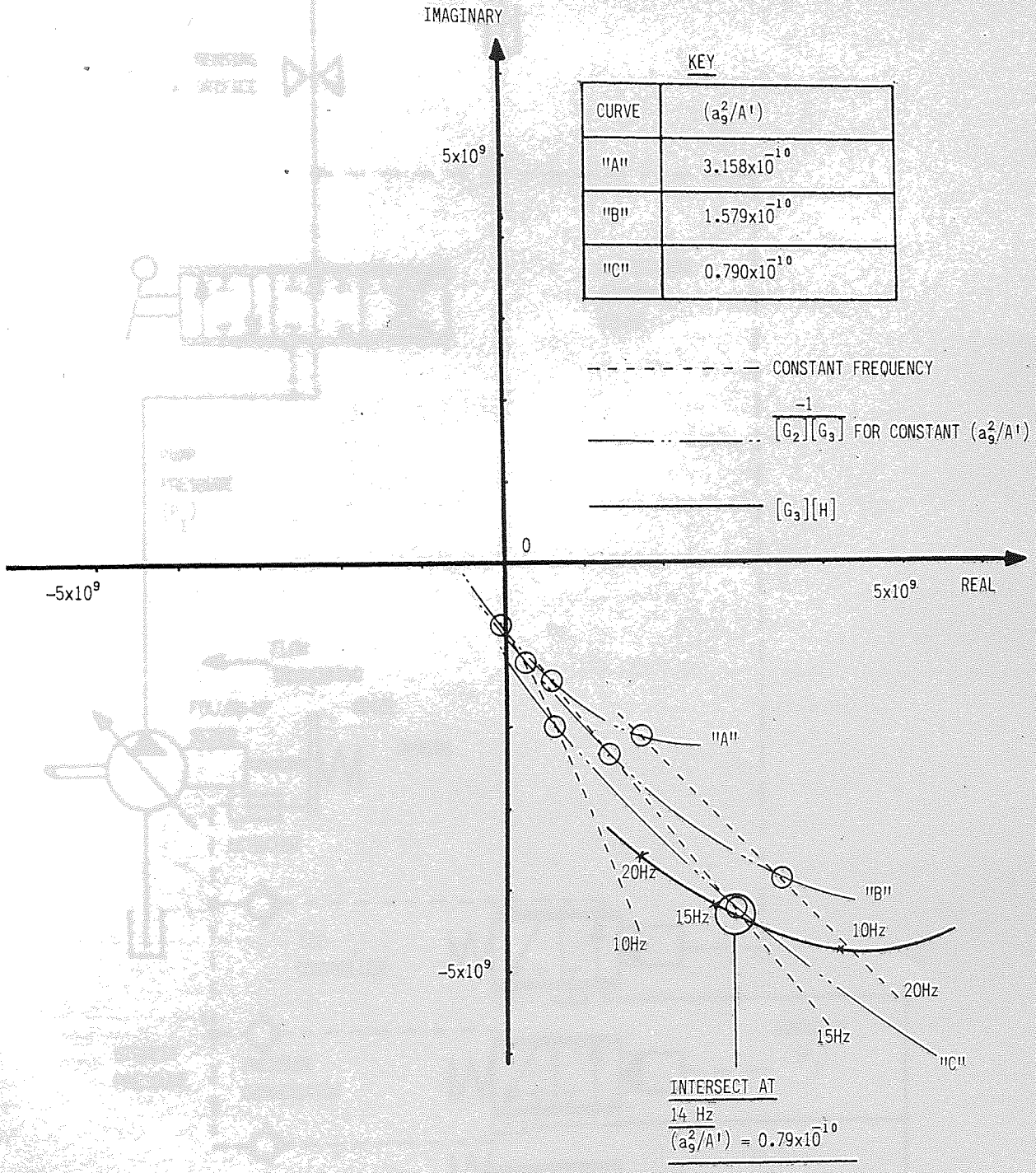

Fig 3.7 NYQUIST PLOT FOR THE CCS CONTROLLER IN THE STAND-BY CONDITION

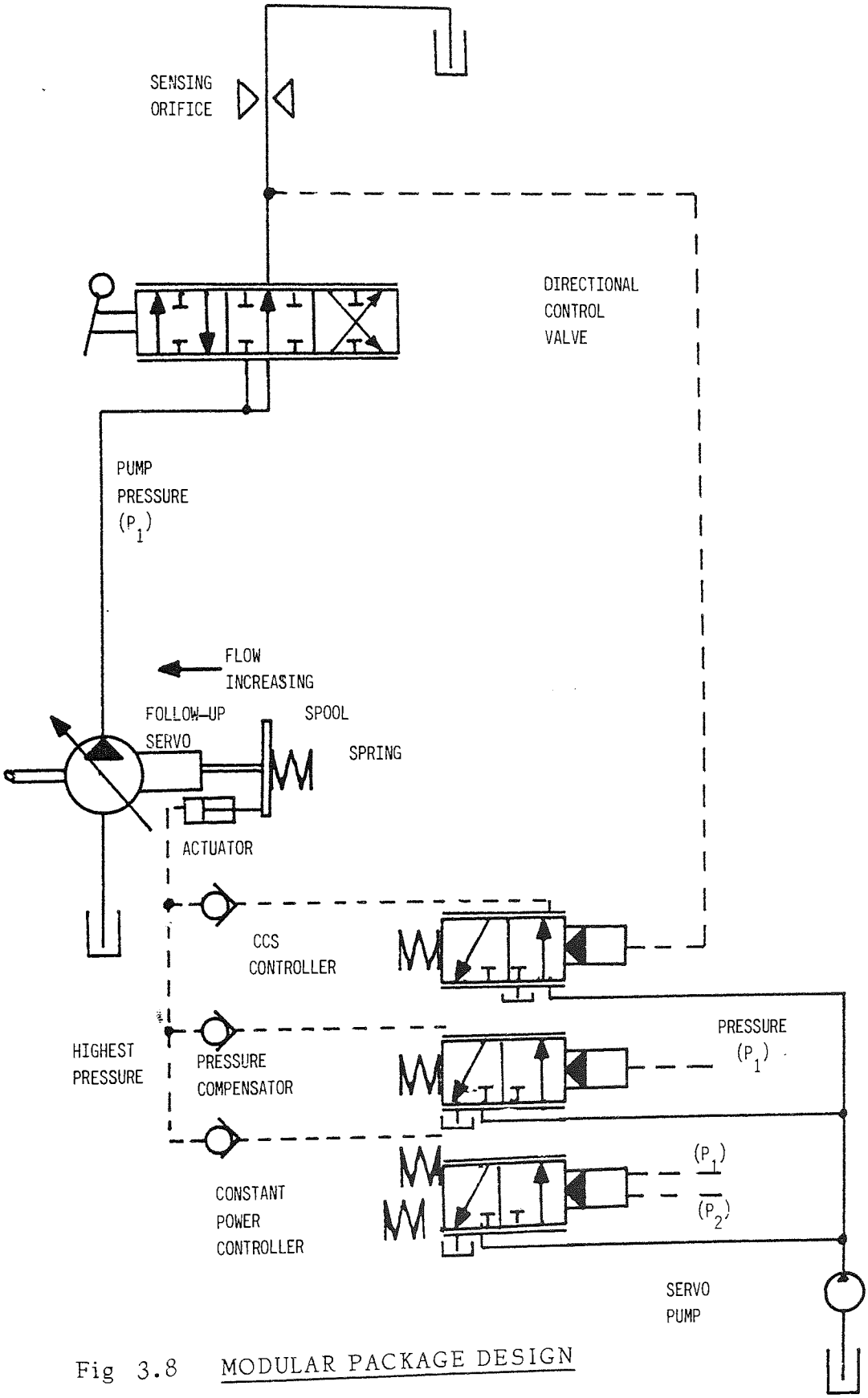

Fig 3.8 MODULAR PACKAGE DESIGN

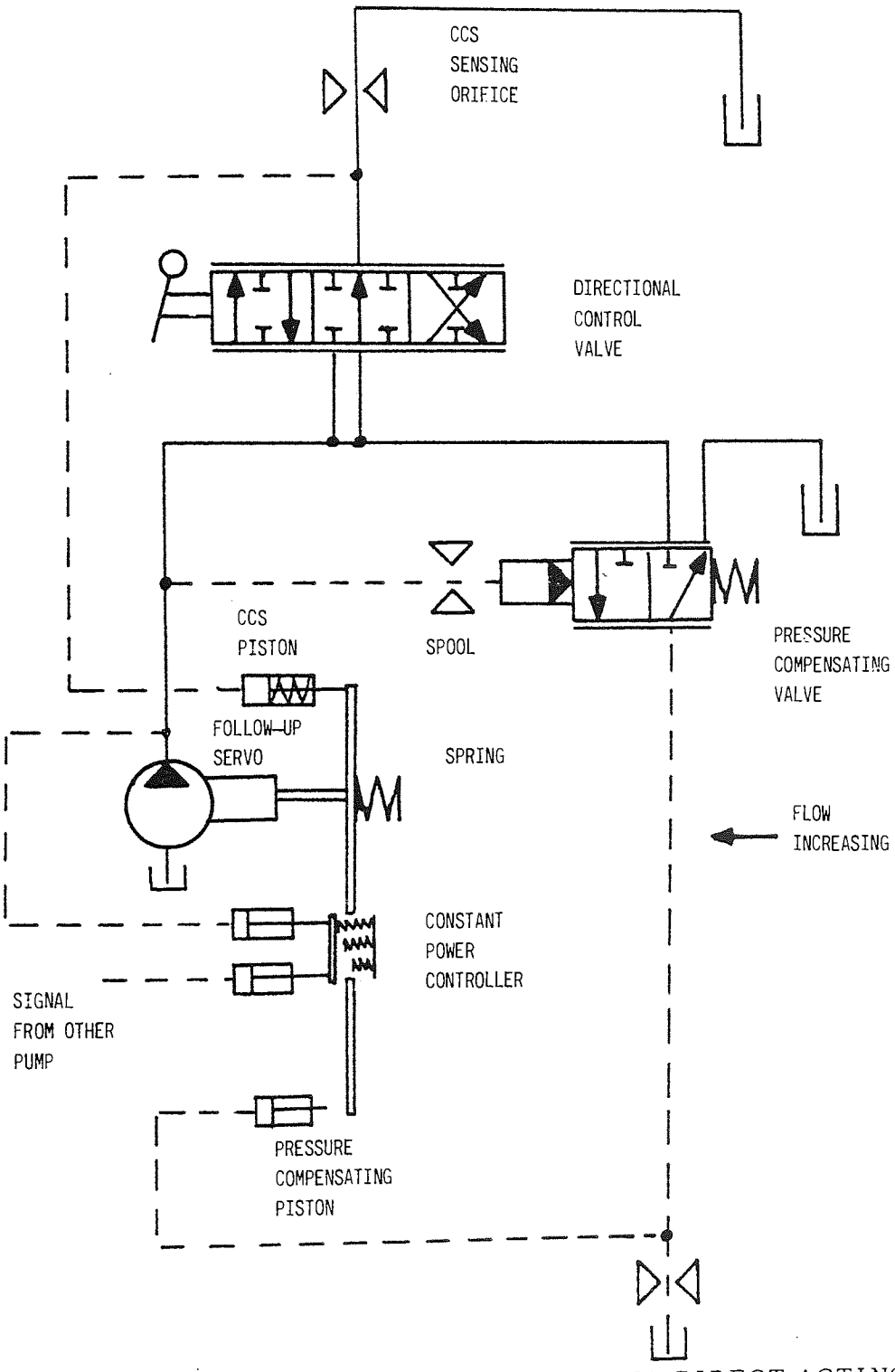

Fig 3.9 A SKETCH OF THE PROPOSED DIRECT ACTING PACKAGE DESIGN

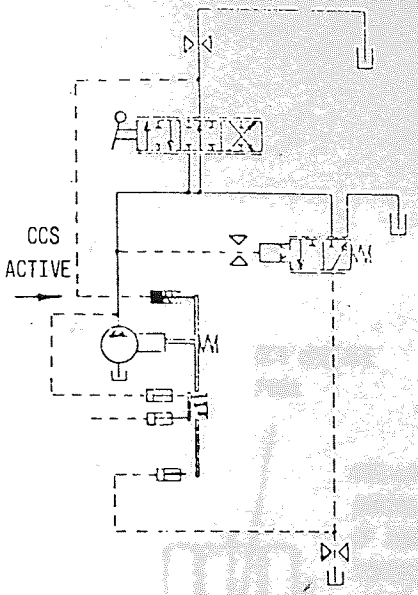

(a) PUMP UNDER CCS CONTROL

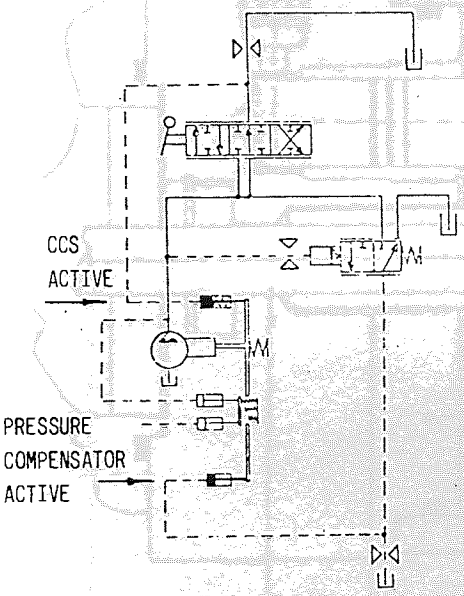

(b) PRESSURE JUST EXCEEDS THE COMPENSATOR CRACKING PRESSURE AND BOTH CONTROLLERS ARE ACTIVE

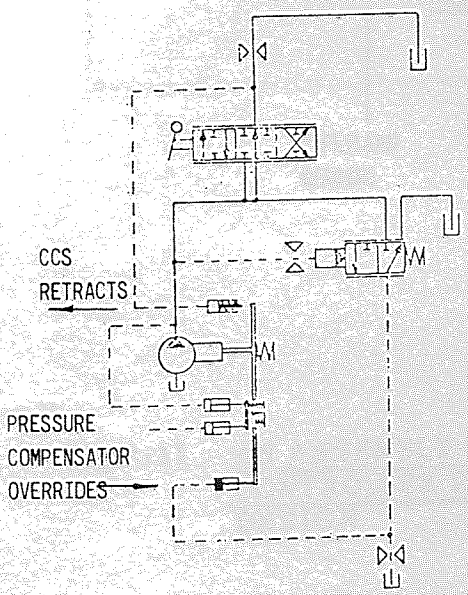

(c) AS PRESSURE CONTINUES TO RISE THE COMPENSATOR OVERRIDES THE CCS CONTROLLER

Fig 3.10 OPERATION OF THE DIRECT ACTING PACKAGE DESIGN

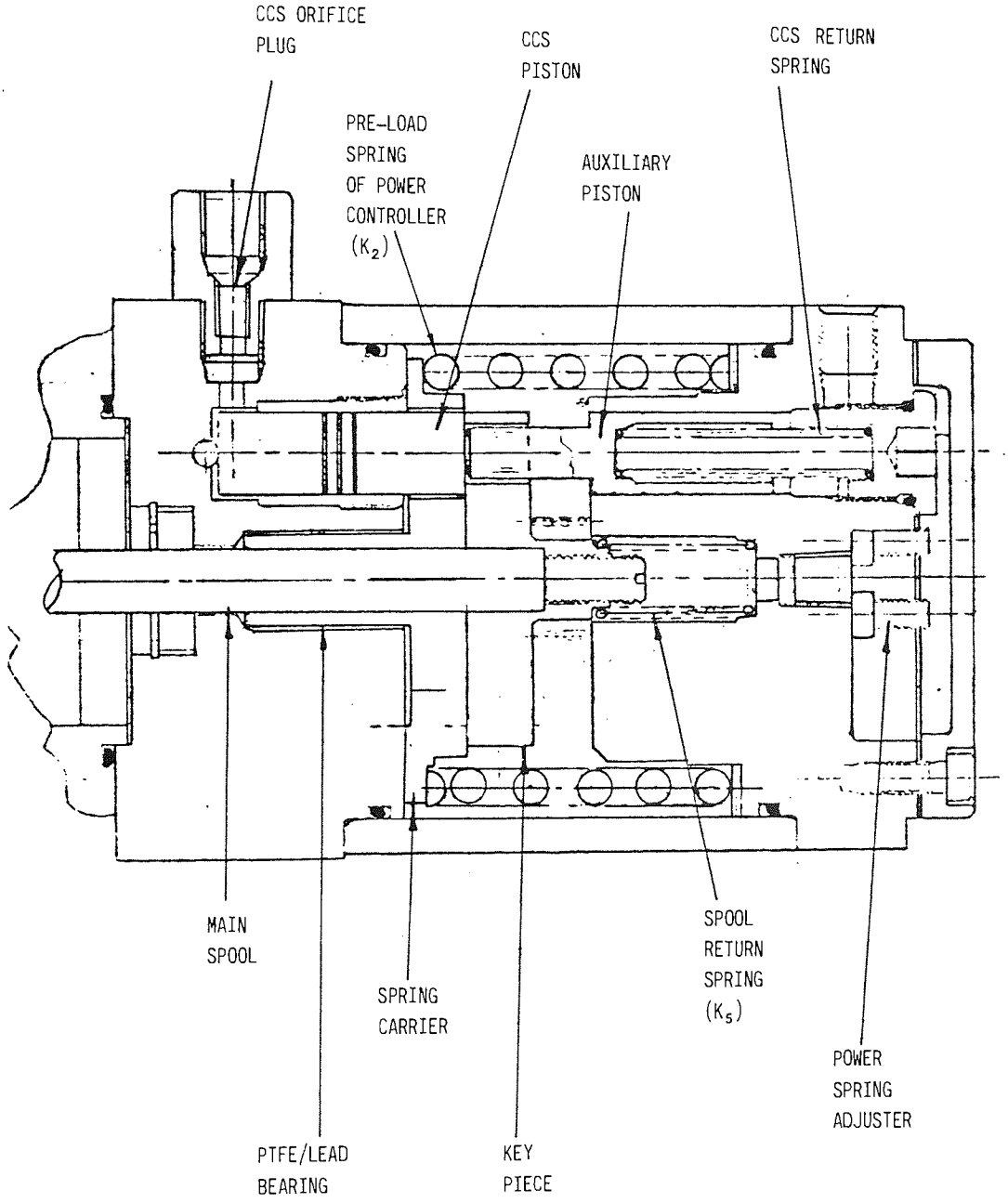

Fig 3.11 AN ASSEMBLY DRAWING OF THE HYDRO-MECHANICAL CONTROLLER PACKAGE SHOWING THE CCS PISTON DESIGN

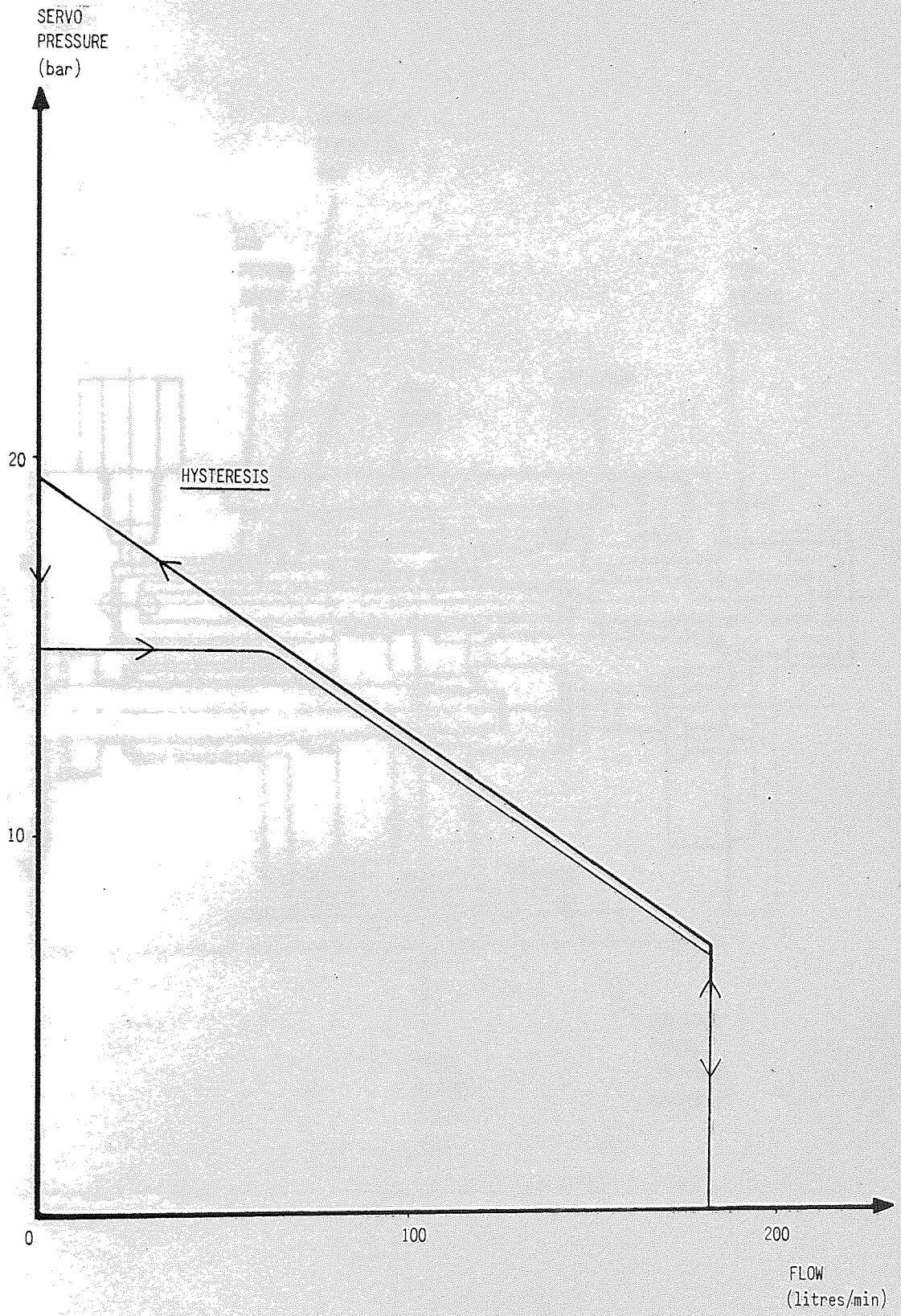

Fig 3.12 INITIAL CHARACTERISTIC OF THE PUMP WITH A REMOTE MANUAL CONTROLLER

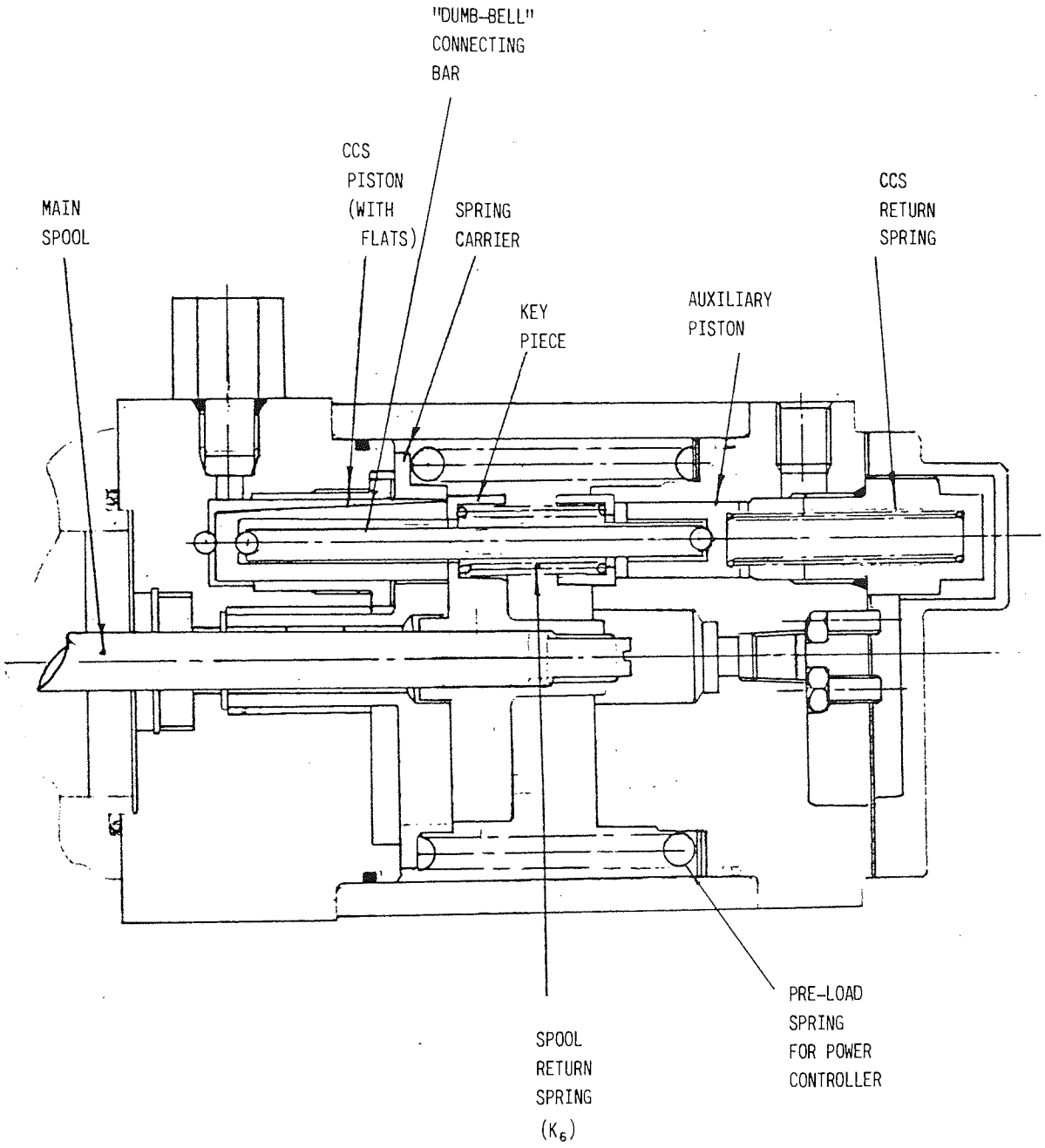

Fig 3.13 AN ASSEMBLY DRAWING OF THE REVISED CONTROLLER PACKAGE SHOWING THE NEW "DUMB-BELL" CCS PISTON DESIGN

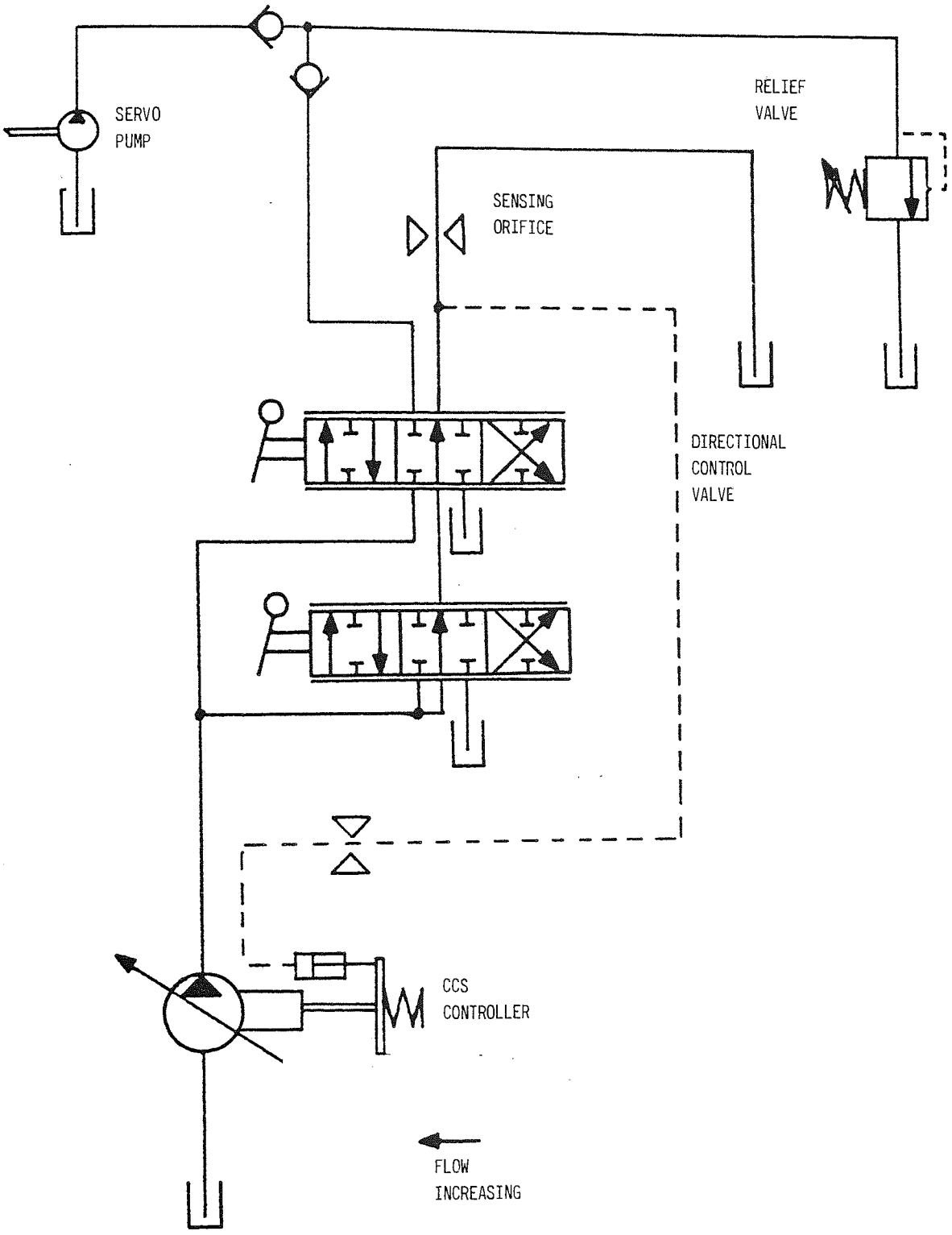

Fig 3.14 HYDRAULIC CIRCUIT USED TO EVALUATE THE CCS CONTROLLER

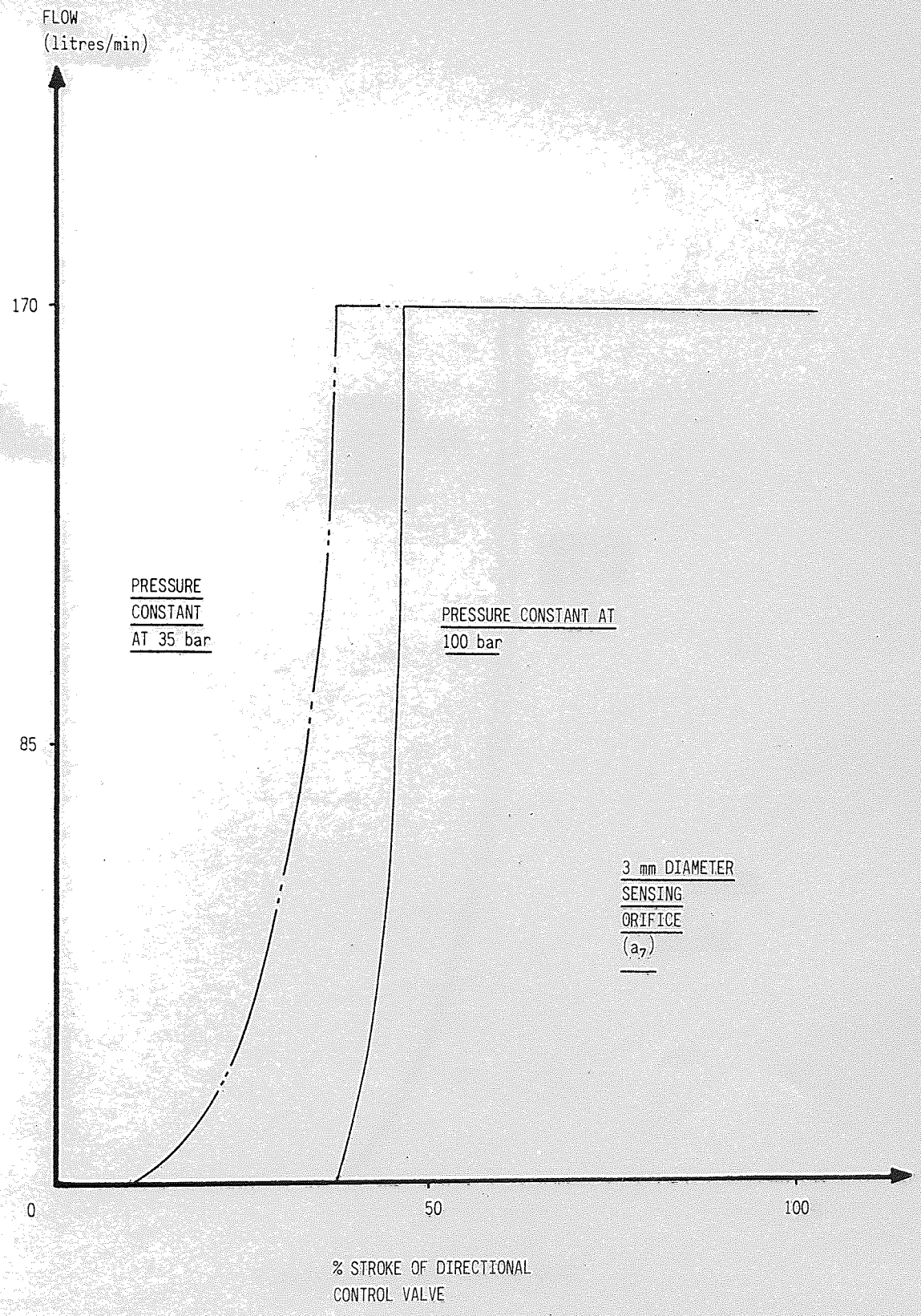

Fig 3.15 CCS CONTROLLER CHARACTERISTICS WITH THE NEW PISTON DESIGN

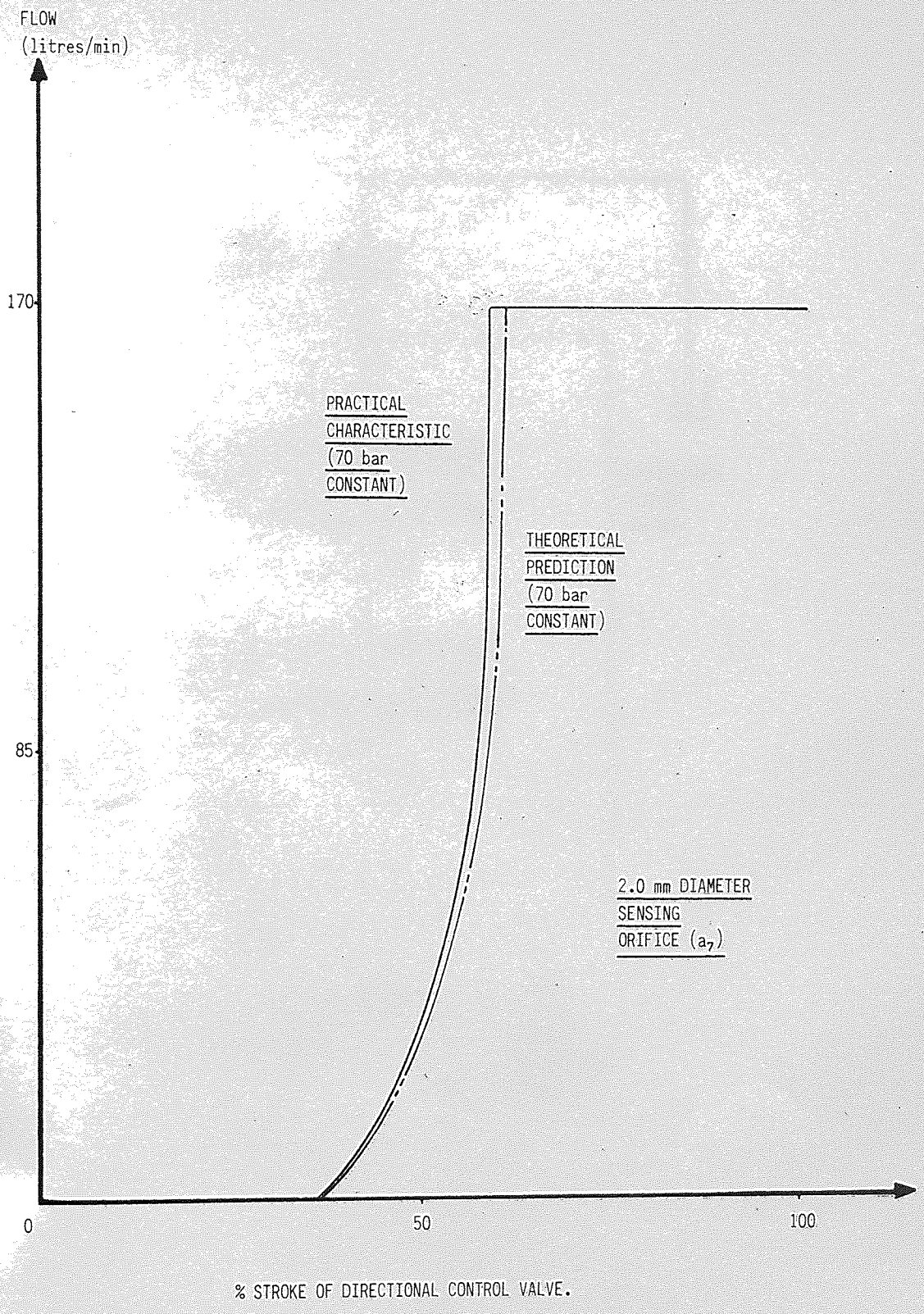

Fig 3.16 A COMPARISON BETWEEN THEORETICAL AND PRACTICAL METERING CHARACTERISTICS FOR THE CCS CONTROLLER

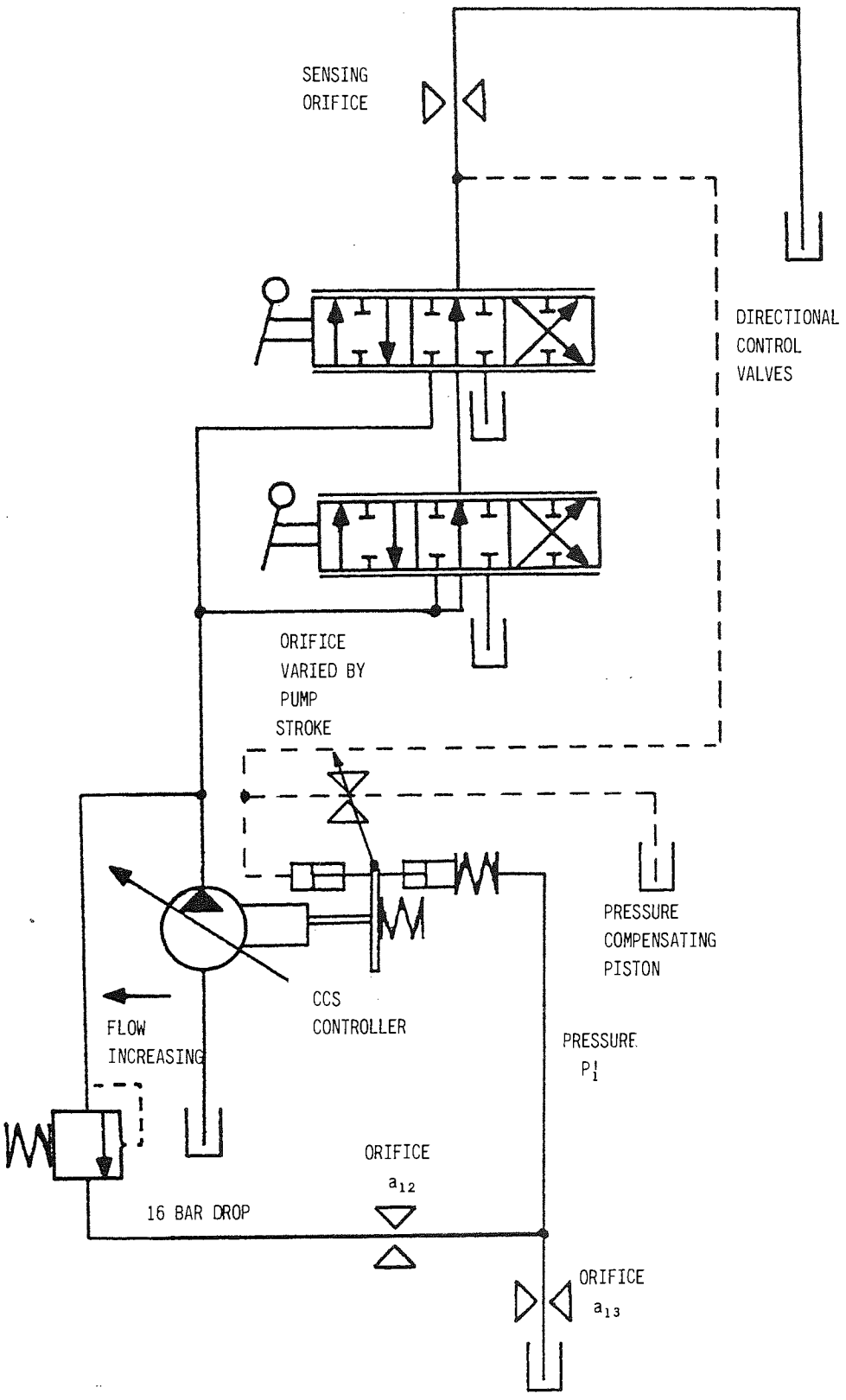

Fig 3.17 PRESSURE COMPENSATED CCS CIRCUIT

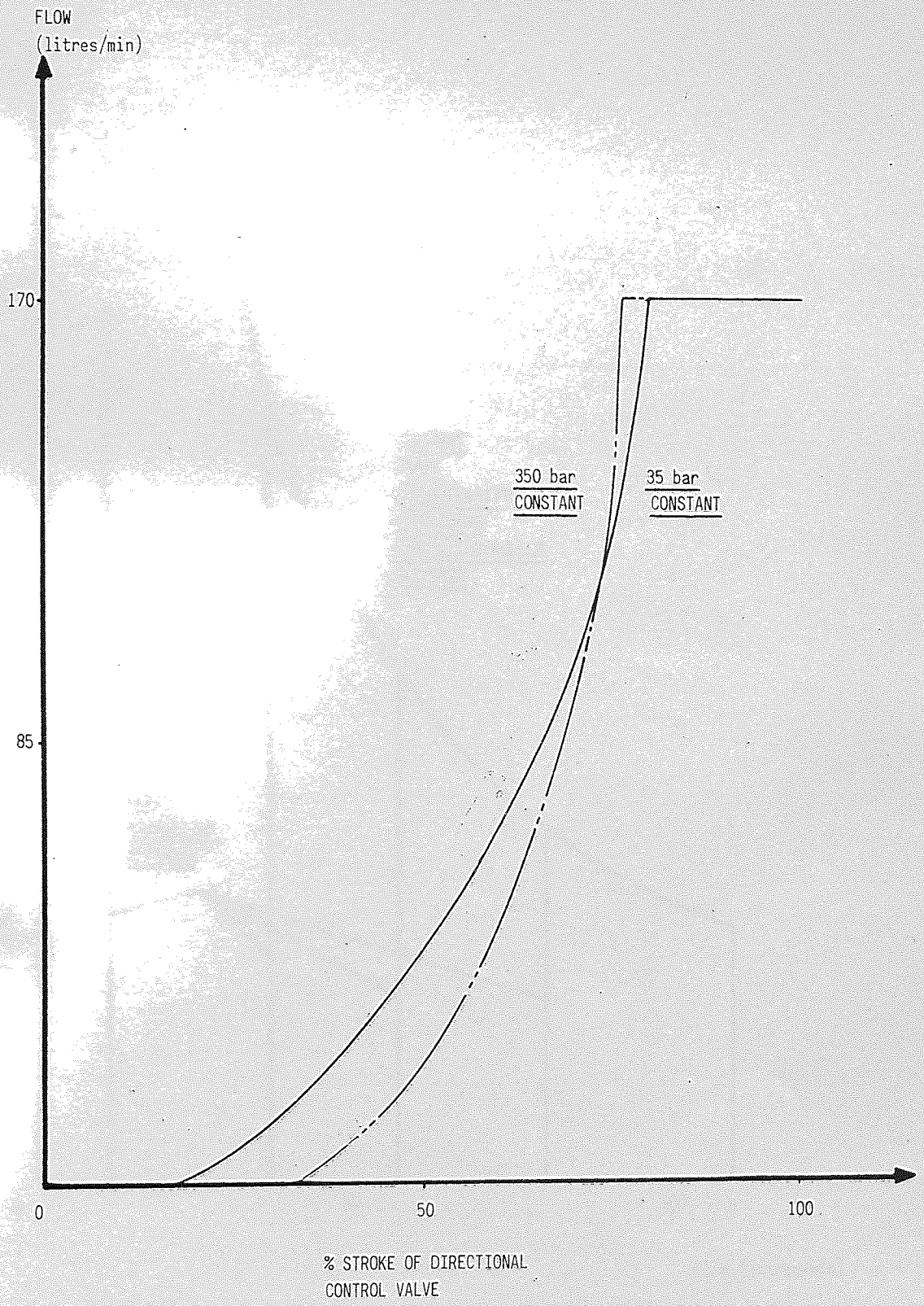

Fig 3.18 PREDICTED METERING CURVES FOR THE CCS CONTROLLER WITH LOAD COMPENSATION

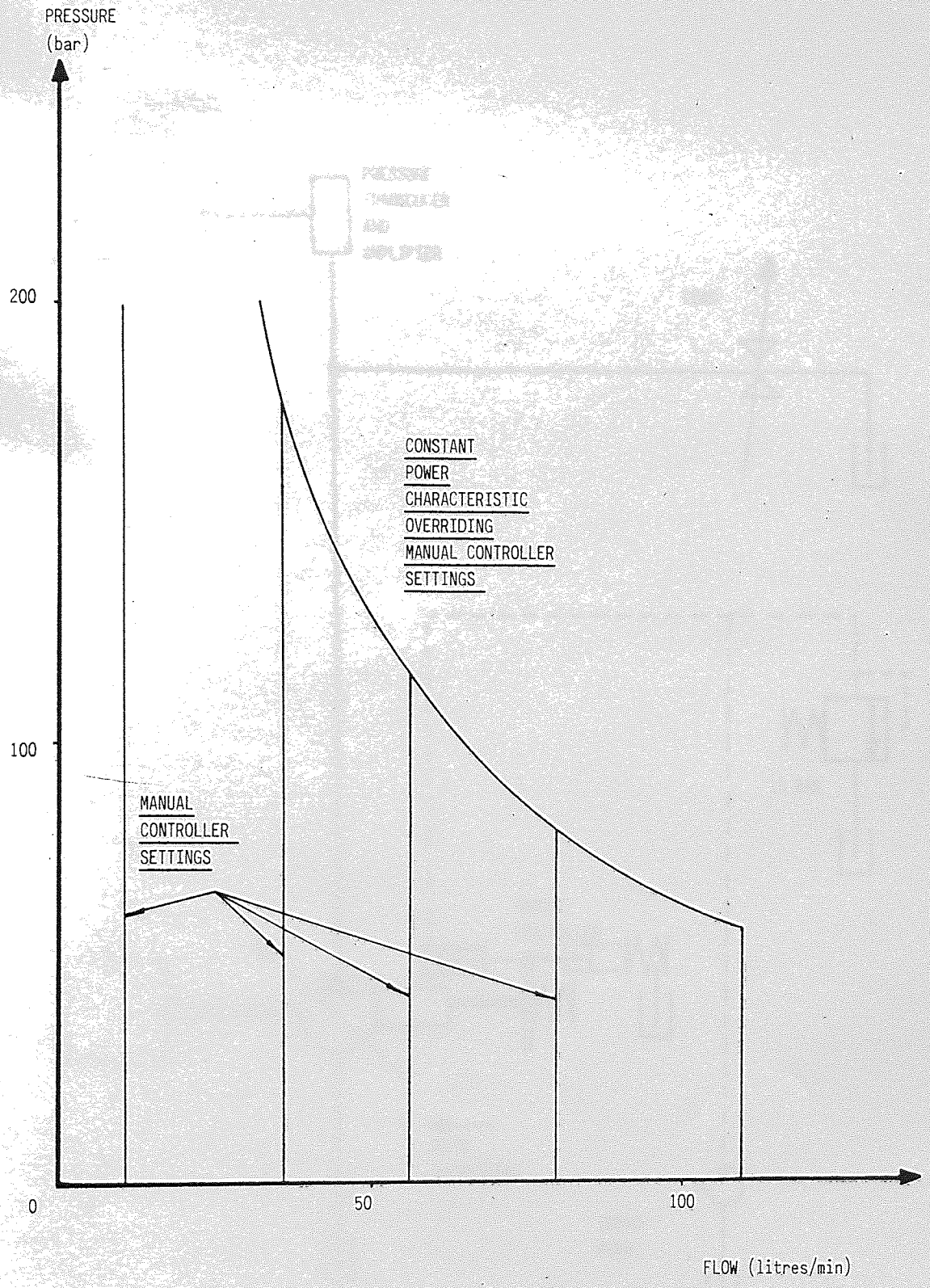

Fig 3.19 CHARACTERISTIC OF THE MANUAL CONTROLLER WITH CONSTANT POWER OVERRIDE

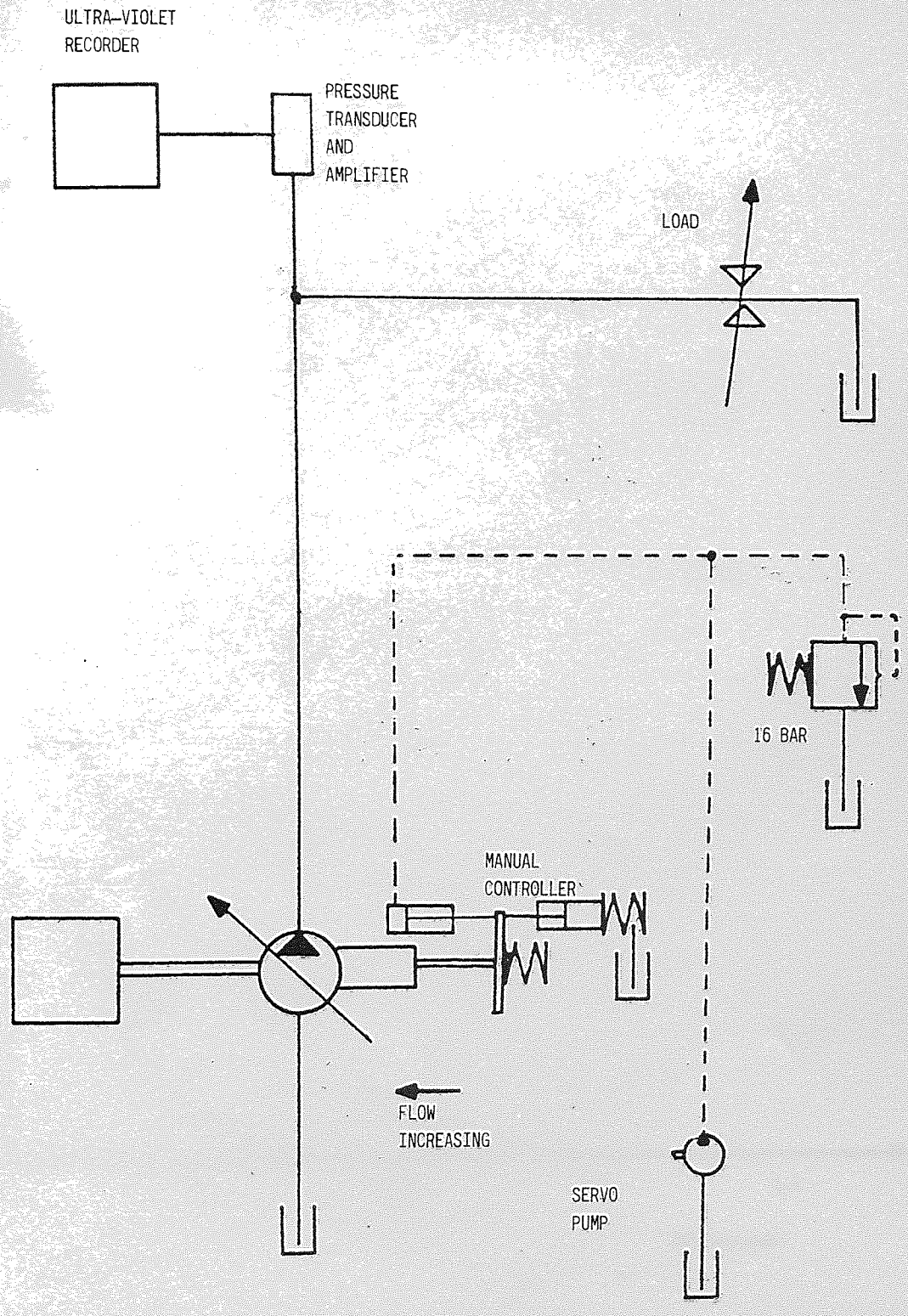

Fig 3.20 THE HYDRAULIC CIRCUIT USED TO DETERMINE THE RESPONSE TIME OF THE PUMP

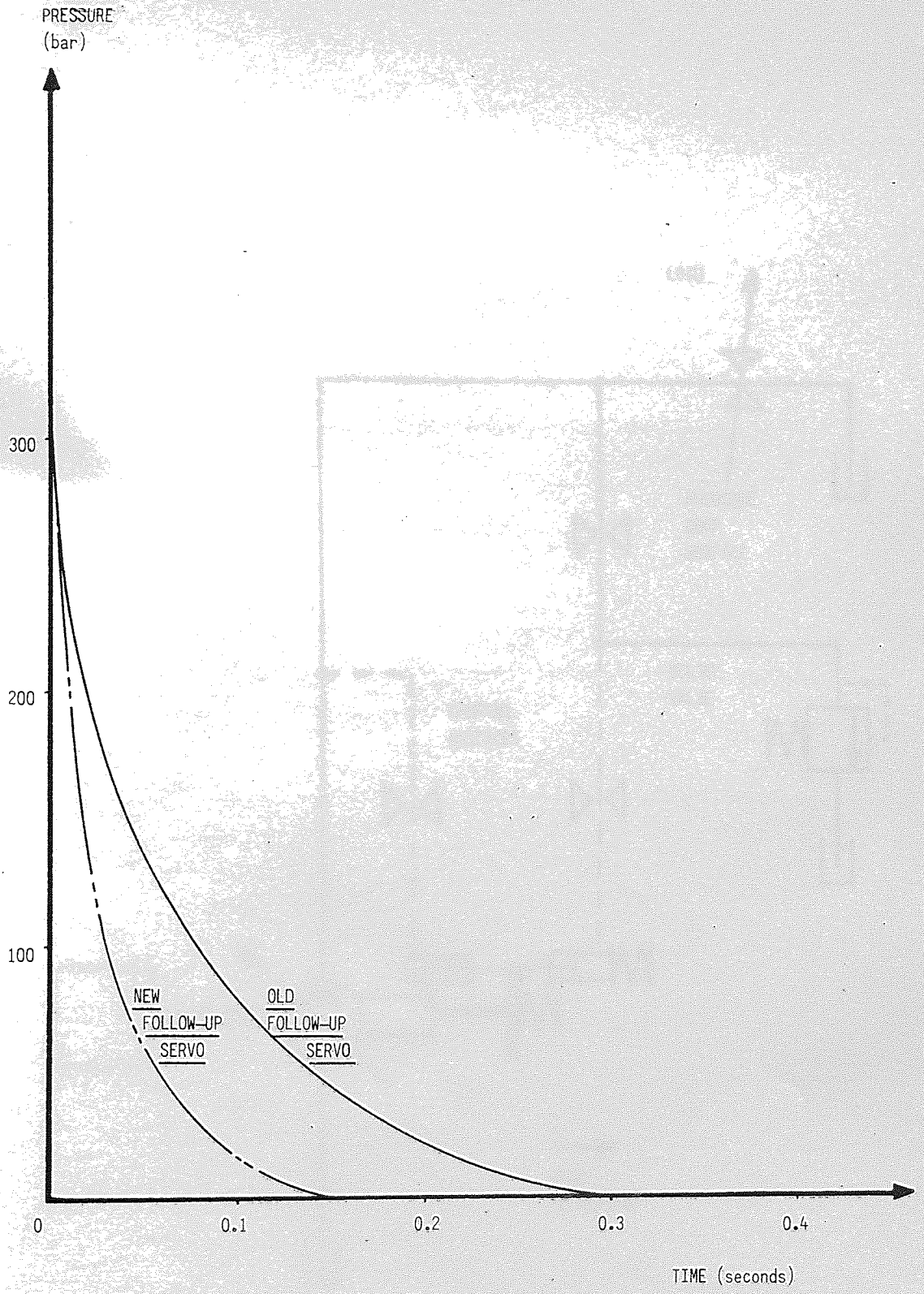

Fig 3.21 RESPONSE OF THE PUMP (FROM MAXIMUM TO MINIMUM FLOW) WITH THE NEW AND OLD FOLLOW-UP SERVO DESIGNS

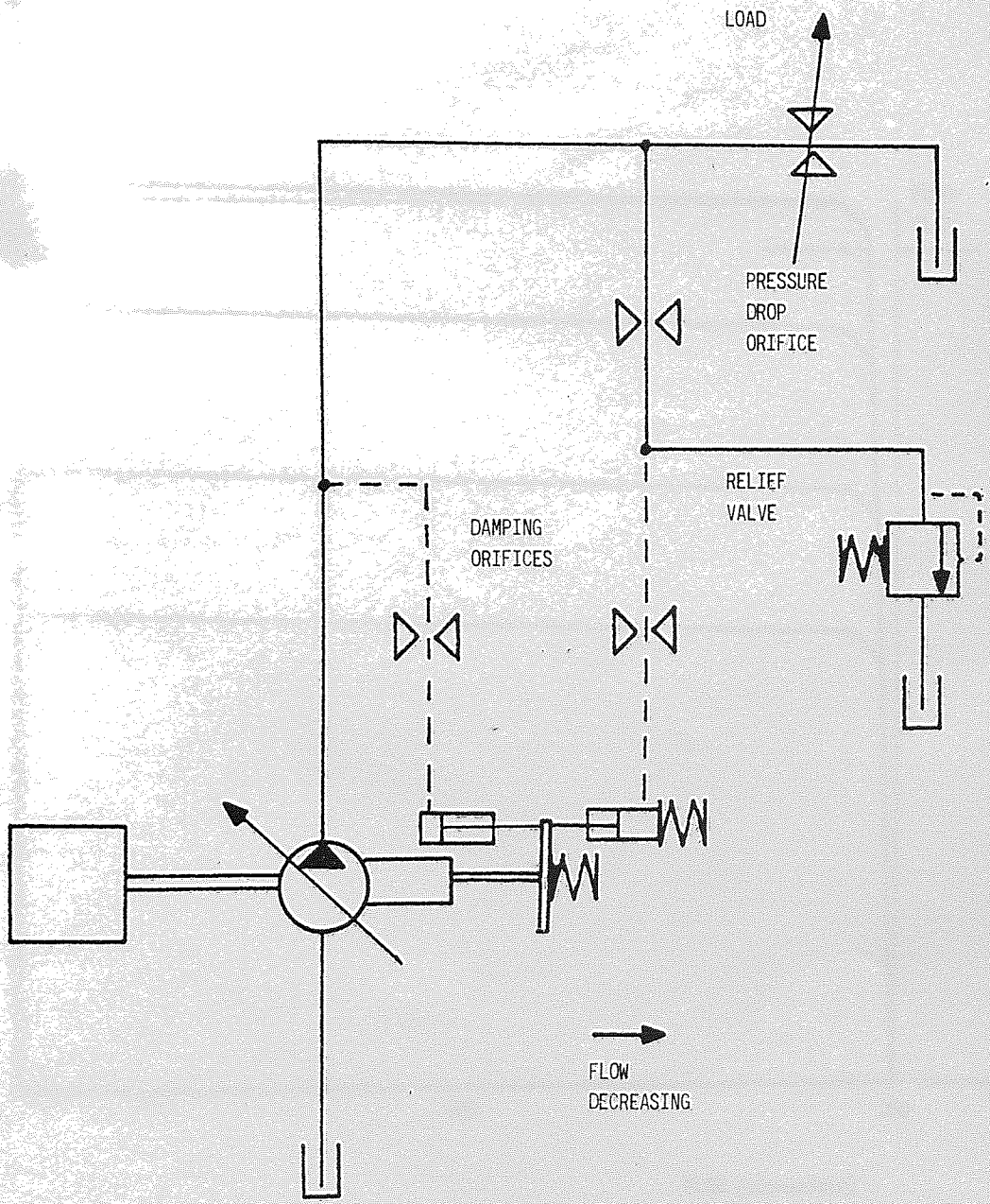

Fig 3.22 PROPOSED NEW PRESSURE COMPENSATING NETWORK

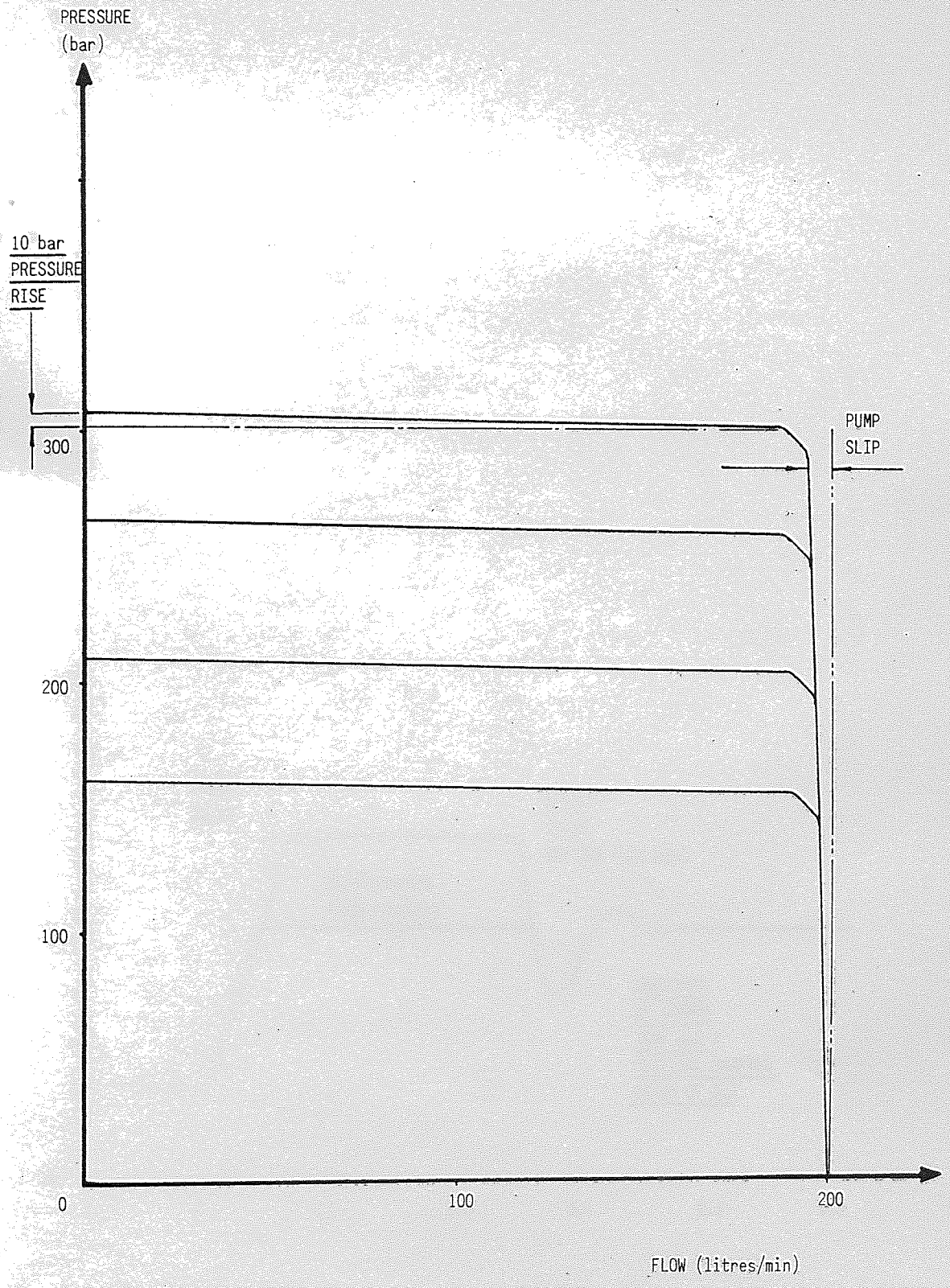

Fig 3.23 A FAMILY OF PRESSURE COMPENSATING CHARACTERISTICS FOR THE NEW, DIRECT ACTING CONTROLLER

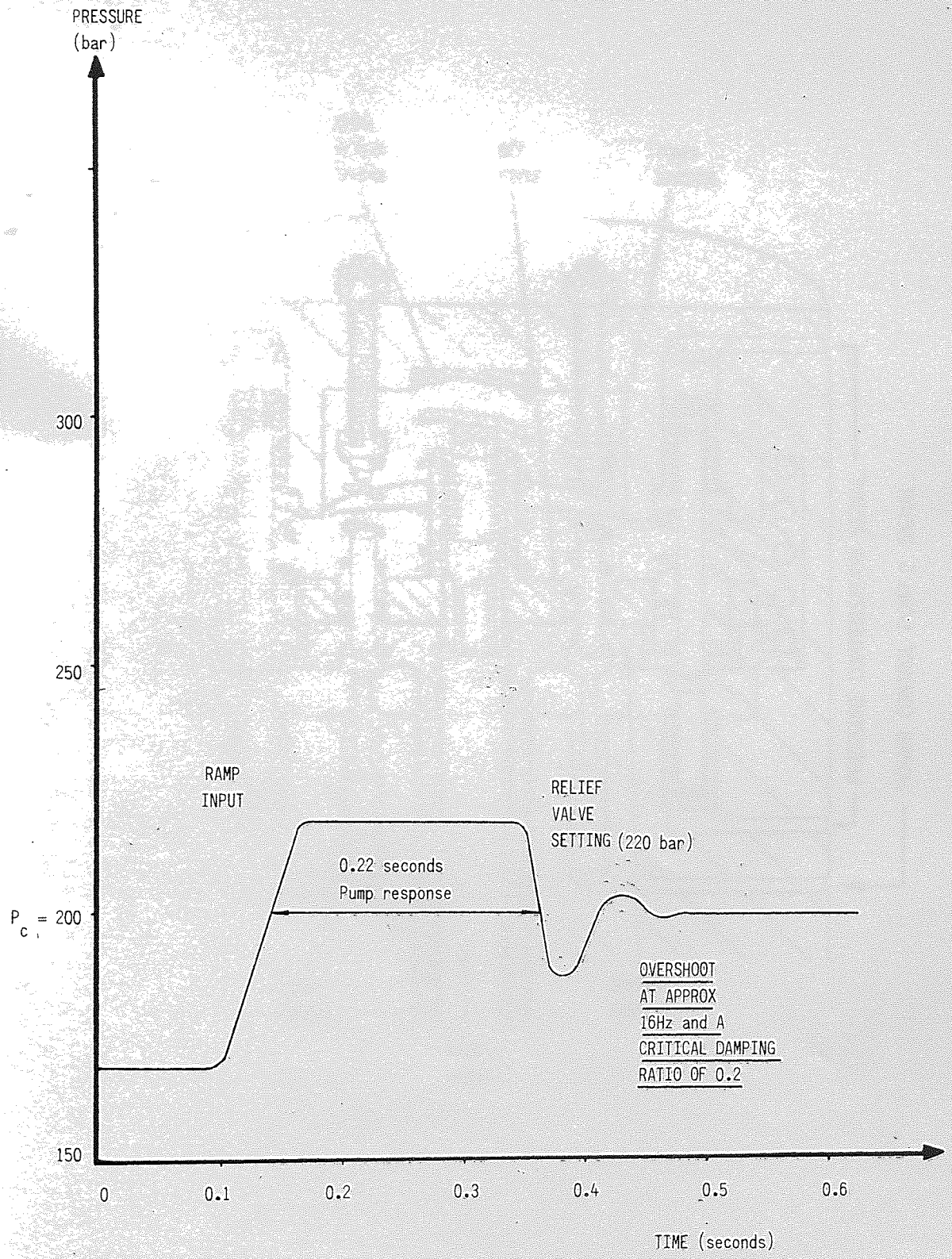

Fig 3.24 RESPONSE OF PUMP WITH A DIRECT ACTING PRESSURE COMPENSATOR TO A RAMP INPUT

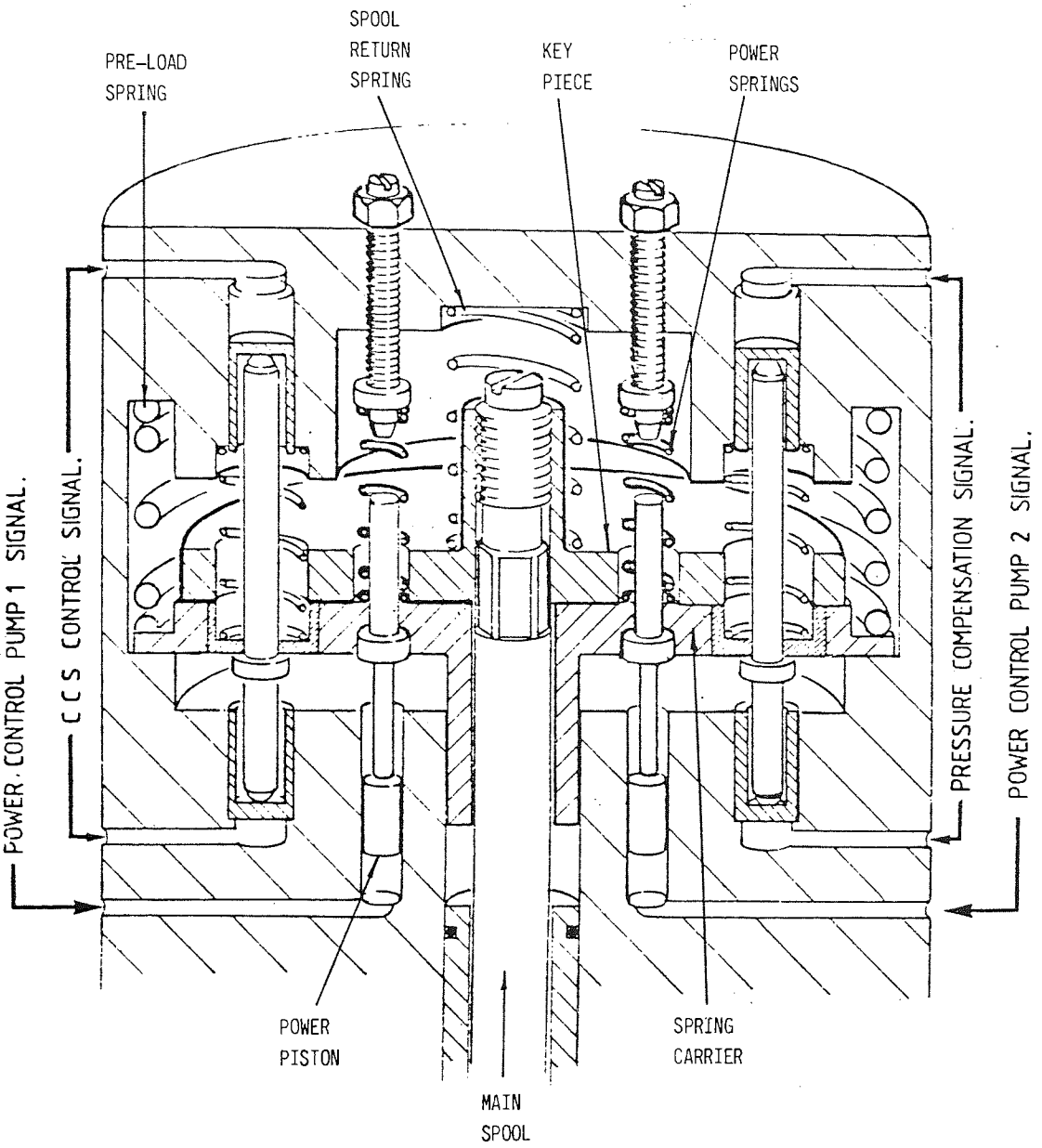

Fig 3.25 A SECTIONED VIEW OF THE NEW CONTROLLER PACKAGE

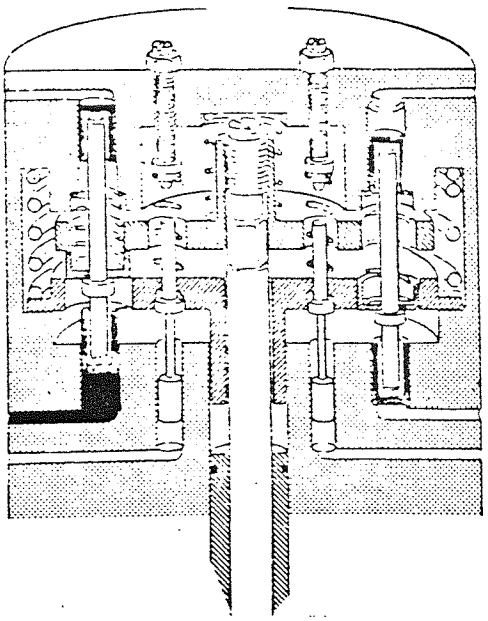

(a) MANUAL CONTROL
(low flow)

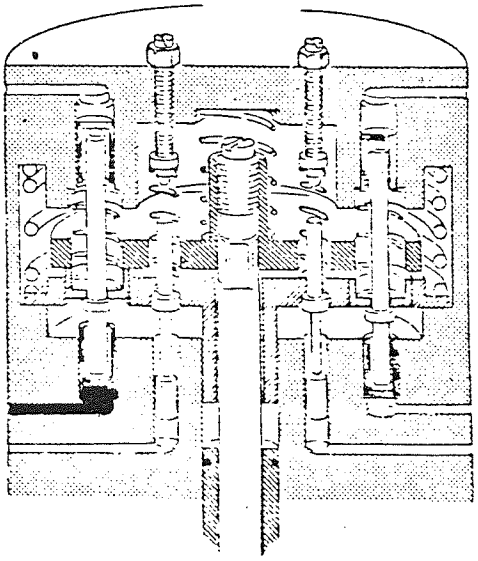

(b) MANUAL CONTROL
(high flow)

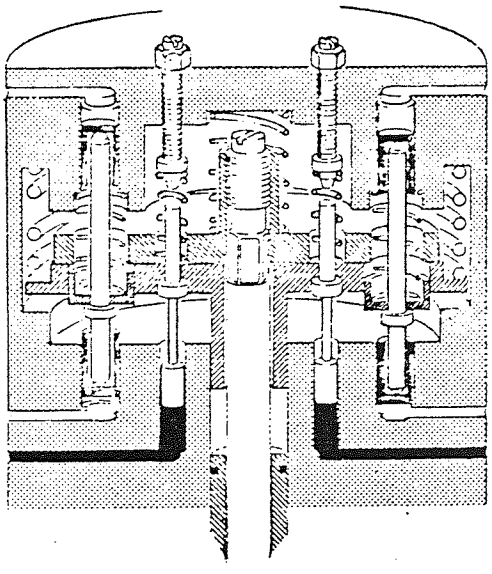

(c) POWER CONTROL

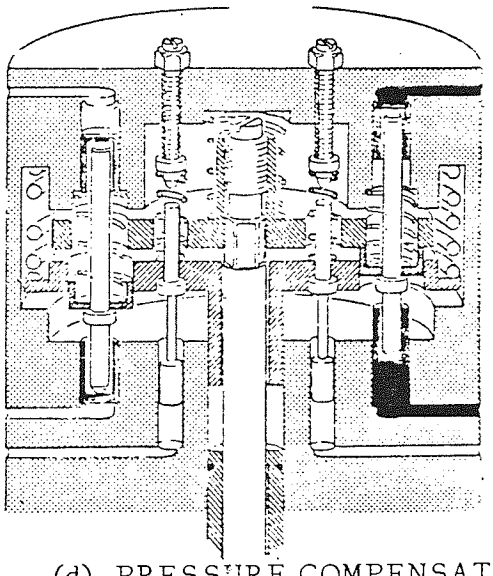

(d) PRESSURE COMPENSATIC

CONTROL PRESSURE

Fig 3.26 OPERATION OF THE NEW CONTROLLER PACKAGE

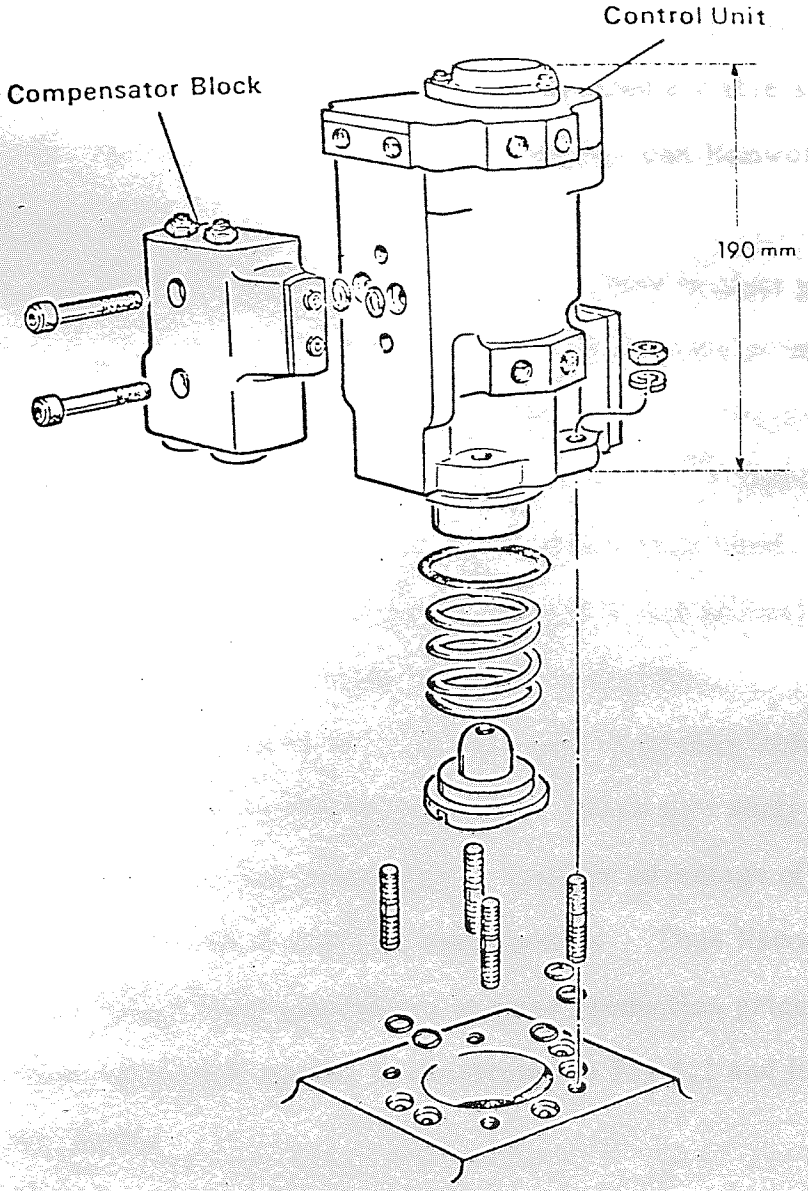

Fig 3.27 ILLUSTRATION OF THE NEW CONTROLLER PACKAGE

CHAPTER 4

FEASIBILITY STUDY INTO A MICRO-PROCESSOR BASED CONTROLLER

4.1 INTRODUCTION

The hydro-mechanical controller package, described in the previous chapter, fulfils the technical requirements of the design specification given in Appendix A 1. However, before it can be considered a viable solution two very important questions must be answered, namely, can Hamworthy produce it and at what cost?

This design is far more complex than any other product presently produced and its manufacture may well create some serious problems. For example, to ensure the correct quality of components will require an estimated £$\frac{1}{4}$ million of new machine tools. This represents a large capital investment at a time when interest payments are at an extremely high level. Also, extra staff will probably be required to plan and progress this product through the factory thus increasing the overhead costs of the factory.

It was realised that these problems could be greatly reduced by using a micro-processor based controller package. Hence this study was undertaken to determine if such a system was viable. Another advantage of an electronically controlled package is that it would be very flexible. Thus Hamworthy could offer customers tailor made controllers at mass production prices.

Such an electronic system is illustrated in Fig 4.1 and it consists of three distinct parts.

1. Position and Pressure Transducers
2. Electro-hydraulic interfaces
3. A micro-processor based electronic control circuit

Each of these must be cheap and reliable if they are to form a viable package. HOLZBOCK investigated the use of micro-processors to control hydraulic equipment and concluded that the least developed of the above areas was low cost sensors. Thus initially, a study was undertaken into the

transducers presently available and special attention was given to pressure sensors.

The variety of pressure transducers on the market was vast but universally too expensive. In an attempt to reduce costs its requirements were analysed and a low performance specification formulated. This was circulated to the leading manufacturers with a covering letter asking if they could supply a low cost, reliable unit. Several manufacturers were interested and supplied samples for evaluation. To ensure the reliability of the transducers they were subjected to an accelerated life test of which two designs look promising to date.

Selection of a suitable position transducer was much easier as linear, variable displacement transformers (LVDT's) are reliable and relatively inexpensive in quantity.

The second area to be investigated was the electro-hydraulic interface. Initially it was thought that a device with a low dynamic performance would be adequate and the leading servo-valve manufacturers were asked if they could supply a suitable, low cost unit. Two were forthcoming and it was suggested that a third interface, used by Hydreco, should also be evaluated. These units were tested in two control modes, firstly in manual control to determine the system's linearity, hysteresis and accuracy, then in pressure compensation to assess the stability of the design.

For the initial evaluation of the interfaces it was proposed to use analogue control circuitry because it was thought that the use of a micro-processor, at this stage, may introduce new problems and cause incorrect conclusions to be drawn.

Hamworthy had shown great interest in the solenoid device used by Hydreco and it was suggested that even if it did not meet the requirements of pressure compensation, then there may be a market for it in a simple manual

control mode alone. An interface for this solenoid was designed and built. In the interim period a simplified mathematical model of the controller in the pressure compensating mode was made with a view to designing electronic stabilising networks. The results of both of these efforts were disappointing. The manual controller was very non-linear and the mathematical model indicated that the system was only marginally stable with a compensating network that had an unacceptably large time constant.

The idea of using a solenoid as an interface was therefore dropped and a new pump stroking interface was designed which used a high performance servo-valve. Initially it was envisaged that a two stage servo-valve was required but from the work on the hydro-mechanical controller, it was felt that the inclusion of this extra stage may adversely affect the stability of the system. A design was then conceived which enabled a single stage servo-valve to directly control the position of the pump by the inclusion of a piston to react the natural de-stroking force of the pump.

A mathematical model was made of the design and the results indicated that, with some compensating networks, the design would be adequately stable. A controller was built and proved to be stable in both the position and pressure control loops.

The next stage of the study was to determine the required conditions for a micro-processor to fulfil the requirements of the design specification. Basically these were to monitor the pump and CCS pressures of up to three pumps, determine the minimum flow for each pump and output these flows as demanded positions to the electro-hydraulic interfaces.

To evaluate the effect of a micro-processor upon the analogue system, a micro-processor development kit was extended to include analogue to digital (A to D) and digital to analogue (D to A) converters. This was inserted in the pressure control loop as a scaler.

The test revealed that the micro-processor induced a limit cycle into the system whose amplitude and frequency depended upon the speed of the pump and the sampling rate of the micro-processor. Initially this was attributed to the resolution and phase lag associated with the micro-processor system. However subsequent tests and analysis revealed this not to be the case.

The effect of alliasing was then investigated and using the micro-processor in an open loop mode confirmed that this was the cause of the problem. However, the magnitudes of these aliased signals were far greater than expected and a subsequent investigation revealed that the pressure ripple from the pump was being amplified by an electrical problem.

Time did not permit this fault to be rectified but it is suggested that, once this has been overcome, the use of a micro-processor to interactively control a pump is technically feasible.

4.2 THE INVESTIGATION INTO PRESSURE AND POSITION TRANSDUCERS

Pressure and position transducers are required to provide the necessary feedback signals for the controller. At the outset of this study it was considered that the existence of a cheap, reliable pressure transducer was unlikely. If such a unit could not be found then the electro-hydraulic controller would not be feasible. It was therefore decided to start this study with a market survey for a suitable pressure transducer and, if this was unsuccessful, then the study could be terminated and considerable resources saved.

The required performance of the pressure transducer was analysed and it was concluded that a fairly large measuring error would be acceptable. The following design guide was circulated to fifty manufacturers and they were asked whether a unit could be made for £5 (1978 prices) at an annual rate of 50,000, (this represents Hamworthy's estimated total requirement for both

electro-hydraulically controlled pumps and valves).

Pressure Range	0 to 350 bar
Measuring error (total)	± 2% (fsd)
Life	10,000 hours or 10^7 cycles

As a result of the survey six transducers were received for evaluation. They encompassed a wide selection of designs ranging from strain gauged beams to silicon diaphrams. To assess the reliability of life of these transducers an arduous accelerated life test was designed which subjected the units to a square wave pressure pulse of 0 to 300 bar, peaking to 350 bar, at a frequency of 45 Hz, all at a temperature between 70 and 80°C. It was estimated that the rate of change in pressure during this test was approaching 100,000 bar/s which was ten times more severe than would be experienced on a machine.

The results from this test are most encouraging and to date two transducers have met the target cost and design specification.

The selection of a suitable type of position transducer was easier because there were only two fundamentally different designs to choose from at the required price. These were potentioneters and LVDTs. Of these, the LVDT is the more reliable because it contains no wearing parts. However LVDTs require oscillator/demodulator circuits, which are an additional expense compared with potentiometers.

Several manufacturers were asked to quote for supplying both types of transducer and the resulting prices, including the electronics for the LVDT, were very similar. Thus it was proposed to use LVDTs to monitor pump position.

4.3 THE DESIGN OF THE ELECTRO-HYDRAULIC INTERFACE

Traditionally servo-valves have been used in aerospace and industrial applications where high accuracy is required but the number of units is small.

However recently, servo-valve manufacturers have become aware of the potential for their products in the high volume, earth moving machinery and crane markets, as predicted by MASKREY & THAYER. Two manufacturers have designed special low cost units to meet this new demand and they were approached by Hamworthy to supply prototypes for evaluation.

While these units were being made it was suggested that the solenoid based interface, used by Hydreco to control valve position, should be evaluated. This unit had the advantages that it was cheap, did not require a servo supply, used no quiescent flow and was fail safe. It was believed that it would be suitable for all control modes but even if it was not, then there may still be a market for it as a simple pump position controller. The Hydreco design was adapted for use on the piston pump and details of it are given in Appendix A 8.

It was proposed that the electro-hydraulic interfaces need only be evaluated in manual and pressure compensating control modes. From the results of the manual controller the linearity, hysteresis and following error of the interface could be evaluated. From the work on the hydro-mechanical controller it was known that pressure compensation was the most difficult control option to stabilise. Thus, if the interface was successful in this mode it would also be suitable for CCS and constant power control.

In between designing and manufacturing the solenoid based interface a simplified, mathematical model of it was produced to predict the stability of the system in the pressure compensating control mode and details of it are included in Appendix A 8. The results from the model indicated that the system was very unstable, requiring an unacceptably large phase lag filter with a 10.0 second time constant, before the instability was eliminated. No electronic control circuitry was therefore made for the controller in pressure compensation. However, the interface was used to control pump position. The resulting characteristic of position against that demanded was very non-

linear and it was concluded that if this design was to be pursued position feedback must be incorporated to overcome this problem.

The next pump controller design was based upon a high performance, low cost, single stage servo valve and a schematic of the proposed system is shown in Fig 4.2. The single stage valve controls the position of a self-centralising, amplifying spool which directs flow to (or from) the pump position control pistons. The design is an integrating system and so pump position is fed back to the control circuit and subtracted from the demand signal. While there is no difference between these signals the pump stroke remains constant.

The advantage of this design is that it uses pump pressure for control and so no servo pump is required. However, previous work on hydro-mechanical pressure compensating networks indicated that, the fewer stages required in the design, the more stable the system.

A new, simpler design, shown in Fig 4.3, was therefore proposed in which the single stage servo-valve directly controls the position of the pump. The difficulty in doing this is that the flow from the valve is very limited and so the driving pistons must be small if a reasonable response time is to be achieved. However, reducing the size of the control pistons implies that there will be insufficient force to control the pump. The design shown in Fig 4.3 overcomes this problem by balancing the pump reaction force, in the plane of the controller, with a small piston at pump pressure. Thus, the required force to control the pump has been reduced to a reasonably low level and smaller pistons can satisfactorily be used.

This new system was mathematically modelled and details of it are given in Appendix A 9. The results from the simulation indicated that with no stabilising networks the position loop was only marginally stable, as shown in Fig 4.4. A lag/lead network was then introduced into the forward path and its effect was to increase the stability margins to satisfactory values, as shown on Fig 4.5

The pressure loop also required compensation to achieve satisfactory stability margins. This consisted of a phase lead plus a lag/lead network and the resulting pressure OLTF is shown on Fig 4.5.

The position loop was then tested and, as predicted in Appendix A 9, the resulting flow characteristic varied by ± 5% depending upon the operating conditions of the pump. This was due to external factors, such as speed, changing the reaction force of the pump. However, it was found that this could be virtually eliminated by increasing the forward loop gain of the system.

Some increase in gain came from increasing the servo supply to 70 bar but this was considered to be the maximum desirable value and hence further increases were achieved electronically.

The result of this was that the position loop was still stable but a limit cycle of ± 3% of maximum travel at 25 Hz was introduced.

With the forward loop gain set to 1025 the electronic circuit was saturating and this was causing the system to oscillate. One of the advantages of saturation is that phase lead can be introduced into the system without affecting the gain, as this is already at a maximum. It was therefore suggested that the amplitude of the limit cycle could be reduced if the lag/lead network were to be replaced by a phase lead system. The time constant of the lead network was chosen to coincide with the natural frequency of the pump to partially offset the phase lag introduced by its motion. The result of this was to reduce the amplitude of the limit cycle to ± 2% of maximum travel and the frequency rose to 55 Hz.

To gain a better understanding of the system the effect of saturation was included in the model given in Appendix A 9. The model predicted limit cycling but at a far higher frequency than occurred in practice. A subsequent investigation revealed that the transistor output stage of the electronic circuit was producing a large phase lag and that the saturation of the circuit was

affecting the frequency response of the servo-valve.

The frequency response of the electronic control circuit, with the phase lead network, was then measured using a frequency response analyser and the results are given in Fig 4.6.

With regard to the servo-valve the operating conditions in practice were, a current input of ± 100% of maximum and a servo supply pressure of 70 bar. These were significantly different from the conditions used to produce the frequency response given in Fig A 9.2 and the manufacturers estimated that the bandwidth of the valve under these new conditions would be only 25% of that assumed. Thus the time constant (T) for the servo-valve used in Appendix A 9 should be 0.0072 rather than 0.0018 seconds.

These two effects were included in the stability analysis and the resultant Nyquist plot is shown in Fig 4.7. This indicated that the system should limit cycle at 80 Hz with an amplitude of ± 1.7%.

No further attempt was made to improve the correlation between the practical and theoretical results as the accuracy of the model was considered sufficient to explain the behaviour of the system.

Attention was then turned to further improving the performance of the control loop. To fully compensate for the phase lag created by the pumps motion, a second phase lead network was introduced at 6 Hz. The effect of this was to reduce the amplitude of the limit cycle to ± 0.5% of maximum travel and raise the frequency to 75 Hz.

This flow ripple was barely perceptible and it was considered to be advantageous as it would reduce hysteresis, rather like dither.

The close loop frequency response of the position loop was then measured and the results are plotted on a Bode diagram in Fig 4.8. The transfer function of the load in the stalled state and the gain of the pressure compensating circuit were then added to produce the pressure compensating open loop transfer

function (OLTF) of the system in its least stable state.

The reason for using the theoretical transfer function for the load and deducing the pressure OLTF, rather than directly measuring it, was for safety. Exciting the pump in a closed outlet condition could lead to extreme over pressurisation and could easily damage the pump.

The gain margins shown on Fig 4.8 were initially too low and so a lag/lead network was introduced at low frequency to give some attenuation at higher frequencies. The resulting OLTF is shown in Fig 4.9 and it illustrates that the gain and phase margins were increased to the acceptable values of 12 db and 30° respectively.

This controller was then tried in practice and the system was indeed stable and the final design of the electronic control circuit is described in Appendix A 10.

It was then proposed that the single stage servo-valve driving the scheme shown in Fig 4.3 should be used to test the effect of a micro-processor upon the pressure compensating control loop.

4.4 THE EFFECT OF A MICRO-PROCESSOR UPON THE ANALOGUE PRESSURE COMPENSATING CONTROLLER

The use of a micro-processor based system to control the flow from hydraulic pumps is not as straightforward as using analogue circuitry because of problems associated with sampling the control signal. These problems are that the process introduces a time delay into the loop, a resolution into the characteristic and can create false signals due to 'aliasing'.

To evaluate the effect of a micro-processor it was decided to include one in the forward path of the analogue pressure compensating controller. A RCA 1802D micro-processor kit was fitted with A to D and D to A converters. The maximum sampling rate of the system was then measured on an oscilloscope and found to be 1 KHz.

The micro-processor was then inserted in the pressure compensating loop as a scaler and a program was written to vary its sampling rate. The effect of the micro-processor was to induce a limit cycle into the system. The magnitude and frequency varied with sampling rate and speed and a series of recorded results are shown in Fig 4.10. The maximum amplitude was ± 5 bar which was not acceptable.

Initially it was thought that this could be the effect of resolution. The 8-bit A to D converter gave 255 discrete output levels to cover the analogue input range. With the first test the input signal was set to give the maximum resolution. When the cycling was noticed the resolution was decreased in order to establish if this was the cause of the problem. The result was that no difference in the limit cycling was noticed with the number of sampling levels as low as 25.

Attention was then turned to determining the phase lag associated with digitising an analogue signal. TOU demonstrates that the effect of the D to A converter is similar to a simple lag network with a time constant equal to twice the reciprocal of the sampling rate. Thus, with a sampling rate of 1 KHz the break frequency is 500 Hz. This was an order of magnitude greater than the bandwidth of the pressure compensating controller and it was therefore concluded that it would have an insignificant effect upon stability.

TOU also illustrates that the act of sampling the analogue signal affects the frequency response of the system. However, this again is dominant at (and above) half the sampling frequency and so, for the same reason as above, its effect was considered to be very small.

It was then proposed that these oscillations were due to aliasing errors caused by a mis-match between the sampling frequency and the frequencies of the components in the pressure signal. A digital computer, with a very high sampling rate, was used to perform a Fourier analysis on the pressure signal

at different speeds. The results of these tests are shown in Fig 4.11.

The Shannon theorem of sampling states that, to avoid aliasing, the sampling frequency must be twice the highest frequency present in the signal.

The Fourier analysis results at 2500 rpm indicate that the dominant frequencies are 291, 875 and 2042 Hz. The latter two being well above half the maximum sampling rate of the micro-processor. This would confuse the micro-processor and cause it to oscillate the system.

To categorically prove that the limit cycling was caused by aliasing the micro-processor was used in an open loop mode to sample the pressure signal. The operating conditions were set equal to those for pressure compensation except that the pump was mechanically fixed at a low stroke and therefore, there was no control loop.

The speed and pressure of the pump and the sampling rate of the micro-processor were set equal to the conditions specified in Fig 4.10 and the signal from the D to A converter was monitored on an oscilloscope. The resulting output signals, given in Fig 4.10, coincided with the magnitudes and frequencies of the limit cycling, also given in Fig 4.10, and so it was concluded that aliasing was indeed the cause of the problem.

To further demonstrate the effect of aliasing the micro-processor was used to monitor the sine wave output of a function generator and again, the output was monitored on an oscilloscope. This clearly showed how low frequency, aliased signals could be generated from a very high frequency input. It also illustrated that the system was indeed similar to a filter, as indicated by TOU, and that the aliased signal was attenuated as the input frequency was increased. With a sampling and input frequency of 1 KHz, the attenuation was approximately -20 db.

This indicated that aliasing should not be a problem. The Fourier analysis, shown in Fig 4.11, revealed that the maximum amplitudes of the

pressure ripple, at 875 Hz, was 5 bar. Therefore, with a 1 KHz sampling rate, the aliased signal should be approximately only one tenth (-20 db) of this and at ± 0.5bar it would be quite acceptable. Clearly, aliasing alone was not creating the large magnitude of the limit cycling.

It was then proposed that there may be a fault in the electronic circuit. A subsequent investigation revealed that the lag/lead network in the pressure compensating network, shown in Appendix A10, was not behaving correctly. It was attenuating low frequency noise, as the mains component in the pressure transducer signal was eliminated. However, the pressure ripple from the pump was amplified to an equivalent value of ± 50 bar.

This signal was then sampled by the micro-processor and thus, with -20 db attenuation, the resulting aliased signals had a magnitude of approximately ± 5 bar.

Of course, this same effect was also present when the pressure compensating control circuit was purely analogue. However, in this case, the attenuation at the pumps fundamental frequency from Fig 4.9, is at least -45 db. Thus, an input of ± 50 bar at 175 Hz (fundamental pump frequency for 1500 rpm), would produce a pressure ripple of only ± 0.3 bar.

Time did not permit this electrical fault to be rectified but it was suggested that the most likely cause of the problem was the use of low quality components.

4.5 DISCUSSION ON THE MICRO-PROCESSOR BASED CONTROLLER PACKAGE

From the results of the previous section it was concluded that a micro-processor based controller is technically feasible. To gain an idea of its cost, the requirements of the most complex installation, shown in Fig 4.1, were considered. This consisted of three electro-hydraulic interfaces (as illustrated in Fig 4.3), six pressure transducers, one magnetic pick-up and one micro-computer. The costs of the first three of these was readily available but the requirements of the micro-computer needed more consideration.

Regarding the sampling rate of the micro-computer, the most critical component is the A to D converter. Although very fast converters are available, they are expensive. To keep the cost of the system to a reasonable level requires the use of fairly slow units such as the 16 channel version offered by National Semi-conductor. This has a maximum sampling rate of approximately 6 KHz. Thus with seven channels the sampling rate per transducer is at 857 Hz. In practice some sampling rate capability will be lost due to multiplexing and therefore a more practical figure would be 800 Hz. From the results shown in Fig 4.10, once the amplifier problem has been rectified, such a rate should be more than adequate.

The second point to consider in selecting an A to D converter is the resolution required. The cheapest units are 8-bit devices and give 255 discrete output values for the complete range of the analogue input signal. With respect to pressure compensation, if the micro-processor is required to monitor the complete pressure range of the pump, then the number of samples available for the pressure compensating control band will be only 25, 10% of maximum. Whether this would be a problem was tested earlier in the Chapter and the results indicated that such a poor resolution would not affect the system.

In conclusion therefore, an 8-bit, 16 channel, National Semi-conductor A to D converter, part number ADC0816CCN, should be adequate for this application.

The output stage of the system, the D to A converter, should not create any problems as very low cost units are capable of outputting signals at rates in excess of 10 KHz.

This application should not pose a serious problem to any n-mos micro-processor, such as the Intel 8085. This has a machine cycle time of approximately 1.3 μs. The majority of operations require two machine cycles thus some 480 should be able to be executed in between samples if each

transducer is monitored at 800 Hz. A block diagram outlining the necessary control program for the micro-processor is shown in Fig 4.12 and it was estimated that this would only require 200 operations. The selection of the micro-processor should therefore be based upon price and it is recommended that a review of available units should be performed in the near future.

Using this information a comparative cost study was then undertaken between the electro-hydraulic and hydro-mechanical controller packages, taking into account machine tool depreciation, interest payments and component costs. This revealed that the electro-hydraulic system was approximately 60% more expensive than the hydro-mechanical controller.

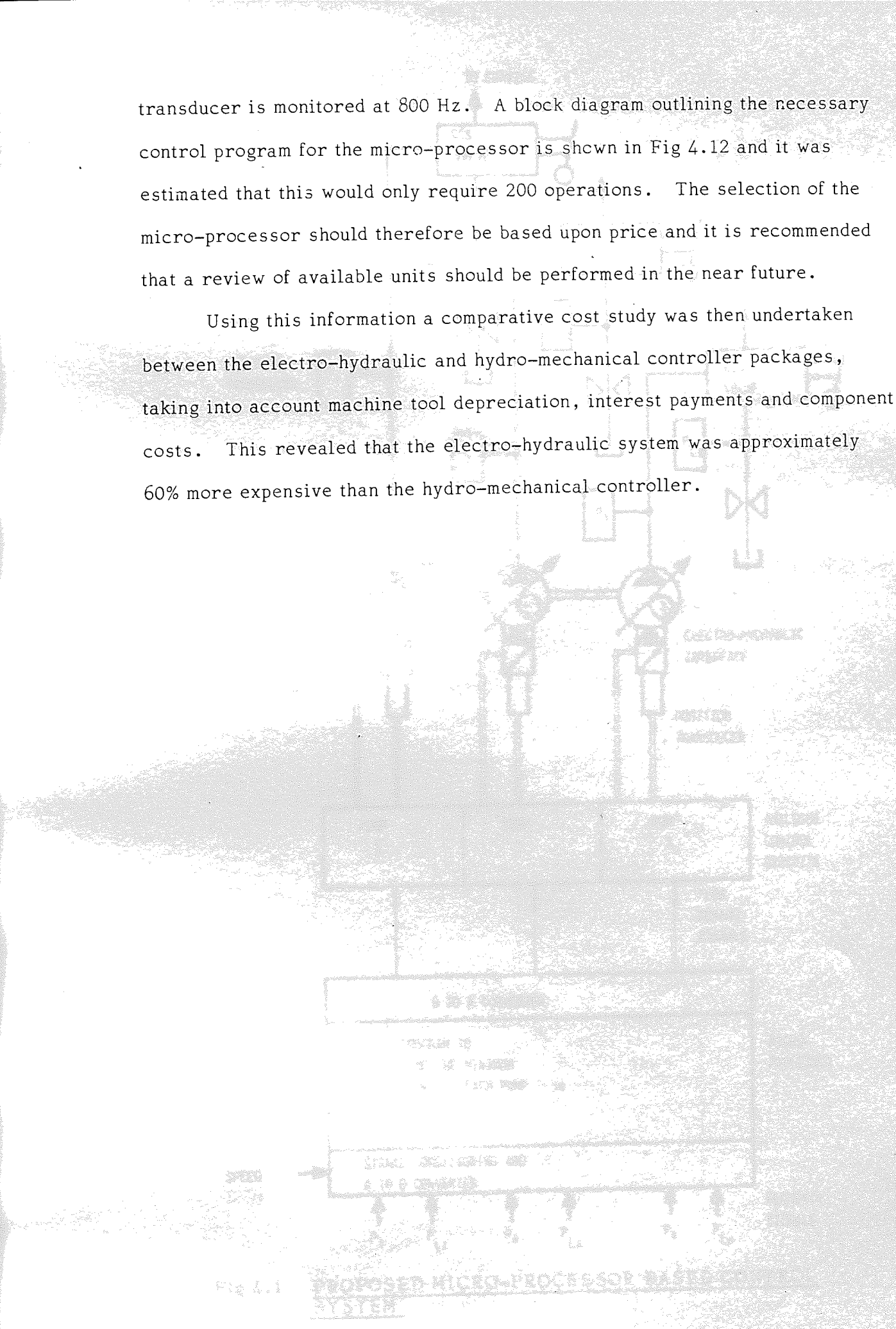

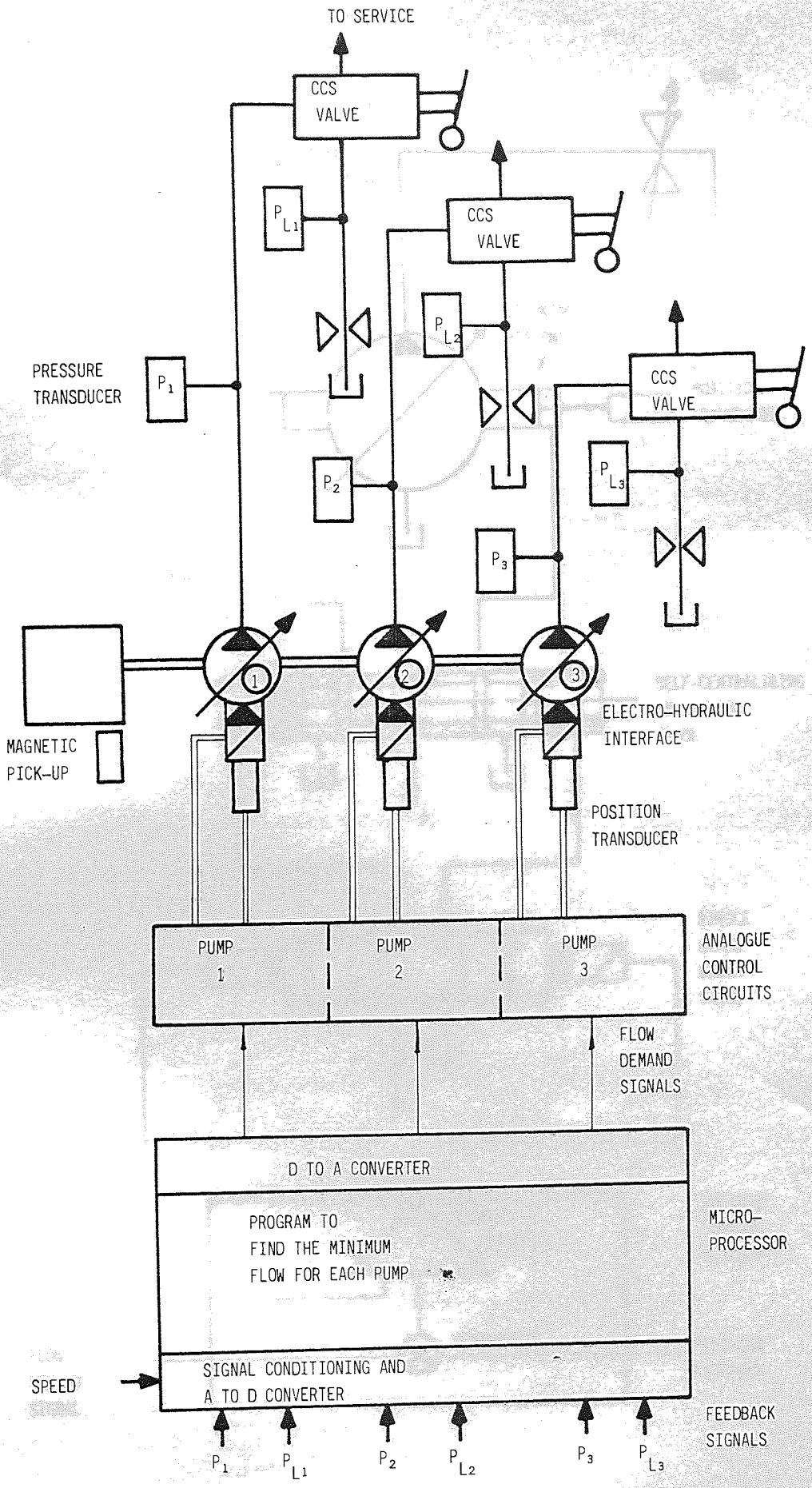

Fig 4.1 PROPOSED MICRO-PROCESSOR BASED CONTROL SYSTEM

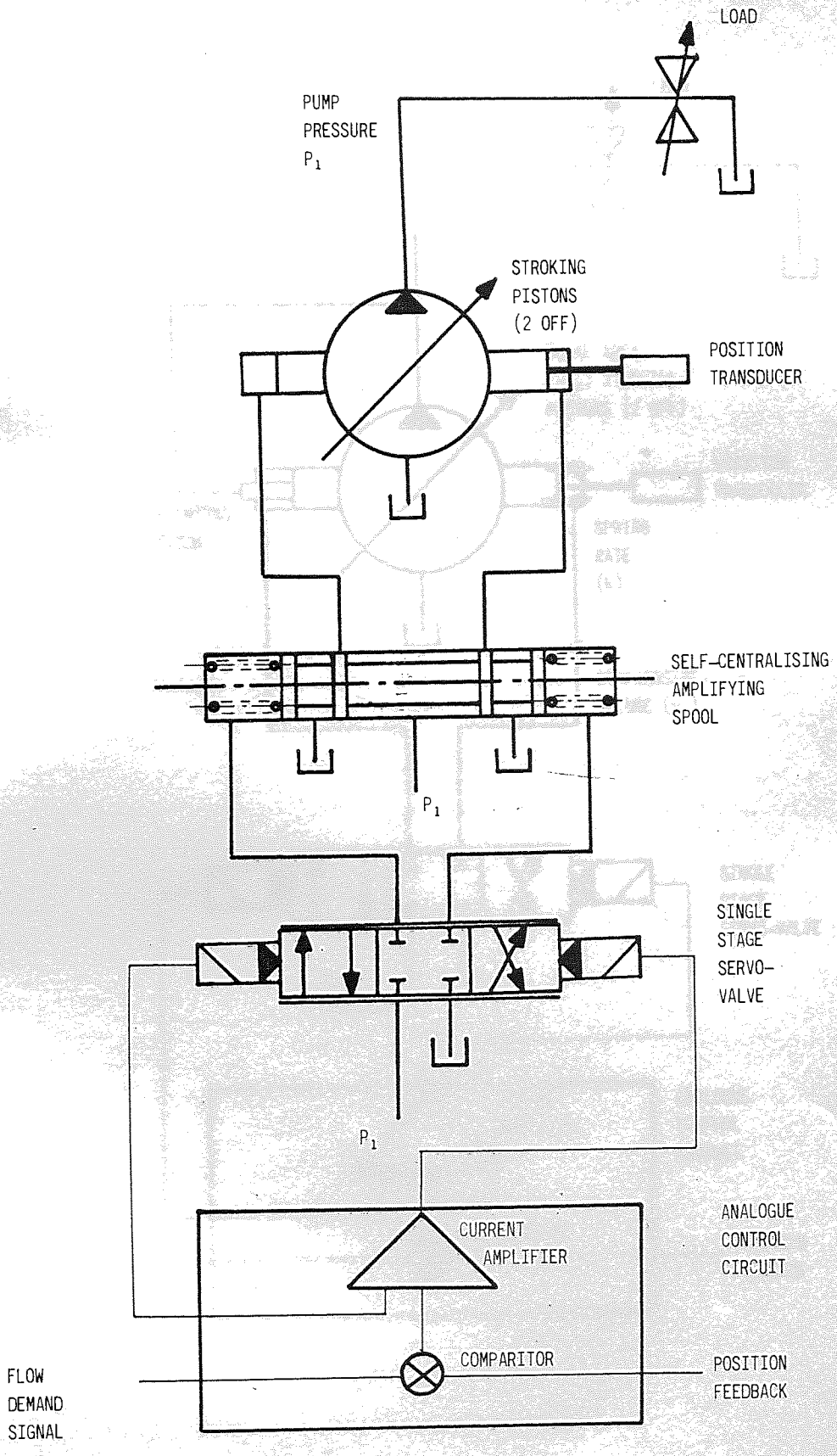

Fig 4.2 PROPOSED TWO STAGE ELECTRO-HYDRAULIC POSITION CONTROLLER

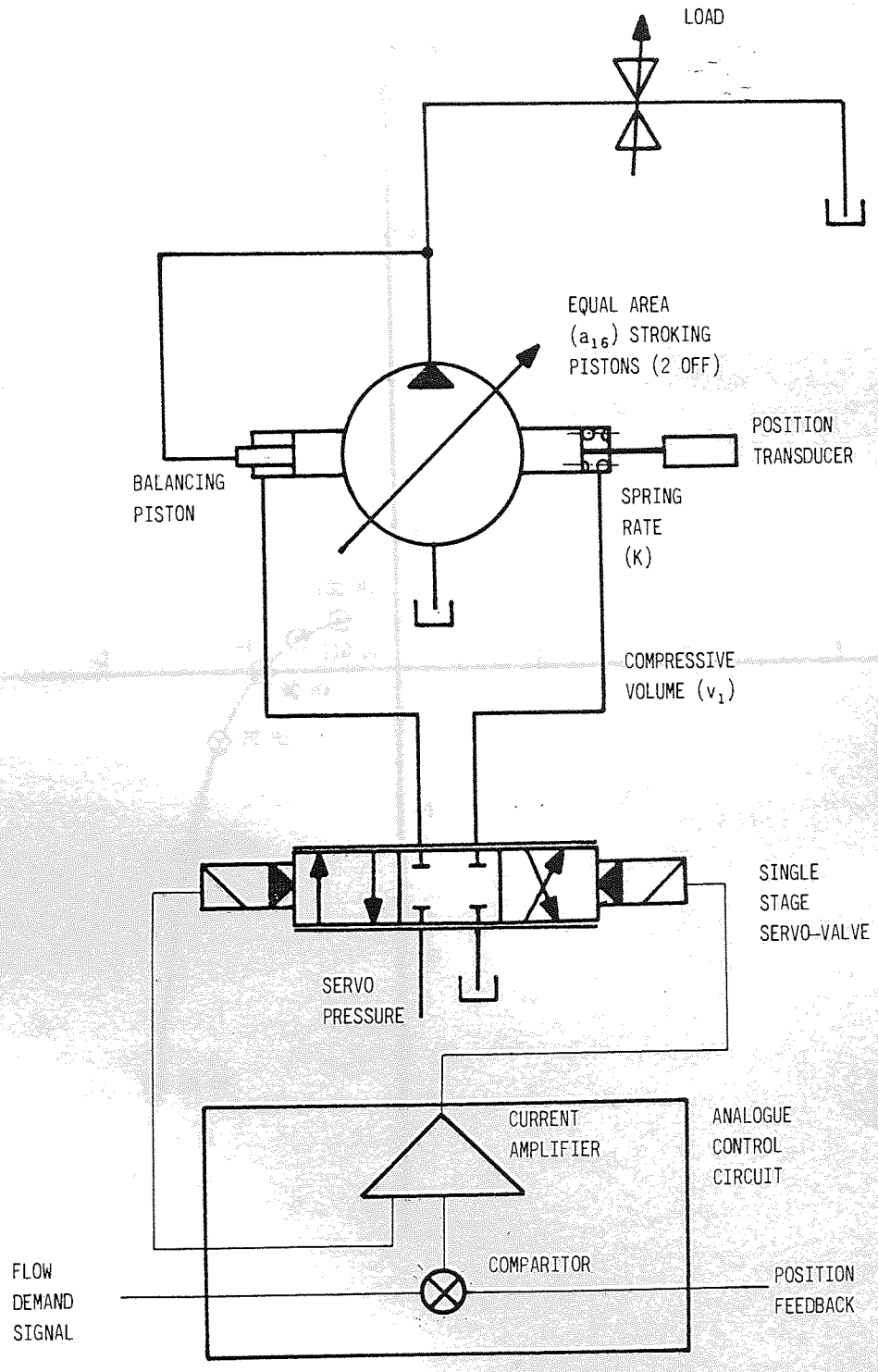

Fig 4.3 ADOPTED ELECTRO-HYDRAULIC POSITION CONTROLLER

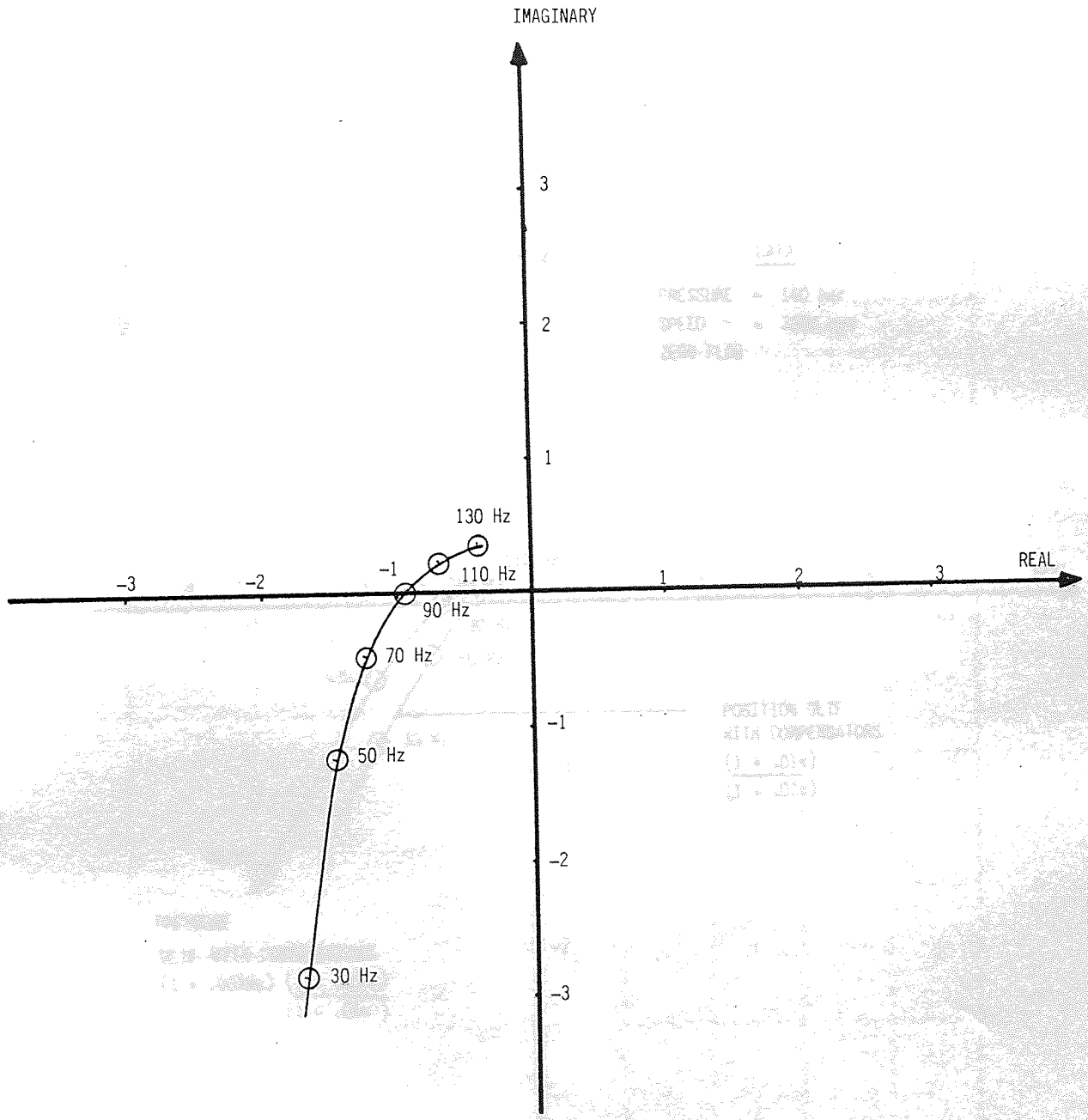

Fig 4.4 NYQUIST PLOT FOR THE POSITION CONTROL LOOP (UNCOMPENSATED)

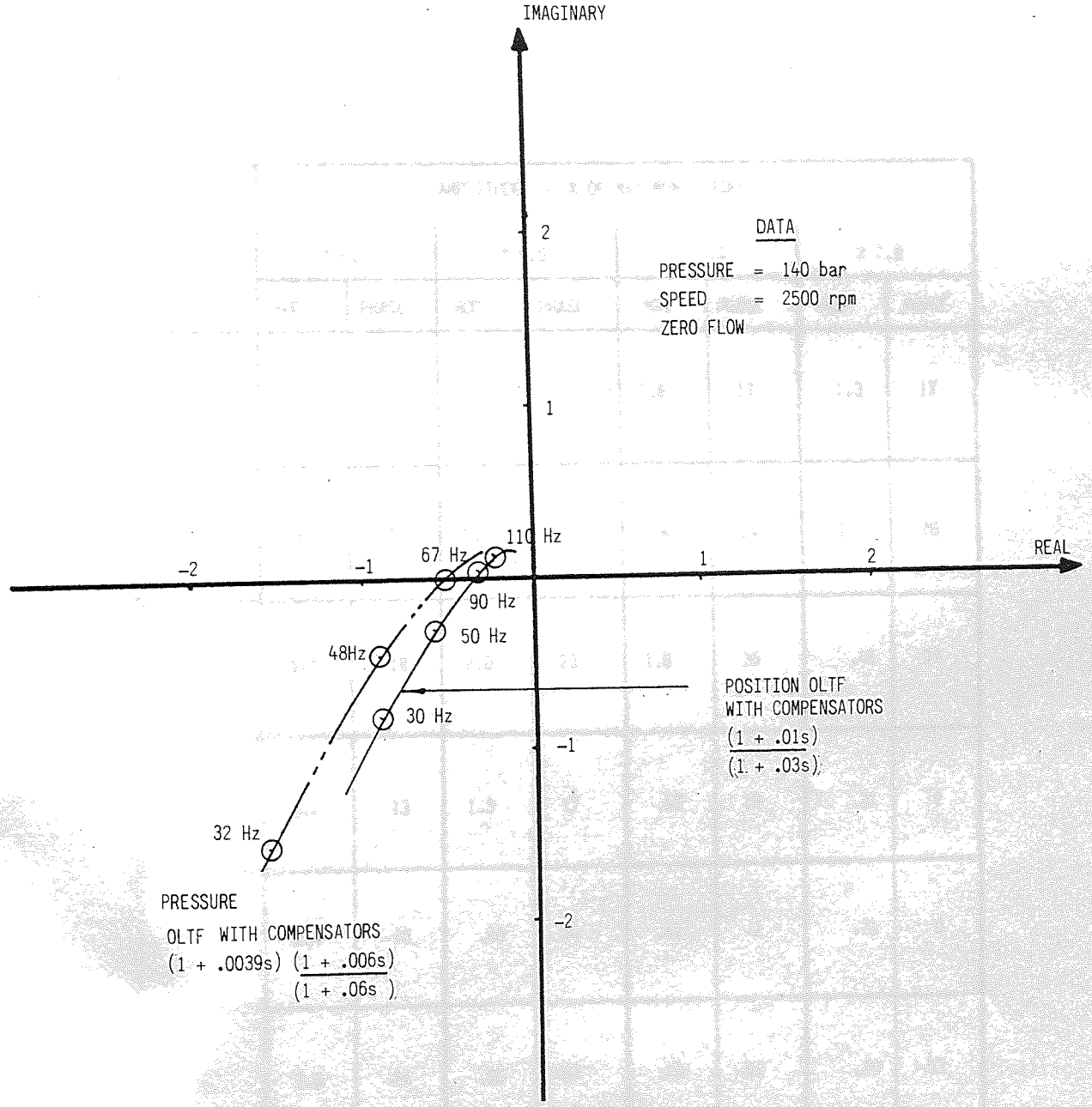

Fig 4.5 NYQUIST PLOTS FOR THE STABLE POSITION AND PRESSURE COMPENSATING CONTROL LOOPS

FREQUENCY (Hz)	AMPLITUDE – % OF MAXIMUM STROKE							
	± 0.2		± 0.5		± 1.0		± 2.0	
	MOD	PHASE	MOD	PHASE	MOD	PHASE	MOD	PHASE
5	18	8	6	14	2.6	17	1.3	17
10	18	24	5.2	24	2.4	24	1.1	26
50	6.0	18	2.0	23	1.0	26	.46	27
100	3.7	13	1.3	17	.60	19	.31	19
200	2.4	–10	.90	–4	.42	–2	.21	0
500	2.0	–84	.80	–67	.40	–59	.20	–53

EQUIVALENT TO TRANSFER FUNCTIONS
$[G_g][G_s]$

Fig 4.6 PRACTICAL RESULTS FOR THE FREQUENCY RESPONSE OF THE SATURATING CONTROL CIRCUIT

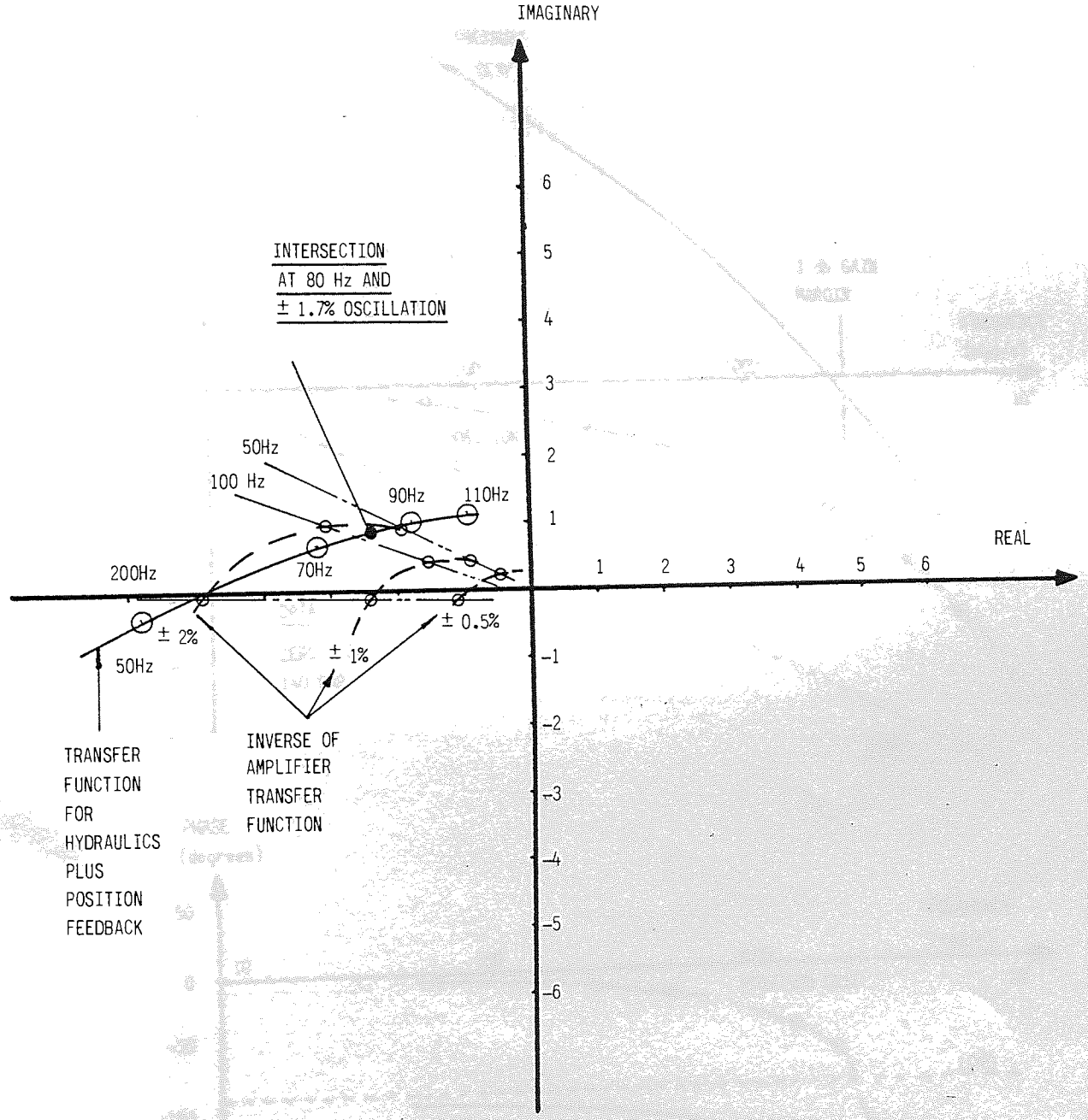

Fig 4.7 NYQUIST PLOT FOR THE PREDICTION OF LIMIT CYCLING IN THE POSITION CONTROL LOOP

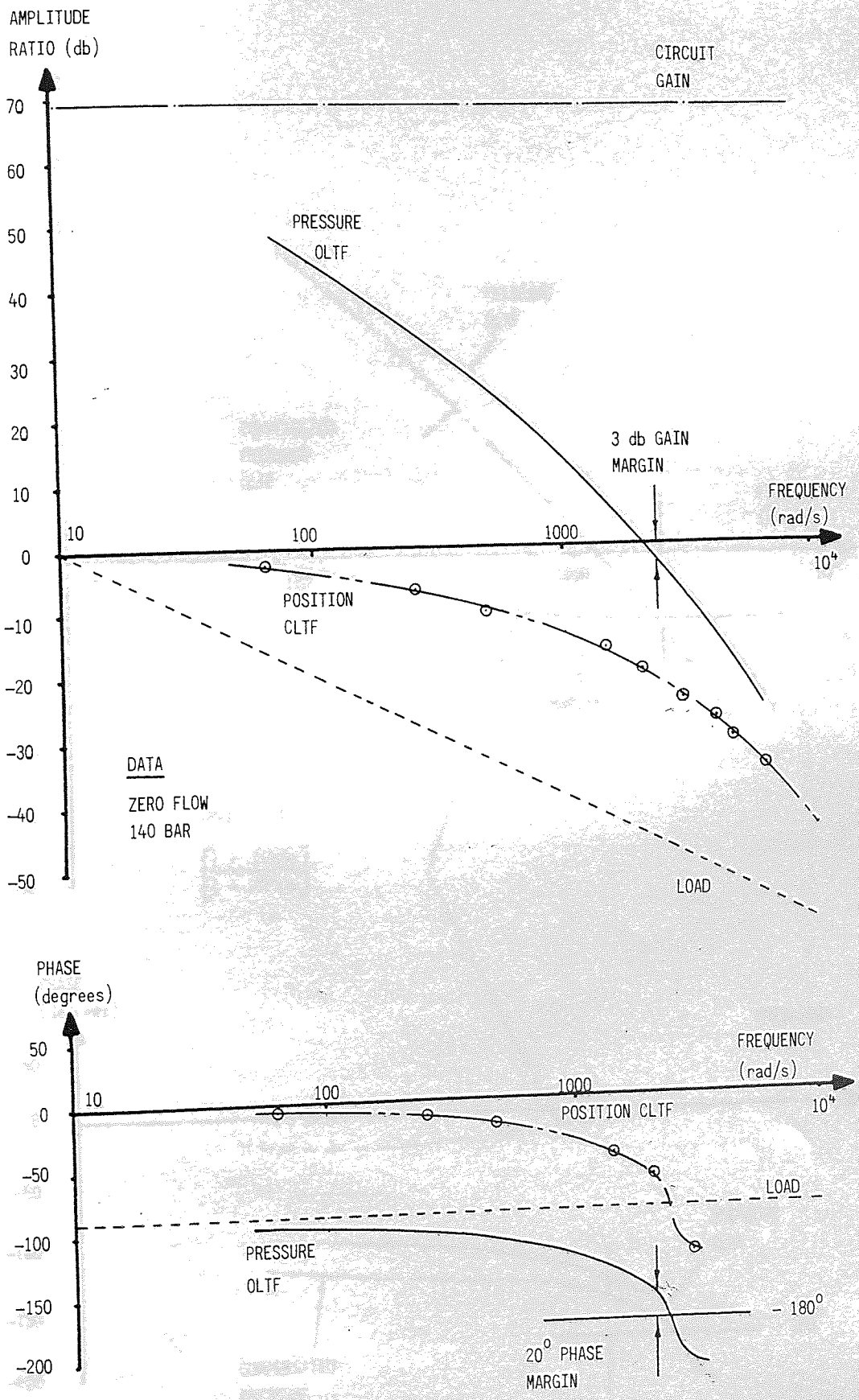

Fig 4.8 A BODE PLOT OF THE PRESSURE COMPENSATION OLTF FOR THE LEAST STABLE OPERATING CONDITION

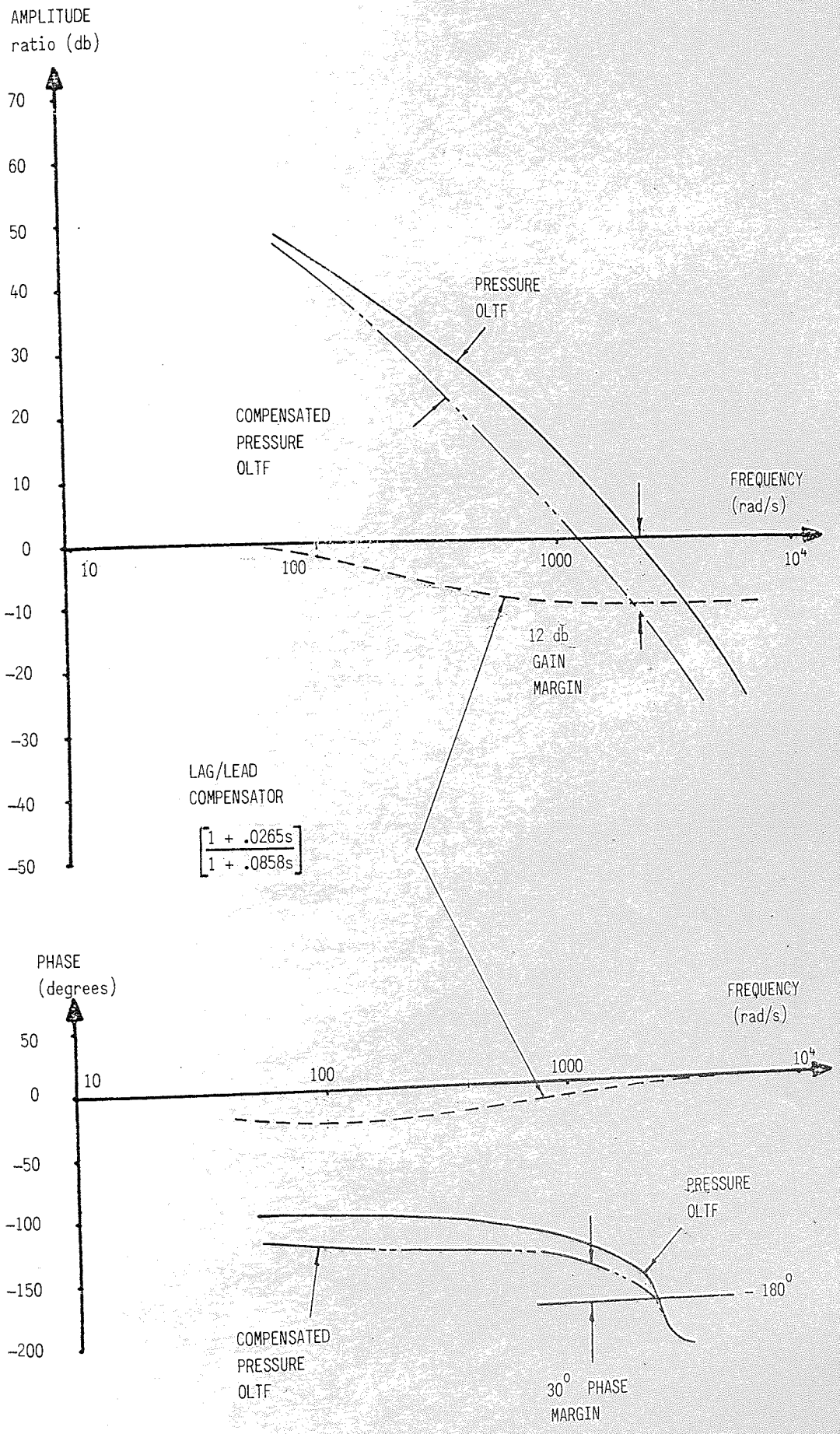

Fig 4.9 A BODE PLOT TO SHOW THE STABILISING EFFECT OF A LAG/LEAD NETWORK UPON THE PRESSURE OLTF

PUMP SPEED (rpm)	SAMPLING RATE (Hz)	LIMIT CYCLE (CLOSED LOOP)		LIMIT CYCLE (OPEN LOOP 'ALIASED' SIGNALS)	
		AMPLITUDE * (bar)	FREQUENCY † (Hz)	AMPLITUDE * (bar)	FREQUENCY † (Hz)
2500	1000	± 3	25	± 3	24
2500	500	± 5	12	± 5	12
2500	300	± 4	25	± 4	25
1500	1000	± 3	14	± 4	14
1500	500	± 4	25	± 4	24
1500	300	± 5	12	± 5	14

* Estimated accuracy ± 1 bar

† Estimated accuracy ± 1 Hz

Fig 4.10 THE AMPLITUDE AND FREQUENCY OF THE MICRO-PROCESSOR INDUCED LIMIT CYCLES AND ALIASED SIGNALS

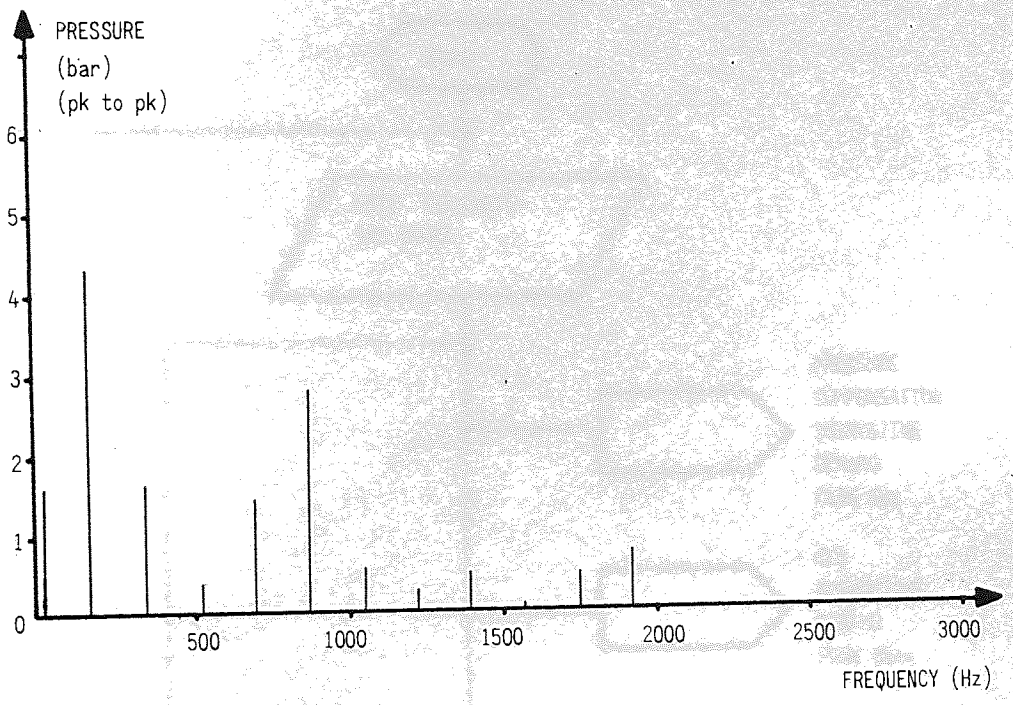

(a) 1500 rpm

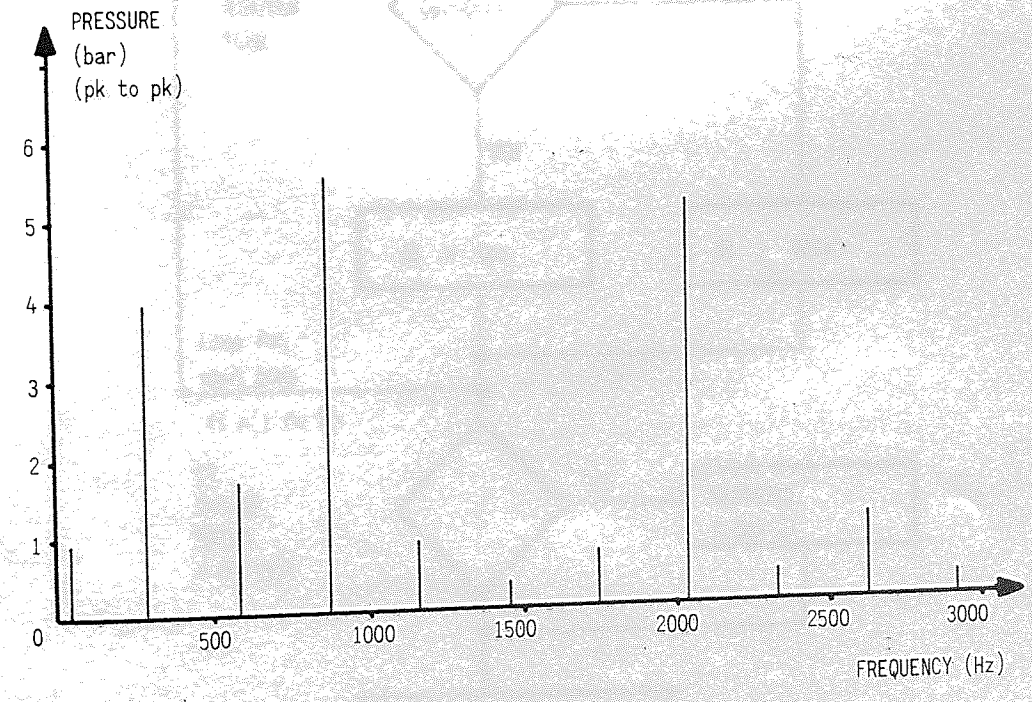

(b) 2500 rpm

Fig 4.11 FOURIER ANALYSIS OF THE PRESSURE RIPPLE AT 1500 AND 2500 RPM

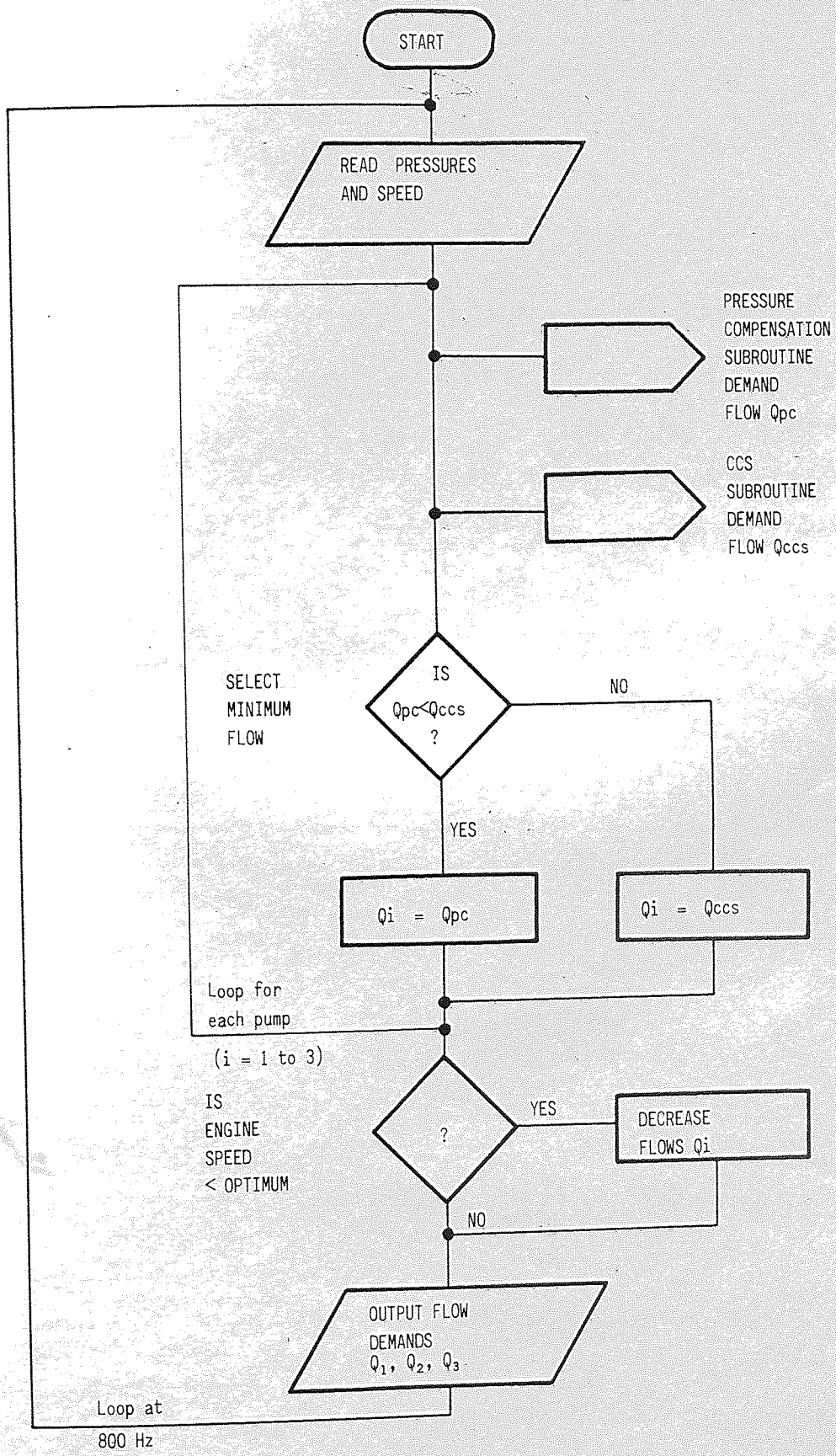

Fig 4.12 A SIMPLIFIED BLOCK DIAGRAM OF THE MICRO-PROCESSOR CONTROL PROGRAM TO CATER FOR A TRIPLE PUMP INSTALLATION

CHAPTER 5

CONCLUSION TO THE PROJECT

It is believed that the use of mathematical models has accelerated the design of the control options, increased the probability of achieving successful products and in most cases improved their performance.

The possible exception was the realisation of the pressure compensating controller. It could be argued that if more time had been spent upon its synthesis and simulation then it is conceivable that the final solution may have been found at the outset. In defence of the approach taken it must be remembered that this was an industrial project and consequently there were considerable commercial pressures to obtain results.

The outcome of this project with respect to the hydro-mechanical controller package is that Hamworthy now has a prototype controller package which:

1. Will fit all three sizes of piston pump.
2. Can contain any combination of the following control modes:
   (a) Manual - biased to full or zero flow.
   (b) Constant power.
   (c) Load compensated CCS.
   (d) Pressure compensation
3. Will be stable in all control options in any installation.
4. Has a CCS metering characteristic which is virtually independent of load.
5. Has a pressure compensator with an operating band of only 5% of the cracking pressure, (the specification allowed for a 10% band).
6. Gives a time response, for a 77 ml/rev pump, of 0.15 seconds (apart from pressure compensation where the response is 0.22 seconds).

To date fifty controllers have been ordered for stock and future customer prototype evaluation. Two have been requested by a Norwegian company for marine applications and their requirement was for dual 77 ml/rev pumps fitted with constant power + manual override controllers. Also a British excavator manufacturer has supplied Hamworthy with one of their machines in order to evaluate the piston pump. The combination of control options they wish to test is load compensated CCS + pressure compensation + power control.

Other customers have requested less complicated control options but they encompass a considerable range such as manual (biased to full flow), manual (biased to zero flow) and power control. This illustrates that there is a considerable mixture of control options required and it looks likely that the decision to design such a universal controller package will be proved correct.

With regard to the electro-hydraulic system, the achievements of this project are that:

1. Low cost pressure and position transducers have been found and proven to be reliable.
2. A low cost, high performance servo-valve has been successfully interfaced to the pump. This system has a high positioning accuracy and is adequately stable in the very arduous control task of pressure compensation.
3. The effect of a micro-processor upon systems stability has been shown to be negligible, once the minor problem in the electronic circuit has been overcome.

It is therefore concluded that a micro-processor based controller is technically feasible but comparing the present day costs of the micro-processor and hydro-mechanical controllers reveals that the electronic design is approximately 60% more expensive. It is therefore concluded that Hamworthy should manufacture the hydro-mechanical package to meet present day and near future requirements.

However, the concept of micro-processor control should not be abandoned because the relative costs of the system, compared with the hydro-mechanical package, is decreasing and eventually the electro-hydraulic design will be the cheaper. An example of this process is that Intel now offer their 2920 micro-processor with on-board memory, A to D and D to A converters.

Another important consideration is whether the same micro-processor control system could be applied to other products such as hydraulic valves. If so, then this would make the use of the system more attractive on the pump.

From these two points it is therefore suggested that the hydro-mechanical controller should be an interim solution and that Hamworthy should proceed with the design of a micro-processor controlled pump. They should find a small market * for it now, so that they can re-coup some of their expenditure and gain valuable experience with the system. Then, when the economies of offering the micro-processor controller as the standard option are favourable, Hamworthy would be in the powerful position of having several years experience.

Hamworthy could quickly and cheaply offer suitable systems if they used standard development kits extended to include A to D and D to A converters. These units are reasonably priced and they would allow Hamworthy to determine the market potential for the product, as well as offering the customer an opportunity of programing the system to give the precise characteristics

---

* One possible market for such a system is in mining machinery. As a result of the work on electro-hydraulically controlled pumps, Hamworthy was able to supply a French company with an electronic, position controlled pump. This company are interfacing the pump to a micro-processor. Clearly, if Hamworthy had been able to supply a complete system, they would have been very interested.

Another possible market is machine tools. The system could be used to give a sequence of flow rates to, say, a hydraulic press and also perform the safety function of monitoring guard switches.

required. If the reaction to the system were to prove favourable then a purpose built micro-processor system could be designed to meet production requirements.

APPENDIX A1

DESIGN SPECIFICATION FOR THE CONTROLLER PACKAGE

A 1.1 CONTROL OPTIONS

(i) CCS — The controller shall have the capability of altering the output flow of the pump so that it corresponds exactly with the total flow required by the various circuit services, plus the flow required to operate the controller.

(ii) Torque (Constant Power at Constant Speed)

This function shall maintain the torque of the prime mover constant.

(iii) Pressure Compensation

When the pressure of the system reaches a predetermined level, this controller shall reduce the flow from the pump until it is in a stand-by condition.

(iv) Remote Manual

The flow output of the pump shall be proportional to a variable, external pressure signal.

A 1.2 OPERATION OF THE PACKAGE

(i) Combinations of Controllers

All the above functions shall be made available in any combination with the exception of the CCS and manual options.

(ii) Overriding

With any combination of functions in the package the one demanding the least flow shall override all other control signals.

A 1.3 THE RANGE OF PUMPS TO BE CONTROLLED

(i) The controller shall be fully interchangeable of all three sizes of

variable displacement pumps in the Hamworthy range.

(ii) Each pump shall have one controller.

(iii) Up to a maximum of any three variable displacement pumps may be driven from the same shaft. The controller must be capable of controlling the total power taken from the prime mover.

A 1.4 GENERAL PERFORMANCE REQUIREMENTS

(i) Pressure Range

20 to 350 bar.

(ii) Flow Losses

For the 77 ml/rev pump a flow loss of up to a maximum of 16 l/min will be acceptable for the most complex control combination. This shall comprise:

10 l/min maximum for CCS

4 l/min maximum for pressure compensation

2 l/min for the follow-up servo

A proportional change in these figures will be acceptable on other sizes of pump.

(iii) Stability

Each controller must be adequately stable under all operating conditions and there shall be no interaction between different control functions.

(iv) Time Response

The required response time of the 77 ml/rev pump to stroke and de-stroke, is 300 ms when the temperature of the system is 50°C and the pressure is 200 bar.

A corresponding change in this figure will be acceptable for the other sizes of pumps.

(v) Life 10,000 hours or 10^7 cycles, whichever occurs first.

A 1.5 PERFORMANCE OF THE CCS CONTROLLER

(i) The controller shall require no adjustment.

(ii) The maximum pressure drop across the sensing orifice shall be 20 bar.

(iii) The controller must function satisfactorily regardless of pump flow and pressure.

A 1.6 PERFORMANCE OF THE TORQUE CONTROLLER

(i) This function shall be tailored to each individual installation.

(ii) It shall be able to cope with all sizes of prime movers likely to be encountered in the mobile earth moving, crane, mining and marine markets.

(iii) The unit shall, if possible, have external adjustment.

(iv) In equal size multi-pump installations, the flow from each pump must be within 4 l/min of each other.

A 1.7 PERFORMANCE OF THE PRESSURE COMPENSATOR

(i) The pressure rise from the cracking to the stalled pressure shall be at most 10% of the crack pressure.

(ii) The controller shall operate at pressures between 138 and 350 bar.

(iii) If possible the controller should be externally adjustable.

A 1.8 PERFORMANCE OF THE MANUAL CONTROLLER

(i) The controller shall require no adjustment.

(ii) The flow shall be proportional to an external pilot pressure ranging from 10 to 20 bar.

A 1.9 ENVIRONMENTAL CONSIDERATIONS

(i) Temperature Range – Operational 25 to 80°C
Survival –30 to 100°C

(ii) Contamination – The controller shall function satisfactorily in applications which incorporate a 25µm nominal filter.

(iii) Types of Fluids

(a) HM 32 to 38 inc Mineral Oil (min. viscosity 8.5 cSt).

(b) HFB 68 Invert Emulsion (60/40)

(c) HFA 1 Dilute Emulsion (5/95)

(d) HFC 46 to 68 Water Glycol

APPENDIX A2

MATHEMATICAL MODEL OF THE ORIGINAL CONSTANT POWER CONTROLLER

A 2.1 INTRODUCTION

A schematic of this controller is shown in Fig 2.5. For simplicity just one pump will be considered in the mathematical model, as shown in Fig A 2.1. A simple block diagram for the complete system is given in Fig A 2.2 and consists of four basic units. Firstly, pump pressure (P_1) is sensed by the two power pistons. These act against the spring pack and they control the position of the spool (X). As this spool moves, it creates an imbalance between the follow-up servo and pump. This forces the pump into a new position (Y) and hence changes its output flow (Q_p). Finally, the load senses this change in flow and alters the pressure of the system (P_1).

To build a mathematical model, the transfer functions of each block must be determined. However, most of these stages contain non-linear equations, which are difficult to solve. To simplify this problem the equations are linearised, using the small pertabation technique. Once the linearised transfer functions have been determined, they can be combined to form the open loop transfer function (OLTF) for the system.

To solve this equation and determine the stability of the system requires two limitations to be imposed:

1. The solution is only valid in a very small region about the particular operating point considered.
2. The stability margins are based upon a sinusoidal excitation signal.

The first limitation is necessary for the equations to be linearised and the second is necessary to evaluate the OLTF and produce a Nyquist plot. By assuming that the excitation signal is a sine wave allows the substitution of "$j\omega$" for the Laplace operator "s". Thus, for a particular excitation

frequency "ω", the OLTF can be determined as a complex number and plotted on an Argand diagram. This process is repeated for various frequencies and the resulting points form the Nyquist locus. If this passes to the right of the "-1" point then, at the operating point considered, the system is stable.

The evaluation of the OLTF is a tedious process and so to speed this up a computer program, written in BASIC, was devised. This program is fully documented in this Appendix but, because it is relatively straightforward, descriptions of similar subsequent programs are not given.

A 2.2 DETERMINATION OF THE OPEN LOOP TRANSFER FUNCTION (OLTF)

The assumptions for all the mathematical modelling of pump stability are the same as those used by GREEN & CROSSLEY which are:

1. Fluid inertia effects will tend to be at high frequencies and can therefore be neglected.
2. The bulk modulus (β) is a difficult quantity to measure because of air entrainment. A figure of 1.03 GPa has been used to allow for this, rather than the accepted figure of 1.7 GPa for SAE 10 oils.
3. Cavitation was assumed to be absent in the system.
4. Pressure losses, other than those across valves or orifices, were neglected.
5. Viscosity, density and bulk modulus were assumed to be constant.
6. The system volume was difficult to estimate and a value was calculated as accurately as possible for the system.
7. The slip of the pump was assumed to be zero as the volumetric efficiency of the pump is in excess of 96%. In any case any slip would have a stabilising effect.
8. Any viscous, speed or turbulence effects acting on the control ring, were ignored.

9. The coefficient of discharge for valves and orifices was held constant at 0.65.

10. The flow forces on the follow-up servo are small and were therefore neglected.

11. The relative velocity between the spool and follow-up servo is small and hence viscous damping effects can be ignored.

12. The flow used by the controller is small and can therefore be ignored. In any case such flow would tend to stabilize the system.

A 2.2.1 THE TRANSFER FUNCTION FOR THE MAIN SPOOL $[G_1]$

A free body diagram for the main spool is shown in Fig A 2.3. As the system is in equilibrium the forces must balance and therefore

$$M_1 \ddot{X} + L_1 \dot{X} + \Sigma KX + \text{spring pre-load} + \text{friction} - 2 P_1 a_1 = 0$$

Applying the small pertabation technique and representing a small change in a variable by its lower case letter gives

$$\frac{\partial}{\partial X}(M_1 \ddot{X})\, x + \frac{\partial}{\partial X}(L_1 \dot{X})\, x + \frac{\partial}{\partial X}(\Sigma K X)\, x + \frac{\partial}{\partial X}(\text{spring pre-load})\, x - \frac{\partial}{\partial P}(2 a_1 P_1)\, p_1 + \frac{\partial}{\partial X}(\text{friction})\, x = 0$$

The spring pre-load and coulomb friction are independent of X thus

$$M_1 \ddot{x} + L_1 \dot{x} + \Sigma K x = 2 a_1 p_1$$

or, inserting "s" the Laplace operator and rearranging the equation,

$$[G_1] = \left[\frac{x}{p_1}\right] = \left[\frac{2 a_1}{M_1 s^2 + L_1 s + \Sigma K}\right] \quad \text{A 2.1}$$

A 2.2.2 THE TRANSFER FUNCTION FOR THE FOLLOW-UP SERVO [G_2]

Fig A 2.4 shows how the follow-up servo operates. In the steady state, Fig A 2.4 (a), the metered pressure acting upon the piston equals the pump reaction force. If the main spool is now moved to the left, to de-stroke the pump, as shown in Fig A 2.4(b), the flow of oil to the piston is restricted and the metered pressure falls. As it does so the pump reaction force pushes the pump to the left and the supply of oil is re-established. This causes the metered pressure to rise and the system is restored to a steady state condition at a lower flow. Conversely when the spool is moved to the right more flow is demanded as shown in Fig A 2.4(c). Initially the servo force overcomes the pump reaction and the piston is forced to follow the movement of the spool. However, as it catches up the meter-out hole is uncovered and the metered pressure drops until the servo force again just equals the pump reaction force.

The pump reaction force is caused by the timing of the pump and it has been measured at various pump speeds and pressures. The result of these tests is that this force can be considered to be equivalent to a cylinder of area 284.7 mm^2 at pump pressure (P_1).

A free body diagram for the pump control ring and the follow-up servo is given in Fig A 2.5. Equating forces for equilibrium and linearising

$$p_2 = \frac{C_1 p_1 - (M_2 s^2 + K)y}{a_2} \quad \text{A 2.2}$$

To determine the relationship between the displacements of the spool and pump, to the metered pressure (P_2), it is necessary to consider the flow of oil through the follow-up servo. Applying the theorem of continuity to the cylinder at pressure P_2 gives

$$Q(\text{in}) + a_2 \dot{Y} = Q(\text{out}) + \text{compressibility flow}$$

As this chamber is small, the compressibility flow will be small and

can therefore be neglected. Therefore linearising the equation

$$q(in) + a_2 sy = q(out) \quad - \quad A\ 2.3$$

The flow entering the cylinder (Q(in)) can be expressed in terms of the flow area and pressure drop across the meter-in port of the follow-up servo by the relationship

$$Q(in) = C_d \; a(in) \sqrt{\frac{(P_1 - P_2)\ 2}{\rho}}$$

or in its linearised form

$$q(in) = C_x' (y - x) + C_p (p_1 - p_2) \quad - \quad A\ 2.4$$

where $$C_x' = C_d \sqrt{\frac{2\ (P_1 - P_2)}{\rho}} \quad \frac{\partial a(in)}{\partial (Y-X)}$$

$$Cp = \frac{Cd\ a(in)}{\sqrt{2\rho\ (P_1 - P_2)}}$$

A diagram of the metering areas of the follow-up servo is shown in Fig A 2.6 and it can be shown that

$$a(in) = r^2 \left[\cos^{-1} \frac{(X-Y)}{r} - \frac{1}{2} \sin \left(2 \cos^{-1} \frac{(X-Y)}{r}\right) \right]$$

$$\frac{\partial a(in)}{\partial (Y-X)} = \frac{r}{\sqrt{1 - \frac{(X-Y)^2}{r^2}}} \left[1 - \cos \left(2 \cos^{-1} \frac{(X-Y)}{r}\right) \right]$$

Applying the orifice square law relationship to the flow out of the cylinder

$$Q(out) = C_d \; a(out) \sqrt{\frac{2\ P_2}{\rho}}$$

or in its linearised form

$$q(out) = C_x' (x-y) + C_p' p_2 \quad - \quad A\ 2.5$$

where $$C_x' = C_d \sqrt{\frac{2\ P_2}{\rho}} \quad \frac{\partial a(out)}{\partial (X-Y)}$$

$$C_p' = \frac{C_d\ a(out)}{\sqrt{2\rho\ P_2}}$$

Fig A 2.7 shows the lap of the follow-up servo and it can be shown that

$$a(out) = r^2 \left[\cos^{-1} \left(\frac{L_2 - 2r - X + Y}{r} \right) - \frac{1}{2} \sin \left(2 \cos^{-1} \left(\frac{L_2 - 2r - X + Y}{r} \right) \right) \right]$$

$$\frac{\partial a(out)}{\partial (X-Y)} = \frac{r}{\sqrt{1 - \left(\frac{L_2 - 2r - X + Y}{r^2} \right)^2}} \left[1 - \cos \left(2 \cos^{-1} \left(\frac{L_2 - 2r - X + Y}{r} \right) \right) \right]$$

Combining equations A 2.3, A 2.4 and A 2.5 results in

$$(C_x + C'_x + a_2 s)y + C_p p_1 - (C_x + C'_x)x - (C_p + C'_p)\, p_2 = 0 \qquad - \text{A } 2.6$$

Substituting for p_1 from equation A 2.1

$$\left((C_x + C'_x) + a_2 s \right) y + \frac{C_p}{2a_1} (M_1 s^2 + L_1 s + \Sigma K) x - (C_x + C'_x)x - (C_p + C'_p)\, p_2 = 0 \qquad - \text{A } 2.7$$

Now combining equations A 2.1 and A 2.2 produces

$$p_2 = \frac{C_1}{2a_1 a_2} (M_1 s^2 + L_1 s + \Sigma K) x - (M_2 s^2 + K) \frac{y}{a_2} \qquad - \text{A } 2.8$$

Finally, the transfer function for the follow-up servo $[G_2]$ can be determined from equations A 2.7 and A 2.8

$$[G_2] = \left[\frac{y}{x}\right] = \left[\begin{array}{l} \frac{M_1}{2a_1a_2}\left((C_p+C'_p)C_1 - C_p a_2\right)s^2 \\ + \frac{L_1}{2a_1a_2}\left(C_1(Cp+Cp') - Cpa_2\right)s \\ + \frac{\Sigma K}{2a_1a_2}\left(C_1(Cp+Cp') - Cpa_2\right) \\ + (C_x+C'_x) \\ \hline \frac{M_2}{a_2}(Cp+Cp')s^2 + a_2 s \\ + (C_x+C'_x) + \frac{K}{a_2}(Cp+Cp') \end{array}\right] \quad - \text{A } 2.9$$

A 2.2.3 THE TRANSFER FUNCTION FOR THE PUMP $[G_3]$

The relationship between pump flow (Q_p) and controller position (Y) is

$$Qp = Vp \frac{N}{60}\left(1 - \frac{Y}{\hat{Y}}\right)$$

Linearising this gives

$$q_p = -\frac{(V_p N)}{60\hat{Y}} \cdot y$$

or $$[G_3] = \left[\frac{q_p}{y}\right] = -\left[\frac{VpN}{60\hat{Y}}\right] \quad - \text{A } 2.10$$

A 2.2.4 THE TRANSFER FUNCTION FOR THE HYDRAULIC LOAD [H]

The hydraulic load for the majority of applications can be considered as a directional control valve and an accumulator. Applying the principle of continuity to the load

$$Qp = Qv + Qc$$

or in its linearised form

$$q_p = q_v + q_c \quad - \text{A } 2.11$$

The flow through a directional control valve is proportional to the square root of the pressure drop so

$$Q_v = C_d\, a_v \sqrt{\frac{2\, P_1}{\rho}}$$

Thus for a particular valve opening (a_v) the change in flow (q_v) is

$$q_v = \frac{C_d\, a_v}{\sqrt{2\rho\, P_1}}\, p_1 \qquad \text{- A 2.12}$$

The compressibility flow (Q_c) can be determined by considering the compressibility of the oil thus,

$$\text{Change in Volume } \Delta v = \frac{v}{\beta} \cdot \Delta P_1$$

Differentiating both sides of this equation with respect to time gives

$$Q_c = \frac{d\,\Delta v}{dt} = \frac{v}{\beta} \cdot \frac{dP_1}{dt}$$

or linearising and using the Laplace operator "s"

$$q_c = \frac{v}{\beta}\, s\, p_1 \qquad \text{- A 2.13}$$

Combining equations A 2.11, A 2.12 and A 2.13 produces the transfer function for the load

$$[H] = \left[\frac{p_1}{q_p}\right] = -\left[\frac{1}{\frac{v}{\beta}.s + \frac{c_d\, a_v}{\sqrt{2\rho\, p_1}}}\right] \qquad \text{- A 2.14}$$

A 2.2.5 THE FORWARD LOOP TRANSFER FUNCTION [G]

This is defined as the product of the transfer functions in the forward path

$$[G] = [G_1]\,[G_2]\,[G_3]$$

Combining equations A 2.1, A 2.9 and A 2.10 gives

$$[G] = \left[\frac{(V_p N)}{(60\hat{Y})} \left(\frac{(C_p+C'_p)\,C_1 - C_p\,a_2}{a_2} \right) \left[M_1 s^2 + L_1 s + \Sigma K + \frac{2a_1 a_2\,(C_x+C'_x)}{(C_p+C'_p)C_1 - C_p a_2} \right] \right]$$

$$\frac{}{s^4 \left[M_1 M_2 \left(\frac{C_p + C'_p}{a_2} \right) \right]}$$

$$+s^3 \left[M_1 a_2 + M_2 (C_p+C'_p) \frac{L_1}{a_2} \right]$$

$$+s^2 \left[M_1 (C_x+C'_x) + L_1 a_2 + M_2 (C_p+C'_p) \frac{\Sigma K}{a_2} + M_1 \frac{K}{a_2} (C_p+C'_p) \right]$$

$$+s \left[L_1 (C_x+C'_x) + a_2 \Sigma K + L_1 K (C_p+C'_p)/a_2 \right]$$

$$+ (C_x+C'_x)\Sigma K + \Sigma K . \frac{K}{a_2} (C_p+C'_p) \Bigg]$$

- A 2.15

and the OLTF can be determined from equations A 2.14 and A 2.15 where,

$$OLTF = [G]\,[H] \qquad \text{- A 2.16}$$

This equation has not been expanded as the computer program was designed to perform this task and produce a Nyquiste plot, for any operating point.

A 2.3 DETERMINATION OF SYSTEM PARAMETERS

A 2.3.1 THE METERING AREAS OF THE FOLLOW-UP SERVO

The steady state force balance for the control ring and follow-up servo is

$$C_1 P_1 = a_2 P_2$$

Now by considering the flow through the servo P_2 can be expressed as

$$P_2 = \frac{P_1}{1 + \left(\frac{a(out)}{a(in)}\right)^2}$$

Re-arranging these equations gives

$$\frac{a(out)}{a(in)} = \sqrt{\frac{a_2}{C_1} - 1}$$

- A 2.17

Thus the metering areas are independent of pump position and pressure. The ratio of a(out) to a(in) can be calculated for various values of (Y-X) and the relative displacement, which makes the two sides of equation A.17 equal, is the actual value for the servo

For $C_1 = 2.842 \times 10^{4}$ m²

$Q_2 = 1.512 \times 10^{3}$ m²

$r = 3.815 \times 10^{4}$ m

$L_2 = 3.815 \times 10^{4}$ m

Then $a(out) = 1.009 \times 10^{7}$ m²

$a(in) = 4.830 \times 10^{8}$ m²

$\frac{\partial a(out)}{\partial (X-Y)} = 5.635 \times 10^{4}$ m

$\frac{\partial a(in)}{\partial (Y-X)} = 6.793 \times 10^{4}$ m

A 2.3.2 THE VOLUME OF OIL BETWEEN THE PUMP AND THE LOAD

It was important to determine the worst realistic load for the pump so that stability could be guaranteed for all installations. A study of several earth moving machines revealed that, the minimum volume of oil between the pump and valve was approximately 0.75 litres (including the dead volume in the pump) and the largest was 5 litres.

These values were used in equation A 2.14 to determine which constituted the worst case from a stability view point. The result of these calculations was that the smaller volume gave the higher gain at virtually 90° phase lag for frequencies above 2 Hz. As this was within the bandwidth of the controller it represented the worst load and was therefore used in all subsequent stability calculations.

A 2.3.3 THE RATE OF THE SPRING PACK

The selection of the springs in the pack, plus the gaps before they are introduced, is dependent upon the particular installation. However, in general the lower the spring rates and the larger the gaps, then the more unstable the system will be. The design case considered for the stability of the power controller was for the lowest power level likely to be required which was 22.4 KW (30 H P) per pump. This satisfied the above condition of using the lowest spring rates and the largest gaps.

The subsequent spring rate/position characteristics were used in the model and it was established that the system was at its least stable when only the pre-load spring was engaged. This was confirmed by test results. If the next spring was brought into contact at too low a flow, then the system went unstable. Whereas, when correctly set the system was adequately stable.

The spring rate was therefore altered in the program depending upon the considered operating conditions and was 17.65 KN/ m for the unstable and 35.30 KN/m for the stable states at a flow of 50% of maximum.

A 2.3.4 MODEL DATA

a_1	=	$0.001512\ m^2$
a_2	=	$6.951 \times 10^{-6}\ m^2$
L_1	=	7 N/(m/s)
ρ	=	$860\ Kg/m^3$
K	=	$1.75 \times 10^4\ N/m$
M_1	=	.238 Kg
M_2	=	11.384 Kg
V_p	=	$77 \times 10^{-6}\ m^3/rev$
N	=	2300 rpm (for this particular application)
$\hat{Y}$	=	.0075 m
a_v	=	$1.604 \times 10^{-5}\ m^2$
P_1	=	89 bar
Q	=	88.5 (l/min)

A 2.4 THE COMPUTER PROGRAM FOR DETERMINING THE OLTF FOR THE POWER CONTROLLER

A 2.4.1. INTRODUCTION

The requirement for the program is that given the operating pressure and flow the computer calculates the parameters of the OLTF and then generates the Nyquist points for various frequencies.

A 2.4.2 DESCRIPTION OF THE PROGRAM

The flow chart for the program is given in Fig A 2.8. Initially the operating conditions of pressure (bar) and flow (l/min) are inserted and converted into SI units. Next, the system parameters are put into the program again in SI units. From these values the terms in the forward loop transfer function (FLTF) can be calculated.

The headings for the answers are then written and the determination of the Nyquist points can commence. Initially the real and imaginary parts for the FLTF are calculated and these are used to find the gain and phase of the FLTF. The phase then has to be adjusted by multiples of π to account for which quadrant the solution is in. This is done by examining the signs of the real and imaginary parts of the FLTF.

The gain and phase of the OLTF can then be found by respectively multiplying and adding the feedback transfer function terms to the FLTF. These are then written under their respective headings against the initial frequency.

The OLTF is evaluated for a series of different frequencies up to 80 Hz, when the program is terminated.

A 2.4.3 PROGRAM NOMENCLATURE

SYMBOL USED IN MATHEMATICS	PROGRAM SYMBOL
P_1 Pump pressure	P1
Q_p Pump flow	Q
π	P
V_p Displacement of Pump	V9
a_1	A1
a_2	A2
L_1	L1
$Cd\sqrt{2/\rho}$	H
K	K
M_1	M1
M_2	M2
N	N
$\hat{Y}$	T
a_v	A9
ΣK	K2
v	V
β	B
C_1	C1
a(out)	A3
a(in)	A4
$\partial a(out)/\partial(X-Y)$	I3
$\partial a(in)/\partial(Y-X)$	I4
P_2	P2
C_x	C2
C'_x	C3
C_p	C4
C'_p	C5
$C_x+C'_x$	C6
$C_p+C'_p$	C7
$(C_p+C'_p)C_1 - C_p a_2$	C8
$\Sigma K + \frac{2a_1a_2(C_x+C'_x)}{(C_p+C'_p)C_1 - C_p a_2}$	Eø

SYMBOL USED IN MATHEMATICS	PROGRAM SYMBOL
$(C_x+C'_x)\Sigma K+\Sigma K.K\ (C_p+C'_p)/a_2$	Fø
$L_1(C_x+C'_x) + a_2\Sigma K + \frac{L_1K(C_p+C'_p)}{a_2}$	F1
$M_1(C_x+C'_x) + L_1a_2 + M_2(C_p+C'_p)\frac{\Sigma K}{a_2} + M_1K(C_p+C'_p)/a_2$	F2
$M_1a_2 + M_2\ (C_p+C'_p)L_1/a_2$	F3
$M_1M_2\ (C_p+C'_p)/a_2$	F4
$\frac{(V_pN)}{(60\hat{Y})}\ \frac{(C_p+C'_p)C_1-C_pa_2)}{a_2}$	F5
Frequency (Hz)	N1
ω (rad/s)	W1
ω^2	W2
ω^3	W3
ω^4	W4
Real part of numerator of FLTF	R1
Imaginary part of numerator of FLTF	I5
Modulus of FLTF	M3
Phase of numerator of FLTF	V3
Phase of denominator of FLTF	V4
Phase of FLTF (degrees)	V5
Gain of OLTF	M4
Phase of OLTF	V6

A 2.4.4 PROGRAM LISTING

```
CONSTP  06/05/80  10:46:16
10  INPUT P1,Q
20  P1=P1*1E5
30  Q=Q/60000
40  P=3.1415926
50  V9=77E-6
60  A1=6.951E-6
70  A2=1.512E-3
80  L1=7
90  H=.65*SQR(2/860)
100  K=1.75E4
110  M1=0.238
120  M2=11.384
130  N=2300
140  T=.0075
150  K2=1.765E4
160  V=0.75E-3
170  B=1.03E9
180  C1=2.847E-4
190  A3=1.009E-7
200  A4=4.33E-8
210  I3=5.635E-4
220  I4=6.793E-4
230  REM   CALCULATE TERMS IN FLTF
240  A9=Q/(H*SQR(P1))
250  P2=P1*C1/A2
260  C2=H*SQR(P1-P2)*I4
270  C3=H*SQR(P2)*I3
280  C4=.65*A4/SQR(2*860*(P1-P2))
290  C5=.65*A3/SQR(2*860*P2)
300  C6=C2+C3
310  C7=C4+C5
320  C8=C7*C1-C4*A2
330  E0=(2*A1*A2*C6/C8)+K2
340  F0=C6*K2+K2*K*C7/A2
350  F1=L1*C6+A2*K2+L1*K*C7/A2
360  F2=M1*C6+L1*A2+M2*C7*K2/A2+M1*K*C7/A2
370  F3=M1*A2+M2*C7*L1/A2
380  F4=M1*M2*C7/A2
390  F5=(V9*N/(60*T))*C8/A2
400  REM   PRINT HEADINGS
410  PRINT
420  PRINT"FREQUENCY        MOD                PHASE"
430  PRINT"  (HZ)                              (DEGREES)"
440  REM   SET INITIAL VALUE OF FREQUENCY
450  H1=0
460  REM   CALCULATE REAL AND IMAGINARY PARTS
```

```
470   W1=N1*2*P
480   W2=W1*W1
490   W3=W1*W2
500   W4=W2*W2
510   R1=E0-W2*M1
520   I5=W1*L1
530   R2=F0-W2*F2+W4*F4
540   I6=F1*W1-F3*W3
550   M3=F5*SQR(R1^2+I5^2)/SQR(R2^2+I6^2)
560   V3=ATN(I5/R1)
570   IF R1>0 THEN 590
580   V3=P+V3
590   V4=ATN(I6/R2)
600   IF R2<0 THEN 630
610   IF I6<0 THEN 650
620   GOTO 660
630   V4=P+V4
640   GOTO 660
650   V4=2*P+V4
660   V5=(V3-V4)*180/P
670   REM   CALCULATE GAIN AND PHASE OF OLTF
680   M4=M3/SQR((V*W1/B)^2+(H*A9/SQR(P1))^2)
690   V6=V5-(ATN((V*W1/B)/(H*A9/SQR(P1))))
700   REM   OUTPUT ANSWERS
710   PRINT TAB(4);W1;TAB(14);M4;TAB(27);V6
720   REM   LOOP FOR OTHER FREQUENCIES
730   IF W1>78 THEN 760
740   W1=W1+2
750   GOTO 460
760   STOP
770   END
```

A 2.4.5 SAMPLE OUTPUT

(1) TWO SPRINGS ENGAGED

```
RUN

CONSTP   06/05/80   10:33:24
?
80,83.5

FREQUENCY      MOD          PHASE
  (HZ)                    (DEGREES)
     0        .935043        0
     2        .909407      -13.5404
     4        .84336       -25.7751
     6        .758991      -36.0336
     8        .673969      -44.2993
    10        .597036      -50.8776
    12        .530763      -56.1347
    14        .474847      -60.3873
    16        .427999      -63.8832
    18        .388783      -66.8038
    20        .355906      -69.285
    22        .3283        -71.4269
    24        .305108      -73.3052
    26        .285661      -74.9778
    28        .269439      -76.4903
    30        .25605       -77.8799
    32        .245207      -79.1778
    34        .236714      -80.4117
    36        .230467      -81.6076
    38        .226451      -82.7921
    40        .224758      -83.9942
    42        .225611      -85.2435
    44        .229421      -86.5993
    46        .236879      -88.1107
    48        .249141      -89.8759
    50        .26818       -92.0492
    52        .297531      -94.9035
    54        .34398       -98.9754
    56        .421665      -105.467
    58        .560767      -117.533
    60        .785672      -143.985
    62        .783546      -190.153
    64        .499301      -222.253
    66        .317941      -236.68
    68        .220153      -244.033
    70        .162455      -248.414
    72        .125299      -251.327
    74        .0997534     -253.418
    76        .0813324     -255.003
    78        .0675424     -256.256
    80        .0569227     -257.276
READY
```

(2) ONE SPRING ENGAGED

```
RUN

CONSTP   06/05/80   10:42:59
?
89,88.5
```

FREQUENCY (HZ)	MOD	PHASE (DEGREES)
0	1.87004	0
2	1.82069	-13.6836
4	1.69386	-26.0643
6	1.53264	-36.4745
8	1.37146	-44.9006
10	1.22729	-51.6519
12	1.10512	-57.0989
14	1.0044	-61.5642
16	.922739	-65.3006
18	.857581	-68.5004
20	.806784	-71.3107
22	.768817	-73.8483
24	.742835	-76.2122
26	.728743	-78.495
28	.727381	-80.7948
30	.740908	-83.2331
32	.773629	-85.9336
34	.833764	-89.3331
36	.937525	-93.826
38	1.1189	-100.659
40	1.45007	-112.948
42	1.93592	-139.402
44	1.96601	-185.749
46	1.22284	-218.441
48	.761203	-233.25
50	.516291	-240.866
52	.373606	-245.458
54	.28286	-248.553
56	.221253	-250.805
58	.177361	-252.535
60	.144922	-253.919
62	.120251	-255.061
64	.101052	-256.025
66	.0858283	-256.854
68	.0735667	-257.579
70	.0635576	-258.22
72	.0552933	-258.794
74	.0484016	-259.311
76	.0426036	-259.781
78	.0376878	-260.211
80	.0334908	-260.607

```
READY
```

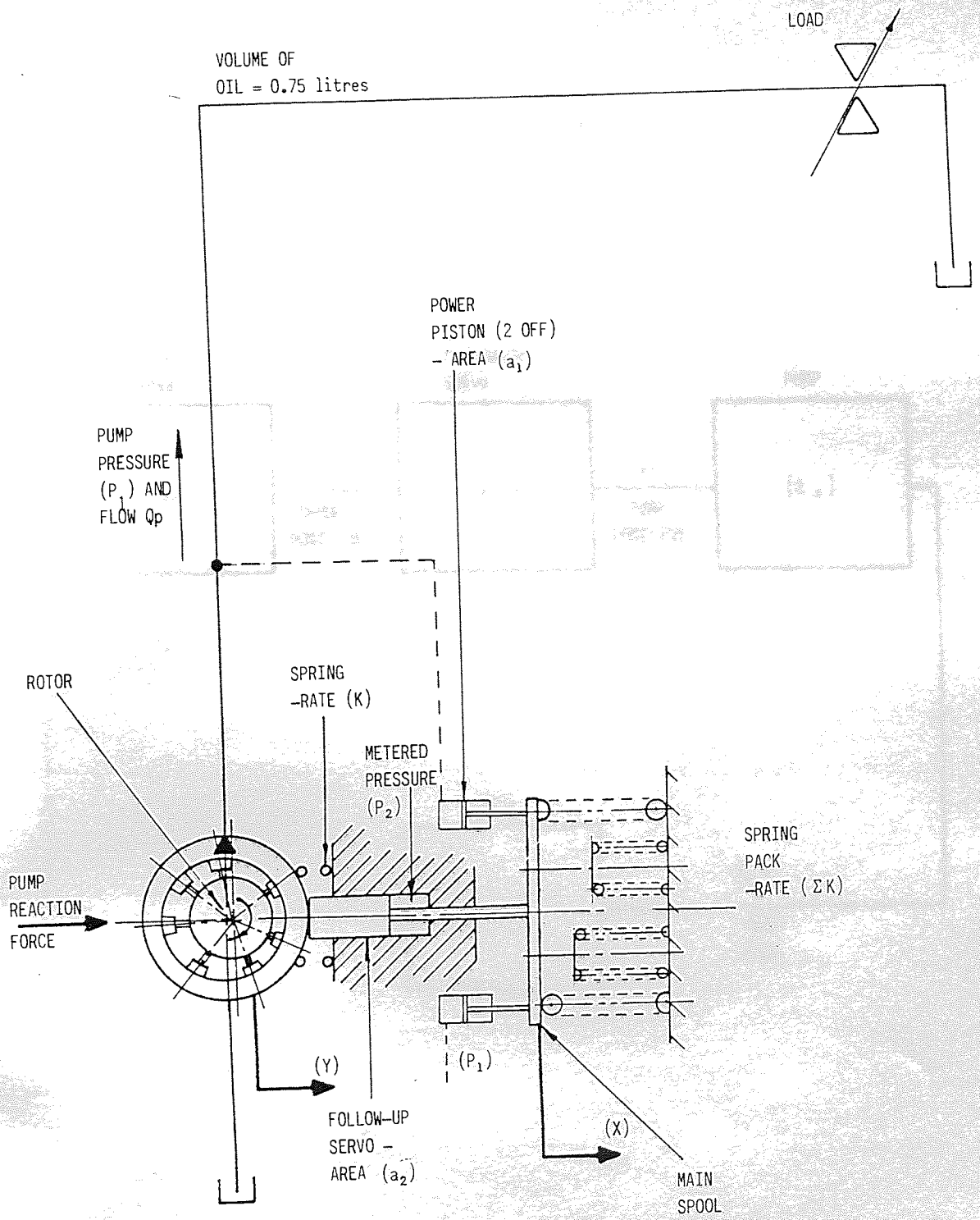

Fig A2.1 SKETCH OF A SINGLE PUMP WITH A POWER CONTROLLER

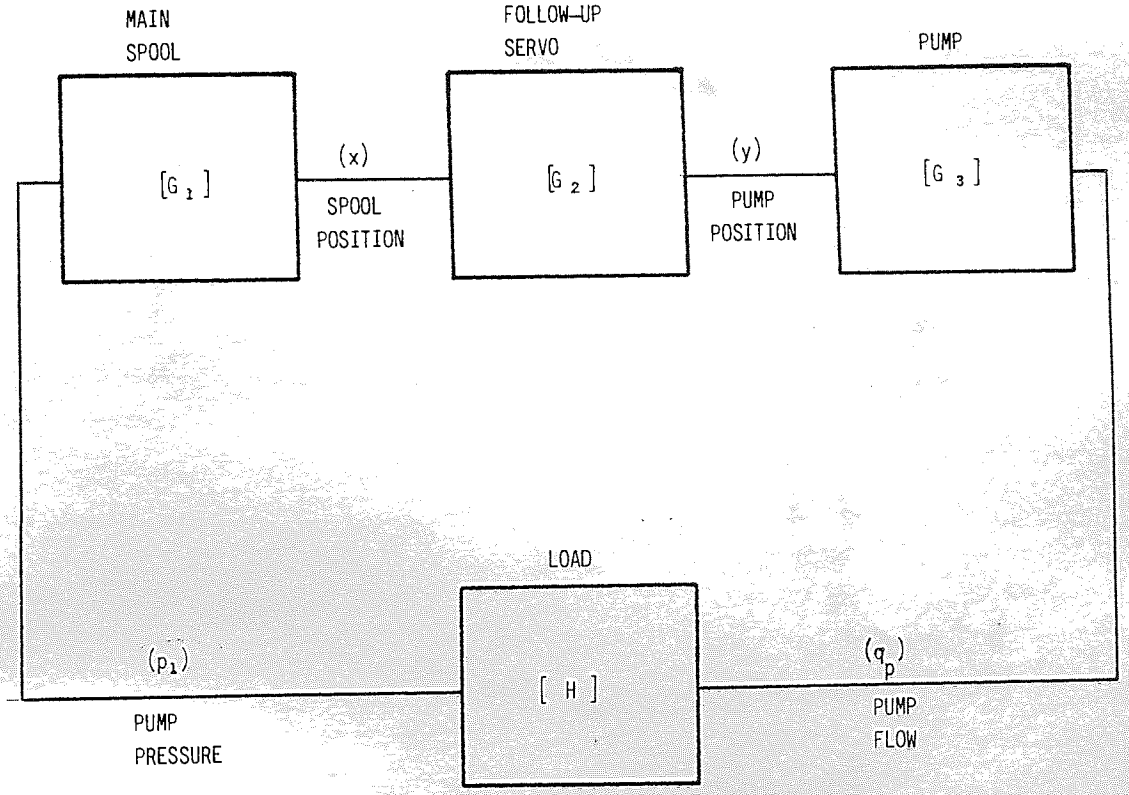

Fig A 2.2 A SIMPLIFIED BLOCK DIAGRAM FOR A PUMP WITH A POWER CONTROLLER

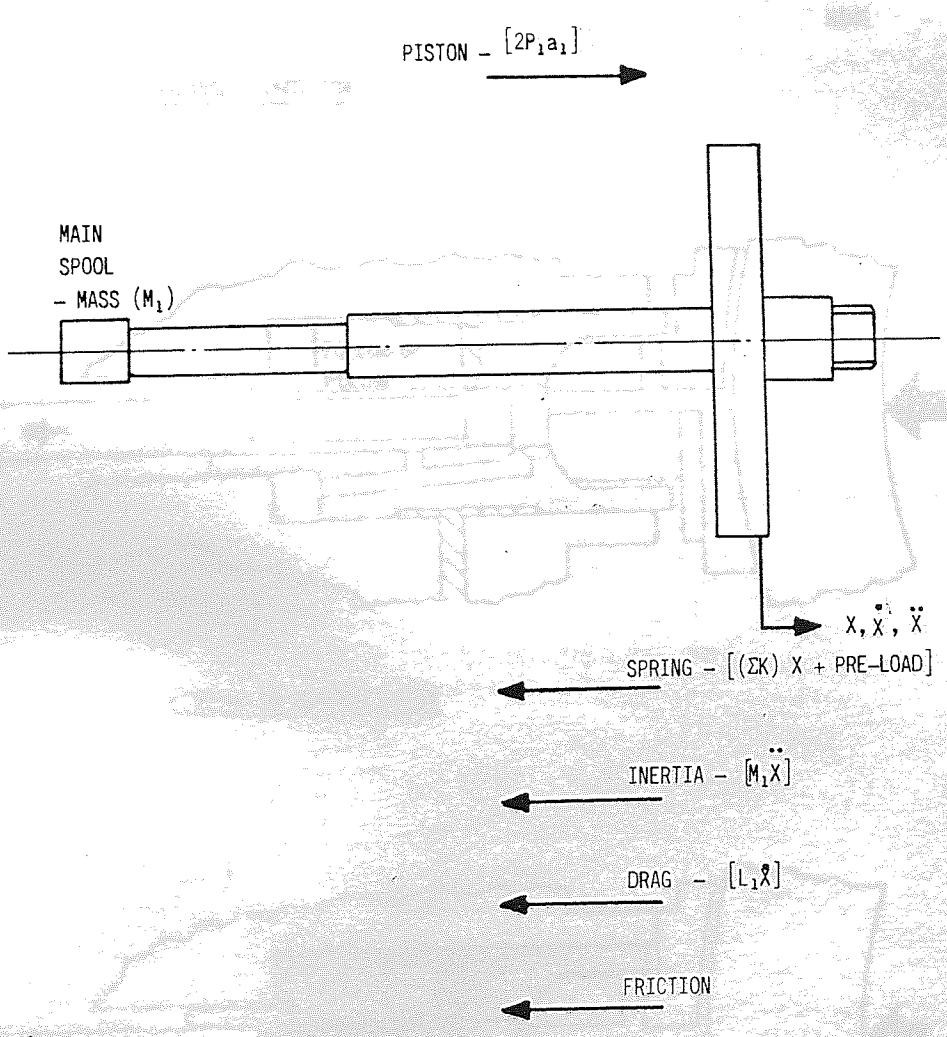

Fig A 2.3 A FREE BODY DIAGRAM FOR THE MAIN SPOOL (IN POWER CONTROL)

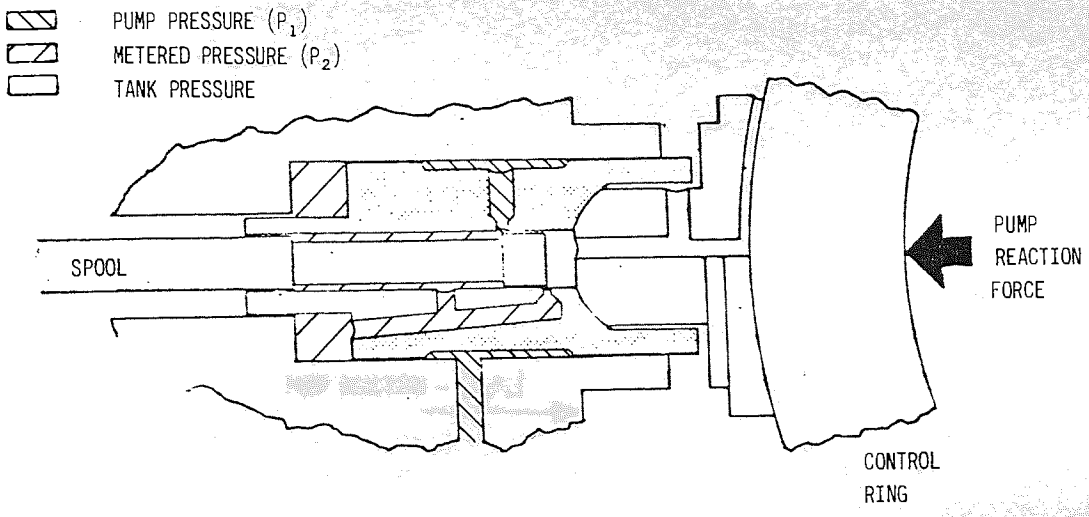

(a) BALANCED CONDITION

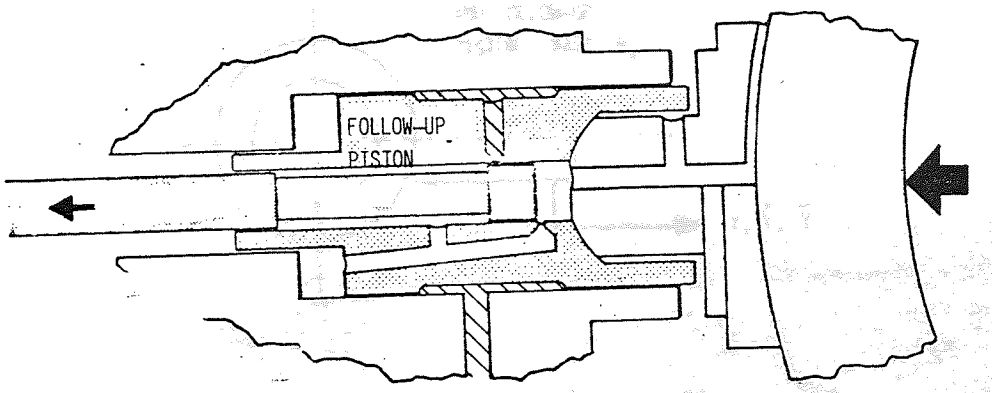

(b) DECREASE IN DEMANDED FLOW

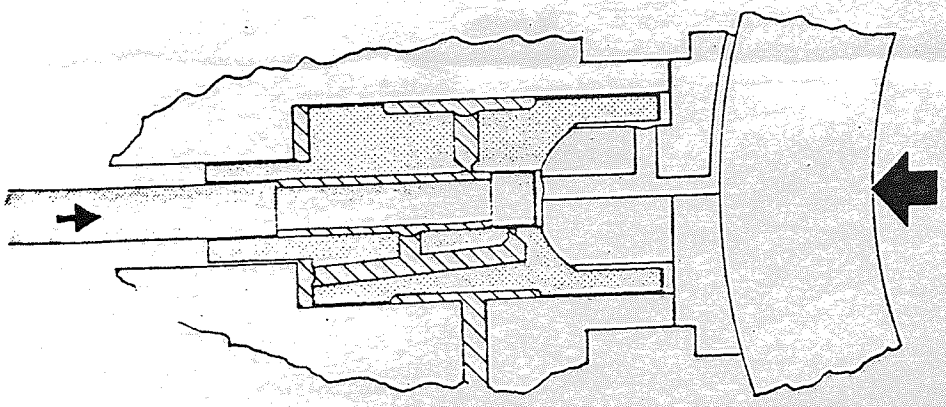

(c) INCREASE IN DEMANDED FLOW

Fig A 2.4 OPERATION OF THE FOLLOW-UP SERVO

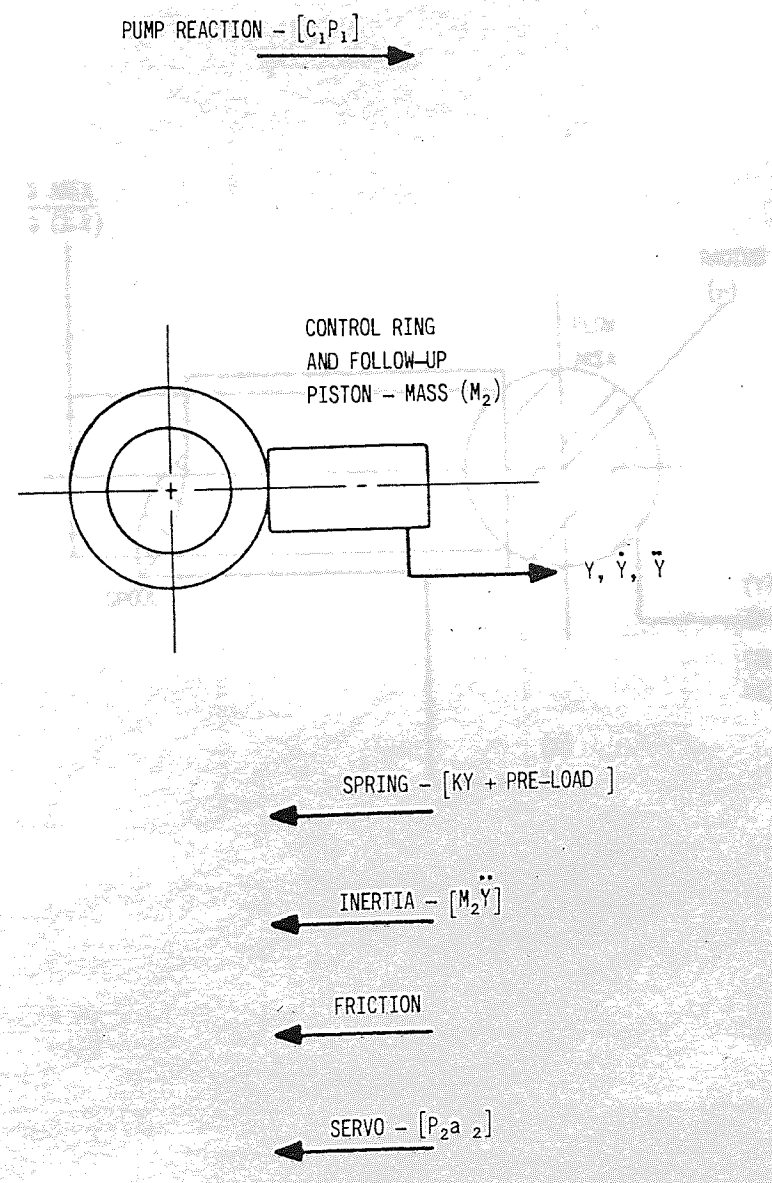

Fig A 2.5 FREE BODY DIAGRAM FOR THE CONTROL RING AND FOLLOW-UP PISTON

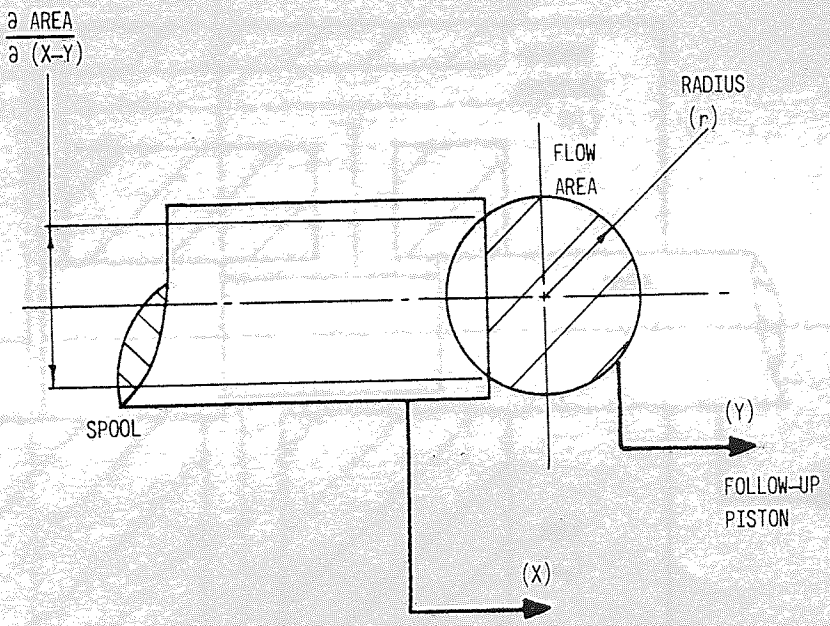

Fig A 2.6 METERING OF THE FOLLOW-UP SERVO

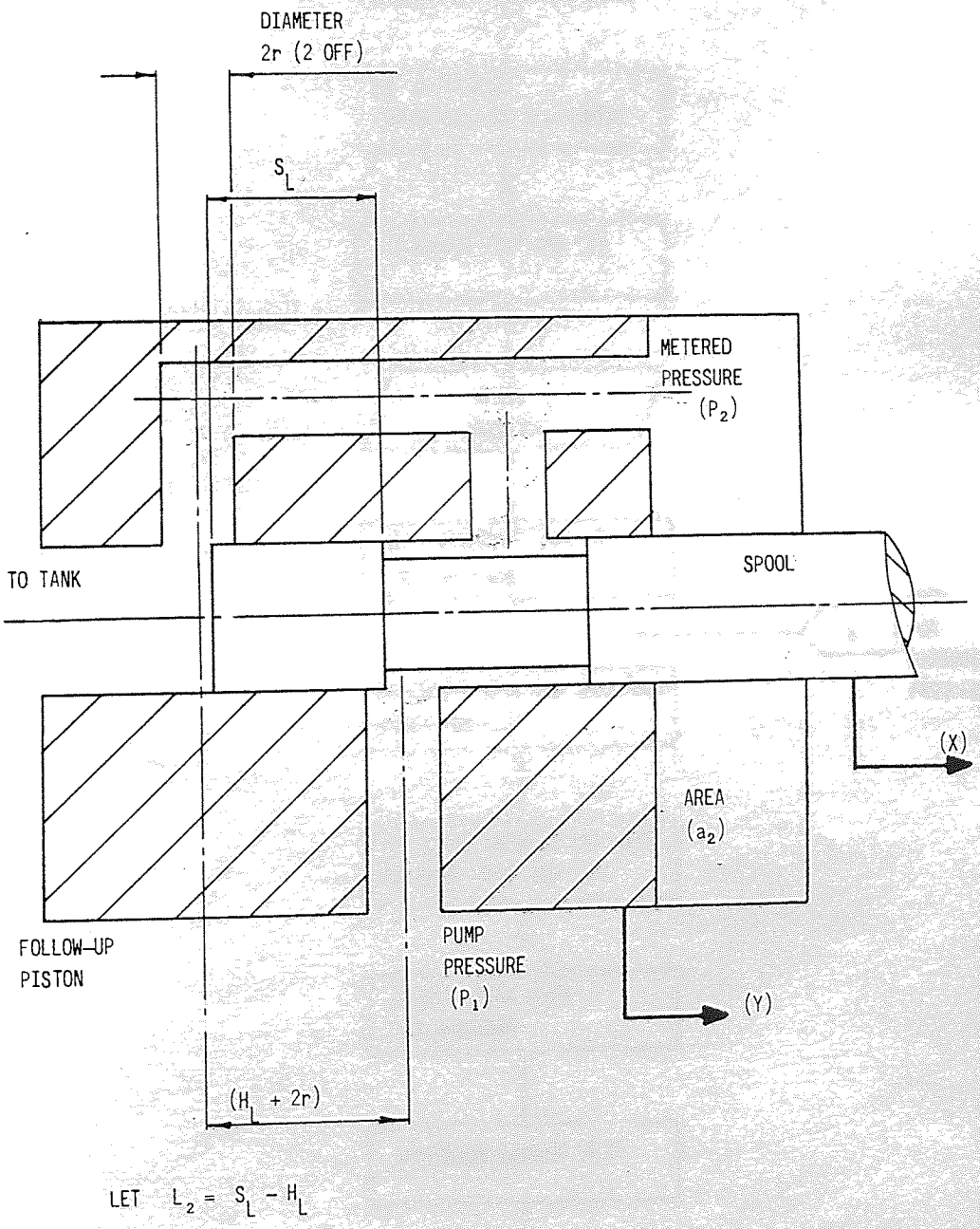

Fig A 2.7 THE LAP OF THE FOLLOW-UP SERVO

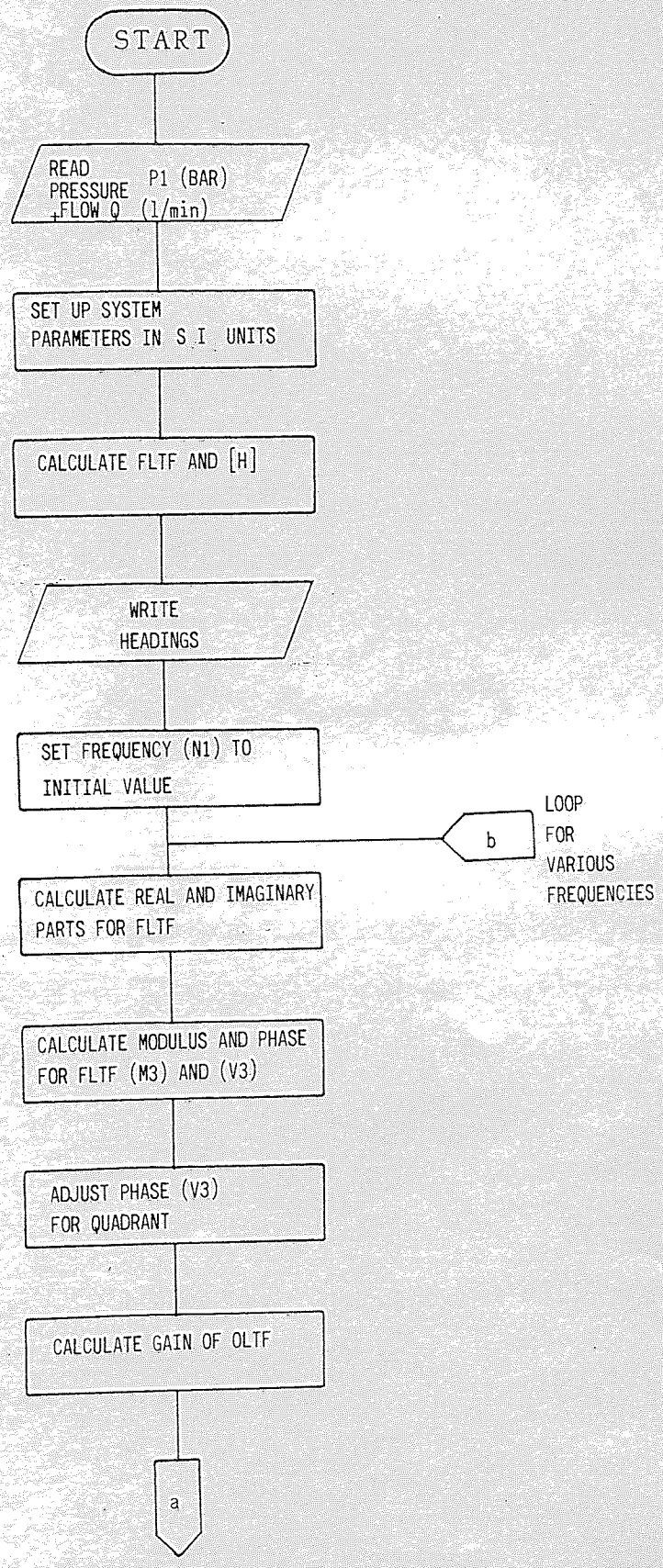

Fig A 2.8 FLOW CHART FOR "CONSTP" - THE COMPUTER PROGRAM TO DETERMINE THE NYQUIST TRACE FOR A POWER CONTROLLER

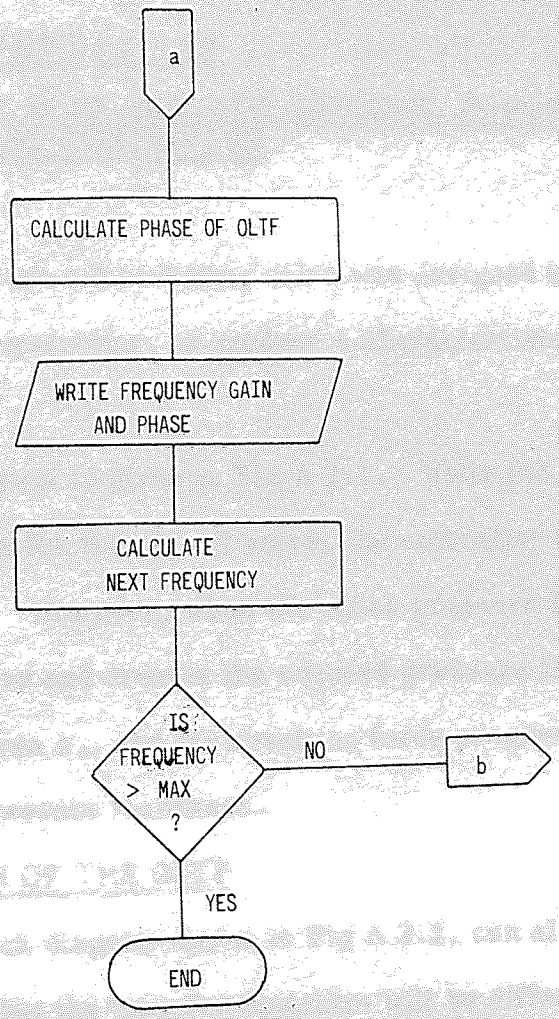

Fig 2.8 (Continued)

APPENDIX A3

DETERMINATION OF THE OLTF FOR THE ORIGINAL POWER AND PRESSURE COMPENSATING CONTROLLER

A 3.1 INTRODUCTION

The original pressure compensating valve was designed to work in conjunction with the power controller, to produce a characteristic similar to that shown in Fig 2.9.

A sketch of the system is given in Fig A 3.1. While the pressure is below the cracking pressure for the cut-off valve, the controller behaves as described in Appendix A 2. However, when the crack pressure is exceeded, flow passes through the valve and creates the metered pressure (Pm). This acts upon a small piston, area a_3, and the resulting force progressively de-strokes the pump, as pressure increases.

A 3.2 DETERMINATION OF THE OLTF

The simplified block diagram shown in Fig A 2.2, can also be applied to this controller, except that the transfer functions will be different.

In determining the OLTF for this controller, the same assumptions have been made as described in Appendix A 2.

A 3.2.1 THE TRANSFER FUNCTION FOR THE MAIN SPOOL [G_1]

The free body diagram in Fig A 2.3, shows the forces associated with the main spool for the power controller. When the compensating valve operates, a further force ($P_m a_3$) acts upon the spool in the opposite direction to that from the spring pack. The resulting linearised equation of motion is

$$2 a_1 p_1 + a_3 p_m = (M_1 s^2 + L_1 s + \Sigma K)x \quad - \quad A\ 3.1$$

A free body diagram for the compensating spool is shown in Fig A 3.2. Assuming that the flow and viscous forces are negligible, the linearised equation of motion is

$$(M_z s^2 + K_4)z = p_1 a_c \quad - \quad A\ 3.2$$

A further relationship between the metered pressure (P_m) and spool travel (Z), can be determined by considering the flow through the valve. Applying the theorem of continuity and ignoring any compressibility flow gives

$$Q(in) = Q(out) + a_3 \dot{x}$$

or linearising

$$q(in) = q(out) + a_3 s x \qquad - \text{A 3.3}$$

Now Q(in)obeys the orifice square law relationship

$$Q(in) = C_d\, a(in) \sqrt{\frac{2(P_1 - P_m)}{\rho}}$$

or in its linearised form

$$q(in) = C_z \cdot z + \alpha (P_1 - P_m) \qquad - \text{A 3.4}$$

where $$C_z = C_d \sqrt{\frac{2(P_1 - P_m)}{\rho}} \frac{\partial a(in)}{\partial Z}$$

$$\alpha = \frac{C_d\, a(in)}{\sqrt{2\rho\,(P_1 - P_m)}}$$

The metering of the compensator spool is shown in Fig A 3.3 and it can be shown that

$$a(in) = r_z^2 \left[\cos^{-1} \frac{(Z - r_z)}{r_z} - \frac{1}{2} \sin \left(2 \cos^{-1} \frac{(Z - r_z)}{r_z}\right) \right] \qquad - \text{A 3.5}$$

$$\frac{\partial a(in)}{\partial Z} = \frac{r_z}{\sqrt{1 - \frac{(Z - r_z)^2}{r_z^2}}} \left[1 - \cos \left(2 \cos^{-1} \frac{(Z - r_z)}{r_z}\right) \right] \qquad - \text{A 3.6}$$

Similarly for the flow out of the valve (Q(out))

$$Q(out) = C_d\, a(out) \sqrt{\frac{2 P_m}{\rho}}$$

or $$q(out) = - C'_z\, z + \alpha' p_m \qquad - \text{A 3.7}$$

where $C_z' = C_d \sqrt{\frac{2 P_m}{\rho}} \frac{\partial a(out)}{\partial Z}$

$$\alpha' = \frac{C_d \, a(out)}{\sqrt{2\rho \, P_m}}$$

$$a(out) = r_z \left[\cos^{-1} \frac{(L_z - 2r_z - Z)}{r_z} - \frac{1}{2} \sin \left(2 \cos^{-1} \frac{(L_z - 2r_z - Z)}{r_z}\right) \right] \quad - \text{A 3.8}$$

$$\frac{\partial a(out)}{\partial Z} = \frac{r_z}{\sqrt{1 - \frac{(L_z - 2r_z - Z)^2}{r_z^2}}} \left[1 - \cos\left(2 \cos^{-1} \frac{(L_z - 2r_z - Z)}{r_z}\right) \right] \quad - \text{A 3.9}$$

Combining equations A 3.3, A 3.4 and A 3.7

$$\alpha p_1 + (C_z + C_z') z = (\alpha + \alpha') p_m + a_3 \, sx \quad - \text{A 3.10}$$

Rearranging equations A 3.1, A 3.2 and A 3.10 gives

$$[G_1] = \left[\frac{x}{p_1}\right] = \left[\frac{\phi_1 s^2 + \phi_2}{\phi_3 s^4 + \phi_4 s^3 + \phi_5 s^2 + \phi_6 s + \phi_7} \right] \quad - \text{A 3.11}$$

where $\phi_1 = M_z \left(\alpha + \frac{2a_1 (\alpha + \alpha')}{a_3}\right)$

$$\phi_2 = K_4 \left(\alpha + \frac{2a_1 (\alpha + \alpha')}{a_3}\right) + a_c (C_z + C_z')$$

$$\phi_3 = M_1 M_z \frac{(\alpha + \alpha')}{a_3}$$

$$\phi_4 = \frac{(\alpha + \alpha')}{a_3} \left(L_1 + \frac{a_3^2}{(\alpha + \alpha')}\right) M_z$$

$$\phi_5 = \frac{(\alpha+\alpha')}{a_3} (M_1 K_4 + M_z \Sigma K)$$

$$\phi_6 = \frac{(\alpha+\alpha')}{a_3} (L_1 + \frac{a_3^2}{(\alpha+\alpha')}) K_4$$

$$\phi_7 = \frac{(\alpha+\alpha')}{a_3} K_4 \Sigma K$$

A 3.2.2 THE TRANSFER FUNCTION FOR THE FOLLOW-UP SERVO

The basic equation of motion for the control ring and follow-up servo is identical to equation A 2.2.

Eliminating p_2 by substituting into equation A 2.6 gives

$$\left[\frac{(C_p + C_p')C_1 - C_p}{a_2} \right] p_1 + (C_x + C_x') \quad x$$

$$= \left[\begin{array}{l} M_2 \frac{(C_p + C_p')}{a_2} s^2 + a_2 s \\ \\ + \frac{(C_p + C_p')}{a_2} K + (C_x + C_x') \end{array} \right] y \quad - \quad \text{A 3.12}$$

Substituting for p_1 from equation A 3.11 and re-arranging produces the transfer function for the follow-up servo $[G_2]$

$$[G_2]=\left[\frac{Y}{X}\right]=$$

$$\left[\left[M_1M_z\frac{(\alpha+\alpha')}{a_3}\gamma\right]s^4+\left[\frac{(\alpha+\alpha')}{a_3}\gamma\frac{(L_1+a_3^2)M_z}{(\alpha+\alpha')}\right]s^3\right.$$

$$+\left[\frac{(\alpha+\alpha')}{a_3}(M_1K_4+M_z\Sigma K)\gamma+(C_x+C_x')M_z\left(\alpha+2a_1\frac{(\alpha+\alpha')}{a_3}\right)\right]s^2$$

$$+\left[\frac{(\alpha+\alpha')}{a_3}\left(L_1+\frac{a_3^2}{(\alpha+\alpha')}\right)K_4\gamma\right]s$$

$$\left.+\left[\frac{(\alpha+\alpha')}{a_3}K_4\Sigma K\gamma+(C_x+C_x')\left[K_4\left(\alpha+\frac{2a_1(\alpha+\alpha')}{a_3}\right)+(C_z+C_z')a_c\right]\right]\right]$$

$$\Big/$$

$$\left[M_2M_z\frac{(C_p+C_p')}{a_2}\left(\alpha+2a_1\frac{(\alpha+\alpha')}{a_3}\right)\right]s^4$$

$$+s^3\left[a_2M_z\left(\alpha+2a_1\frac{(\alpha+\alpha')}{a_3}\right)\right]$$

$$+s^2\left[M_z\left(\alpha+2a_1\frac{(\alpha+\alpha')}{a_3}\right)\left[\frac{(C_p+C_p')}{a_2}K+(C_x+C_x')\right]\right.$$

$$\left.+M_2\frac{(C_p+C_p')}{a_2}\left[K_4\left(\alpha+2a_1\frac{(\alpha+\alpha')}{a_3}\right)+(C_z+C_z')a_c\right]\right]$$

$$+sa_2\left[K_4\left(\alpha+2a_1\frac{(\alpha+\alpha')}{a_3}\right)+(C_z+C_z')a_c\right]$$

$$+\left[\frac{(C_p+C_p')}{a_2}K+C_x+C_x'\right]\left[K_4\left(\alpha+2a_1\frac{(\alpha+\alpha')}{a_3}\right)+(C_z+C_z')a_c\right]$$

where $\gamma=\dfrac{(C_p+C_p')C_1}{a_2}-C_p$ – A 3.13

A 3.2.3 THE OLTF FOR THE POWER CONTROLLER WITH PRESSURE COMPENSATION

The transfer functions for the pump $[G_3]$ and the hydraulic load $[H]$ are identical to those in Appendix A 2 and are given by equations A 2.10 and A 2.14 respectively. The Nyquist plot of the OLTF can therefore be determined by combining the modulus and phase of these transfer functions, for a series of frequencies. The stability of the system can then be assessed, by applying the Nyquist criterion to the resulting trace.

A 3.3 SYSTEM DATA

The majority of data is identical to that for the power controller and is given in section A 2.3.4. The values of new or changed parameters for this combined control function are:

$a_3 = 3.865 \times 10^{-5}\ m^2$

$M_z = 2.695 \times 10^{-3}\ kg$

$K_4 = 6.151 \times 10^{4}\ N/m$

$a_c = 1.600 \times 10^{-5}\ m^2$

$r_z = 0.257 \times 10^{-3}\ m$

$L_z = 0.56 \times 10^{-3}\ m$

$N = 2500\ rpm$

$\Sigma K = 1.398 \times 10^{5}\ N/m$ (for flows less than 25% of maximum).

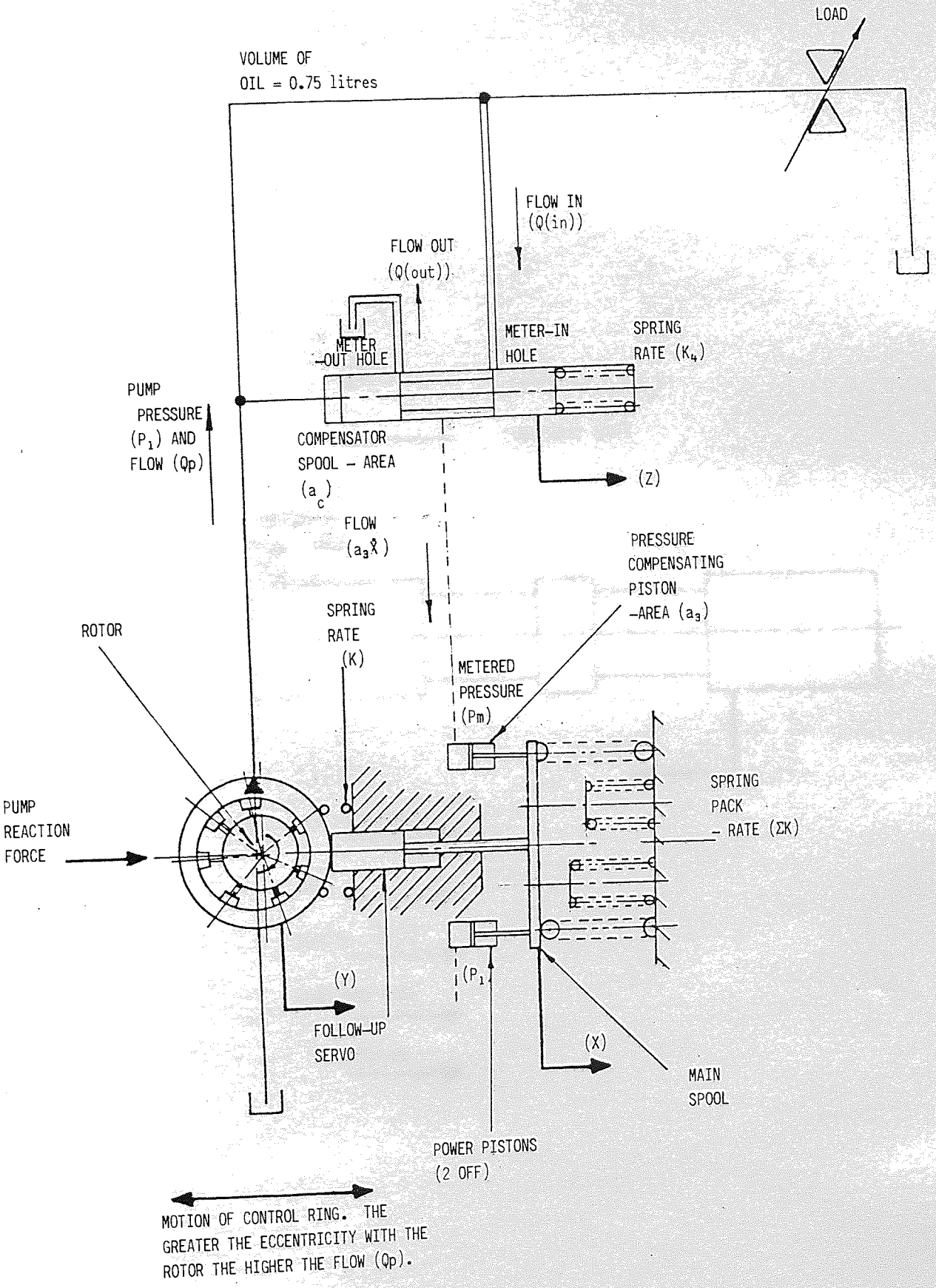

Fig A 3.1 A SKETCH OF THE ORIGINAL POWER AND PRESSURE COMPENSATING CONTROLLERS

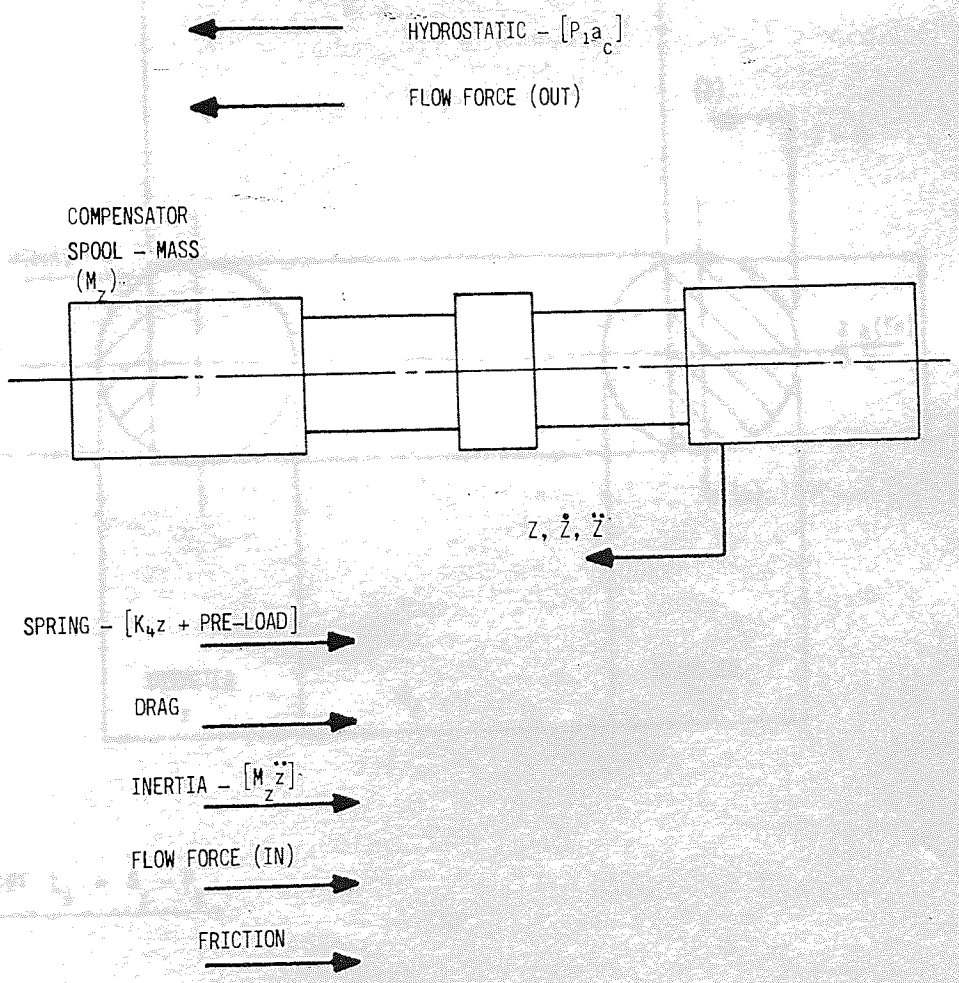

Fig A 3.2 FREE BODY DIAGRAM FOR THE COMPENSATOR SPOOL

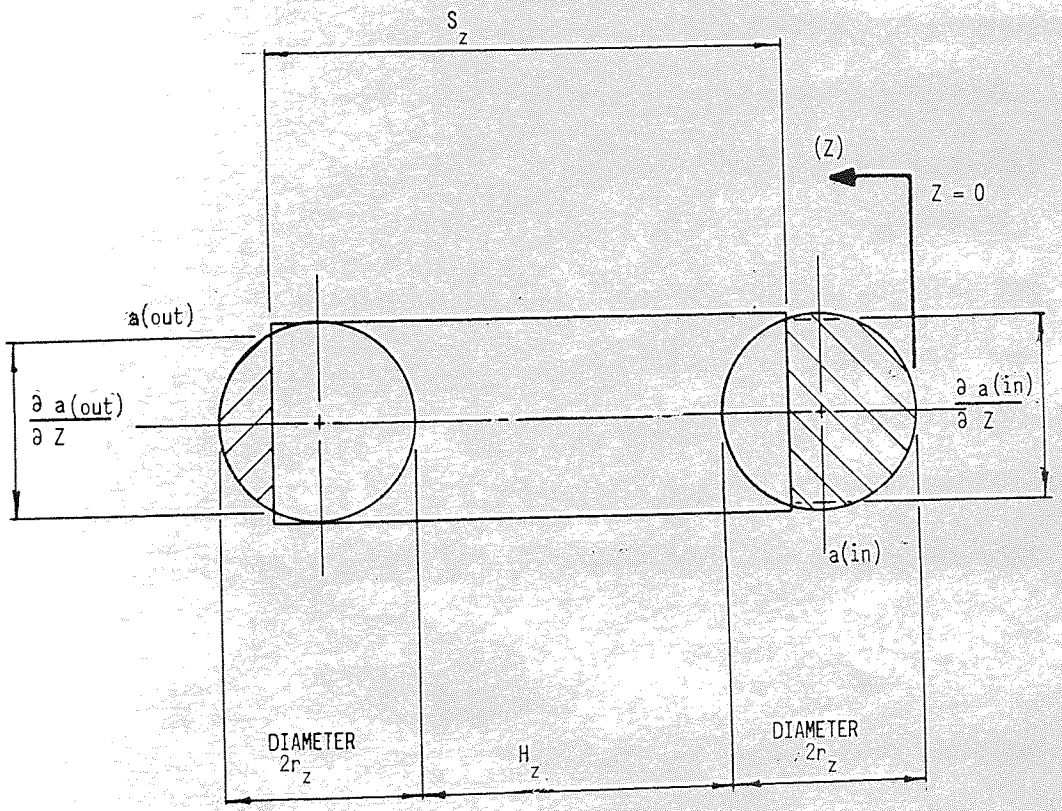

LET $L_z = S_z - H_z$

Fig A 3.3 METERING AREAS OF THE COMPENSATOR VALVE

APPENDIX A4

DETERMINATION OF THE OLTF FOR THE NEW DESIGN OF PRESSURE COMPENSATING NETWORKS

A 4.1 INTRODUCTION

The design of the new pressure compensating network is very similar to the previous system, described in Appendix A 3, except for different metering and the inclusion of a damping orifice.

Also, this system was designed to operate independently of a constant power controller and so the power pistons and spring pack are not present. A typical pressure/flow characteristic for this system is given in Fig 2.7(a).

A schematic of the system is shown in Fig A 4.1. For pressures less than that required to overcome the pre-load in the spring, rate K_4, the pump remains on full flow. However, when this pressure is exceeded, flow passes through the valve creating the metered pressure (P_m). This pressure is sensed by the compensating piston, area a_3, which acts upon the main spool. As P_m increases, the spool moves to the right and the pump is progressively de-stroked.

A 4.2 DETERMINATION OF THE OLTF

In determining the OLTF, the same assumptions have been made as those given in Appendix A 2.

The simplified block diagram for the power controller, shown in Fig A 2.2 can, with different transfer functions, represent the pressure compensating network. The determination of these new transfer functions are given in the following sections.

A 4.2.1 THE TRANSFER FUNCTION FOR THE MAIN SPOOL [G_1]

A free body diagram for the main spool is shown in Fig A 4.2 and the linearised equation of motion is

$$(M_1 s^2 + L_1 s + K_3)x = a_3 p_m \qquad \text{A 4.1}$$

Fig A 4.3 shows the free body diagram for the compensating valve and the linearised equation of motion is

$$(M_z s^2 + K_4)z = p_3 a_c$$

From the results of the previous pressure compensating model, the effect of spool mass (M_z) was shown to be small and so its effect in this model has been ignored. The equation can therefore be simplified to

$$K_4 z = p_3 a_c \qquad - \quad A\ 4.2$$

To relate z, p_1 and p_m the theorem of continuity was applied to the volume at metered pressure (P_m) thus, neglecting compressibility flow

$$Q(in) = Q(out) + a_2 \dot{X}$$

or linearising

$$q(in) = q(out) + a_2 sx \qquad - \quad A\ 4.3$$

Applying the orifice square law relationship for Q(in)

$$Q(in) = C_d a(in) \sqrt{\frac{2 (P_1 - P_m)}{\rho}}$$

or in its linearised form

$$q(in) = C_z z + \alpha(p_1 - p_m) \qquad - \quad A\ 4.4$$

where C_z and α are defined in equation A 3.4.

Similarly

$$Q(out) = C_d a_4 \sqrt{\frac{2 P_m}{\rho}}$$

and linearising gives

$$q(out) = \alpha' p_m \qquad - \quad A\ 4.5$$

where

$$\alpha' = \frac{C_d a_4}{\sqrt{2\rho P_m}}$$

Combining equations A 4.3, A 4.4 and A 4.5 yields

$$C_z z + \alpha p_1 = (\alpha+\alpha')p_m + asx \quad - \quad A\ 4.6$$

The final relationship required before the transfer function $[G_1]$ can be determined, relates the pressures p_1 and p_3. Applying the theorem of continuity to the volume at pressure P_3 and again neglecting compressibility effects gives

$$Q(in) = a_c \dot{Z} \quad - \quad A\ 4.7$$

or in its linearised form

$$q(in) = a_c s z \quad - \quad A\ 4.8$$

Q(in) is through the damping orifice and so applying the square law relationship for pressure and flow

$$Q(in) = C_d a \sqrt{\frac{2 (P_1 - P_3)}{\rho}} \quad - \quad A\ 4.9$$

or linearising

$$q(in) .= \mu(p_1 - p_3) \quad - \quad A\ 4.10$$

where

$$\mu = \frac{C_d a}{\sqrt{2 \rho (P_1 - P_3)}} \quad - \quad A\ 4.11$$

From equation A 4.7 it can be seen that, as $\dot{Z}$ is zero in the steady state, q(in) is also zero. Substituting this into equation A 4.9 yields the result that p_3 equals p_1. This implies that the orifice has no effect – which is obviously wrong and so a different approach to the analysis was required.

The effect of the damping orifice is to create a damping force which opposes motion of the compensator spool. This damping stabilizes an otherwise unstable system. This results in the spool continually oscillating, or limit cycling, with a magnitude and frequency dependent upon the whole system.

To account for this it is necessary to introduce a relationship between the damping force and the amplitude of the limit cycle. This can be achieved

by assuming that the motion of the spool is harmonic thus,

$$Z = A \sin \omega t$$

where A = The maximum amplitude of the oscillation.

Differentiating this equation with respect to time gives the velocity of the spool which has a maximum value of

$$\hat{\dot{Z}} = A\omega \qquad - \text{ A 4.12}$$

Substituting A 4.12 into equation A 4.7 gives

$$\hat{Q}(in) = a_c A\omega$$

Now substituting this into equation A 4.9 and re-arranging results in

$$|P_1 - P_3| = \left[\frac{a_c A\omega}{C_d a}\right]^2 \frac{\rho}{2} \qquad - \text{ A 4.13}$$

Thus, from equations A 4.11 and A 4.13

$$\mu = \frac{(C_d a)^2}{\rho a_c A \omega} \qquad - \text{ A 4.14}$$

The relationship between p_1 and p_3 can therefore be determined, for various amplitudes, by combining equations A 4.8 and A 4.10

$$p_3 = p_1 - \frac{a_c}{\mu} sz \qquad \text{A 4.15}$$

The transfer function for the main spool can now be determined by combining and re-arranging equations A 4.1, A 4.2, A 4.6 and A 4.15 to give

$$[G_1] = \left[\frac{x}{p_1}\right] = \left[\frac{\frac{a_3}{(\alpha+\alpha')}\left[\alpha K_4 + C_z a_c + \frac{\alpha a_c^2 s}{\mu}\right]}{\left[M_1 \frac{a_c^2}{\mu}\right] s^3 + \left[M_2 K_4 + \frac{a_c^2}{\mu}\left(L_1 + \frac{a_3^2}{(\alpha+\alpha')}\right)\right] s^2 + \left[K_4\left(L_1 + \frac{a_3^2}{(\alpha+\alpha')}\right) + K_3 \frac{a_c^2}{\mu}\right] s + K_3 K_4}\right] \qquad - \text{ A 4.16}$$

A 4.2.2 THE COMBINED TRANSFER FUNCTION FOR THE MAIN SPOOL AND FOLLOW-UP SERVO $[G_1]\,[G_2]$

Combining equations A 3.12 and A 4.16 and re-arranging gives $[G_1]\,[G_2]$, the transfer function for the main spool and the follow-up servo

$$[G_1]\,[G_2] = \left[\frac{y}{p_1}\right] = \gamma \left[\frac{\begin{array}{l} M_2\,\lambda_1\,s^3 + (M_2\,K_4 + \lambda_1\,\lambda)s^2 \\ + \left(K_4\lambda + K_3\lambda_1 + \dfrac{\alpha\lambda_1\lambda_3}{\gamma}\right)s \\ + K_3K_4 + \dfrac{\lambda_3}{\gamma}(\alpha\,K_4 + C_z\,a_c) \end{array}}{\begin{array}{l} s^5\,\lambda_4\,M_z\,M_1\,\lambda_1 \\ + s^4\,(\lambda_4\,M_2\,(M_1\,K_4 + \lambda_1\,\lambda) + a_2\,M_1\,\lambda_1) \\ + s^3 \left[\begin{array}{l} (\lambda_4\,K + C_x + C_x')\,M_1\,\lambda_1 \\ + (M_1\,K_4 + \lambda_1\,\lambda)a_2 \\ + M_2\,\lambda_4\,(K_4\lambda + K_3\lambda_1) \end{array} \right] \\ + s^2 \left[\begin{array}{l} K_3\,K_4\,M_2\,\lambda_4 + a_2\,(K_4\lambda + K_3\lambda_1) \\ + (C_x + C_x' + K\,\lambda_4)\,(M_2\,K_4 + \lambda_1\lambda) \end{array} \right] \\ + s \left[\begin{array}{l} a_2\,K_3\,K_4 \\ + (C_x + C_x' + \lambda_4\,K)\,(K_4\lambda + K_3\lambda_1) \end{array} \right] \\ + K_3\,K_4\,(C_x + C_x' + \lambda_4\,K) \end{array}} \right] \qquad \text{A 4.17}$$

where $\gamma = (C_p + C_p')/a_2 - C_p$

$$\lambda = L_1 + \frac{a_3^2}{\alpha+\alpha'}$$

$$\lambda_1 = \frac{a_c^2}{\mu}$$

$$\lambda_2 = C_x + C_x' + (C_p + C_p')\frac{K}{a_2}$$

$$\lambda_3 = a_3\,(C_x + C_x')/(\alpha+\alpha')$$

$$\lambda_4 = \frac{C_p + C_p'}{a_2}$$

A 4.2.3 DETERMINATION OF THE NYQUIST PLOT

The method used to determine the Nyquist plot in the previous Appendices cannot be directly applied in this case because the damping of the compensating spool is dependent upon the amplitude of the limit cycle.

The approach adopted to take this into account is similar to that used for describing functions.

The Nyquist criterion was derived by considering the denominator of the closed loop transfer function (CLTF) and equating this to zero (for infinite amplitude).

$$1 + [G][H] = 0$$

or

$$[G][H] = -1$$

The describing function technique uses a slightly different approach and re-writes this equation so, in this particular case

$$[G_3][H] = -\frac{1}{[G_1][G_2]} \qquad \text{A 4.18}$$

where $[G_3]$ is given by equation A 2.10

$[H]$ is given by equation A 2.14

$[G_1][G_2]$ is given by equation A 4.17

The right hand side of this equation represents the locus of the "-1" point for various amplitudes and frequencies. Where this curve intersects the $[G_3][H]$ locus, at the same frequency, determines the frequency and amplitude of the limit cycle.

A 4.2.4 MODEL DATA

The majority of data is identical to that used in the previous models except that

$$a_3 = 1.963 \times 10^{-5} \text{ m}^2$$
$$K_3 = 3.495 \times 10^{4} \text{ N/m}$$
$$K_4 = 4.369 \times 10^{4} \text{ N/m}$$
$$a_4 = 5.0265 \times 10^{-7} \text{ m}^2$$
$$r_z = 0.4 \times 10^{-3} \text{ m (2 off)}$$
$$(a^2/A) = \text{variable}$$

A 4.2.5 THE MAGNITUDE OF THE LIMIT CYCLE

Considering the effect of the limit upon the overall hydraulic system lead to the design criteria that the maximum pressure oscillation should be ± 0.5 bar.

Once the frequency (ω) and amplitude (A) of the limit cycle have been determined, for a particular damping orifice diameter, then from equation A 4.13.

$$P_3 = P_1 \pm \left[\frac{a_c A \omega}{C_d a} \right]^2 \frac{\rho}{2}$$

Thus the magnitude of the pressure ripple (P_r) is

$$P_r = \pm \left[\frac{a_c A \omega}{C_d a} \right]^2 \frac{\rho}{2} \qquad \text{A 4.19}$$

A 4.3 THE EFFECT OF USING A LARGER DIAMETER SPOOL UPON THE MODEL OF THE PRESSURE COMPENSATING NETWORK

The results from the model indicated that an unsuitably small orifice was required to limit the pressure ripple to an acceptable level. To overcome this problem a new design for the valve was conceived and is shown in Fig 3.4. The main difference between this new valve and the previous one was that pump pressure acted upon different areas at each end of the spool. Thus the hydrostatic force on the spool was proportional to the difference between these areas (a_c) but, the damping term was a function of the full spool area (a_s).

In theory there was no limit to the diameter of the compensator spool and the larger the spool, the bigger the damping orifice could be for the same degree of stability. However, a practical limit of 25 mm was imposed because of overall envelope consideration. A scaled assembly drawing of the valve is shown in Fig A 4.4 and it illustrates just how large the valve had become.

The transfer function $[G_1][G_2]$ given in equation A 4.17 is still valid if

$$a_c = a_5 - a_6$$

However, the damping coefficient (μ) must be changed to

$$\mu = \frac{(C_d\ a)^2}{\rho\ a_5\ A\omega} \qquad - \qquad \text{A 4.20}$$

Similarly the equation for the pressure ripple A 4.19 becomes

$$P_r = \pm \left[\frac{a_5\ A\ \omega}{C_d\ a}\right]^2 \frac{\rho}{2} \qquad - \qquad \text{A 4.21}$$

With these alterations the model was valid for the larger design of spool. The parameters of the system were then adjusted to give the most stable results and the modifications to the previous model data were

$a_3 = 4.909 \times 10^{-6}\ m^2$

$a_4 = 1.131 \times 10^{-6}\ m^2$

$a_5 = 4.909 \times 10^{-4}\ m^2$

$a_6 = 4.589 \times 10^{-4}\ m^2$

$a_c = 3.20 \times 10^{-5}\ m^2$

$K_3 = 1.223 \times 10^4 N/m$

$K_4 = 1.398 \times 10^5 N/m$

$r_z = 4.00 \times 10^{-4}\ m$ (2 off)

An additional feature of the valve, shown in Fig A 4.4, was the inclusion of a cascade of orifices. Results from the model indicated that a 0.66 mm diameter orifice was required to limit the pressure ripple to ± 0.5 bar. In order to increase the size of this orifice, without affecting the performance of the valve, four 0.94 mm diameter orifices were used in series.

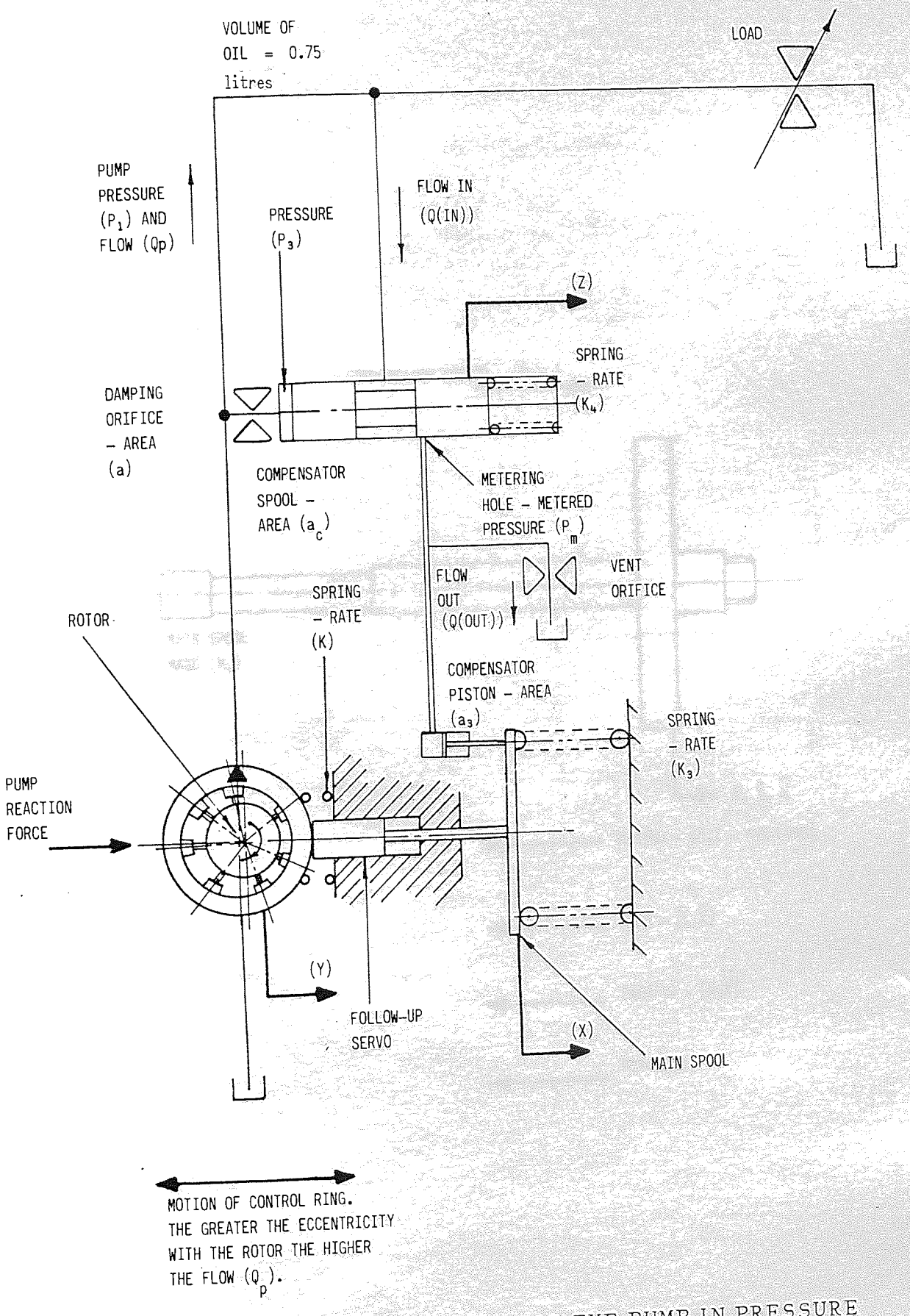

Fig A 4.1 A SCHEMATIC DIAGRAM FOR THE PUMP IN PRESSURE COMPENSATION

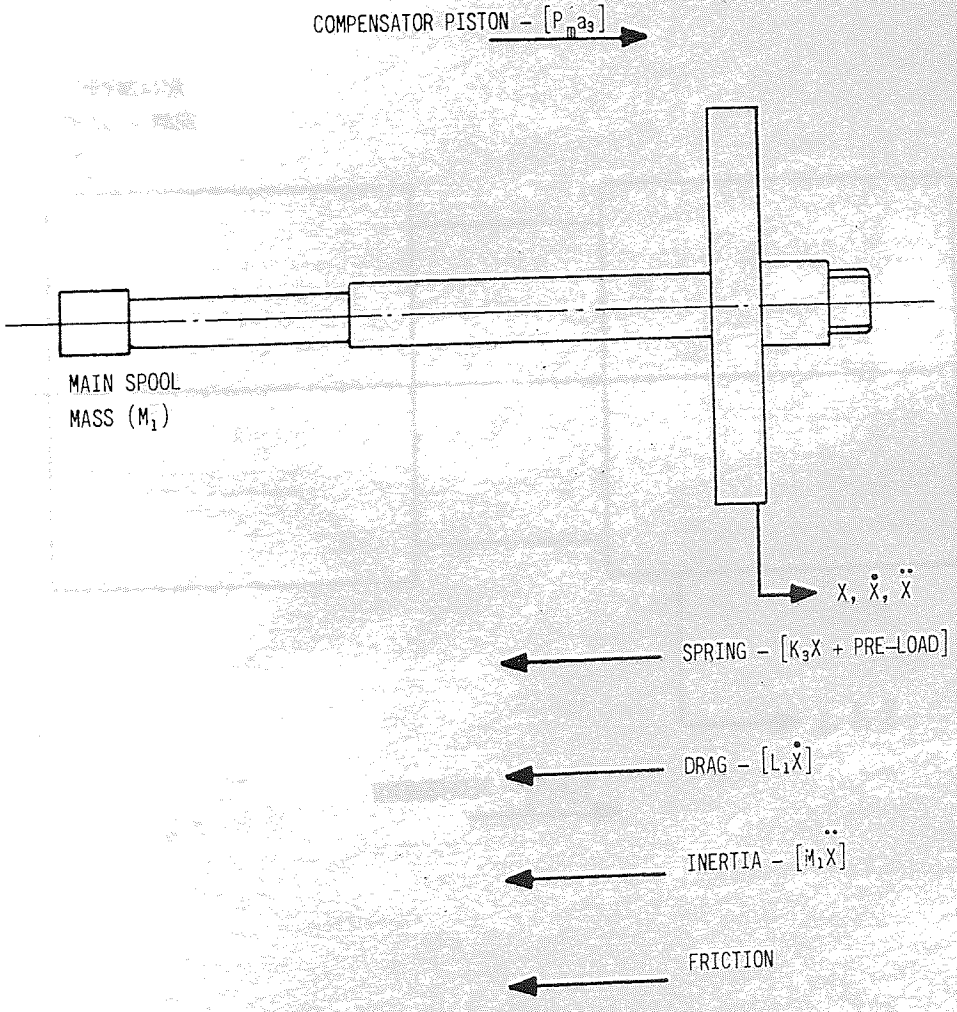

Fig A 4.2 A FREE BODY DIAGRAM FOR THE MAIN SPOOL (IN PRESSURE COMPENSATION)

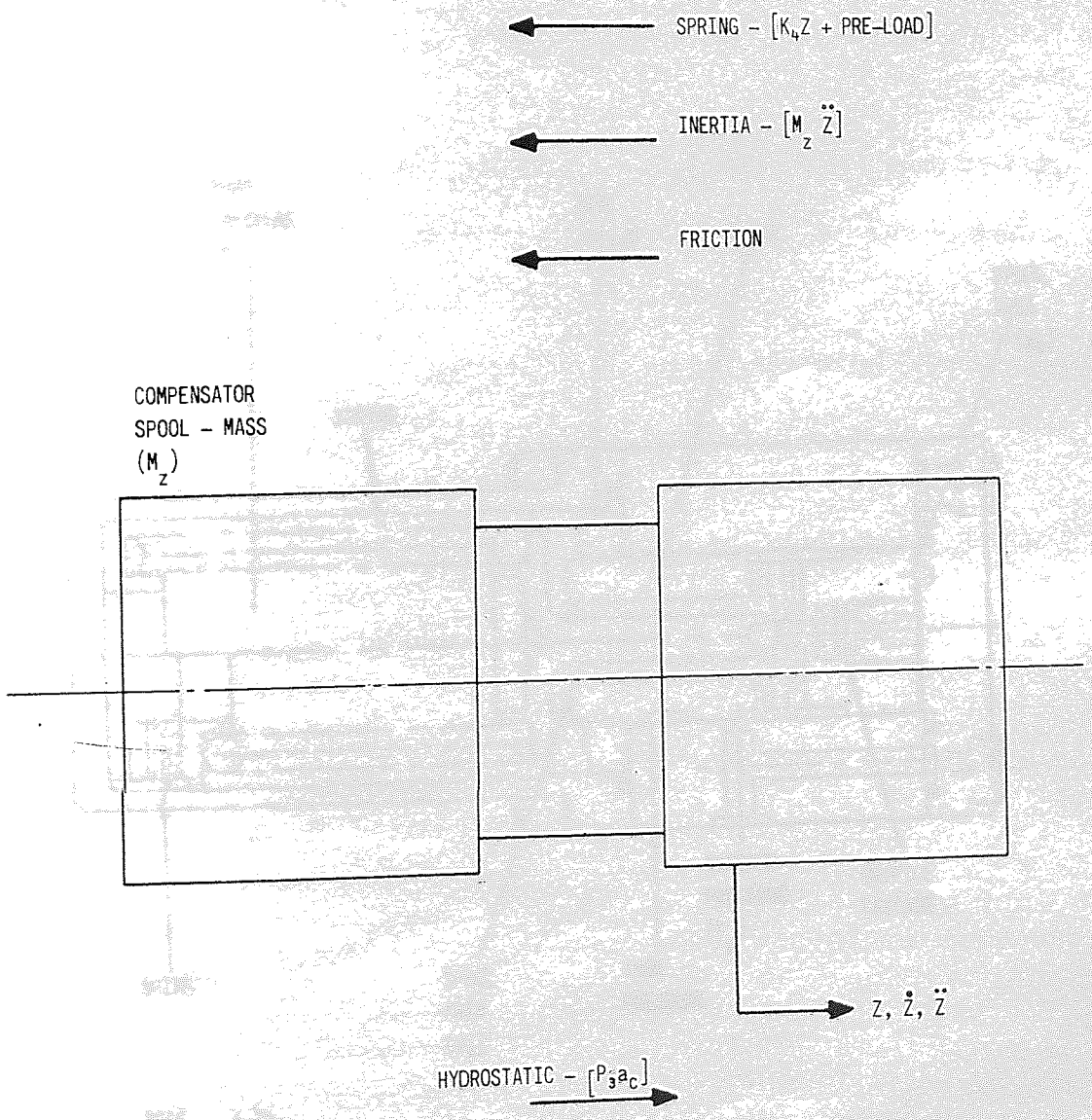

Fig A 4.3 A FREE BODY DIAGRAM FOR THE COMPENSATING SPOOL

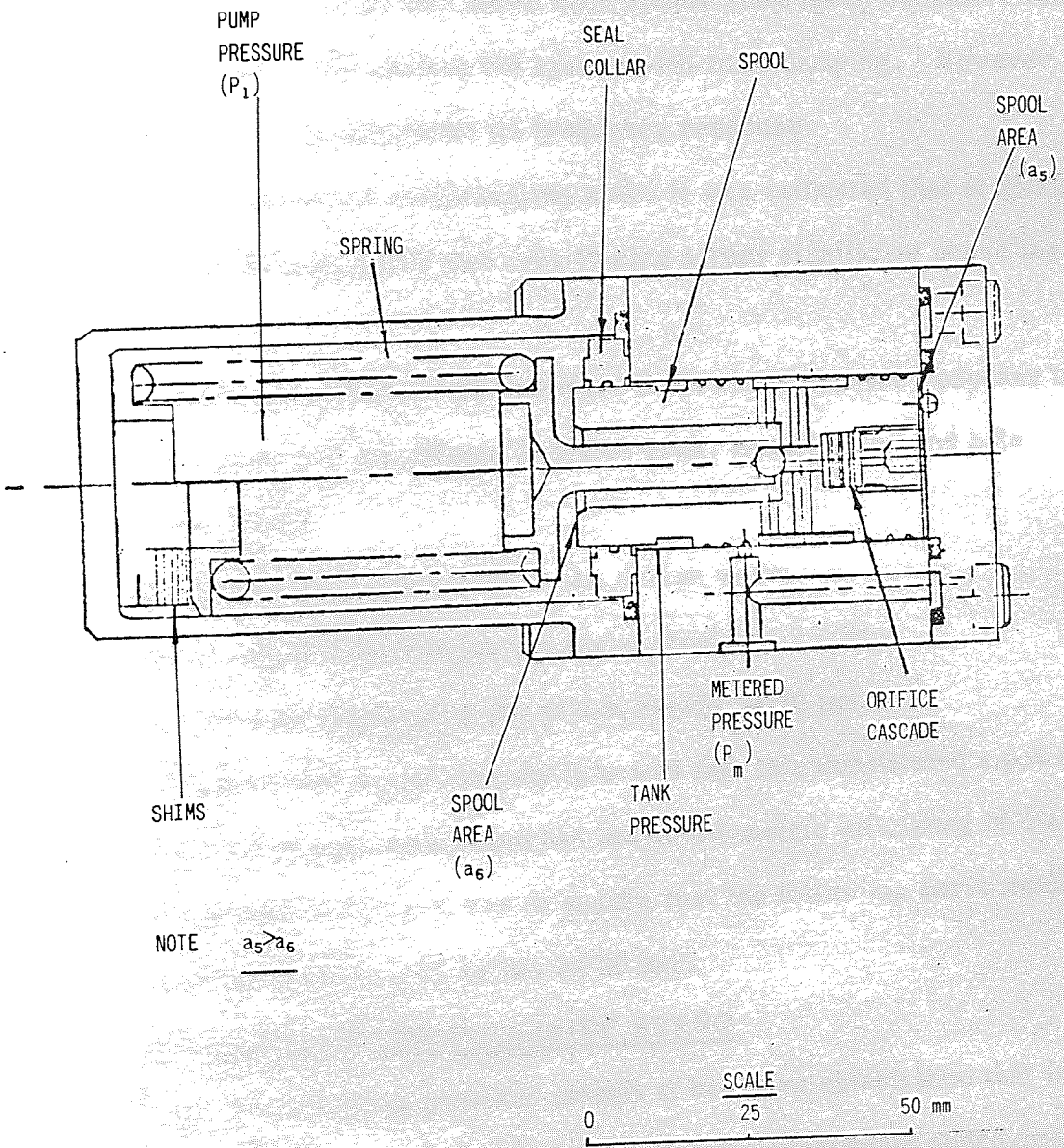

Fig A 4.4 AN ASSEMBLY DRAWING OF THE LARGER DIAMETER PRESSURE COMPENSATING VALVE

APPENDIX A5

THE RE-DESIGN OF THE FOLLOW-UP SERVO

A 5.1 INTRODUCTION

A description of the operation of the follow-up servo is given in Appendix A 2.

The original design was based upon steady state force considerations together with a view to providing the system with some damping. However, no attempt was made to determine its frequency response.

From the pressure compensating model it was estimated that at 250 bar and 10 Hz the follow-up servo was contributing a very significant phase lag of 37°.

A mathematical model was therefore made of the dynamic response of the follow-up servo and the effects of piston area, metering lap and hole diameter were tested.

The steady state limitations to the design were:

1. The maximum flow through the servo should be 2 l/min.
2. The minimum diameter of the piston should be 30 mm.

The reason for minimising the flow was that this constituted a power loss which would be seen as a reduction in the volumetric efficiency of the pump. The second constraint was to ensure that the follow-up servo could control the pump at pressures as low as 20 bar.

A 5.2 THE MODEL OF THE FOLLOW-UP SERVO

From the results of previous models it had been established that the term γ, defined in equation A 3.13, was small and a reasonable approximation on which to base a comparative study was that from equation A 3.12

$$\left[\frac{Y}{X}\right] \simeq \left[\frac{(C_x+C_x')\,a_2}{M_2(C_p+C_p')s^2 + a_2^2 s + (C_p+C_p')K + a_2(C_x+C_x')}\right] \quad - \text{A 5.1}$$

A 5.3 MODEL PREDICTIONS FOR THE FOLLOW-UP SERVO

The data for the original follow-up servo was used in the model and the results for a pressure of 250 bar are given in Fig A 5.1 for frequencies from 1 to 15 Hz.

The parameters of the system were then varied in order to optimise the design within the imposed practical limitations. Generally, the smaller the diameter of the piston and the higher the flow through the valve, then the better the dynamic performance.

The final results are given in Fig A 5.2 and, with reference to Fig A 2.7, they were achieved with

$$a_2 = 6.28 \times 10^{-4}\ m^2$$

$$r = 7.5 \times 10^{-4}\ m$$

$$L_2 = 2.4 \times 10^{-3}\ m$$

From comparing Figs A 5.1 and A 5.2 it was concluded that because the pressure compensating network was particularly sensitive to phase lag, there were considerable advantages to changing to the new design.

To update all previous models to include this new servo the flow areas through the valve had to be altered. Refering to Section A 2.3.1.

$$a(out) = 2.646 \times 10^{-7}\ m^2$$

$$a(in) = 2.388 \times 10^{-7}\ m^2$$

$$\frac{\partial\, a(out)}{\partial\, (X-Y)} = 1.216 \times 10^{-3}\ m$$

$$\frac{\partial\, a(in)}{\partial\, (X-Y)} = -1.184 \times 10^{-3}\ m$$

Also the new piston area of $6.28 \times 10^{-4}\ m^2$ had to be included.

FREQUENCY (Hz)	MODULUS	PHASE (DEGREES)
1	.997	- 4.3
2	.989	- 8.6
3	.975	- 12.8
4	.957	- 16.9
5	.935	- 20.8
6	.910	- 24.5
7	.883	- 28.0
8	.855	- 31.3
9	.826	- 34.4
10	.796	- 37.2
11	.767	- 39.9
12	.739	- 42.4
13	.711	- 44.7
14	.685	- 46.8
15	.660	- 48.8

Fig A 5.1 FREQUENCY RESPONSE FOR THE ORIGINAL FOLLOW-UP SERVO AT 250 BAR

FREQUENCY (Hz)	MODULUS	PHASE (DEGREES)
1	1.000	- 0.9
2	1.000	- 1.7
3	.999	- 2.6
4	.998	- 3.4
5	.997	- 4.2
6	.996	- 5.1
7	.995	- 6.0
8	.993	- 6.8
9	.992	- 7.6
10	.990	- 8.5
11	.988	- 9.3
12	.985	- 10.1
13	.983	- 11.0
14	.980	- 11.8
15	.977	- 12.6

Fig A 5.2 FREQUENCY RESPONSE FOR THE NEW FOLLOW-UP SERVO AT 250 BAR

APPENDIX A6

THE STABILITY MODEL FOR THE CCS CONTROLLER

A 6.1 INTRODUCTION

A schematic diagram for this controller is shown in Fig A 6.1 and a description of its operation is given in Section 2.6.

From the results of the Hydreco CCS system it was established that the stand-by condition constituted the least stable state. Therefore, this model was simplified by designing it to only cater for this particular operating condition.

The assumptions made in determining the model are the same as those described in Appendix A 2.

A 6.2 THE OLTF FOR THE SYSTEM

The block diagram for the power controller, shown in Fig A 2.2, can also be applied to the CCS system. The individual transfer functions must therefore be determined before the OLTF can be calculated.

A 6.2.1 THE TRANSFER FUNCTION FOR THE MAIN SPOOL $[G_1]$

A free body diagram for the main spool is shown in Fig A 6.2. Using the small pertabation technique the resulting linearised equation of motion is

$$p_m a_8 = (M_1 s^2 + L_1 s + K_7) x \qquad - \text{ A 6.1}$$

In order to determine $[G_1]$ it is necessary to relate the pump pressure (P_1) to the CCS piston pressure (P_m). This can be done by considering the flow through the volume at pressure P_m. By continuity and assuming that compressibility effects are small

$$Q(in) = Q(out)$$

$$\text{or} \quad q(in) = q(out) \qquad - \text{ A 6.2}$$

The flow into this volume (Q(in)) passes through the damping orifice and so applying the square law relationship for pressure and flow

$$Q(in) = C_d a_9 \sqrt{\frac{2}{\rho}(P_1 - P_m)} \quad - \text{A 6.3}$$

linearising gives

$$q(in) = \mu' (p_1 - p_m) \quad - \text{A 6.4}$$

where $$\mu' = \frac{C_d a_9}{\sqrt{2\rho (P_1 - P_m)}} \quad - \text{A 6.5}$$

The flow leaving the volume is proportional to the velocity of the main spool thus

$$Q(out) = a_8 \dot{X}$$

or $$q(out) = a_8 sx \quad - \text{A 6.6}$$

Combining equations A 6.2, A 6.4 and A 6.6 gives

$$p_m = p_1 - \frac{a_8}{\mu'} sx \quad - \text{A 6.7}$$

The damping term μ' is dependent upon the velocity of the main spool and is similar to the term μ in Appendix A 4. Thus the CCS system will behave in a similar manner to the pressure compensating controller, by oscillating with an amplitude dependent upon the size of the damping orifice (a_9). Assuming this oscillation is harmonic, it allows the following relationship to be used for the velocity of the main spool

$$\dot{X} = A'\omega \cos \omega t$$

where A' = The maximum amplitude of the oscillation. Therefore the maximum velocity is

$$\hat{\dot{X}} = A' \omega \quad - \text{A 6.8}$$

Thus the maximum flow into the considered volume is

$$\hat{Q}(in) = a_8 A'\omega \quad - \text{A 6.9}$$

Combining equations A 6.3 and A 6.9 and rearranging gives

$$p_m = p_1 \pm \left[\frac{a_8 A'\omega}{C_d a_9}\right]^2 \frac{\rho}{2} \quad - \text{A 6.10}$$

Also, combining equations A 6.3, A 6.8 and A 6.5 yields

$$\mu' = \frac{(C_d\, a_9)^2}{\rho a_8 A' \omega} \qquad - \text{ A 6.11}$$

The transfer function for the main spool $[G_1]$ can now be determined by substituting for p_m from equation A 6.7 in A 6.1

$$[G_1] = \left[\frac{x}{p_1}\right] = \left[\frac{\dfrac{a_8}{M_1 s^2 + (L_1 + a_8^2)s + K_7}}{\bar{\mu}'}\right] \qquad - \text{ A 6.12}$$

A 6.2.2 THE TRANSFER FUNCTION FOR THE FOLLOW-UP SERVO $[G_2]$

The transfer function for the follow-up servo can be determined by combining equations A 3.12 and A 6.12 thus

$$[G_2] = \left[\frac{y}{x}\right] = \left[\frac{\left[\dfrac{(C_p + C_p')}{a_2} \quad C_1 - C_p\right]\left[\dfrac{M_1 s^2 + (L_1 + a_8^2)\, s}{\bar{\mu}'} + K + \dfrac{(C_x + C_x')a_2}{((C_p + C_p')C_1 - C_p a_2)}\right]}{M_2 \dfrac{(C_p + C_p')}{a_2} s^2 + a_2 s + (C_p + C_p')K + (C_x + C_x')}\right]$$

$$- \text{ A 6.13}$$

A 6.2.3 COMBINING THE TRANSFER FUNCTIONS TO FORM THE OLTF

The transfer function for the pump $[G_3]$ is given by equation A 2.10. Assuming the flow to the CCS piston is small in comparison to the flow from the pump then $[H]$, the transfer function for the load, can be expressed

$$[H] = \left[\frac{p_1}{q_p}\right] = -\left[\frac{1}{\frac{v}{\beta} \cdot s + \frac{C_d\, a_7}{\sqrt{2\rho\, P_1}}}\right] \qquad - \text{ A 6.14}$$

The determination of system stability is identical to that described in section A 4.2.3 and involves the intercept point for the equation

$$[G_3]\ [H] = -\frac{1}{[G_1]\ [G_2]} \qquad - \text{ A 6.15}$$

Where $[G_1]\ [G_2]$ represents the amplitude dependent transfer function and can be derived from equations A 6.12 and A 6.13 giving

$$[G_1][G_2] = \left[\frac{y}{p_1}\right] = \left[\frac{a_8\gamma \left[M_1 s^2 + \lambda_5 s + K + (C_x + C_x')/\gamma \right]}{\begin{array}{l} M_1 M_2 \lambda_7 s^4 \\ + s^3 (M_1 a_2 + M_2 \lambda_7 \lambda_5) \\ + s^2 (M_1 \lambda_6 + \lambda_5 a_2 + K_7 M_2 \lambda_7) \\ + s (\lambda_5 \lambda_6 + K_7 a_2) \\ + K_7 \lambda_6 \end{array}}\right]$$

$$- \text{ A 6.16}$$

where $\gamma = (C_p + C_p')/a_2 - C_p$

$\lambda_5 = L_1 + \dfrac{a_8^2}{\mu'}$

$\lambda_6 = (C_p + C_p')K/a_2 + C_x + C_x'$

$\lambda_7 = (C_p + C_p')/a_2$

A 6.2.4 RESULTS FROM THE CCS STABILITY MODEL

The required steady state characteristic for the system was that the flow from the pump should be at a maximum when the CCS pressure was 3 bar and at a minimum when p_m = 20 bar. This determined the relationship between a_8 and K_7 as the stroke of the 77 ml/rev pump was 7.50 mm.

Various values for a_8 wereused and it was found that the larger the piston then the larger the damping orifice (a_9), for the same amplitude of limit cycle. A practical limitation on the diameter of the CCS piston was imposed at 13 mm because of envelope considerations for the complete controller package.

Fig 3.7 shows the resulting Nyquist trace when the following values were used in the model

$$K_7 = 3.32 \times 10^4 \text{ N/m}$$

$$a_7 = 4.15 \times 10^{-6} \text{ m}^2$$

$$a_8 = 1.327 \times 10^{-4} \text{ m}^2$$

(All other parameters are given in previous Appendices).

Using the stability criterion described in Appendix A 4 it can be deduced that the system will oscillate at 14 Hz, with (a_9^2/A') at $0.79 \times 10^{-10} \text{ m}^2$.

From equation A 6.10 the pressure ripple P_r' is given by

$$P_r' = \pm \left[\frac{a_8 A' \omega}{C_d a_9}\right]^2 \frac{\rho}{2} \qquad - \quad \text{A 6.17}$$

Inserting the intersect values into this equation gives a predicted pressure ripple of ±3 bar when a 0.40 mm diameter damping orifice is used.

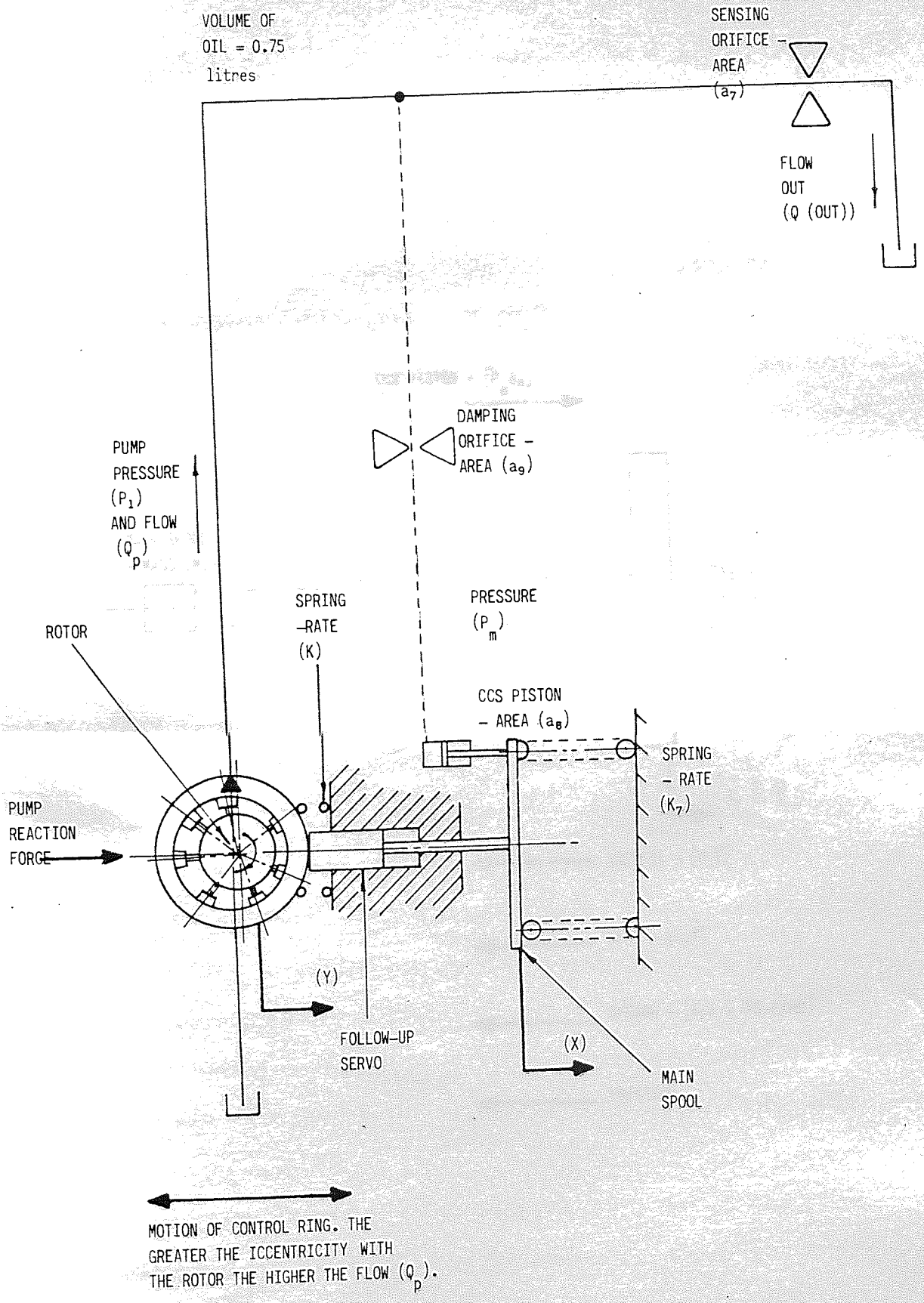

Fig A 6.1 A SKETCH OF THE CCS CONTROLLER

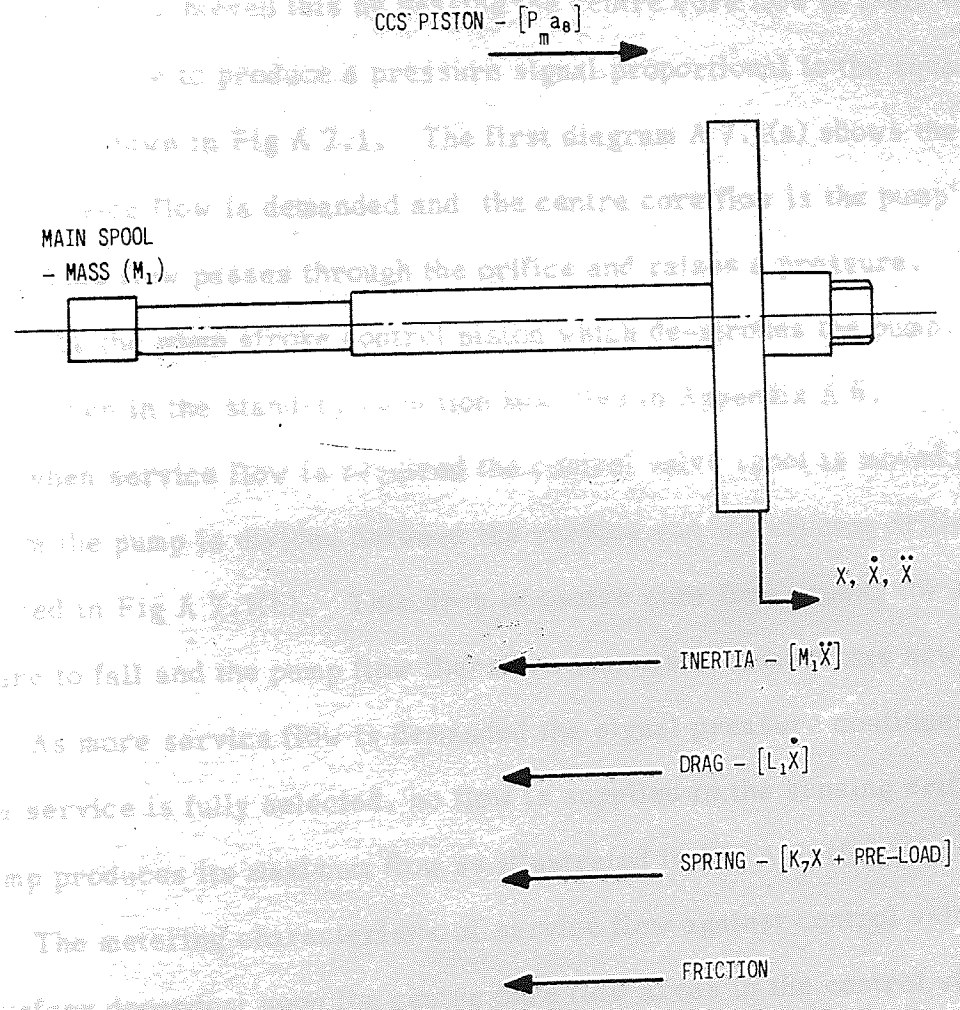

Fig A 6.2 FREE BODY DIAGRAM FOR THE MAIN SPOOL (IN CCS CONTROL)

APPENDIX A7

DETERMINATION OF THE STEADY STATE METERING CHARACTERISTICS FOR THE CCS CONTROL SYSTEM

A 7.1 INTRODUCTION

The CCS system comprises of both a variable displacement pump and a special directional control valve. The two are matched so that a movement of the valve signals the pump to change its stroke. Thus the pump only provides sufficient flow to satisfy the demand.

Hydreco achieved this by passing the centre core flow of their valve through an orifice to produce a pressure signal proportional to the square of the flow, as shown in Fig A 7.1. The first diagram A 7.1(a) shows the system when no service flow is demanded and the centre core flow is the pump's output. This flow passes through the orifice and raises a pressure. This is sensed by the pump stroke control piston which de-strokes the pump. The system is then in the stand-by condition modelled in Appendix A 6.

When service flow is required the control valve spool is moved and the flow from the pump is divided between the service and the sensing orifice as illustrated in Fig A 7.1(b). This drop in centre core flow causes the signal pressure to fall and the pump flow therefore increases to meet this new demand.

As more service flow is demanded the signal pressure continues to fall. When a service is fully selected, no flow is supplied to the sensing orifice and the pump produces its maximum flow as illustrated in Fig A 7.1(c).

The metering characteristic of service flow against control valve travel is therefore dependent upon the centre core flow areas in the control valve spool and the sensing orifice.

An extra complication to determining this characteristic comes from the introduction of a variable orifice on the CCS piston, which was introduced to extend the metering band of the system.

The first model was representative of the first system to be tested and a comparison of results is shown in Fig 3.16. The curves were in reasonable agreement and so the model was extended to include pressure compensating networks.

A schematic diagram of the circuit which gave the best results is shown in Fig 3.17 and the predicted metering characteristic for the extremes of pressure are shown in Fig 3.18.

A 7.2 THE MODEL FOR THE CCS STEADY-STATE METERING CHARACTERISTIC (UNCOMPENSATED)

A schematic diagram for the CCS controller with a variable orifice in the pump controller is shown in Fig A 7.2.

The required relationship is between the travel of the directional control valve (W) and the flow to the service (Qs).

The area a_{10} is related to valve travel (W). This relationship can be determined by considering the shape of the notches on the spool shown in Fig A 7.3. These notches were produced using a grinding wheel.

The metering area (a_{10}) can be approximated to a triangle as shown in Fig A 7.3. Joining the two metering areas together forms a square of area

$$a_{10} \simeq \frac{H^2}{2} \qquad - \quad A\ 7.1$$

To relate H to W consider the grinding wheel used to produce the notch shown in Fig A 7.4.

The general equation for a circle is

$$(W - W')^2 + (H - H')^2 = R^2 \qquad - \quad A\ 7.2$$

The centre of the grinding wheel is at co-ordinates $(O, -H_1)$ thus equation A 7.2 becomes

$$W^2 + (H + |H_1|)^2 = R^2$$

$$\text{or} \quad H = \sqrt{R^2 - W^2} - |H_1| \qquad - \quad A\ 7.3$$

Substituting into equation A 7.1 gives

$$a_{10} = \frac{1}{2}\left[\sqrt{R^2 - W^2} - |H_1|\right]^2 \quad - \quad A\ 7.4$$

or for simplicity

$$a_{10} = f(W) \quad - \quad A\ 7.5$$

The orifice a_{11} varies with main spool travel and is formed by grinding tapered flats on the CCS controller piston. The resultant metering area is shown in Fig A 7.5. From the diagram

$$u = R - X \tan\theta \quad - \quad A\ 7.6$$

and the total flow area is therefore given by

$$a_{11} = 2R_1^2\left[\cos^{-1}\left(\frac{R_1 - X\tan\theta}{R_1}\right) - \frac{1}{2}\sin\left(2\cos^{-1}\left(\frac{R_1 - X\tan\theta}{R_1}\right)\right)\right] - \quad A\ 7.7$$

or for simplicity

$$a_{11} = f(X) \quad - \quad A\ 7.8$$

The equation relating Q_s and W can now be determined by considering the flow through the system

$$Qp = Qs + Q_1 + Q_2 \quad - \quad A\ 7.9$$

Assuming that the orifice square law relationship for pressure and flow is valid for all restrictions with equal coefficients of discharge then

$$Q_2 = C_d\, a_7\sqrt{\frac{2\,Pm}{\rho}} \quad - \quad A\ 7.10$$

$$Q_1 = C_d\, a_{11}\sqrt{\frac{2\,Pm}{\rho}} \quad - \quad A\ 7.11$$

and

$$(Q_1 + Q_2) = C_d\, a_{10}\sqrt{\frac{2}{\rho}(P_1 - P_m)} \quad - \quad A\ 7.12$$

Combining these three equations

$$P_m = \left[\frac{P_1}{1 + \left(\frac{a_7 + a_{11}}{a_{10}}\right)^2}\right] \quad - \quad A\ 7.13$$

Substituting this into equation A 7.12 produces

$$(Q_1 + Q_2) = C_d\, a_{10} \sqrt{\frac{2\,P_1}{\rho\left(1 + \frac{a_{10}^2}{(a_7 + a_{11})^2}\right)}} \quad - \quad A7.14$$

The flow from the pump, in the steady state, is given by

$$Q_p = \frac{V_p\, N}{60}\left(1 - \frac{X}{\hat{X}}\right) \quad - \quad A\ 7.15$$

The steady state forces acting upon the main spool are shown on Fig A 7.2. For equilibrium they must balance so

$$P_m\, a_8 = K_7 X + F \quad - \quad A\ 7.16$$

Thus, combining equations A 7.13, A 7.15, A 7.16 and rearranging gives

$$Q_p = \frac{N\, V_p}{60}\left[1 - \left[\frac{\frac{P_1\, a_8}{\left(1 + \frac{(a_7 + a_{11})^2}{a_{10}^2}\right)} - F}{\hat{X}\ K_7}\right]\right] \quad - \quad A\ 7.17$$

The relationship between service flow and control valve travel can now be established by combining equations A 7.5, A 7.8, A 7.9, A 7.14 and A 7.17 thus

$$Q_s = \frac{N\, V_p}{60}\left[1 - \left[\frac{\left[\frac{P_1 a_8}{1 + \frac{(a_7 + f(x))^2}{f(W)^2}}\right] - F}{\hat{X}\ K_7}\right]\right] - C_d\, f(W) \sqrt{\frac{2\,P_1}{\rho\left(1 + \frac{f(W)^2}{(a_7 + f(x))^2}\right)}} \quad - \quad A\ 7.18$$

where from equations A 7.16 and A 7.13

$$X = \frac{P_1 a_8}{K_7\left(1 + \frac{(a_7 + f(x))^2}{f(W)^2}\right)} - \frac{F}{K_7} \qquad \text{A 7.19}$$

To solve equation A 7.18 for a particular load pressure (P_1) and control valve stroke (W) requires the determination of pump stroke (X) from equation A 7.19. This is greatly simplified by the use of a computer and an iterative solution technique.

The determination of the service flow (Q_s) is then a matter of straightforward substitution into equation A 7.18.

The values of the parameters used in the model were

N	=	2500 rpm
V_p	=	77 ml/rev
a_8	=	1.327×10^{-4} m^2
F	=	40.0 N
a_7	=	0
K_7	=	1.66×10^4 N/M
ρ	=	860 Kg/m^3
C_d	=	0.65
R	=	0.0508 m
$\lvert H_1 \rvert$	=	0.0493 m
R_1	=	0.0065 m
L_N	=	0.0244 m
θ	=	3^o

A 7.3 DETERMINATION OF THE PRESSURE COMPENSATED CCS SYSTEM

The effect of a pressure dependent metering characteristic is that the higher the load the smaller the control range of the valve. This effect can be severe and many valves at high pressure are on/off rather than proportional devices. Hydreco had claimed that their CCS system was independent of pressure. Hence the CCS system was an attractive option to include in the package because, it would not only save energy, but also overcome this problem of poor load control at high pressures.

This would make the Hamworthy pump very attractive to crane manufacturers because their business is the control of large loads.

When the first Hamworthy CCS system was tested and found to be pressure dependent it was decided that, if CCS was to be a viable proposition, a way of overcoming this must be found.

The solution came by examining the pressure dependent terms in equation A 7.18. The term

$$- C_d f(w) \sqrt{\frac{2 P_1}{\rho\left(1 + \frac{f(w)^2}{(a_7 + f(x))^2}\right)}}$$

represents the flow through the sensing orifice (a_7) and variable orifice (a_{11}) and is generally small compared with the flow from the pump. The term

$$- \left[\frac{\left[\frac{P_2 a_8}{1 + \frac{(a_7 + f(x))^2}{f(w)^2}} \right] - F}{K_7} \right]$$

is more significant and it represents the CCS command signal.

From the results of the CCS tests it was evident that the gain of the controller to changes in pressure was too high. Increasing the spring rate (K_7) would overcome this but it would also affect the stand-by pressure.

The method finally used to overcome this, without altering the stand-by pressure, was to introduce an opposing piston to the CCS signal. Initially this was thought to be sufficient but from the results of the model it was predicted that the pre-load (F) would adversely affect the characteristic. The signal to the opposing piston was therefore modified to eliminate the pre-load from the equation for pressures above that at stand-by.

A schematic of how this was achieved hydraulically is shown in Fig 3.17 and if P_1' is the pressure behind the opposing piston area (a_8), then the new equation for the equilibrium of the main spool is

$$P_m \; a_8 = F + K_7 X + P_1' \; a_8 \qquad - \quad A\ 7.20$$

The relief valve shown in Fig 3.17 was set equal to (F/a_8). Therefore by considering the flow through the network,

$$P_1' = \left[\frac{P_1}{1 + \frac{a_{13}^2}{a_{12}^2}} \right] - \frac{F}{a_8} \qquad - \quad A\ 7.21$$

Combining equations A 7.20, A 7.21, A 7.13 and re-arranging gives

$$X = \frac{P_1 a_8}{K_7} \left[\left(\frac{1}{1 + \frac{(a_7 + a_{11})^2}{a_{10}^2}} \right) - \left(\frac{1}{1 + \frac{a_{13}^2}{a_{12}^2}} \right) \right] \qquad - \quad A\ 7.22$$

This is equivalent to the term from equation A 7.18 under consideration. The magnitude of the CCS signal, in square brackets, is the same in both of these equations but the pressure gain in the new system has been greatly reduced. Thus the spool position (X) moves less for a given change in pressure (P_1).

This can be more easily understood by considering the characteristics of the terms in the equations. These are shown in Fig A 7.6 for percentage changes in flow. The ratio (a_{13}/a_{12}) was set to make both expressions equal at zero flow. The third curve on the graph represents the difference between the two terms.

Returning to comparing the new and old CCS systems, the signal for both is the same but in the new design the overall signal is much smaller. Thus, the magnitude of the pressure gain for the new system is much smaller by the ratio of B_1/B_2 for the flow "Q" in Fig A 7.6.

Equation A 7.18, relating service flow (Q_s) to control valve travel (W), can therefore be modified to include the pressure compensating network

$$Q_s \text{ (compensated)} = \frac{N V_p}{60} \left[1 - \frac{P_1 a_8}{\hat{X} K_7} \left[\frac{1}{\frac{(1+(a_7+f(x))^2)}{f(w)^2}} - \frac{1}{\left(1 + \frac{a_{13}}{a_{12}}^2\right)} \right] \right] - C_d f(w) \sqrt{\frac{2 P_1}{\rho\left(1 + \frac{f(w)^2}{(a_7+f(x))^2}\right)}} \quad - \text{A 7.23}$$

and

$$X = \frac{P_1 a_8}{K_7} \left[\frac{1}{\left(1 + \frac{(a_7+f(x))}{f(w)^2}\right)^2} - \frac{1}{\left(1 + \frac{a_{13}}{a_{12}}^2\right)} \right] \quad - \text{A 7.24}$$

The method of solving this equation is, as before, to use an interactive process.

The model for the new, pressure compensated, CCS system predicted that for pressures between 35 and 350 bar the metering characteristic should be between the curves given in Fig 3.18.

The actual values of the pressure dividing orifices a_{12} and a_{13} were such that the circuit used the minimum flow and yet they were large enough to be contaminant insensitive. The values chosen were

$$a_{13} = 4.869 \times 10^{-7} \text{ m}^2$$

and

$$(a_{13}/a_{12}) = 0.592$$

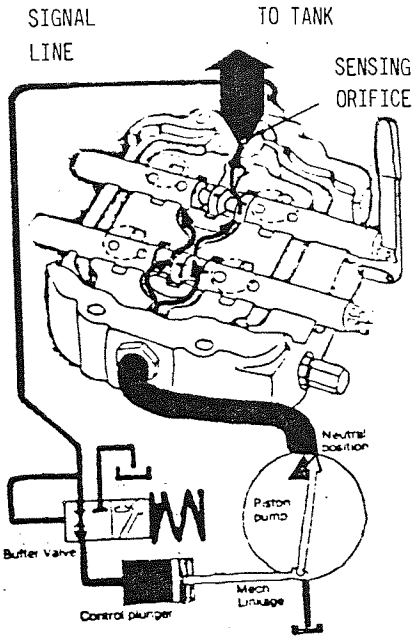

(a) ZERO SERVICE FLOW (STAND-BY)

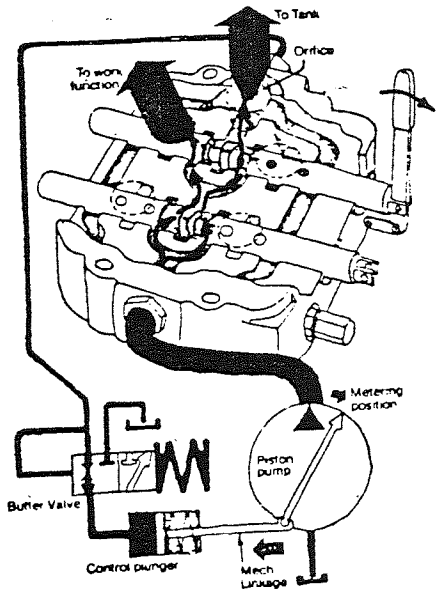

(b) PARTIAL SELECTION OF THE VALVE

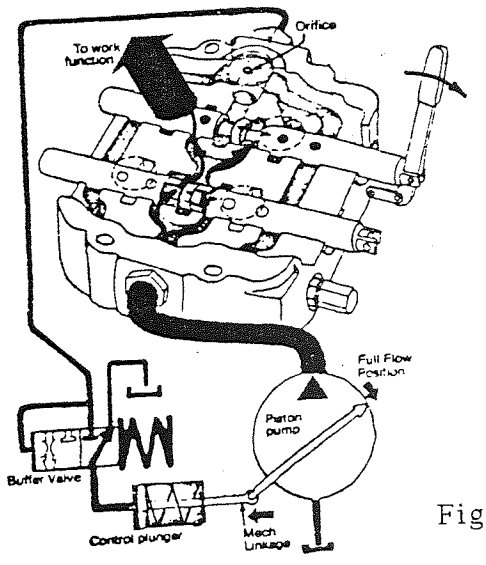

(c) FULL VALVE SELECTION

Fig A7.1 OPERATION OF THE HYDRECO CCS SYSTEM

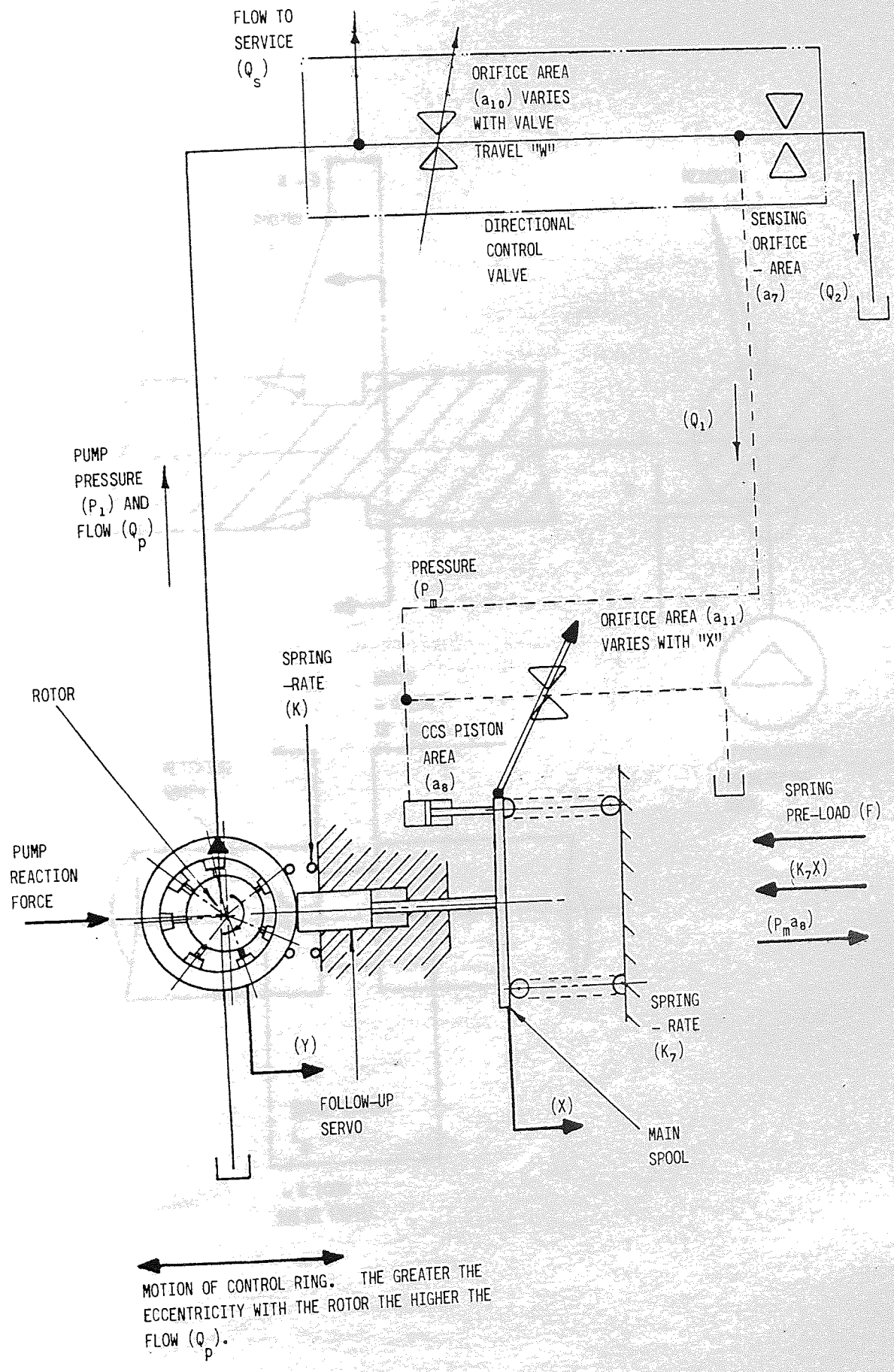

Fig A 7.2 A SKETCH OF THE CCS SYSTEM INCLUDING A VARIABLE ORIFICE IN THE CONTROLLER PISTON

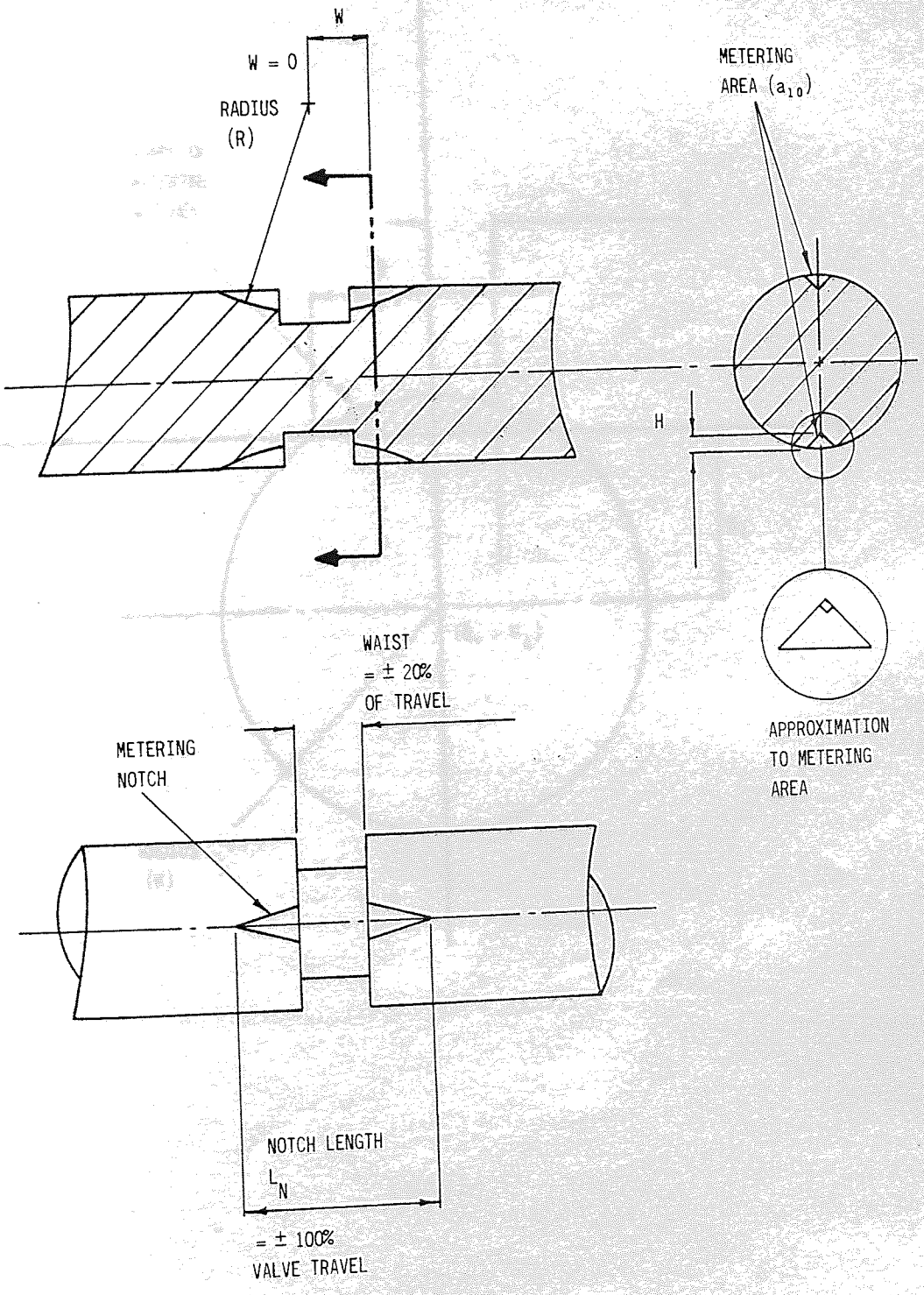

Fig A 7.3 AN ILLUSTRATION OF THE SPECIAL CCS SPOOLS

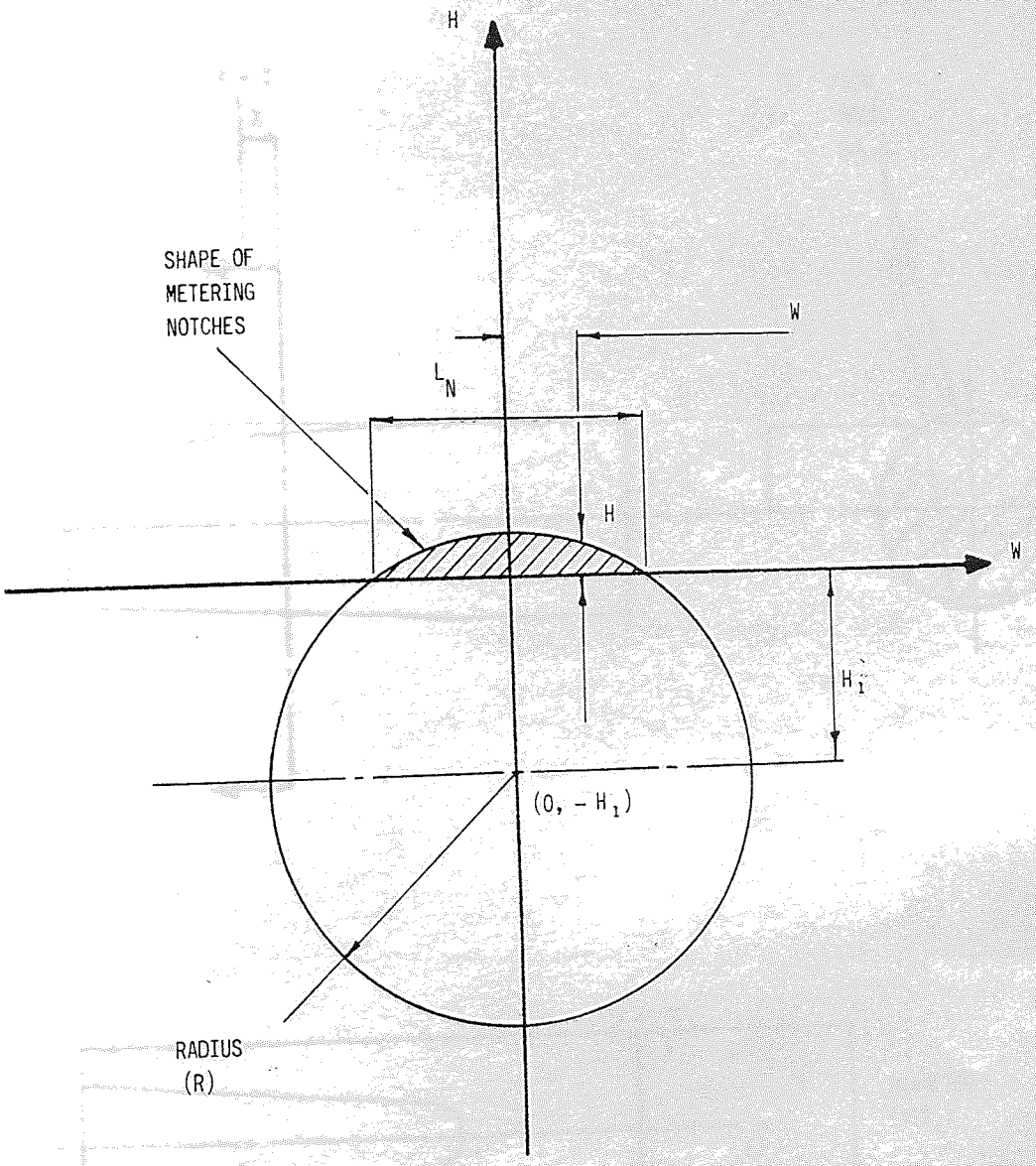

Fig A 7.4 A SKETCH OF THE GRINDING WHEEL USED TO PRODUCE THE CCS SPOOL METERING NOTCHES

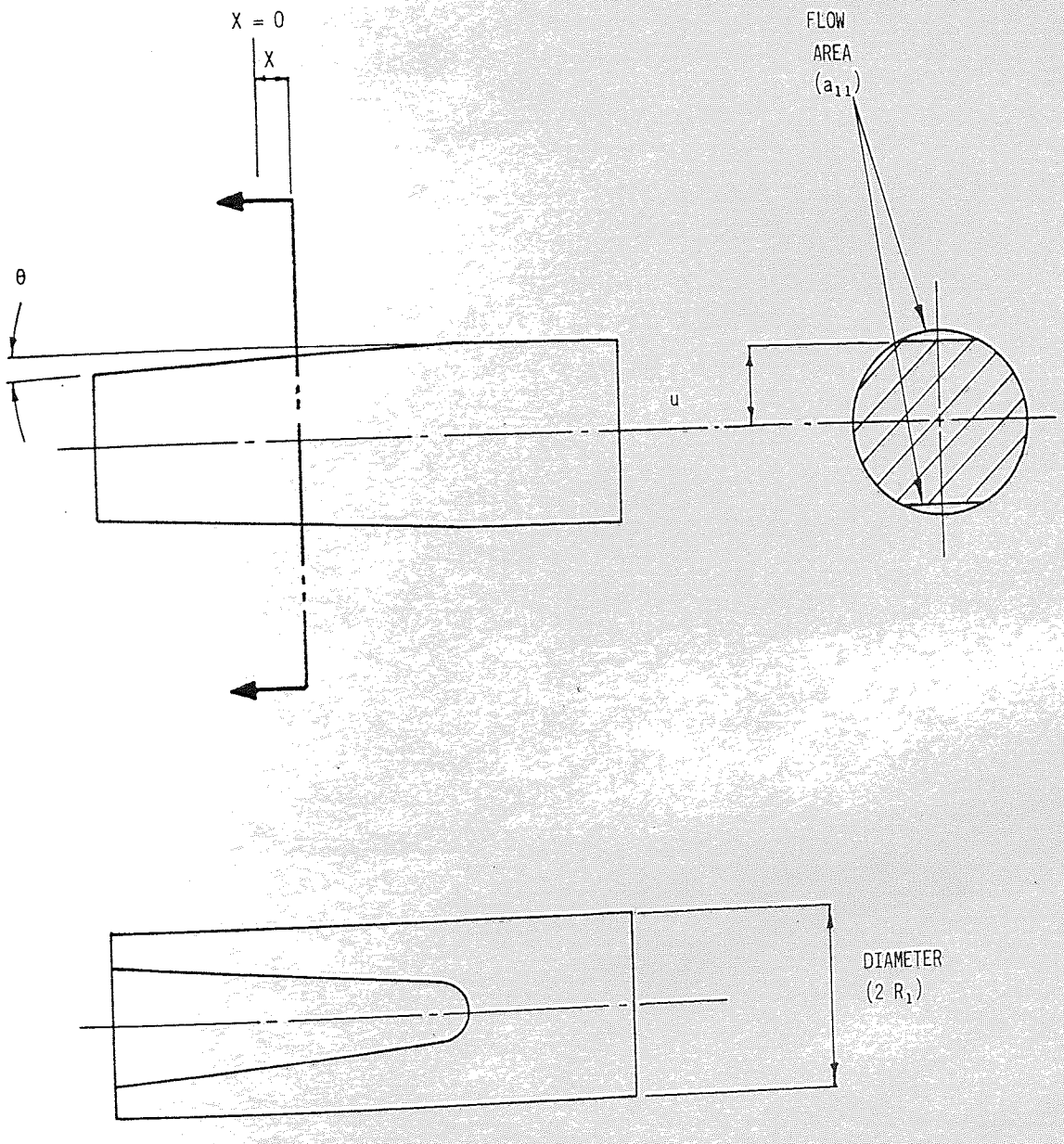

Fig A 7.5 A SKETCH OF THE CCS CONTROLLER PISTON WITH TAPERED FLATS

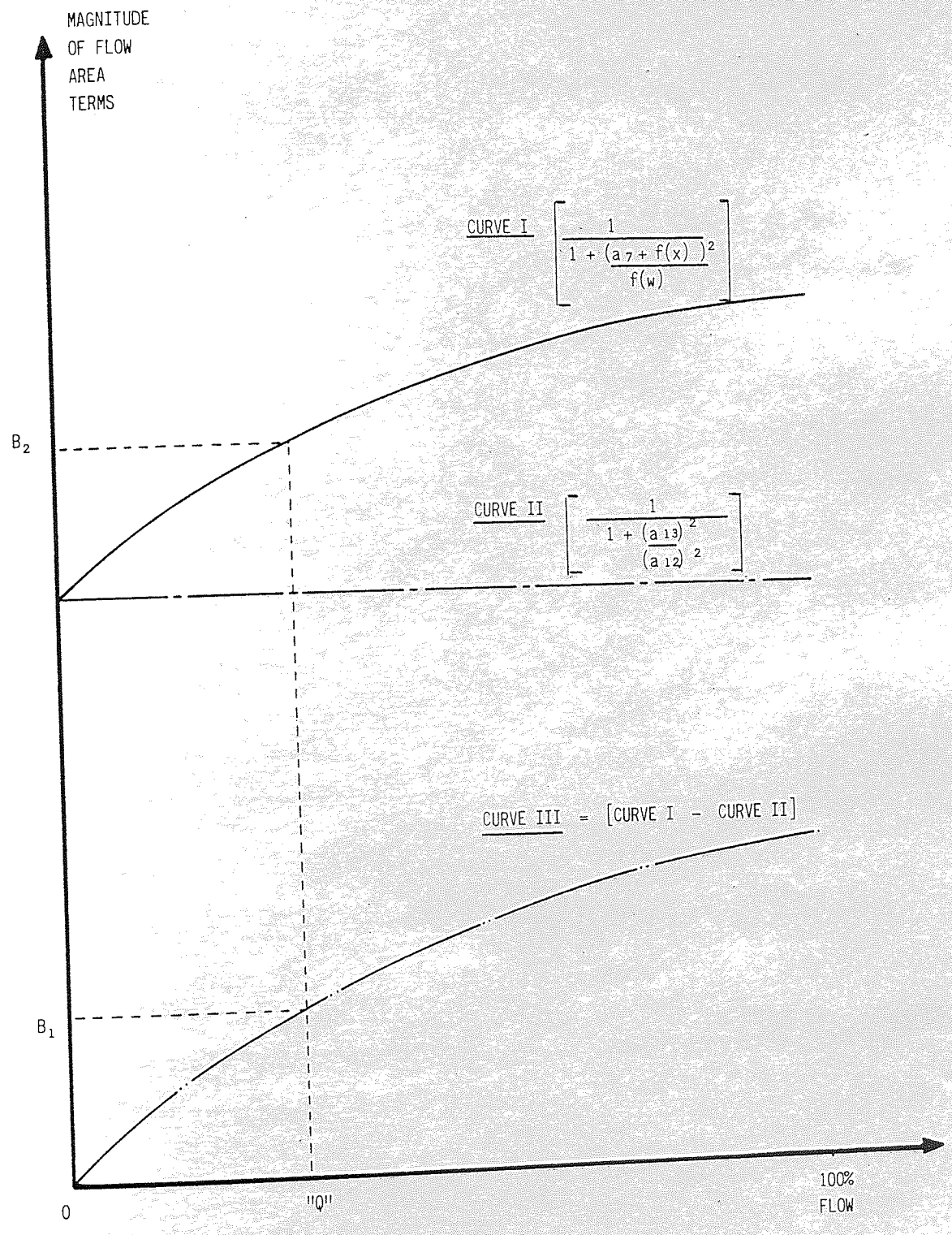

Fig A 7.6 GENERAL CHARACTERISTICS FOR THE FLOW AREA TERMS IN THE CCS METERING EQUATIONS

APPENDIX A8

THE DESIGN OF THE PROPORTIONAL, SOLENOID BASED, ELECTRO-HYDRAULIC CONTROLLER

A 8.1 INTRODUCTION

Hydreco had designed a proportional, solenoid based, position controller for use on directional control valves. This worked well and so the design was adopted to control the position of a piston pump.

An assembly drawing of the system is shown in Fig A 8.1. The principle of operation is that of force feedback. The design consists of a push/pull, internally spring biased solenoid, acting against a spool. As more current is supplied to the solenoid the force on the spool increases and the spool moves. As it does so, flow is vented from behind the control piston and the metered pressure drops. The natural reaction force of the pump then overcomes the piston force and the pump moves to a lower stroke. As the pump moves the force feed-back through the feed-back spring increases. This opposes the increase in force from the solenoid and centralises the spool. The stroke of the pump can be increased by the reverse process.

A typical flow/voltage characteristic is shown in Fig A 8.2 and it shows the large degree of non-linearity of the system.

A 8.2 THE SIMPLIFIED STABILITY MODEL FOR THE SOLENOID BASED CONTROLLER

The main problem associated with modelling this system was that there was no information available regarding the frequency response of the solenoid. Also, at the time, there was no drive circuitry available and so the response could not be measured.

It was therefore decided to model a pressure compensating controller and assume that the solenoid had an infinite bandwidth as this would give a valuable insight into how the system would behave. Also, if the system was unstable with this assumption, then it would most definitely be unstable in practice.

A 8.2.1 THE EQUATION OF MOTION FOR THE SPOOL

A schematic of the controller is shown in Fig A 8.3 which includes the pressure feedback signal to the control circuit. The control circuit produces the pressure compensating characteristic and its output is sensed as a position demand to the pump.

The majority of assumptions given in Appendix A 2 have been used in this analysis, with the exception that the flow forces on the spool are now significant in comparison with the driving forces and cannot be neglected.

Fig A 8.4 shows the metering of the valve. The flow forces on the spool can be determined by the following analysis.

$$\text{Force} = \text{rate of change in momentum} \quad - \quad \text{A 8.1}$$

In the direction of spool travel

$$\text{Momentum} = \text{mass x velocity cos } 69^{\circ} \quad - \quad \text{A 8.2}$$

The angle the flow enters and leaves the spool was set to 69° which is the value used by BLACKBURN[2] et al. Combining the above equations

$$\text{Force} = \frac{d}{dt} (\text{mass x velocity cos } 69^{\circ})$$

In the steady state velocity is constant and therefore

$$\text{Force} = \dot{m} \cos 69^{\circ} \text{ x velocity} \quad - \quad \text{A 8.2}$$

where $\dot{m}$ = rate of change of mass

= density (ρ) x flow (Q)

$$= \rho Q \quad - \quad \text{A 8.3}$$

Now, if a_p is the flow area through the port then

$$Q = a_p \text{ x velocity} \quad - \quad \text{A 8.4}$$

Combining equations A 8.2, A 8.3 and A 8.4 gives

$$\text{Force} = \rho a_p \cos 69^{\circ} \text{ x (velocity)}^2 \quad - \quad \text{A 8.5}$$

Applying Bernoulli's equation across the orifice produces

$$\Delta P = \frac{1}{2} \rho \text{ x (velocity)}^2$$

and so from equation A 8.5

$$\text{Force} = 2\, a_p\, \Delta P \cos 69^\circ \quad - \quad \text{A 8.6}$$

Applying this equation to the flow Q(in) in Fig A 8.4 gives

$$(\text{Flow force})_{in} = F(in) = 2a(in)(P_1 - P_4) \cos 69^\circ C_d$$

and linearising

$$f(in) = C_2 (p_1 - p_4) + C_3 x \quad - \quad \text{A 8.7}$$

where $C_2 = 2\, a(in) \cos 69^\circ C_d$

and $C_3 = 2 (P_1 - P_4) \cos 69^\circ \frac{\partial a(in)}{\partial X} C_d$

A diagram showing the metering of the valve is given in Fig A 8.5.

The equation relating the area a(in) to spool travel is

$$a(in) = r_2^2 \left[\cos^{-1} \frac{(r_2 - X)}{r_2} - \frac{1}{2} \sin 2 \cos^{-1} \frac{(r_2 - X)}{r_2} \right]$$

$$- \quad \text{A 8.8}$$

and $$\frac{\partial a(in)}{\partial a\, X} = \frac{r_2}{\sqrt{1 - \frac{(r_2 - X)^2}{r_2^2}}} \left[1 - \cos \left(2 \cos^{-1} \frac{(r_2 - X)}{r_2} \right) \right]$$

$$- \quad \text{A 8.9}$$

The corresponding equation for the flow force associated with Q(out) is

$$(\text{Flow force})_{out} = F(out) = 2\, a(out)\, P_4 \cos 69^\circ$$

and upon linearising

$$f(out) = C_4\, p_4 - C_5\, x \quad - \quad \text{A 8.10}$$

where $C_4 = 2\, a(out) \cos 69^\circ\, C_d$

$$C_5 = 2\, P_4 \cos 69^\circ \frac{\partial a(out)}{\partial X} C_d$$

$$a(out) = r_2^2 \left[\cos^{-1} \frac{(L_v - r_2 - X)}{r_2} - \frac{1}{2} \sin 2 \cos^{-1} \frac{(L_v - r_2 - X)}{r_2} \right] \quad - \text{A 8.11}$$

$$\frac{\partial a(out)}{\partial X} = \frac{r_2}{\sqrt{1 - \frac{(L_v - r_2 - X)^2}{r_2^2}}} \left[1 - \cos 2 \cos^{-1} \frac{(L_v - r_2 - X)}{r_2} \right] \quad - \text{A 8.12}$$

A free body diagram for the spool is shown in Fig A 8.6. The linearised equation of motion is

$$f_s = \delta_1 x + K_{10} y + C_2 p_1 - (C_2 + C_4) p_4 \quad - \text{A 8.13}$$

where $\delta_1 = K_{10} + K_{11} + C_3 + C_5 + L_3 s + M_3 s^2 \quad - \text{A 8.14}$

A 8.2.2 THE EQUATION OF MOTION FOR THE PUMP

A free body diagram for the pump is shown in Fig A 8.7. The resulting linearised equation of motion, neglecting the force $K_{10}(Y+X)$ because it is small, is

$$C_1 p_1 + \delta_2 y = a_{14} p_4 \quad - \text{A 8.15}$$

where $\delta_2 = K_8 + K_9 + M_2 s^2 \quad - \text{A 8.16}$

A 8.2.3 CONSIDERATION OF FLOW THROUGH THE VALVE

Applying the principle of continuity to the volume of oil at pressure P_4, shown in Fig A 8.4, and neglecting the compressibility flow gives

$$Q(in) = a_{14}\dot{Y} + Q(out) \quad - \quad A\ 8.17$$

or in its linearised form

$$q(in) = a_{14} s y + q(out) \quad - \quad A\ 8.18$$

Q(in) and Q(out) are related to the pressures P_1 and P_4 by the square law equation for flow through an orifice and so in their linearised forms

$$q(in) = C_6 x + C_7 (p_1 - p_4) \quad - \quad A\ 8.19$$

and

$$q(out) = -C_8 x + C_9 p_4 \quad - \quad A\ 8.20$$

where

$$C_6 = C_d \sqrt{\frac{2 (P_1 - P_4)}{\rho}} \frac{\partial a(in)}{\partial X}$$

$$C_7 = \frac{C_d\ a(in)}{\sqrt{2 \rho (P_1 - P_4)}}$$

$$C_8 = \sqrt{\frac{2}{\rho} P_4} \frac{\partial a(out)}{\partial X}$$

$$C_9 = \frac{C_d\ a(out)}{\sqrt{2 \rho P_4}}$$

Combining equations A 8.18, A 8.19 and A 8.20 gives

$$(C_6 + C_8)x + C_7 p_1 = (C_7 + C_9)p_4 + a_{14} sy \quad - \quad A\ 8.21$$

A 8.2.4 COMBINING THE EQUATIONS TO FORM THE FLTF

From equation A 2.14 and A 2.10

$$y = \delta_3 p_1 \quad - \quad A\ 8.22$$

where

$$\delta_3 = \frac{-60 \hat{Y}}{V_p N} \left[\frac{v}{\beta} s + \frac{C_d a_v}{\sqrt{2 \rho P_1}} \right] \quad - \quad A\ 8.23$$

Substituting for y in equation A 8.15 gives

$$p_4 = (C_1 + \delta_2 \delta_3) \frac{p_1}{a_{14}} \quad - \quad A\ 8.24$$

Combining equations A 8.21, A 8.22 and rearranging

$$x = \left[\frac{\frac{(C_7 + C_9)(C_1 + \delta_2 \delta_3)}{a_{14}} + a_{14} s \delta_3 - a_7}{(C_6 + C_8)} \right] p_1$$

– A 8.25

A very basic block diagram for the system is shown in Fig A 8.8. The combined transfer function for the solenoid, pump and load is $[G_4]$ and this is given by combining and rearranging equations A 8.13, A 8.22, A 8.24 and A 8.25

$$[G_4] = \left[\frac{p_1}{f_s}\right] = \left[\frac{1}{\frac{\delta_1 (C_7 + C_9)(C_1 + \delta_2 \delta_3)}{a_{14} (C_6 + C_8)} + \frac{\delta_1 a_{14} s \delta_3}{(C_6 + C_8)} - \frac{C_7 \delta_1}{(C_6 + C_8)} + K_{10} \delta_3 + C_2 - \frac{(C_2 + C_4)(C_1 + \delta_2 \delta_3)}{a_{14}}} \right]$$

– A 8.26

Multiplying the denominator out by substituting equations A 8.14, A 8.16 and A 8.23 gives

$$[G_4] = \left[\frac{p_1}{f_s}\right] = \frac{1}{\gamma_4 M_2 M_3 \gamma_3 \quad s^5}$$

$$+ s^4 \left[\gamma_4 (M_3 M_2 \gamma_2 + M_2 \gamma_3 L_3) + \frac{a_{14}}{(C_6 + C_8)} M_3 \gamma_3 \right]$$

$$+ s^3 \left[\gamma_4 (M_3 \gamma_3 (K_8 + K_9) + L_3 M_2 \gamma_2 + \gamma_1 M_2 \gamma_3) - \frac{(C_2 + C_4)}{a_{14}} M_2 \gamma_3 + \frac{a_{14}}{(C_6 + C_8)} (M_3 \gamma_2 + \gamma_3 L_3) \right]$$

$$+ s^2 \left[\gamma_4 (M_3 \gamma_2 (K_8 + K_9) + L_3 \gamma_3 (K_8 + K_9) + \gamma_1 M_2 \gamma_2) - C_1 \gamma_4 M_3 + \frac{C_7}{(C_6 + C_8)} M_3 - \frac{(C_2 + C_4)}{a_{14}} M_2 \gamma_2 + \frac{a_{14}}{(C_6 + C_8)} (\gamma_3 \gamma_1 + L_3 \gamma_2) \right]$$

$$+ s \left[\gamma_4 (L_3 \gamma_2 (K_8 + K_9) + \gamma_1 \gamma_3 (K_8 + K_9)) - C_1 \gamma_4 L_3 + \frac{a_{14}}{(C_6 + C_8)} \gamma_1 \gamma_2 + \frac{C_7}{(C_6 + C_8)} L_3 + K_{10} \gamma_3 - \frac{(C_2 + C_4)}{a_{14}} \gamma_3 (K_8 + K_9) \right]$$

$$\left[+ \frac{C_1}{a_{14}} (C_2 + C_4) - \frac{(C_2 + C_4)}{a_{14}} \gamma_3 (K_8 + K_9) + \gamma_4 \gamma_1 \gamma_2 \quad (K_8 + K_9) - C_1 \gamma_4 \gamma_1 + \frac{C_7 \gamma_1}{(C_6 + C_8)} \quad K_{10} \gamma_2 - C_2 \right]$$

– A 8.27

Where $\gamma_1 = K_{10} + K_{11} + C_3 + C_5$

$$\gamma_2 = \frac{60\,\hat{Y}\,C_d\,a_v}{V_p N \sqrt{2\rho P_1}}$$

$$\gamma_3 = \frac{60\,\hat{Y}}{V_p N}\,\frac{v}{\beta}$$

$$\gamma_4 = \frac{(C_7 + C_9)}{(C_6 + C_8)}\,\frac{1}{a_{14}}$$

A 8.2.5 DETERMINATION OF THE FEEDBACK TRANSFER FUNCTION $[H_1]$

The relationship between the solenoid force (F_s) and pump flow is shown in Fig A 8.9(a). Combining this characteristic with the desired pressure compensating curve, Fig 8.9(b), produces the force/pressure trace given in Fig A 8.9(c). Thus, in the control region of the curve where pressure > p_c, the feedback transfer function is

$$[H_1] = [\frac{f_s}{p_1}] = \frac{13.3}{(\hat{P} - P_c)} \qquad - \qquad \text{A 8.28}$$

A 8.2.6 THE OPEN LOOP TRANSFER FUNCTION (OLTF) FOR THE COMPLETE SYSTEM

The OLTF for the system is

$$\text{OLTF} = [G_4][H_1]$$

As the transfer functions are linear, the classic Nyquist criterion can be applied to the resulting locus to test for stability.

A 8.3 RESULTS FROM THE STABILITY MODEL FOR THE SOLENOID CONTROLLER IN PRESSURE COMPENSATION

Once the model was established, for the desired pressure compensating characteristic, there were only a few parameters to vary in order to optimise the design.

These parameters affected the metering of the valve and were the hole diameter and amount of underlap. In general, the larger the underlap the more stable the system. However, the amount of underlap was limited by the requirement for a maximum, steady state flow of 2 litres/min through the controller.

A Nyquist plot of the system, operating under the most unstable conditions, is shown in Fig A 8.10 and this represents the most stable configuration for the controller.

Although instability is not predicted, the system is far from satisfactory because of the gross simplification used for the transfer function of the solenoid. An attempt was made to produce a more stable system by using electrical compensating networks. An example of using a phase lag system is shown in the Bode plot of Fig A 8.11. The resultant OLTF is adequately stable but the time constant for the lag network is 10.0 seconds. Such a system would therefore take approximately 30 seconds to respond to a step input which is far too long as the design specification demands a response of 300 ms.

An investigation of the most significant terms in the stability model revealed that the model was so unstable because of the large magnitude of the flow forces compared with the control signal.

This was considered to be an inherent problem of the design and it was concluded that it should not be pursued.

A 8.3.1 DATA USED IN THE MODEL

M_2 = 11.384 Kg

M_3 = 0.05 Kg

L_3 = 0

a_{14} = 1.276×10^{-3} m^2

K_8 = 74.10 KN/m

K_9 = 18.35 KN/m

C_1 = 2.847×10^{-4} m^2

K_{10} = 1.573 KN/m

K_{11} = 10.485 KN/m

$\hat{Y}$ = 7.5×10^{-3} m

C_d = 0.65

a_v = Variable (= 0 for previous results)

V_p = 77×10^{-6} m^3/rev

N = 2500 rpm

ρ = 860 Kg/m^3

P_1 = VARIABLE (= 350 bar for previous results)

v = 0.75×10^{-3} m^3

β = 1.7 GP_a

r_2 = 2.0×10^{-3} m

L_v = 0.4×10^{-3} m

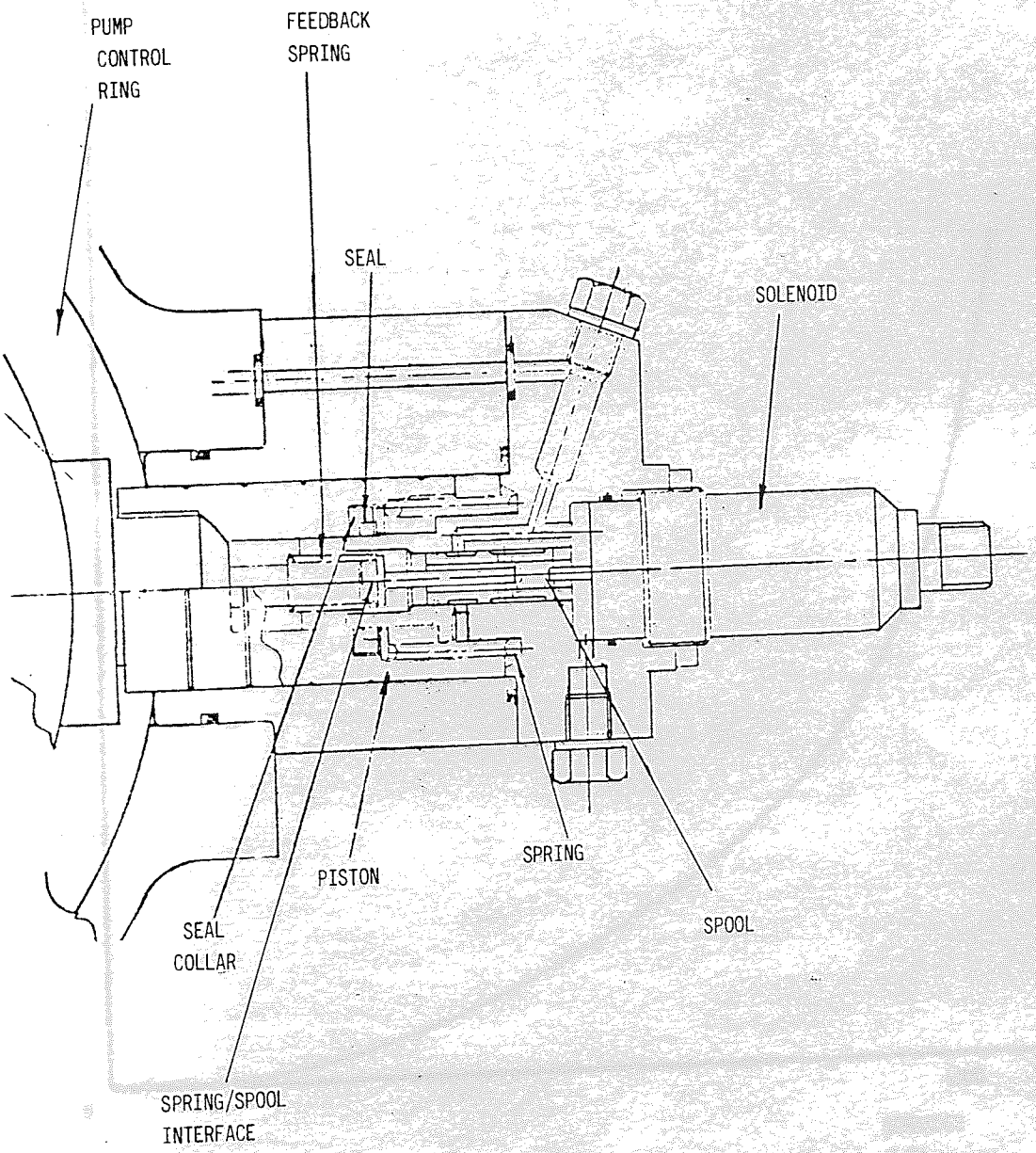

Fig A 8.1 AN ASSEMBLY DRAWING OF THE SOLENOID BASED, ELECTRO-HYDRAULIC CONTROLLER

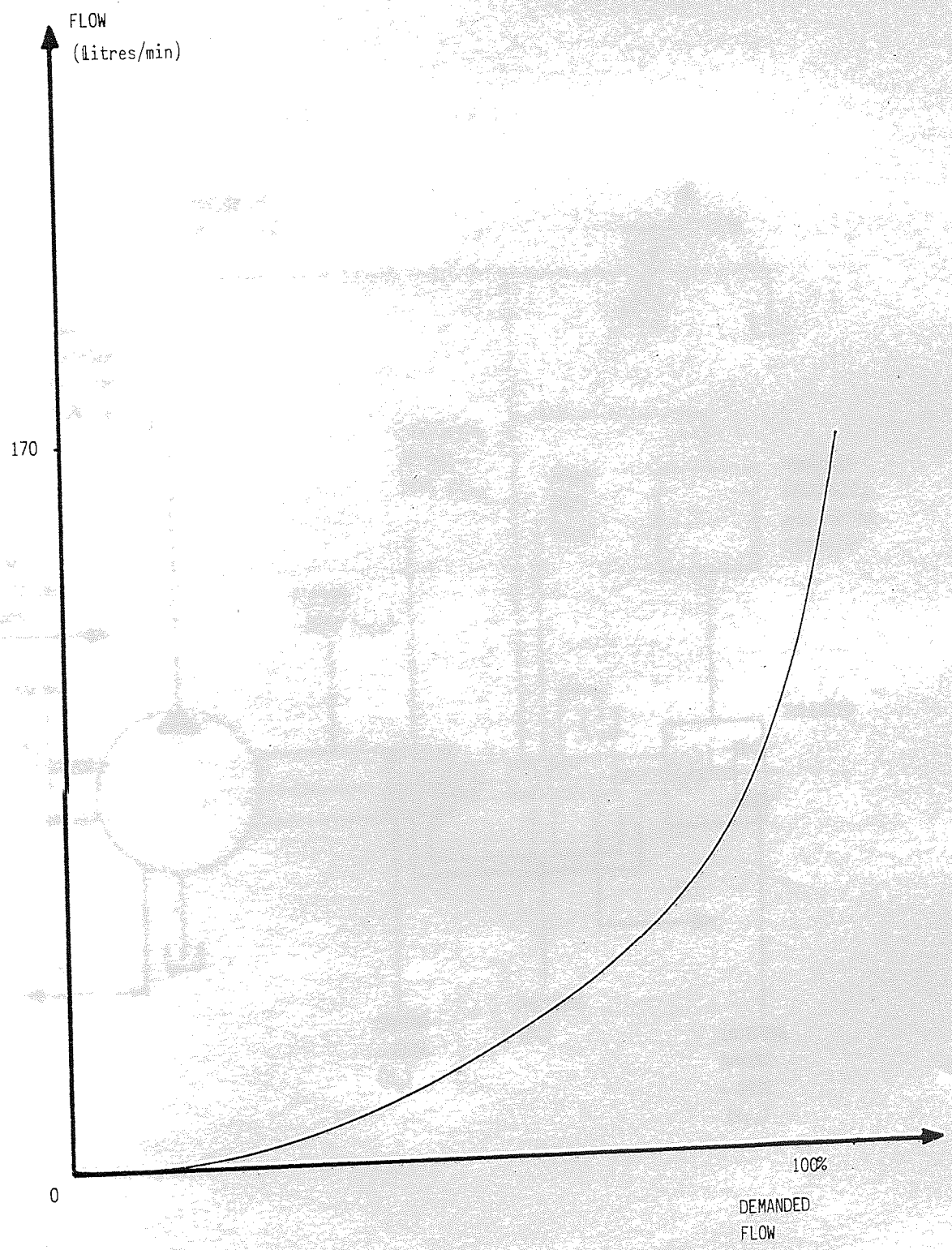

Fig A 8.2 FLOW CHARACTERISTIC FOR THE SOLENOID BASED CONTROLLER

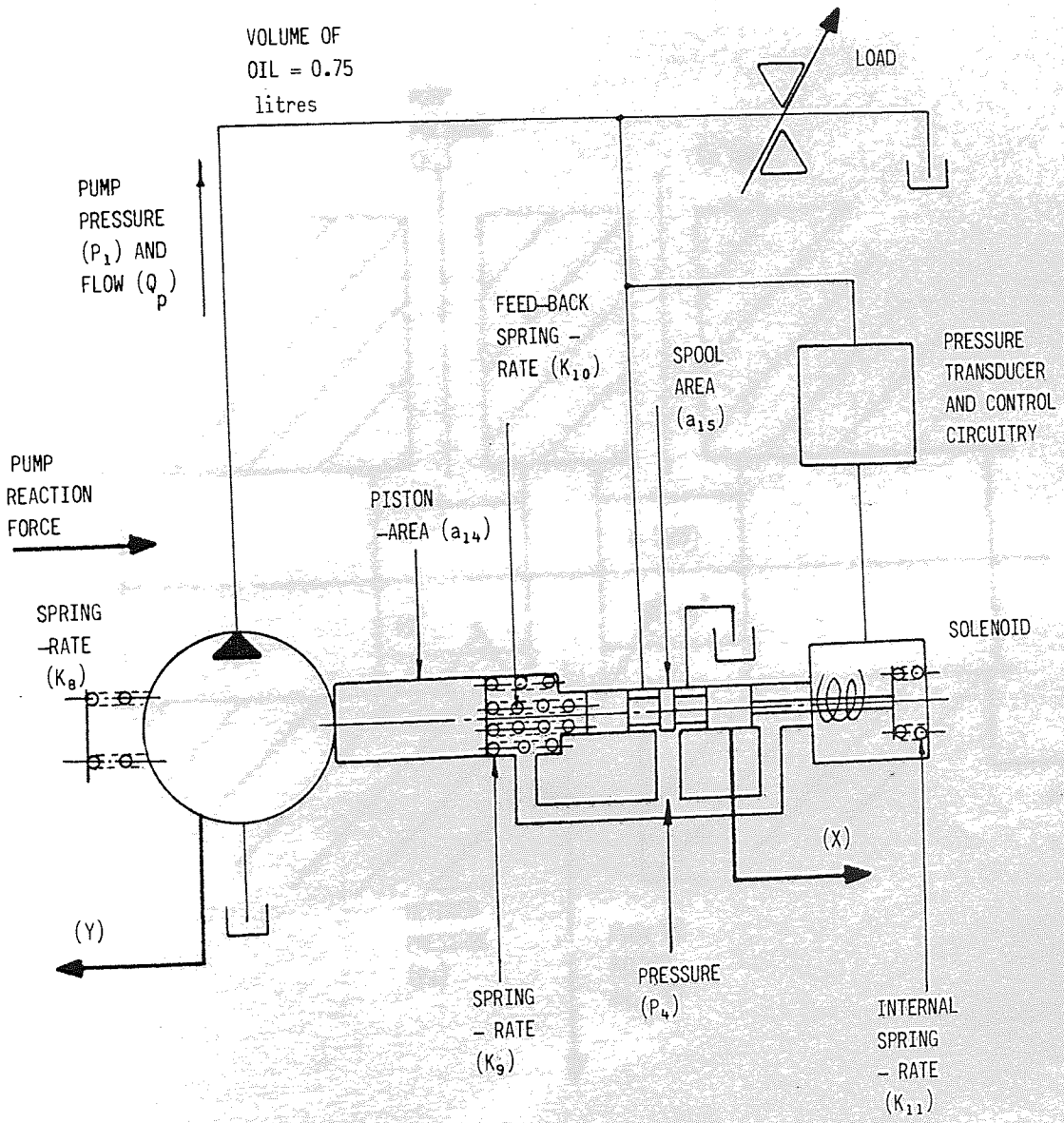

Fig A 8.3 A SCHEMATIC DIAGRAM OF THE SOLENOID CONTROLLER IN PRESSURE COMPENSATION

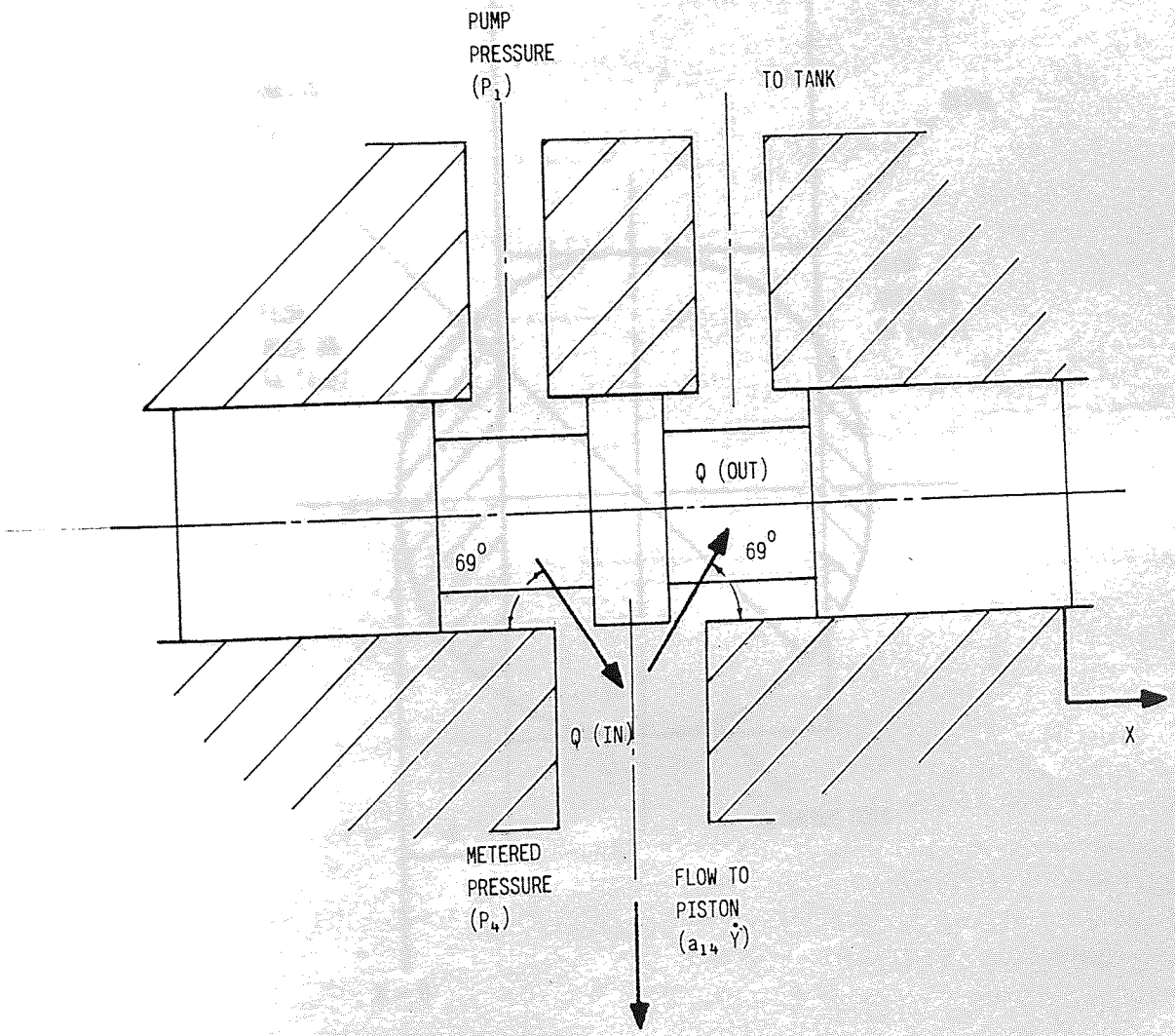

Fig A 8.4 A SKETCH SHOWING THE FLOW THROUGH THE VALVE

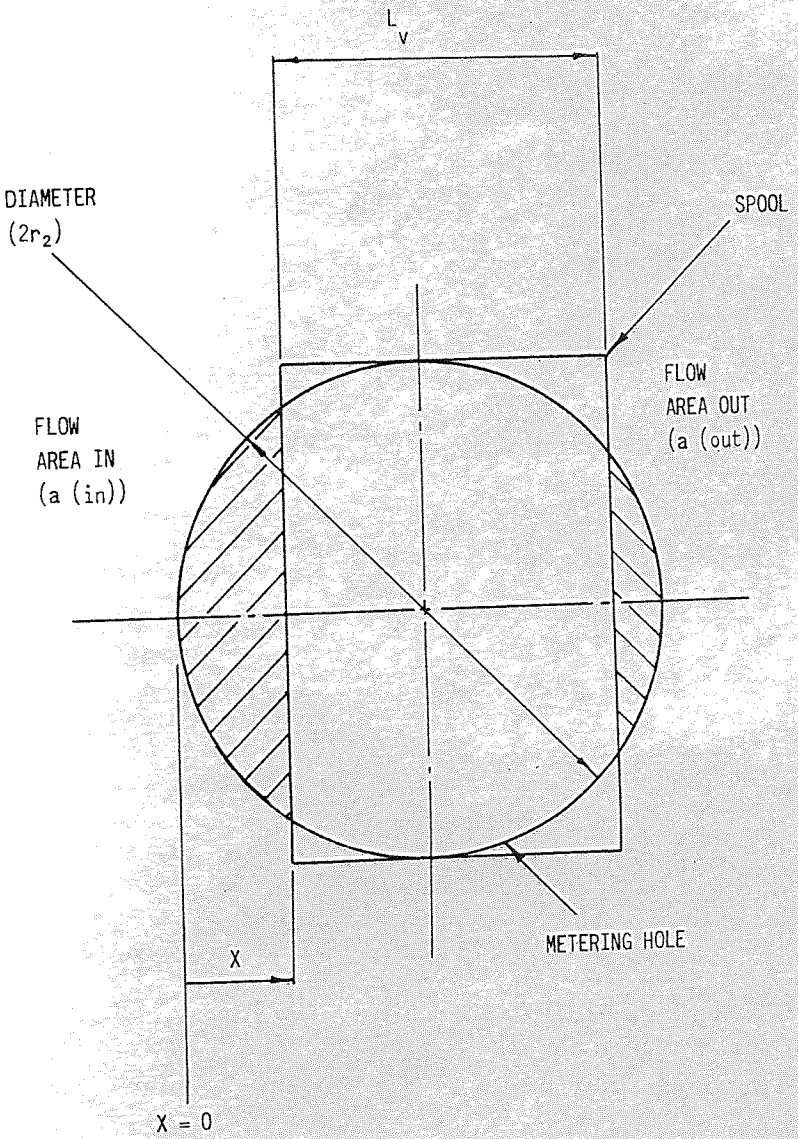

Fig A 8.5 A DIAGRAM OF THE METERING OF THE VALVE

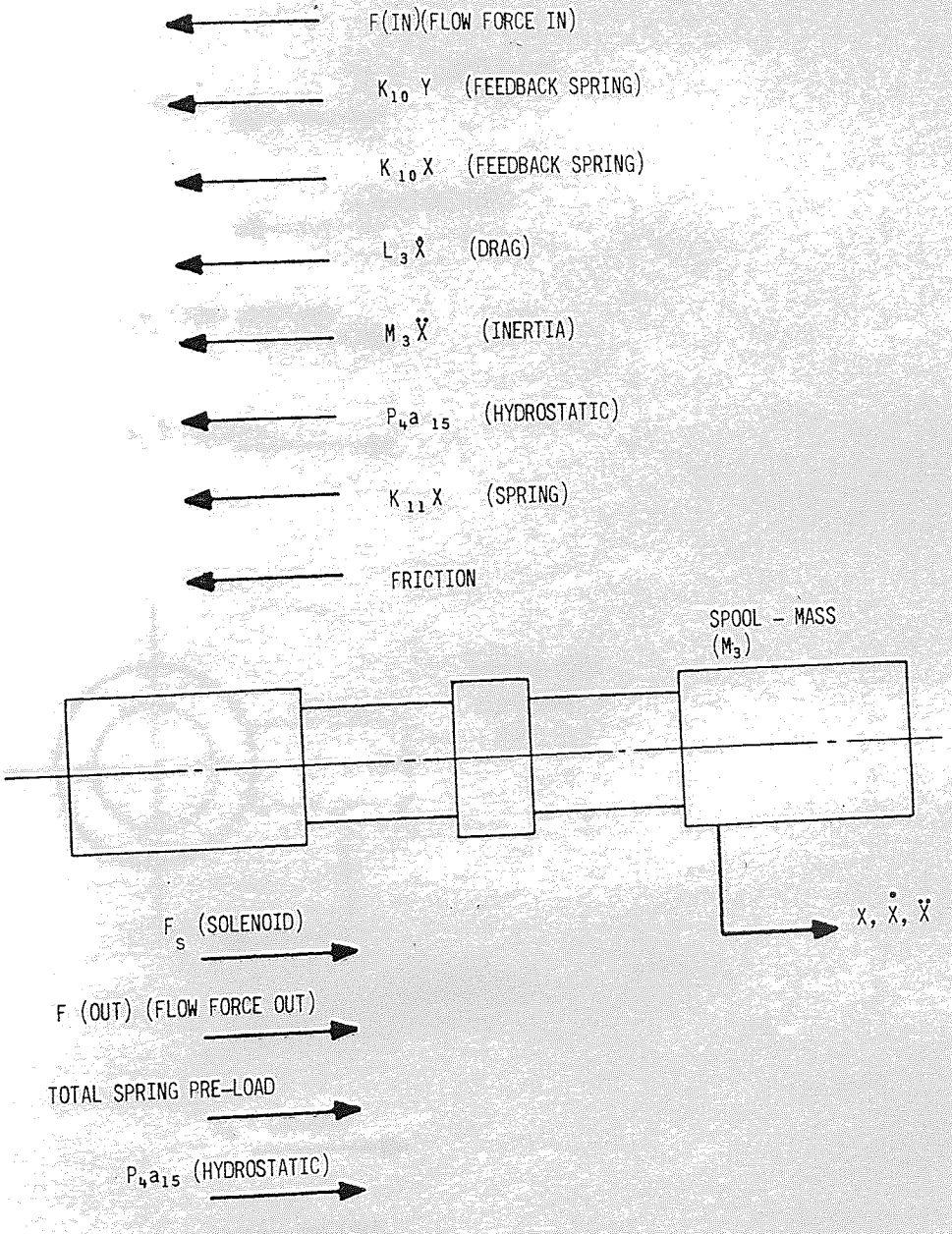

Fig A 8.6 A FREE BODY DIAGRAM FOR THE SPOOL

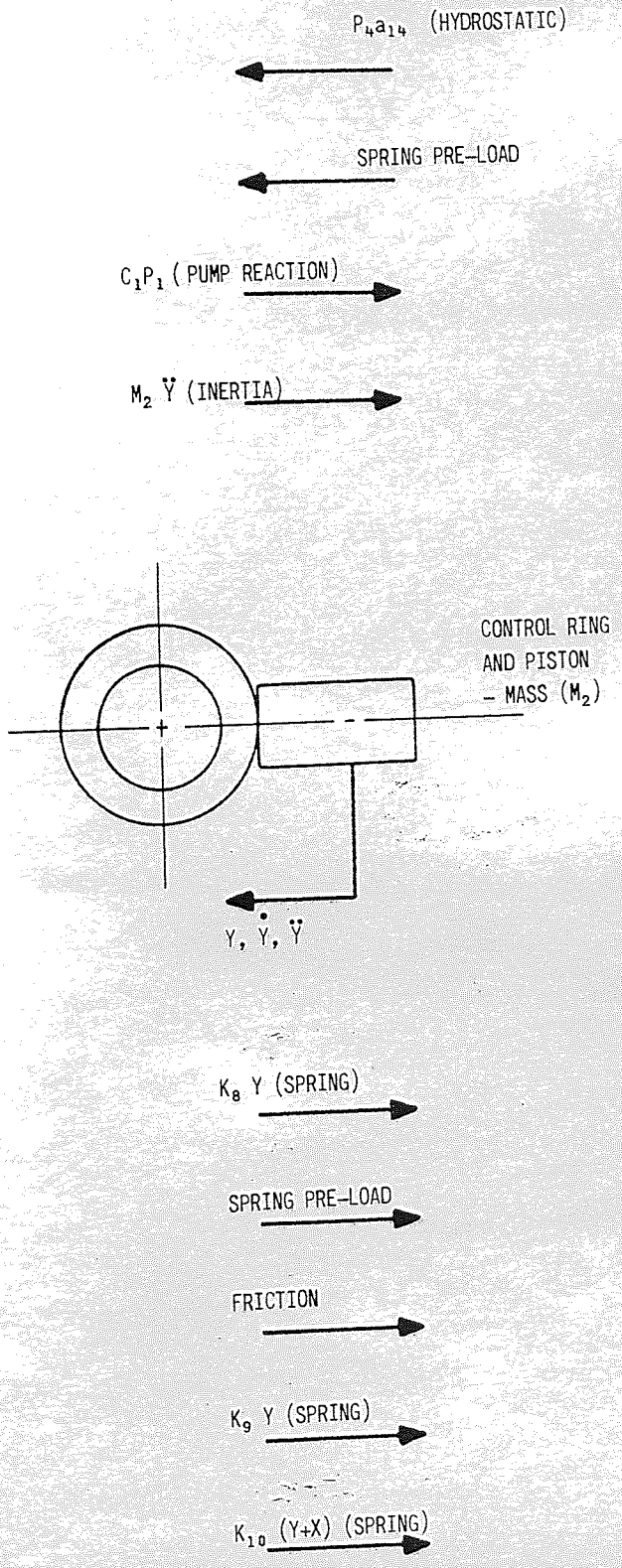

Fig A 8.7 FREE BODY DIAGRAM FOR THE PUMP

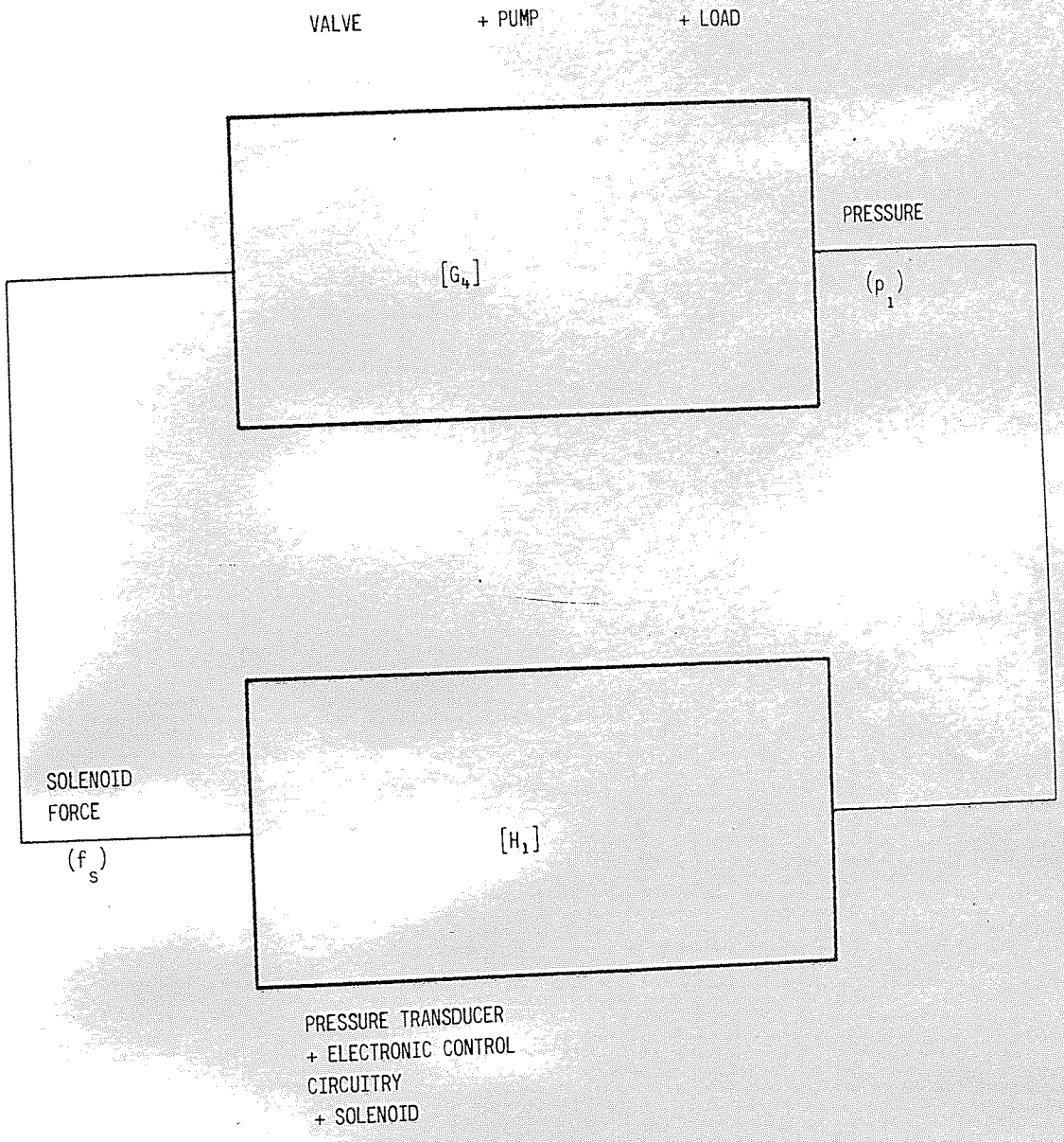

Fig A 8.8 A SIMPLIFIED BLOCK DIAGRAM FOR THE SOLENOID BASED CONTROLLER IN PRESSURE COMPENSATION

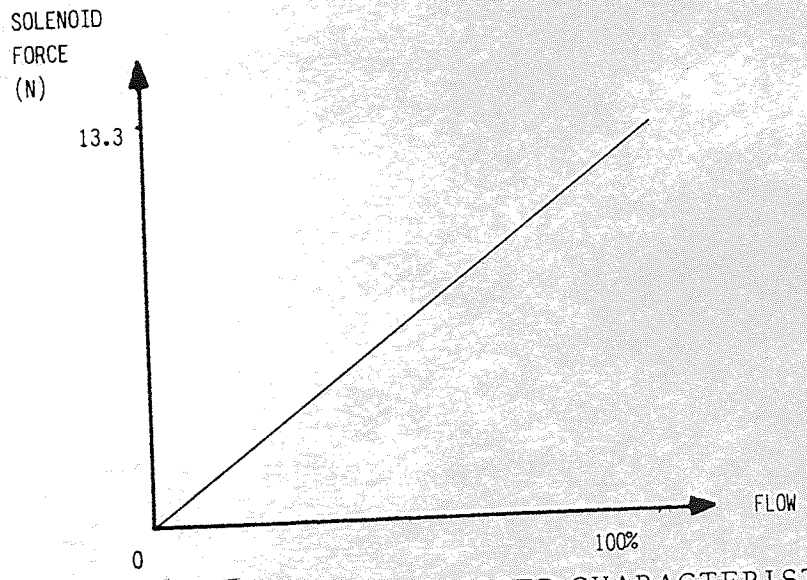

(a) IDEALISED CHARACTERISTIC OF SOLENOID FORCE AGAINST PUMP FLOW

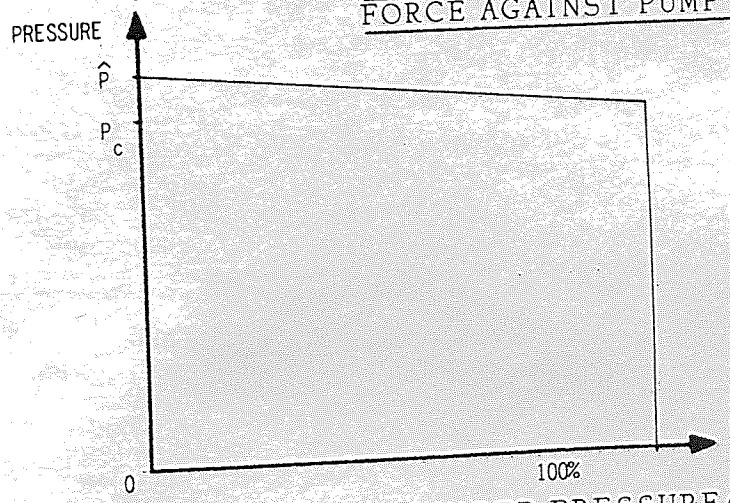

(b) REQUIRED PRESSURE/FLOW CHARACTERISTIC

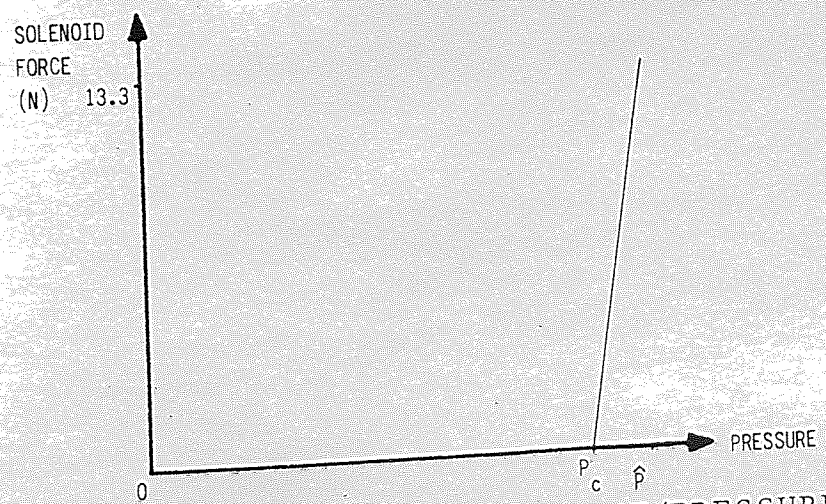

(c) SOLENOID FORCE/PRESSURE CHARACTERISTIC [H_1] REQUIRED FOR PRESSURE COMPENSATION

Fig A8.9 DETERMINATION OF THE TRANSFER FUNCTION [H_1]

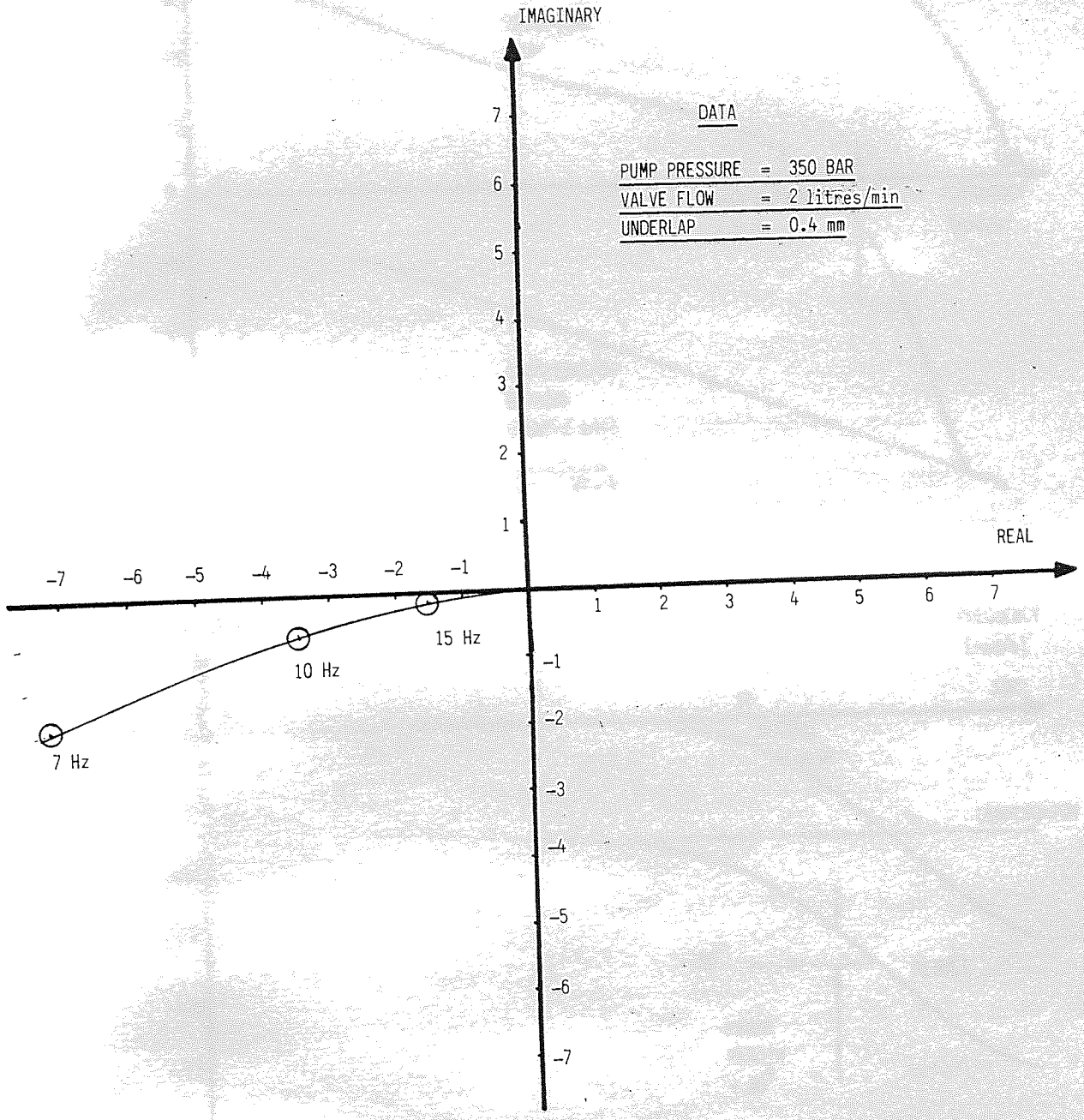

Fig A 8.10 NYQUIST PLOT FOR THE SOLENOID BASED CONTROLLER IN PRESSURE COMPENSATION

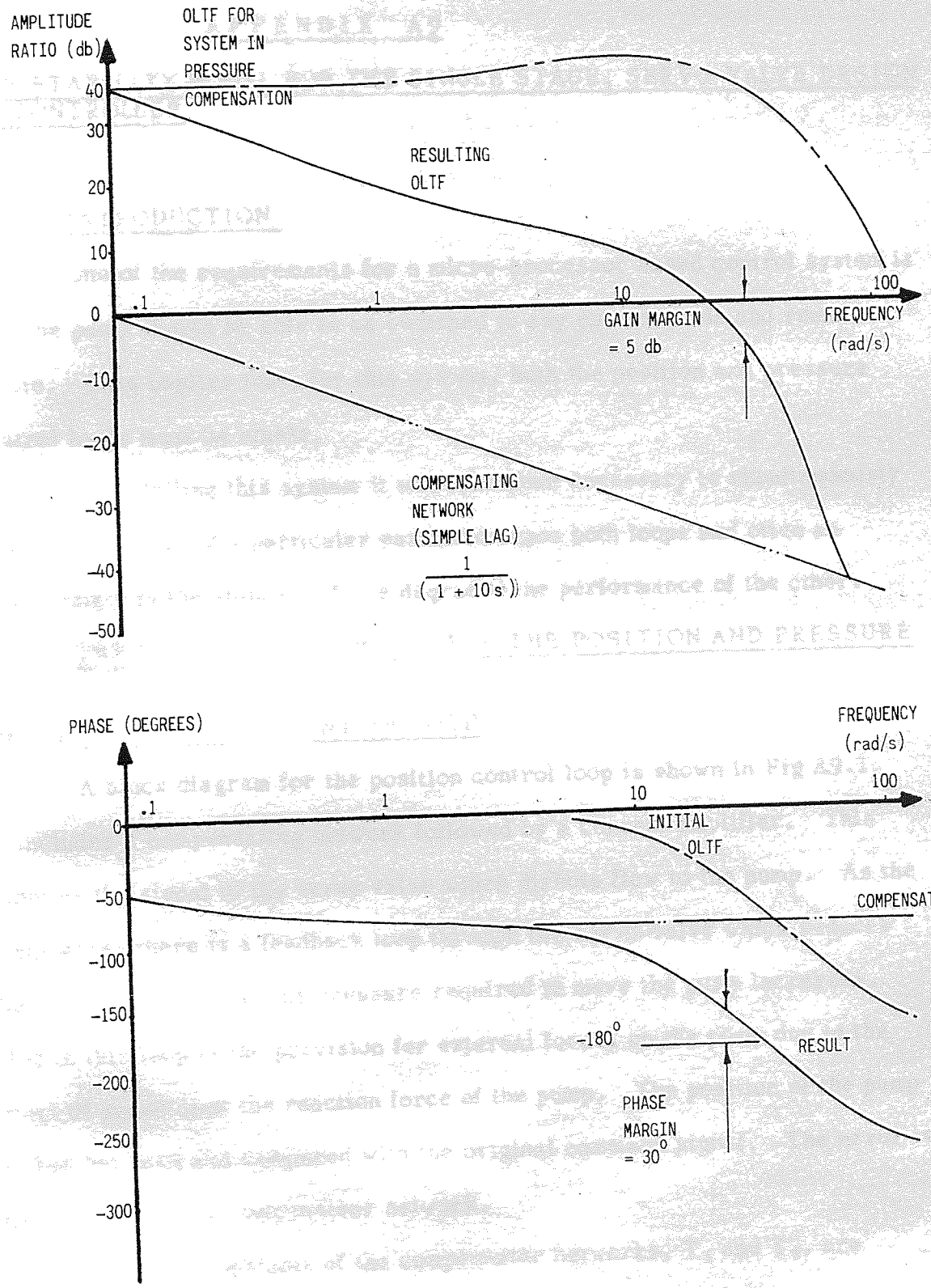

Fig A 8.11 BODE PLOT FOR THE SOLENOID BASED CONTROLLER ILLUSTRATING THE MAGNITUDE OF THE LAG NETWORK NECESSARY TO GIVE SUITABLE STABILITY MARGINS

APPENDIX A9

THE STABILITY MODEL FOR THE SINGLE STAGE, SERVO-VALVE DESIGN OF CONTROLLER

A9.1 INTRODUCTION

One of the requirements for a micro-processor based control system is that the pump should be able to be switched to any control mode and remain stable. This implies that, for this system, both the position and pressure control loops must be stable.

In modelling this system it was therefore necessary to simultaneously monitor the effect of a particular parameter upon both loops and often an improvement in the stability of one degraded the performance of the other.

A9.2 THE MATHEMATICAL MODEL FOR THE POSITION AND PRESSURE CONTROL LOOPS

A9.2.1 THE POSITION CONTROL LOOP

A block diagram for the position control loop is shown in Fig A9.1. It includes a compensating network followed by a current amplifier. This supplies the signal to the servo valve which directs flow to the pump. As the pump moves there is a feedback loop through the servo-valve which reduces the flow to the pump as the pressure required to move the pump increases. Also in this loop is the provision for external forces on the pump due to the effect of speed upon the reaction force of the pump. The position of the pump is then fed back and compared with the original command signal. The error is then altered by the compensator network.

The time constants of the compensator networks, T_1 and T_2, are included as variables to improve system stability. Thus

$$[G_8] = \left[\frac{1 + T_1 s}{1 + T_2 s}\right] \qquad - \quad A9.1$$

The range of the input signal to command zero and maximum flow was set to nominal values of ±10 v and the required gain of the system was initially set to 10 to give an accuracy of ± 5%. The servo-valve required a maximum current of ± .150 A and hence the gain of the current amplifier was

$$[G_9] = 0.15 \text{ (A/V)} \qquad - \text{ A9.2}$$

The dynamic performance of the servo valve was supplied by its manufacturer for a supply pressure of 140 bar and the Bode plot is shown in Fig A9.2. A first order lag was then devised which gave a fairly good representation of its performance and this too is shown in Fig A9.2. Fig A9.3 shows the steady state flow characteristics for the valve for various load pressures.

The characteristics are non-linear and in order to continue with this analysis it is necessary to linearise the relationship about the operating point considered. It was envisaged that the normal operating differential pressure would be in the region of 14 bar and that the current would be between 40 to 100 mA. The rate of change of flow with respect to current under these conditions can therefore be calculated to be 6.8×10^{-4} $(m^3/s)/A$.

The transfer function for the servo-valve is therefore

$$[G_7] = \left[\frac{6.8 \times 10^{-4}}{1 + TS}\right] \qquad - \text{ A9.3}$$

where T = .0018 seconds

The transfer function relating pump position to flow is simply

$$[G_{10}] = \left[\frac{1}{a_{16}s}\right] \qquad - \text{ A9.4}$$

where a_{16} is the area of the drive piston shown in Fig 4.3.

As the pump moves the differential pressure increases. Fig A9.4 is a free body diagram for the control ring and the driving pistons. Equating these forces for equilibrium, dividing through by a_{16} and linearising gives

$$[H_5] = \left[\frac{M_2 s^2 + K}{a_{16}}\right] \quad - \quad A9.5$$

Returning to Fig A9.3 the rate of change in flow with respect to differential pressure about the considered operating point at constant current is given by the slope of the constant current lines at a differential pressure of 14 bar. This gradient is reasonably constant and is approximately -1.60×10^{-11} $(m^3/s)/Pa$. The transfer function $[H_2]$ is therefore

$$[H_2] = \left[\frac{H_2}{1+TS}\right]$$

where $H_2 = -1.60 \times 10^{-11}$

$T = .0018$

A further loss in flow is from compressibility effects in the volume of oil in the pump control cylinders (V_1). The compressibility flow is given by

$$Q_C = \frac{V_1}{\beta} s(\Delta P)$$

Therefore the linearised transfer function $[H_3]$ is

$$[H_3] = \left[\frac{V_1 s}{\beta}\right] \quad - \quad A9.7$$

Finally, pump position is monitored by a transducer and the amplified signal is compared with that demanded. The stroke of a 77 ml/rev pump is 7.5 mm and the amplified signal must equal ± 10 V. The gain of the feedback signal $[H_4]$ is therefore

$$[H_4] = [2666] \quad V/m \quad - \quad A9.8$$

Assuming the external forces are small, the OLTF for the position control loop is given by

$$OLTF = [H_4][G_8][G_9][G_7]\left[\frac{[G_{10}]}{1 + [G_{10}][H_5][H_2+H_3]}\right] \quad - \quad A9.9$$

Combining equations A9.1 to A9.9 gives

$$\text{OLTF (position)} = \left[\frac{0.272\, a_{16}(1+T_1 s)}{(1+T_2 s)\left[\frac{M_2 V_1 T}{\beta} s^4 + \frac{M_2 V_1}{\beta} s^3 + \left(\frac{KV_1}{\beta} T + M_2 H_2 + a_{16}^2 T\right) s^2 + \left(a_{16}^2 + \frac{KV_1}{\beta}\right) s + KH_2 \right]} \right]$$

– A9.10

A9.2.2 THE PRESSURE COMPENSATING CONTROL LOOP

Returning to the block diagram for this controller, shown in Fig A9.1,

$$\text{OLTF (pressure)} = [G_5][G_6][\text{CLTF(position)}][G_3][H] \quad \text{– A9.11}$$

The transfer function for the pressure transducer and electronic control circuit for pressure above that of cracking (P_c), $[G_5]$, is such that 10% of cracking pressure (P_c) gives 20 volts thus

$$[G_5] = \left[\frac{200}{P_c}\right] \quad (V/Pa) \qquad \text{– A9.12}$$

$[G_6]$ represents three variable, first order filters with time constants T_3, T_4 and T_5.

$$[G_6] = \left[\frac{1 + T_3 s}{1 + T_4 s}\right] (1 + T_5 s) \qquad \text{– A9.13}$$

$$[G_3] = -\left[\frac{V_p N}{60\hat{Y}}\right] \qquad \text{– A9.14}$$

(as given by equation A2.10)

$$[H] = \left[\frac{-1}{\left(\frac{V}{\beta}\right)s + \frac{C_d a_v}{\sqrt{2 P_1 \rho}}} \right]$$

– A9.15
(as given by equation A2.14)

and $$[CLTF\ (position)] = \frac{1}{[H_4]} \left[\frac{OLTF\ (position)}{1 + OLTF\ (position)} \right]$$

– A9.16

Combining equations A9.10 to A9.16 and rearranging gives

$$OLTF\ (pressure) = \left[\frac{200}{P_c}\right] \left[\frac{1+T_3 s}{1+T_4 s}\right] \left[\frac{-V_p N}{60 \hat{Y}}\right] \left[\frac{-1}{\frac{V}{\beta} s + \frac{C_d a_v}{\sqrt{2\rho P_1}}}\right] [1 + T_5 s]$$

$$\bullet \left[\frac{0.272\ a_{16}\ (1+T_1 s)/[H_4]}{\frac{M_2 V_1 T T_2 s^5}{\beta} + s^4 \frac{M_2 V_1}{\beta} (T + T_2) + s^3 \left(\frac{M_2 V_1}{\beta} + \frac{(KV_1 T + M_2 H_2 + a_{16}^2 T) T_2}{\beta}\right) + s^2 \left(\frac{(KV_1 T + M_2 H_2 + a_{16}^2 T) + (a_{16}^2 + KV_1) T_2}{\beta}\right) + s \left(\frac{(a_{16}^2 + KV_1)}{\beta} + KH_2 T_2 + 0.272\ a_{16} T\right) + KH_2 + 0.272\ a_{16}} \right]$$

– A9.17

A9.2.3 MODEL DATA

M_2	=	11.384
a_{16}	=	4.3×10^{-4} m^2
V_1	=	4×10^{-5} m^3
T	=	.0018 s
K	=	17.5 KN/m
H_2	=	-1.6×10^{-11} $(m^3/s)/Pa$
T_1	=	.01 s
T_2	=	.03 s
T_3	=	.006 s
T_4	=	.06 s
T_5	=	.0039 s
P_c	=	140×10^5 P_a
N	=	2500 rpm
a_v	=	0 (zero flow condition)
$[H_4]$	=	2666 V/m
v, β, $\hat{Y}$		are given in Appendix A2

A9.2.4 RESULTS FROM THE MODELS

Fig 4.4 is a Nyquist plot for the resulting position OLTF with no auxiliary compensation. This indicates that the loop is only marginally stable. To improve this the effects of the time constants T_1 and T_2 were investigated and it was found that the most favourable results were obtained with a lag/lead network as shown in Fig 4.5.

The model of the pressure loop was then used and initially it predicted that with no compensation it would be unstable. The time constants T_3, T_4 and T_5 were then varied in order to produce satisfactory stability margins and the final result is shown in Fig 4.5.

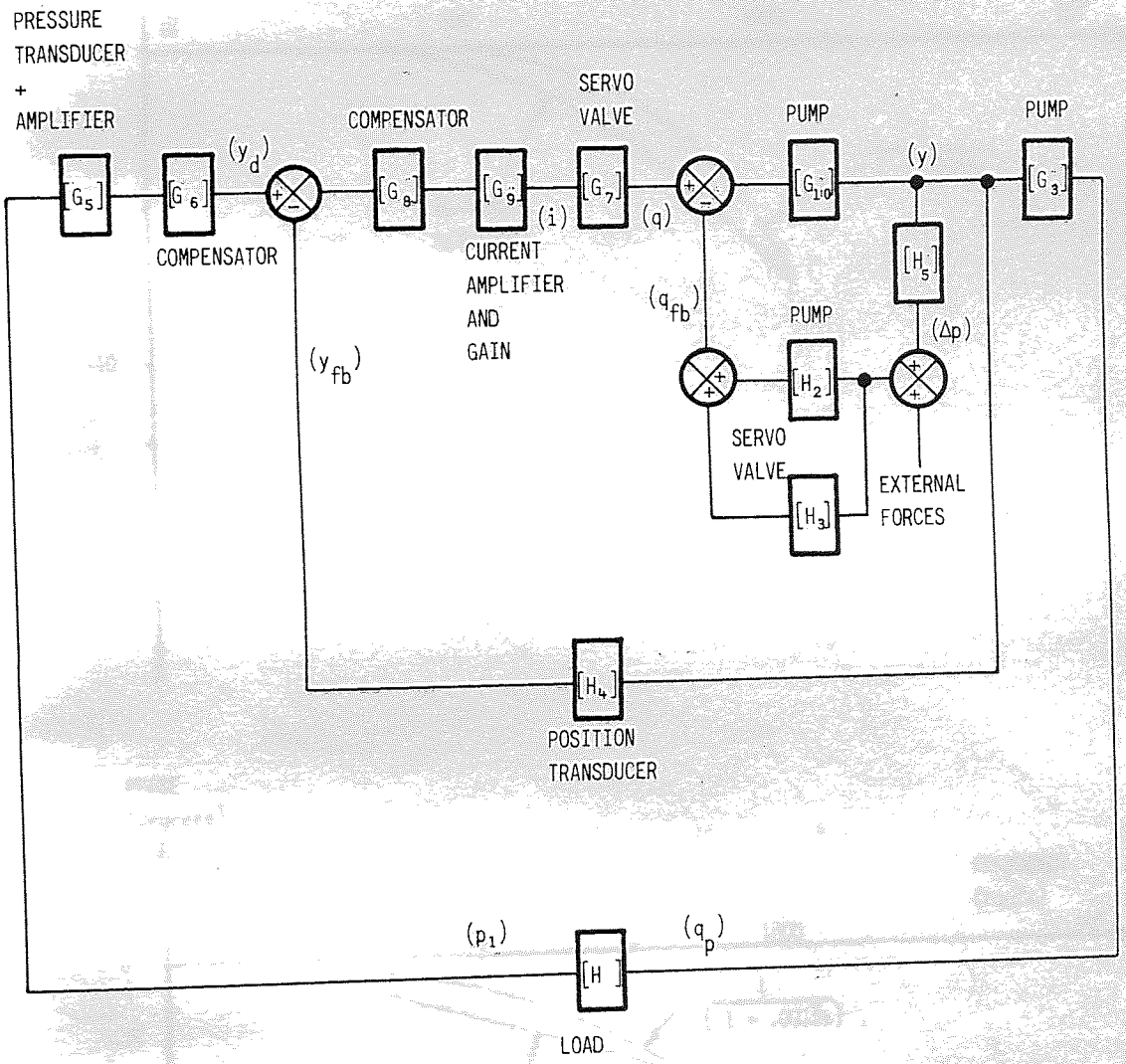

Fig A9.1 BLOCK DIAGRAM FOR THE PRESSURE AND POSITION CONTROL LOOPS INCLUDING COMPENSATING NETWORKS

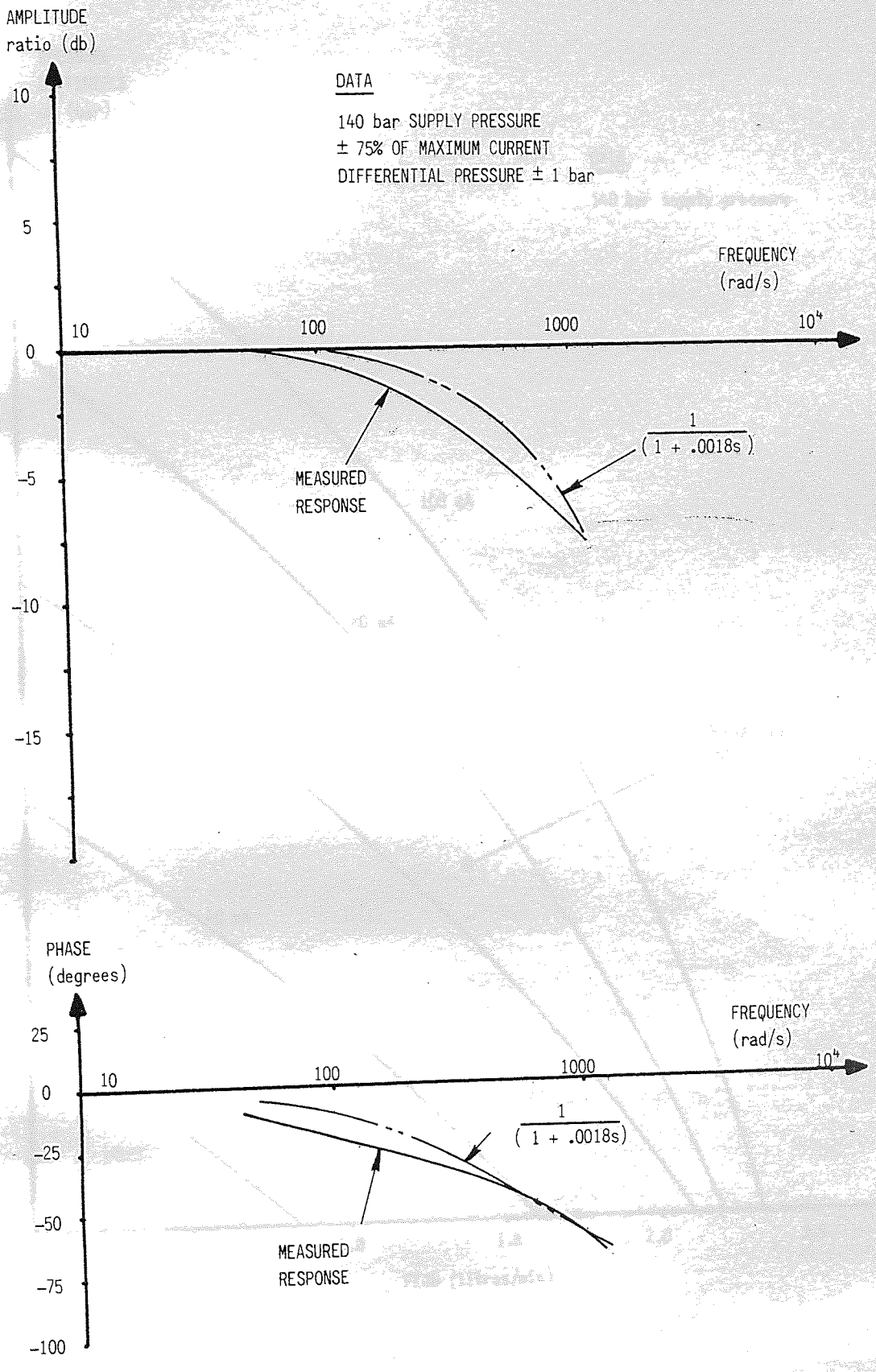

Fig A9.2 THE DYNAMIC PERFORMANCE (FLOW/CURRENT) OF THE SINGLE STAGE SERVO VALVE AND ITS FIRST ORDER APPROXIMATION

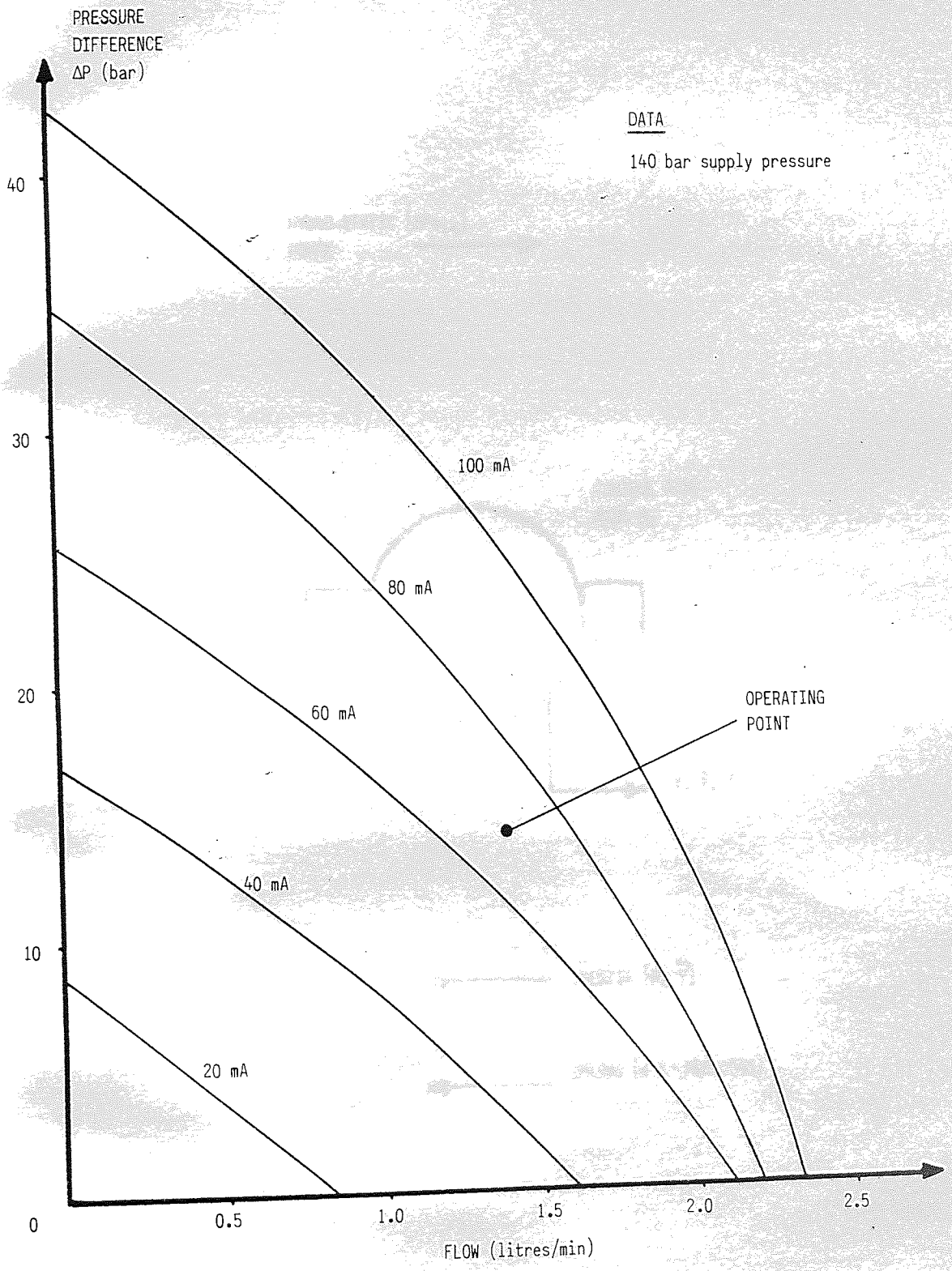

Fig A9.3 THE STEADY STATE FLOW CHARACTERISTIC FOR THE SINGLE STAGE SERVO-VALVE

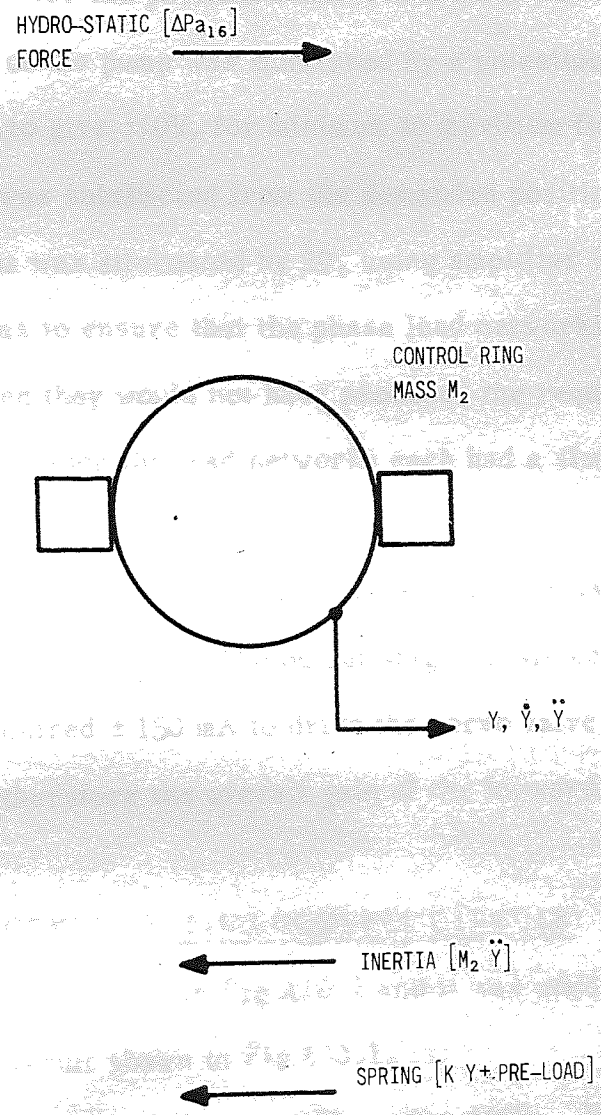

Fig A9.4 A FREE BODY DIAGRAM FOR THE CONTROL RING

APPENDIX A10

THE ELECTRONIC CONTROL CIRCUITS

A10.1 THE POSITION CONTROL LOOP

The circuit diagram for the position control circuit is shown in Fig A10.1. The position of the pump was monitored by a potentiometer and its output was conditioned to give ±10V, for minimum to maximum flow, by amplifier 8. This signal was subtracted from the demanded position signal and the difference between them was attenuated by 39, using amplifier 1.

This attenuation was to ensure that the phase lead networks did not saturate. If they had, then they would not have produced the required phase advantage. For the same reason the lead networks each had a simple filter to limit high frequency amplification.

Amplifier 4 buffered the compensating networks from the saturating amplifier 5, which had a gain of 2000. The output stage consisted of a current boost and this gave the required ± 150 mA to drive the servo valve. The gain of amplifier 7 was 20 and therefore the overall gain of the forward loop was 1025.

A10.2 THE PRESSURE COMPENSATING CONTROL CIRCUIT

The circuit diagram is shown in Fig A10.2 and it was used in conjunction with the position control circuit shown in Fig A10.1.

The pressure transducer used was a CEL series 4000. This gave an output of 0.0343V/bar, thus at 200 bar the output was 6.86 V.

The input from the transducer was through a differential amplifier 1 with a variable offset. This was adjusted to hold the output from the amplifier at -10 v until the pressure exceeded the compensating crack level of 180 bar (6.17V). Thus, for pressures below 180 bar, the circuit demanded full pump flow. However, when pressure exceeded this,the compensating circuit was activated and the pump was progressively de-stroked.

The Bode plot for the pressure compensating loop, shown in Fig 4.9, indicated that the gain margin could be improved by the introduction of a lag/lead network. This was achieved using amplifier 2.

The A to D converter had an input range of 0 to +10V and this gave 255 discrete, digital levels. To alter the resolution of the micro-computer, amplifier 3 was used to change the magnitude of the input signal to the A to D converter. Thus, when this signal ranged from 0 to 1V this was represented by only 25 levels in the micro computer.

The micro-processor attenuated the signal by three and so amplifier 5 was used to condition the final signal to give ± 10V, to be compatible with the requirements of the position control loop.

If the micro-processor was not required in a particular test, this could be accommodated by turning the analogue/digital switch and to keep the circuit gain unchanged, the analogue signal was also attenuated by 3 using amplifier 4.

In general the circuit worked well but, amplifier 2 amplified, rather than attenuated, the pressure ripple of the pump. This did not adversely affect the analogue control loop but it led to serious aliasing problems when the micro-processor was used in the loop. Time did not permit this problem to be rectified but it was thought that the use of higher quality components would eliminate it.

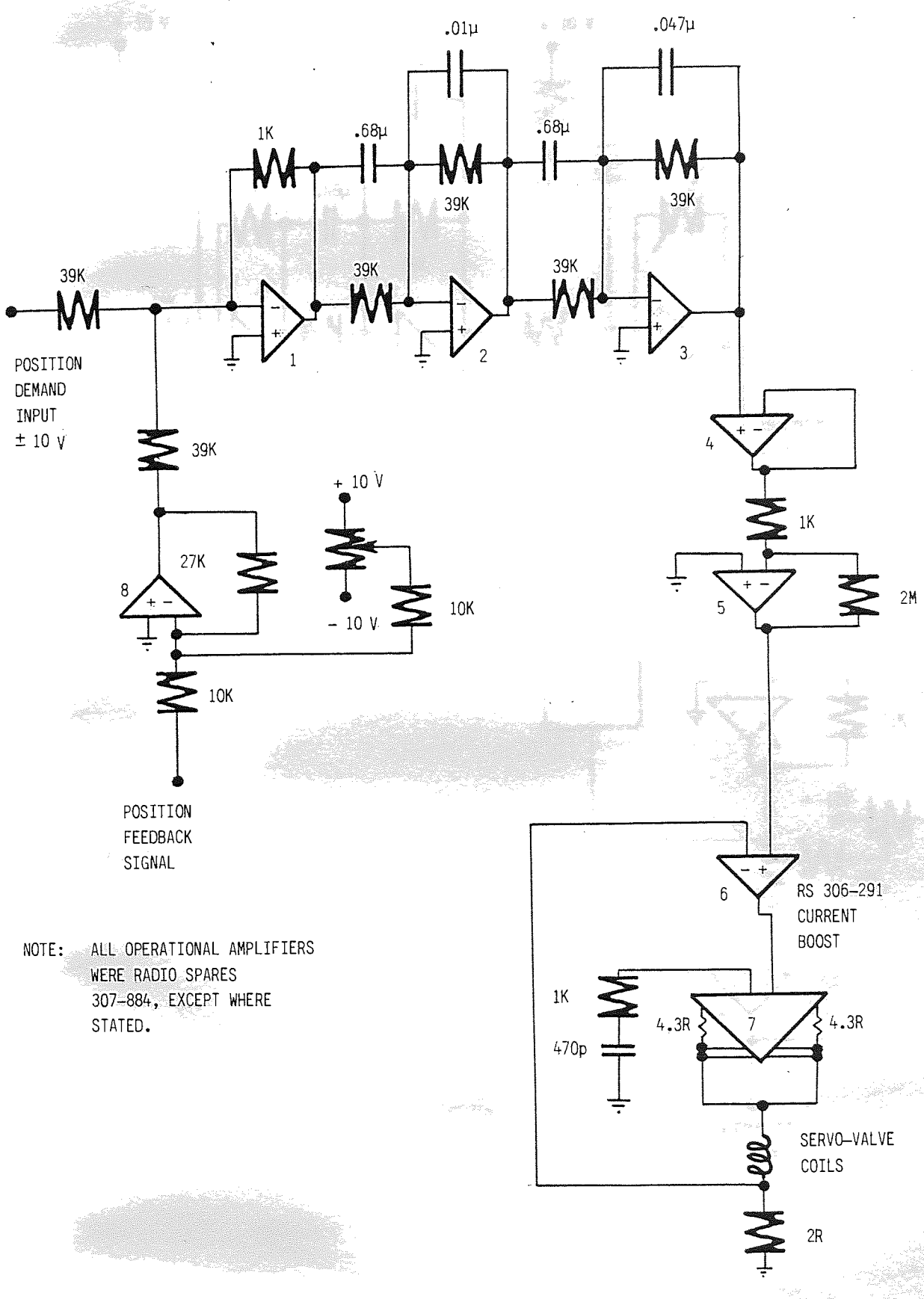

NOTE: ALL OPERATIONAL AMPLIFIERS WERE RADIO SPARES 307-884, EXCEPT WHERE STATED.

Fig A10.1 ELECTRONIC CIRCUIT FOR THE POSITION CONTROL CIRCUIT

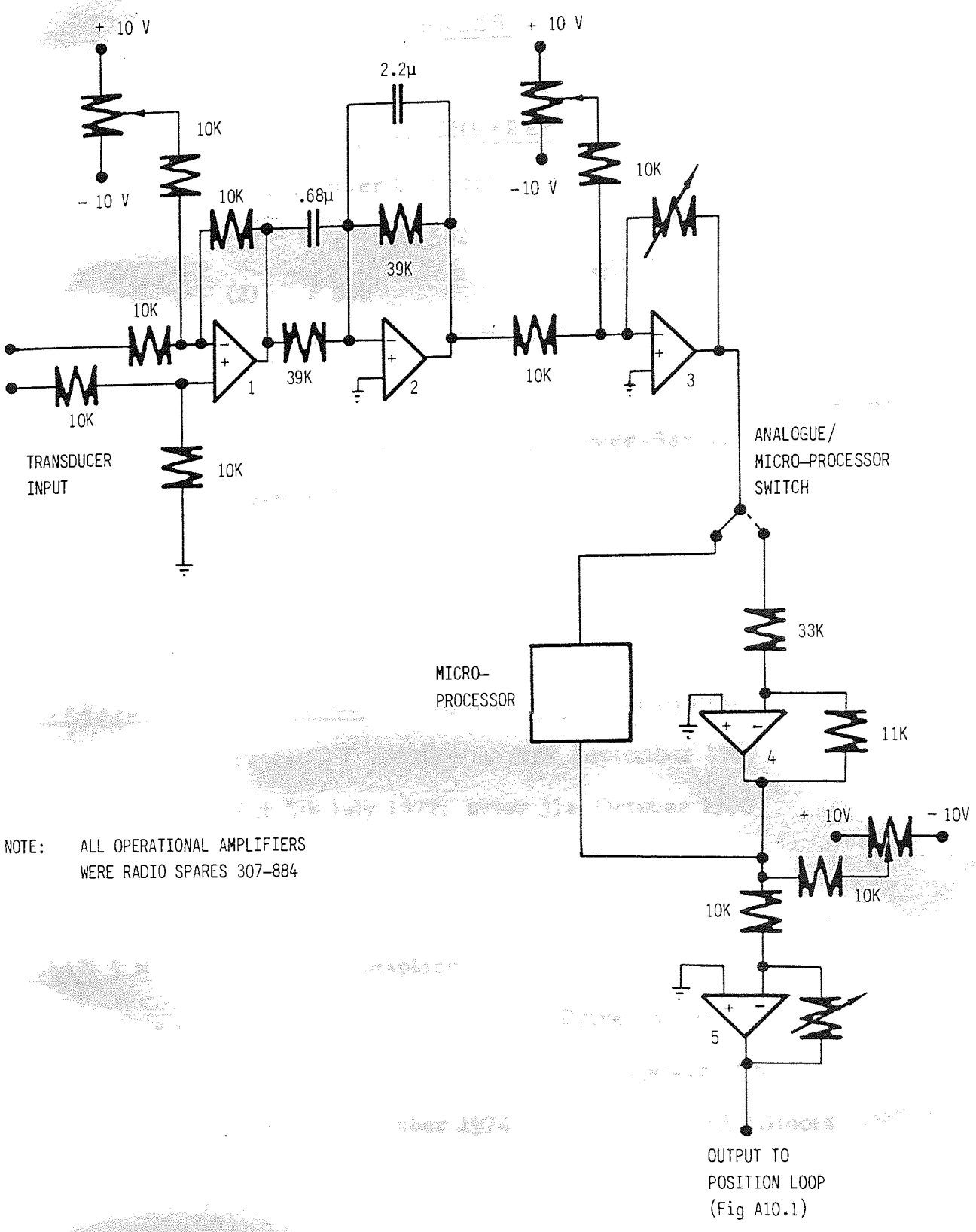

Fig A10.2 ELECTRONIC CONTROL CIRCUIT FOR THE PRESSURE COMPENSATING LOOP

REFERENCES

BLACKBURN J F, REETHOF G, SHEARER J L

"Fluid Power Control"

(1) P 477 and 582

(2) P 300

Technology Press MIT and John Wiley & Sons 1960.

BOULDEN L L "Those Energy-Scrimping, Power-Saving, Hydraulic Systems"

Automation (Cleve) V 22 n 10

October 1975 - P 57 - 61.

CATERPILLAR TRACTOR CO "Hydraulic Control System".

Patent U K 1280048 - 30th September 1969

Pub 5th July 1972; prior 31st October 1968

USA 772246

CLAAR L M "Variable Displacement Pump and Controls - Applied to Variable Speed - Variable Drive Systems"

30th National Conference on fluid power, Chicago Ill USA

12-14th November 1974 (Chicago Ill USA Illinois Inst Technol 1974) P 123 - 43.

CLARK D C "Electronic Controls for Fluid Power"

Hydraul Pneum V 31

6th June 1978 P 70 - 73

DREYMULLER J "Pilot - Operated and Directly Actuated Pressure Control with Variable Delivery Axial Piston Pumps".
4th International Fluid Power Symposium April 16th-18th 1975, B H R A Paper B1.

ERNST W "Design of Pressure - Compensating Controls".
Applied Hydraulics and Pneumatics V 12 n 11
November 1959 P 76 - 77.

FOSTER K "Dynamic Analysis of a Two-Stage Relief Valve".
Proceedings of the conference on Oil Hydraulic Power Transmission and Control.
29th and 30th November 1961.
Instn Mech Engrs, LONDON 1962 Paper 16
P 207 - 215.

GREEN W L and CROSSLEY T R "An analysis of the Control Mechanism used in Variable-Delivery Hydraulic Pumps".
Proc Instn Mech Engrs 1970 - 71
Vol 185 No. 6 P 63-72.

GLICKMAN M "Variable-Delivery Hydraulic Pumps"
(Eng Syst & Prod Co. Hayel Crest Ill)
Plant Eng (Barrington) Ill - V 30 n 5
Mar 4th 1976 - P 85 - 87.

HOLZBOCK W G "Energy-Saving Electro Hydraulic Systems".
Ill Inst of Technol, Chicago 1977 P 324 - 331
33rd National Conference on Fluid Power.

JOYAL T J "Electronic Controls for Hydrostatic Drives"
Mach Des V 48 n 23
October 7 1976 - P 114 - 117

KNOELKER H D, MAZUR J N "Why Better Controls for High Pressure Hydraulics in Construction Machinery".
31st National Conference on Fluid Power, Chicago Ill USA 21 - 23rd October 1975
(Chicago Ill USA Illinois Inst Technol 1975)
P 604 - 29.

MASKREY R H, THAYER W J "A Brief History of Electro Hydraulic Servo-Mechanisms".
ASME V100 n 2
June 1978 - P 110 - 116.

MEISEL W "Remote Control of Variable-Displacement Pumps".
Machine Design V 36 n 10 April 23rd 1964
P 238 - 41.

RIGBY R W "An Integral Control Constant Pressure Device with Built-In-Stabilization for a Variable Delivery Axial Piston Hydraulic Pump".
Proc of the 1st Fluid Power Symposium, paper SP 988,
PP 159 - 169. Cranfield 1969.

RUPPELT K, SCHLINKE G S "Programmed Controls for Axial Piston Pumps and Motors".
Hydraulic, Pneumatic (USA) V 22 n 3 P 88 - 91
March 1969.

STRICKLAND W B "Control Mechanisms for Hydraulic Piston Pumps".
Product Eng V 21 n 8 Aug 1950 - P 120 - 1.

TOU J T "Digital and Sampled - Data Control Systems".
McGraw - Hill Book Co. 1959.

YEAPLE F "Evaluate Hydraulic System Losses by Putting Dollar Valves on Energy".
Prod Eng V 47 n 8
Aug 1976 - P 41 - 42.

YOUNG J E G "Power Conservation Through the Control of Axial Piston Pumps".
30th National Conference on Fluid Power, Chicago Ill USA. 12 - 14th November 1974
(Chicago Ill USA: Ill Inst Technol 1974)
P 39 - 51.